TAMPEREEN TEKNILLINEN YLIOPISTO
TAMPERE UNIVERSITY OF TECHNOLOGY

Heli Koivuluoto

Microstructural Characteristics and Corrosion Properties of Cold-Sprayed Coatings

Julkaisu 882 • Publication 882

Tampere 2010

Tampereen teknillinen yliopisto. Julkaisu 882
Tampere University of Technology. Publication 882

Heli Koivuluoto

Microstructural Characteristics and Corrosion Properties of Cold-Sprayed Coatings

Thesis for the degree of Doctor of Technology to be presented with due permission for public examination and criticism in Konetalo Building, Auditorium K1702, at Tampere University of Technology, on the 4th of June 2010, at 12 noon.

Tampereen teknillinen yliopisto - Tampere University of Technology
Tampere 2010

ISBN 978-952-15-2353-3 (printed)
ISBN 978-952-15-2373-1 (PDF)
ISSN 1459-2045

PREFACE

The work presented in this dissertation was carried out at the Department of Materials Science, Tampere University of Technology during the years 2005-2009. This work was supervised by Prof. Petri Vuoristo to whom I would like to address my deepest gratitude and thank for all his guidance and for giving me the opportunity to prepare this dissertation under his supervision.

In addition, I would like to thank all of the co-authors: Lic.Tech. Juha Lagerbom for his guidance at the beginning of this work, M.Sc. Jonne Näkki for corrosion tests which were performed at KETEK and M.Sc. Mari Honkanen for TEM evaluations. Mr. Werner Krömmer of Linde AG Gas for spraying the high-pressure cold-sprayed coatings and Mr. Mikko Kylmälahti for spraying the low-pressure cold-sprayed coatings are also gratefully acknowledged. Furthermore, I would like to express many thanks to Dr. Minnamari Vippola for her guidance, help and fruitful discussions during this work period. The research assistants, who have assisted me during this work, are also acknowledged. I would also like to express thanks to the members, past and present, of the Surface Engineering Group and to all the staff of the Department of Materials Science for the nice working atmosphere.

I am much obliged for the financial support by the Academy of Finland (2009-2010), the Graduate School on New Materials and Processes (2009), and the KINE-MATEK (2005-2008) project funded by the Finnish Funding Agency for Technology and Innovation (TEKES), the European Regional Development Fund (ERDF), Metso Paper Oy, Outotec Research Oy, Kemira Oy, Oy AGA Ab, TTT Technology Oy, Fincoat Oy, Oseir Oy, and KMT Group Oy. The Jenny and Antti Wihuri Foundation, the Finnish Foundation for Technology Promotion (TES), Walther Alhström Foundation and the City of Tampere are also gratefully acknowledged for their financial supports.

My parents, Merja and Matti, are also gratefully thanked for their supports and encouragements. Finally, my beloved husband Petteri is most deeply thanked for his endless patience, support and encouragement during this hard work.

Tampere, May 2010

Heli Koivuluoto

ABSTRACT

Cold spraying is a thermal spray process which enables production of metallic and metallic-ceramic coatings with dense (very low porosity level) and pure (low oxygen content) structures. Several coating properties such as corrosion resistance and electrical conductivity rely on these properties. Cold spraying consists of two processes: high-pressure cold spraying (HPCS) and low-pressure cold spraying (LPCS) divided by the pressure level used in the processes (40 bar versus 10 bar). Generally, cold spraying is based on higher particle velocities and lower process temperatures than in other thermal spray processes. The coating is formed in a solid state when powder particles impact on a sprayed surface with high kinetic energy, deform and adhere to the substrate or to other particles. Therefore, a high level of plastic deformation and adiabatic shear instability are required for a tight bonding between powder particles and for the formation of dense microstructures. Moreover, in cold spraying, many factors, e.g., powder characteristics and compositions, spraying parameters, and post-treatments affect the formation and properties of the coating.

This work focuses on the characterization of the microstructural properties (microstructure, grain structure, particle deformation, and fracture behavior), corrosion resistance (denseness, impermeability, and corrosion properties), and mechanical properties (hardness and bond strength) of the cold-sprayed metallic and metallic-ceramic coatings. Furthermore, the aim of this work is to find relationship between microscopic details and macroscopic properties and affecting factors for these in order to produce fully dense coatings using cold spray processes. The coating materials are pure metals: Cu, Ta, and Ni, metal alloys: Ni-20Cr, Ni-20Cu, and Ni-30Cu, and metallic-ceramic composites: Cu+Al_2O_3, Ni-20Cr+Al_2O_3, and Ni-20Cr+WC-10Co-4Cr. Structural details are characterized using electron microscopy techniques (SEM, FESEM, and TEM) whereas denseness and corrosion properties are evaluated with corrosion tests (open-cell potential measurements, salt spray tests, and polarization measurements).

Typically, cold-sprayed coatings appeared to be dense without porosity or other defects in their structures according to visual examinations. However, corrosion tests revealed through-porosity in the coating structures, indicating an existence of weak points inside the coatings. Therefore, denseness and impermeability play an important role in the corrosion resistance of the coatings. Good corrosion resistance is based on the formation of a protective oxide layer in case of passivating metals and metal alloys. Fully dense coating structures are required for the capability of the cold-sprayed coatings to act as real corrosion barrier coatings and to perform well in all corrosion tests. Three ways to eliminate or decrease the number of weak points and defects in the coating structures were found. Firstly, the denseness improvement was done with an optimal combination of powder and spraying parameters (HPCS Cu, Ta, and Ni coatings). These combinations are strongly material-dependent. HPCS Ta coatings also have similar corrosion properties with corresponding bulk material, indicating excellent corrosion protection. Secondly, the denseness of metallic coating can be increased by adding ceramic particles into the metallic powder as a powder mixture. These hard particles keep the nozzle clean; activate the sprayed surface; and reinforce the coating by hammering the structure. The significant denseness improvement was observed with HPCS Ni-20Cr+Al_2O_3, HPCS Ni-20Cr+WC-10Co-4Cr and LPCS Cu+Al_2O_3 coatings. In addition to these, thirdly, the denseness improvement of HPCS Ni-20Cu coatings was done with heat treatments due to the void reduction and recrystallization.

TABLE OF CONTENTS

PREFACE i
ABSTRACT iii
TABLE OF CONTENTS iv
LIST OF PUBLICATIONS vi
AUTHOR'S CONTRIBUTION vi
LIST OF SYMBOLS AND ABBREVIATIONS viii

1 INTRODUCTION 1

2 COLD SPRAYING 4
  2.1 High-pressure cold spraying 5
  2.2 Low-pressure cold spraying 6

3 COLD-SPRAYED COATINGS 8
  3.1 Coating formation 8
    3.1.1 Velocities 10
      3.1.1.1 Critical velocity 10
      3.1.1.2 Particle velocity 12
    3.1.2 Particle deformation 14
      3.1.2.1 Plastic deformation 14
      3.1.2.2 Adiabatic shear instability and material jets 16
      3.1.2.3 Bonding 18
  3.2 Coating properties 19
    3.2.1 Effect of powders 19
    3.2.2 Coating structure 20
    3.2.3 Mechanical properties 22
  3.3 Corrosion resistance 24
  3.4 Potential applications of cold-sprayed coatings 28

4 AIM OF THE STUDY 29

5 MATERIALS 30
  5.1 Powder materials 30
  5.2 Substrate materials 30

6 METHODS 31
  6.1 Spraying methods 31
    6.1.1 High-pressure cold spray system 31
    6.1.2 Low-pressure cold spray system 31

6.2 Characterization methods 32
6.2.1 Microscopic techniques 32
6.2.2 Corrosion tests 33
6.2.3 Mechanical testing methods 33
6.2.4 Other methods 34
6.3 Post-treatments 34

7 RESULTS AND DISCUSSION 35
7.1 Microscopic properties of cold-sprayed coatings 35
7.1.1 Microstructure 35
7.1.2 Grain structure 38
7.2 Particle interfaces 40
7.2.1 Metal-metal particle bonding 40
7.2.2 Metal-ceramic particle bonding 42
7.2.3 Particle deformation 43
7.3 Macroscopic properties of cold-sprayed coatings 46
7.3.1 Microhardness 46
7.3.2 Bond strength 47
7.4 Corrosion resistance of cold-sprayed coatings 48
7.4.1 Denseness 48
7.4.2 Corrosion properties 52

8 CONCLUDING REMARKS AND SUGGESTIONS FOR FUTURE WORK 54

REFERENCES 56

LIST OF ORIGINAL PUBLICATIONS

This thesis is based on the original experimental work presented in detail in the following 7 publications, which are referred in the text with corresponding Roman numerals I-VII.

I Heli Koivuluoto, Juha Lagerbom, and Petri Vuoristo, Microstructural Studies of Cold Sprayed Copper, Nickel, and Nickel-30%Copper Coatings, *Journal of Thermal Spray Technology*, 16 (4) 2007, p. 488-497

II Heli Koivuluoto, Juha Lagerbom, Mikko Kylmälahti, and Petri Vuoristo, Microstructure and Mechanical Properties of Low-Pressure Cold-Sprayed (LPCS) Coatings, *Journal of Thermal Spray Technology*, 17 (5-6) 2008, p. 721-727

III Heli Koivuluoto and Petri Vuoristo, Effect of Ceramic Particles on Properties of Cold-Sprayed Ni-20Cr+Al_2O_3 Coatings, *Journal of Thermal Spray Technology*, 18 (4) 2009, p. 555-562

IV Heli Koivuluoto, Jonne Näkki, and Petri Vuoristo, Corrosion Properties of Cold-Sprayed Tantalum Coatings, *Journal of Thermal Spray Technology*, 18 (1) 2009, p. 75-82

V Heli Koivuluoto, Mari Honkanen, and Petri Vuoristo, Cold-sprayed copper and tantalum coatings – Detailed FESEM and TEM analysis, *Surface & Coatings Technology*, 204 (15) 2010, p. 2353-2361

VI Heli Koivuluoto and Petri Vuoristo, Structural Analysis of Cold-Sprayed Nickel-Based Metallic and Metallic-Ceramic Coatings, *Journal of Thermal Spray Technology*, in press, DOI:10.1007/s11666-010-9481-4

VII Heli Koivuluoto and Petri Vuoristo, Effect of Powder Type and Composition on Structure and Mechanical Properties of Cu+Al_2O_3 Coatings Prepared by using Low-Pressure Cold Spray Process, *Journal of Thermal Spray Technology*, in press, DOI: 10.1007/s11666-010-9491-2

AUTHOR'S CONTRIBUTION

Heli Koivuluoto (née Mäkinen) is the main researcher and writer of all the publications. She planned and organized all experiments, performed most of the tests and characterizations, analyzed the results, and prepared the manuscripts. In the publications I and II, Lic.Tech. Juha Lagerbom gave advises and comments on the manuscripts. In the publication IV, M.Sc. Jonne Näkki carried out the polarization measurements and in the publication V, M.Sc. Mari Honkanen performed the TEM studies. In addition, all of the manuscripts were commented by Prof. Petri Vuoristo who also was the supervisor in the research.

PUBLICATIONS ON THE RESEARCH AREA BUT NO INCLUDED IN THE THESIS

VIII Heli Koivuluoto, Jonne Näkki, and Petri Vuoristo, Structure and Corrosion Behavior of Cold-Sprayed Tantalum Coatings, *Thermal Spray 2009: Expanding Thermal Spray Performance to New Markets and Applications,* B. Marple, M. Hyland, Y.-C. Lau, C.-J. Li, R. Lima, G. Montavon (Eds.), ASM International, May 4-7, 2009 (Las Vegas, Nevada, USA), p. 314-319

IX Heli Koivuluoto, Minna Kotilainen, and Petri Vuoristo, Overview of Structure and Properties of High-Pressure and Low-Pressure Cold-Sprayed Coatings, *Welding and Cutting*, (2) 2009, p. 98-104

X Heli Koivuluoto, Minna Kulmala, and Petri Vuoristo, Structural Properties of High-Pressure Cold-Sprayed and Low-Pressure Cold-Sprayed Coatings, *Surface Modification Technologies XXII*, T. Sudarshan, P Nylen (Eds.), September 22-24, 2008, (Trollhättan, Sweden), p. 65-72

XI Heli Mäkinen, Juha Lagerbom, and Petri Vuoristo, Adhesion of cold sprayed coatings: effect of powder, substrate, and heat treatment, *Thermal Spray 2007: Global Coating Solutions*, B. Marple, M. Hyland, Y.-C. Lau, C.-J. Li, R. Lima, G. Montavon (Eds.), ASM International, May 14-16, 2007 (Beijing, China), p. 31-36

XII Heli Mäkinen, Juha Lagerbom, and Petri Vuoristo, Mechanical properties and corrosion resistance of cold sprayed coatings, *Thermal Spray 2006: Building on 100 Years of Success*, B. Marple, M. Hyland, Y.-C. Lau, R. Lima, J. Voyer (Eds.), ASM International, May 15-18, 2006 (Seattle, USA), 6 p

LIST OF SYMBOLS AND ABBREVIATIONS

Greek symbols

ρ	Density
σ_u	Yield strength
σ_{TS}	Tensile strength

Latin symbols

Ø	Diameter
c_p	Specific heat
E_0	Resting potential
E_{corr}	Corrosion potential
E_p or E_{pp}	Passivation potential
F_1	Mechanical calibration factor (for cold spray 1.2)
F_2	Thermal calibration factor (for cold spray 0.3)
i_c	Critical passivation current density
i_{corr}	Corrosion current density
i_p or i_{pp}	Passivation current density
RT	Room temperature, 22ºC
T_i	Impact temperature
T_m	Melting point
$T_{particle}$	Particle temperature
$T_{particle,\ initial}$	Initial particle temperature
T_R	Reference temperature (293 K)
v_{cr} or v_{crit}	Critical velocity needed for coating formation, Eq. 1
$v_{crit}^{th,mech}$	Critical velocity in advanced Eq. 2
$v_{erosion}$	Erosion velocity

Materials abbreviations

Al	Aluminum
$Al+Al_2O_3$	Aluminum+aluminum oxide (composite)
Al_2Cu, Al_4Cu_9	Aluminum-copper intermetallic alloy
Al_2O_3	Aluminum oxide (alumina)
$Al_2O_3-Ti_2O$	Aluminum oxide-titanium dioxide (composite)
$Al-MnO_2$	Aluminum-manganese dioxide (composite)
Al-Si	Aluminum-silicon (alloy)
Al+SiC	Aluminum+silicon carbide (composite)
Al-Zn-Ti	Aluminum-zinc-titanium (composite)
Ag	Silver
Ar	Argon
$Ar-3H_2$	Argon-3%hydrogen
BCC	Body-centered cubic lattice structure
CoNiCrAlY	Cobalt-nickel-chromium-aluminum-yttrium (alloy)
Cu	Copper
$Cu+Al_2O_3$	Copper+aluminum oxide (composite)
CuAl	Copper-aluminum (alloy)
Cu-Al	Copper-aluminum (composite)
Cu_2O	Copper oxide, patina
Cu-Sn	Copper-tin (bronze)
Cu-W-Zn	Copper-tungsten-zinc (composite)
Cu-Zn	Copper-zinc (brass)
FCC	Faced-centered cubic lattice structure
Fe	Iron
Fe52	Carbon steel

H_2SO_4	Sulfuric acid
HCl	Hydrochloride acid
He	Helium
HF	Hydrogen fluoride
MCrAlY	M-chromium-aluminum-yttrium, M=metal (alloy)
N_2	Nitrogen
NaCl	Sodium chloride
Nb	Niobium
Ni	Nickel
Ni+TiC	Nickel-titanium carbide (composite)
NiAl	Nickel-aluminum (alloy)
$NiAl_3$, Ni_3Al	Nickel aluminide (intermetallic alloy)
Ni-Cu	Nickel-copper (alloy)
Ni-30Cu	Monel 400 alloy
Ni-Cr	Nickel-chromium (alloy)
NiO	Nickel oxide
Si	Silicon
SiC	Silicon carbide
SiO	Silicon oxide
Ta	Tantalum
Ta-MnO_2	Tantalum-manganese dioxide (composite)
Ta_2O_5	Tantalum pentoxide
Ti	Titanium
TiMo	Titanium-molybdenum (alloy)
TiO_2	Titanium dioxide
W	Tungsten
WC-Co	Tungsten carbide-cobalt (hardmetal, alloy)
WC-Co-Cr	Tungsten carbide-cobalt-chromium (hardmetal, alloy)
WO_3	Tungsten trioxide
Y_2O_3	Yttrium oxide
Zn	Zinc
Zn-Al	Zinc-aluminum (composite)
Zn/Al/Al_2O_3	Zinc-aluminum-aluminum oxide (composite)
Zr	Zirconium

Methods and other abbreviations

Ag/AgCl	Silver/silver chloride reference electrode
APS	Atmospheric plasma spraying
ARC	Electrical arc spraying
ASM	American Society for Material
ASTM B117	Standard for salt spray test
ASTM G59	Standard for anodic polarization measurements
BSE	Backscattered electrons
CS	Cold spraying
CGT	Cold Gas Technology
DE	Deposition efficiency
EBSD	Electron backscattering diffraction
EDS	Energy dispersive X-ray spectrometer
EN 582	Standard for tensile pull test
FLAME	Flame spraying
FESEM	Field-emission gun-scanning electron microscopy
HPCS	High-pressure cold spraying
$HV_{0.2}$	Vickers hardness, weight of load 200 g
$HV_{0.3}$	Vickers hardness, weight of load 300 g
HVOF	High-velocity-oxygen-fuel spraying
ITAM SB RAS	Institute of Theoretical and Applied Mechanics of the Siberian Branch of the Russian Academy of Sciences

LALPCS	Laser-assisted low-pressure cold spraying
LPCS	Low-pressure cold spraying
Nd:YAG	Neodymium-doped yttrium-aluminum-garnet laser
OCPS	Obninsk Center for Powder Spraying
PIC	Optimal impact conditions
SCE	Saturated calomel electrode
SE	Secondary electrons
SEM	Scanning electron microscopy
TEM	Transmission electron microscopy
VPS	Vacuum plasma spraying
WS	Window of sprayability

1 INTRODUCTION

Coating technology is growing because of its important role in improving, e.g., corrosion resistance, conductivity, and other properties of material in order to decrease costs and increase service life and safety. Thermal spray processes, including flame, arc, plasma, high-velocity oxygen fuel (HVOF) and cold spraying, are the techniques to produce coatings from powder or wire feedstock by spraying molten, semi-molten or solid particles on the substrate and forming the coating. Acceleration of particles can be done by several ways based on energy used: electrical (arc and plasma spraying), chemical (flame and HVOF spraying), or kinetic (cold spraying) energy [1]. Cold spraying is a relatively new spraying method, which has many advantages over other forms of thermal spraying. The advantages are high deposition efficiency, low residual stresses, minimal heat input to substrate, phase and compositional stability, and little need for masking [2]. Furthermore, cold spraying is a cost-effective and environmentally-friendly alternative to e.g., soldering, electroplating, and painting [3].

Cold spraying was developed in the former Soviet Union in the 1980´s at the Institute of Theoretical and Applied Mechanics of the Siberian Branch of the Russian Academy of Sciences, ITAM SB RAS, (Novosibirsk, Russia) [2,4]. The latest thermal spray technique is based on the use of significantly lower process temperatures with high particle velocities than those present in other thermal spray techniques [2,5,6]. Figure 1 shows a diagram of gas temperatures and particle velocities in different thermal spray processes. During the past decades, the trend has turned from the use of thermal energy to the use of increasing amounts of kinetic energy. This opens new advantages, e.g., pure and dense coating formation due to the low or zero-level oxidation during the cold spray process. In addition, heat input is significantly low, not changing the substrate properties, and avoiding oxidation during spraying [3,7]. The other advantages are that phase transformations caused by melting and porosity formation caused by solidification in the other methods can be eliminated by the use of cold spray process [8]. Temperature of the gas is well below the melting point of the sprayed material and thus, particles are not melted in the gas flow [9]. Furthermore, residual stresses are compressive (peening effect of impinging solid particles [3]), offering chances to spray dissimilar materials [3,4].

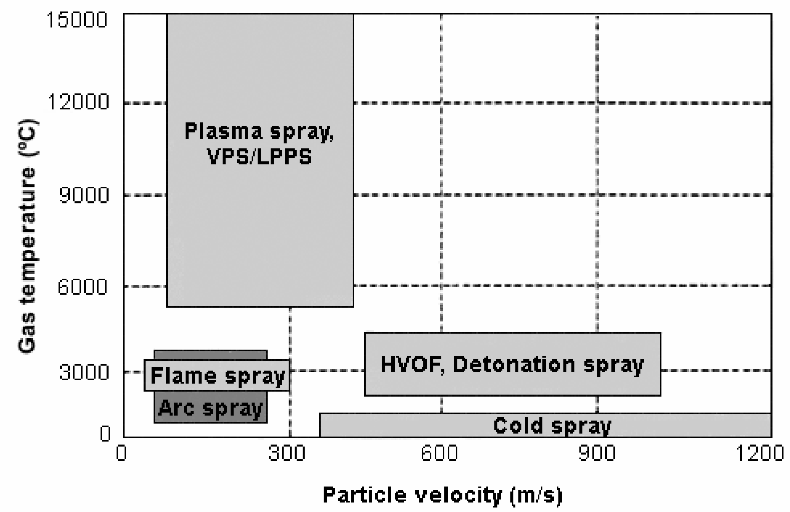

Figure 1. Gas temperatures versus particle velocities in the thermal spray processes. VPS is a vacuum plasma spray and LPPS is a low-pressure plasma spray process [1].

Due to the fact that cold spraying is a solid-state method, oxide inclusions, and void formation can be avoided [9]. Typical defects of this kind in other thermally-sprayed coatings are presented in Fig. 2. The schematic presentation is shown in Fig. 2a and typical cross-sectional structure in Fig. 2b.

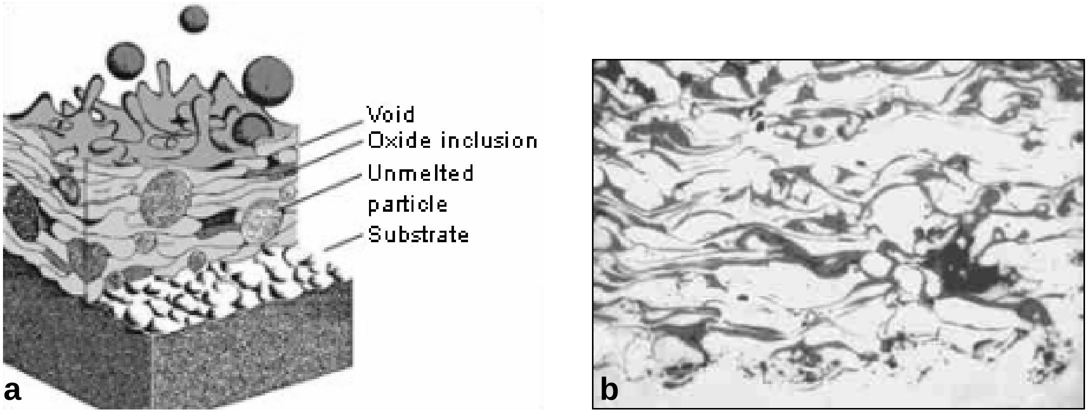

Figure 2. Thermally-sprayed coatings: a) typical defects in the coating structure and b) typical lamellar microstructure with oxide inclusions and pores [10].

Typically, almost all materials can be sprayed using the thermal spray methods. The flame and electric arc spray methods are often used to prepare coatings for less demanding applications. Porosity levels and oxygen contents are higher than in the other processes. Plasma spraying is usually used for manufacturing ceramic coatings [1] and HVOF is used as a method to produce metallic and cermet (hardmetal) coatings [8,11]. Material selection is larger in other thermal spray processes than in cold spraying, including metals, metal alloys, ceramics, cermets, composites, and plastics [1]. In turn, cold spraying is a method to produce metallic and composite coatings and there are limitations of coating materials; ceramic and non-ductile materials cannot be sprayed alone, they will need a ductile component in the composite coating. Thus, this is one requirement for the sprayed material in the cold spraying; the capability to be deformed plastically, i.e., the ductility of the powder is needed. [1,2,4] However, embedded ceramic particles as surface treatments produced by using cold spraying are reported [12-15]. Nevertheless, a relatively wide range of coating materials, e.g., pure metals Al, Cu, Zn, Ni, Ti, Ta, Ag, Ni, Fe, metal alloys, Ni-Cr, Ni-Cu, Ni-Al, Cu-Al, Cu-Sn, Cu-Zn, MCrAlY, CoNiCrAlY [16], stainless steel, and composites, Al-Al_2O_3, Al-Zn-Ti, Cu-W-Zn, Al+SiC, Cu+Al_2O_3, Ni+TiC can be used in cold spray process [1,4,17]. In addition, substrates can be metals, metal alloys, polymers, ceramics, and composites [4].

Comparison between deposition rates and deposition efficiencies of thermal spray methods is presented in Fig. 3 whereas porosity levels and oxygen contents in different thermally-sprayed coatings are shown in Table 1. In cold spraying, the deposition rate is equal or lower than in the other methods. However, the deposition efficiency can be significantly higher in the cold spray process than in the others. It is reported to be as high as 97 % (Cu coating) [18]. In addition, porosity and oxygen contents are lower in cold-sprayed coatings. Generally speaking, porosity and oxygen content decrease with increasing particle velocity (compare Fig. 1 and Table 1).

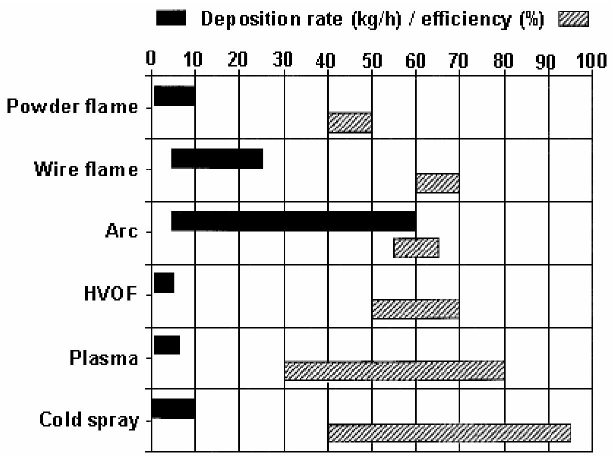

Figure 3. Deposition rates and efficiencies: comparison between different thermal spray methods. After Champagne [1].

Table 1. Porosity and oxygen contents of coatings in different thermal spray methods [1,11,19,20].

Method	Porosity (%)	Oxygen content (%)
COLD SPRAY	0.1 [19]	same as in the powder [1]
HVOF	1 [11]	0.2 [20]
FLAME	10-20 [11]	4-6 [20]
ARC	10-20 [11]	0.5-3 [20]
PLASMA	1-7 [11]	0.5-1 [20]

Normalized costs in different thermal spray processes according to Champagne [1] are summarized in Fig. 4. Capital costs are shown in Fig. 4a. In flame spray and arc spray processes, capital costs are relatively low. On the other hand, in HVOF process, capital costs are higher and they are the highest in the low-pressure or vacuum plasma process. In cold spray process (high-pressure cold spray system), the main capital costs are come from powder feeder and gas heater [1]. Although capital costs in cold spraying are higher than those of in the other methods (expect low-pressure/vacuum plasma spraying), running costs are at the same level as in the powder flame spraying and in addition, lower than in HVOF and plasma spraying. Typically, methods using wires have lower running costs due to cheaper feedstock materials (wire versus powder). Generally speaking, powders incur the main costs. Moreover, gas costs are the highest in the cold spray process and will be even higher if He is used as a process gas. The normalized running costs are illustrated in Fig. 4b.

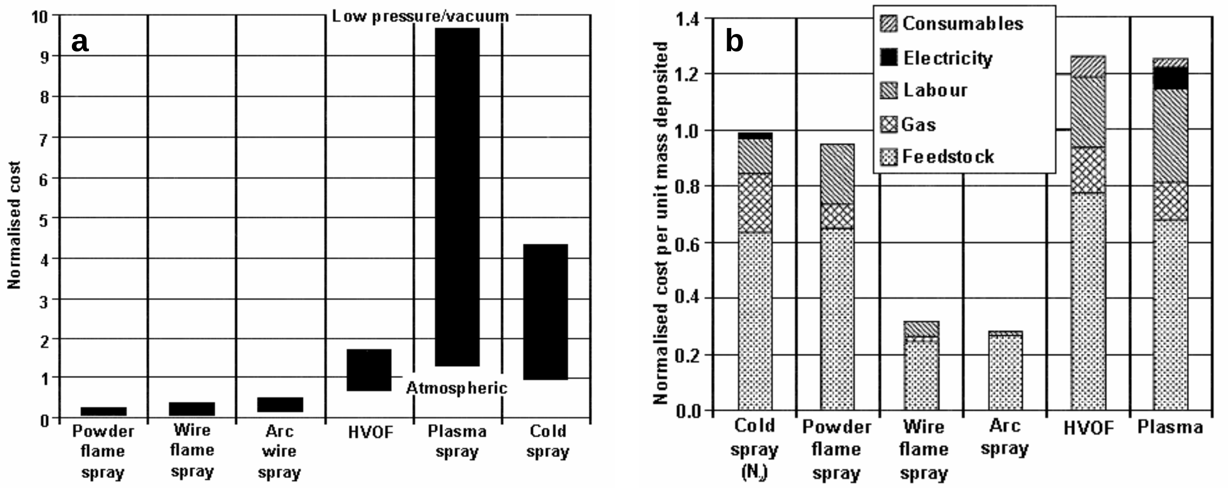

Figure 4. Comparison of normalized costs in different thermal spray processes: a) relative capital costs of copper spraying based on proprietary feedstock and gas cost information and b) comparison of running costs based on the average values of deposition rates and efficiencies for copper. After Champagne [1].

Cold spray process was firstly patented (1994) by Alkhimov et al. [21,22]. In addition, various cold spray related innovations are patented by several authors. Patents include cold spray devices, nozzle design, coating materials, applications etc. Cold spraying, high-pressure cold spraying, low-pressure cold spraying, cold gas dynamic spraying, kinetic metallization, dynamic metallization, and kinetic spraying are all based on the same basic idea of the process.

2 COLD SPRAYING

In a cold spray process, powder particles impact on the surface with high kinetic energy (high velocity), deform, adhere to the substrate or other particles, and thus, depositing the coating [2,4,9,23,24]. A gas (N_2, He or air) is accelerated to supersonic velocity by a converging-diverging de Laval type nozzle. Powder particles are fed into the gas flow and they are accelerated and sprayed on the substrate. [9] This occurs by drag effect [6]. Formation of a cold-sprayed coating depends on the velocity of powder particles. Each material has a specific critical velocity v_{cr}. Above v_{cr} the particles adhere to the substrate, causing plastic deformation and formation of the coating whereas at velocities lower than v_{cr} only erosion and particle rebounding occur without coating building up [1,9,23-26].

In cold spraying, several parameters such as a particle size, particle temperature, substrate material and the properties of the coating material have a remarkable influence on the coating formation and the deposition efficiency [4,5,9]. In addition, good bonding between the cold-sprayed powder particles requires heavy plastic deformation during the particle impacts [1,5,6,23]. For successful bonding, deposition conditions, where oxide layers on the particle surfaces are removed during impact, should be created [5]. The powder particles impinge on the substrate in solid form, well below the powder melting temperature [23]. Furthermore, compressed layer takes form near to the impact surface and leads to the formation of shock waves (bow shock) near to the sprayed surface [27]. The shock layer decreases particle velocity and increases particle temperature [2,28,29]. Particles should go through the shock layer and hence, high kinetic energy is needed. At the same time, thermal softening and adiabatic shear instability play a very important role in the bonding between particles and substrate in the cold spray process [24,30,31].

Additionally, coating quality relies on spraying conditions. Reportedly, the preheating temperature of the process gas has an influence on the particle velocity and the coating quality [1,2,9]. Preheating of the gas increases viscosity of the gas which in turn, increases gas velocity and thus, also particle velocity [32]. Furthermore, higher velocity leads to stronger deformation and therefore, coating structure becomes denser and mechanical properties are improved [33,34]. Higher process temperature together with higher pressure promotes denser coating structure precisely due to the thermal softening and local shear instability [31]. Moreover, in the particle interfaces, the temperature is increased due to the adiabatic localization (and thermal softening) [30]. As a materials processing method, cold spraying is kept very similar to an explosive welding [35,36].

Cold spraying is an effective method of depositing dense coatings with very low porosity and pure coatings with low oxygen content [37]. This is regarded as an advantage to several important material properties, such as electrical conductivity and corrosion resistance [9]. Because the sprayed material undergoes neither phase transformations nor melting during the spray process (solid state process), cold spraying enables, in principle, the production of highly dense metallic coatings [1,9,37]. Oxygen contents are reported to be at the same level in the coating compared with the level in the as-received powder [1,7,23].

The basic idea of particle collision in the cold spray process is presented in Fig. 5. Two particles impact on the substrate overlapping with each other. The impacting particles highly deform, forming ring-type material jets around the particle impact zone. The latter particle also enhances the deformation of the first particle due to the overlapping. In the final state, particles are highly deformed with flattened shapes, having material jets formed in the particle interfaces. [31,38]

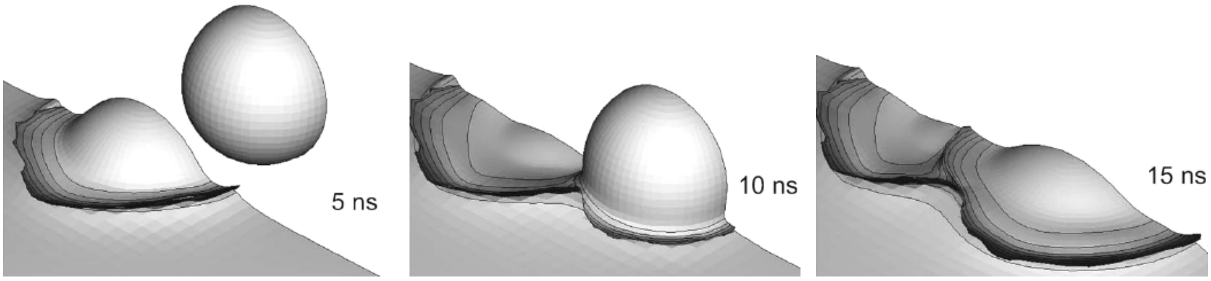

Figure 5. Simulated situation of particle impacts after impact times of 5, 10, and 15 ns from the first particle [31,38].

High gas velocities generate high particle velocities [1,2,6]. For that purpose, the gas is preheated in order to increase the velocity of the particles but also to increase the temperature [1,2,9]. High velocities also result in a high impact deformation at the interfaces of both substrate and coating and between particles [9,39,40]. Furthermore, the gas and particle temperatures significantly affect the quality of the cold-sprayed coatings by improving it with higher temperatures. High temperature leads to high velocity and, thus, to strong impacts. [7,32,41,42] Moreover, because deposition efficiency (DE) depends on the temperature of the gas, DE is reportedly improved at high gas temperatures [39,40,43-45]. Furthermore, substrate pretreatments are reported to have an effect on DE. It can be slightly increased with increasing roughness of grit-blasted substrate. On the other hand, for instance increased traverse speed (100 mm/s versus 20 mm/s) decreases DE of Cu and Ti coatings [44].

2.1 High-pressure cold spraying

Cold spraying is divided into two different processes by the pressure level used; high-pressure cold spray (HPCS) and low-pressure cold spray (LPCS) processes. The HPCS process enables the use of pressure as high as 40 bar and preheating temperature of max. 800ºC (Kinetiks 4000). Typically, pure metal and metal alloys are used as powder materials in the HPCS process. Furthermore, the selection of powder materials is larger with the HPCS process compared to the LPCS process. Typically, metals and metal alloys, e.g., Cu, Al, Ta, Ni, Cu-Sn, NiCr, and Ni-Al are used as a powder material. Figure 6 shows schematic presentation of the HPCS process. Basically, in the HPCS process, high pressurized gas (N_2, He or mixture of these gases) is heated and it flows to the nozzle where powder is fed with carrier gas. Then, the gas-powder flow is fed through the nozzle in which high velocity is generated. After that, particle-gas flow exits the nozzle with high speed and impacts on the sprayed surface. The HPCS process is controlled with a control unit.

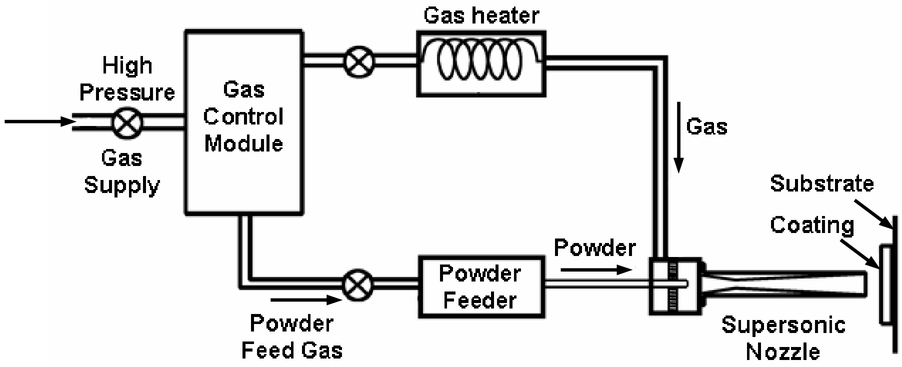

Figure 6. Schematic presentation of cold spray process [46].

In cold spraying, converging-diverging nozzle is used to produce supersonic gas flow in which particles achieve supersonic velocity. Supersonic velocity is created in the nozzle throat, in the diverging part of the nozzle. Powder is fed with carrier gas in axial direction and then, mixed with the main gas forming a particle-gas flow before the nozzle. De Laval type converge/diverge nozzle is the most commonly used. Schematic presentation of one cold spray gun with de Laval nozzle is shown in Fig. 7. The colors indicate temperatures in different regions of the gun, from warmer (red) input to colder (blue) output.

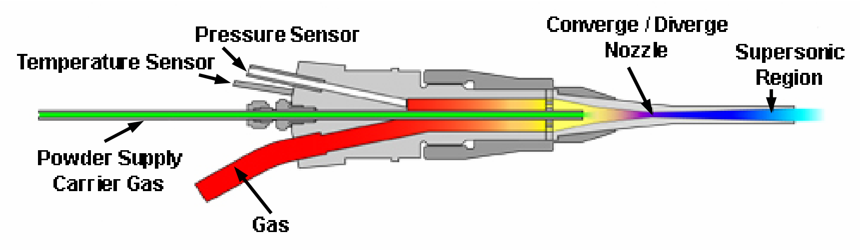

Figure 7. Schematic presentation of cold spray gun. Colors indicate temperatures, in the red areas, temperature is the highest and in the blue areas, temperature is the lowest [47].

2.2 Low-pressure cold spraying

In the LPCS process, preheating temperatures of the process gas are between room temperature (RT) and 650ºC, and pressures between 5 and 9 bar. Usually, compressed air is used as process gas to spray powder mixtures [48]. Typically, LPCS process is a method to spray metallic powders (e.g., Cu, Al, Ni, Zn) with an addition of ceramic powder (Al_2O_3, SiC) as powder mixtures. The main functions of the ceramic powder addition are to activate the sprayed surface and to keep the nozzle of the gun clean. In addition to these, ceramic particles affect the coating by mechanical hammering of the substrate/sprayed layers or by the so-called shot peening via particle impacts [49,50]. The ceramic particle addition in the powder mixtures has also a compacting effect during the impacts, indicating improved coating properties and deposition efficiency of metallic coatings [51-53]. The hard phase can also be used for reinforcing and strengthening the metallic matrix in the LPCS process [54].

The main difference between the spray guns used in the HPCS and LPCS processes is that in the LPCS process, powder is fed to the gas flow perpendicularly (radial injection) to the diverging part of the nozzle as presented in Fig. 8. In addition to that, Papyrin et al. [55] have presented the possibility to inject two powders, e.g., Cu+Al, and Cu+SiC, separately to the nozzle (two powder feeders at the same time) and form composite coatings. Additionally, another difference between the LPCS and HPCS processes is that heating of gas is done only in the spraying gun in the LPCS process whereas in the HPCS process, gas is preheated in the separate heating unit and in addition to that, in the spraying gun. Although powder feed rates are lower in the LPCS process, particle concentration in gas flow can be higher than in the HPCS process [6].

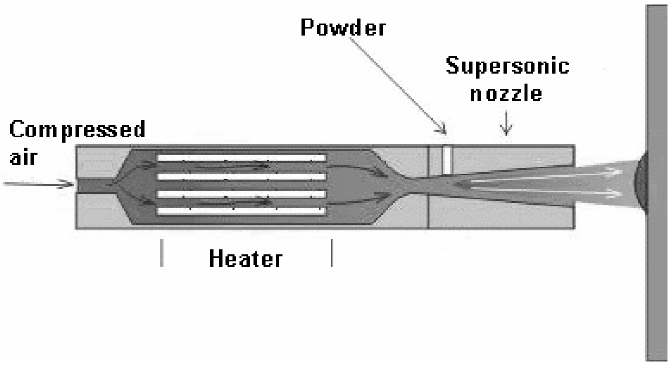

Figure 8. Schematic presentation of spraying gun in LPCS process. Powder is fed radially to diverging part of the converging-diverging type nozzle [49,56].

As a summary, typical spraying parameters used in these two cold spray processes are presented in Table 2. The main differences relate to process gas, pressure level and electrical power used. In addition to these, the HPCS system is a more efficient process with higher gas flow and powder feed rates.

Table 2. Typical spraying parameters used in cold spray processes.

Spraying parameter	HPCS	LPCS
Process gas	N2, He, mixture	Compressed air
Pressure (bar)	7-40	6-10
Preheating temperature (°C)	20-550-800	20-650
Gas flow rate (m^3/min)	0.85-2.5 (N_2), max. 4.2 (He)	0.3-0.4
Powder feed rate (kg/h)	4.5-13.5	0.3-3
Spraying distance (mm)	10-50	5-15
Electrical power (kW)	17-47	3.3
Particle size (µm)	5-50	5-30

These two cold spray processes, the HPCS and LPCS processes, have their own advantages and as methods, they support each other. Generally, cold spray processes offer several advantages, e.g., high deposition efficiency, high deposition rate, high denseness, minimal thermal input to the substrate, compressive residual stresses, no oxidation, and no phase changes. On the other hand, some limitations in the number of cold sprayable materials (i.e., mainly ductile metals and alloys are prosessable by cold spraying), low ductility of the coatings in their as-sprayed state and that cold spraying, as also other thermal spray processes, is a line-of-sight process, can be regarded as disadvantages of the cold spray processes [1]. The main advantages of the stationary HPCS process are a significantly larger material selection and higher quality of the coatings whereas the investment costs of the LPCS equipment are lower than those of the HPCS process. In addition, on-site spraying is possible by using the portable LPCS equipment. Furthermore, both cold spray processes have specific powder characteristics of their own together with optimal spraying parameters to produce high quality coatings. Coating properties are presented in the following Chapters.

3 COLD-SPRAYED COATINGS

Basics of coating formation by cold spraying and more about specific details in cold spraying as the method to produce metallic coatings are presented here. In addition, coating properties, corrosion resistance of the coatings in general, and potential applications are identified.

3.1 Coating formation

As it is generally known, powder particles need certain critical velocity (v_{crit}) for successful coating formation in cold spraying. If particle velocity is below the material-dependent critical velocity, then particles rebound and do not form the coating [24]. However, activation (cleaning) of the sprayed surface occurs [6,23,57]. If the particle velocity is above the critical velocity, then particles adhere to the surface and build-up the coating [24]. Particles are stuck to the surface by plastic deformation or they just penetrate (or are embedded) into the sprayed surface [57].

Formation of the cold-sprayed coating is presented in Fig. 9. First particles cause the build-up the coating (adhered particles) and substrate cratering (rebounded particles) [23,58]. Formation of the cold-sprayed coating is based on two steps: build-up of the first layer (particle-substrate interactions) and deposit of the coating (particle-particle interactions). In the first step, adhesion strength between coating and substrate is defined whereas step 2 defines the cohesive strength of the coating [58]. At the first stage, particle-substrate interactions occur and are affected by substrate and coating materials as well as surface preparation. After that, new incoming particles adhere to the previous particles, deform and realign; now the coating is built-up. At the second stage, particles interact with each other and form the coating structure. [57] During the spraying, metallic bonding and void reduction occur and after that, coating structure is densified and work-hardened [23].

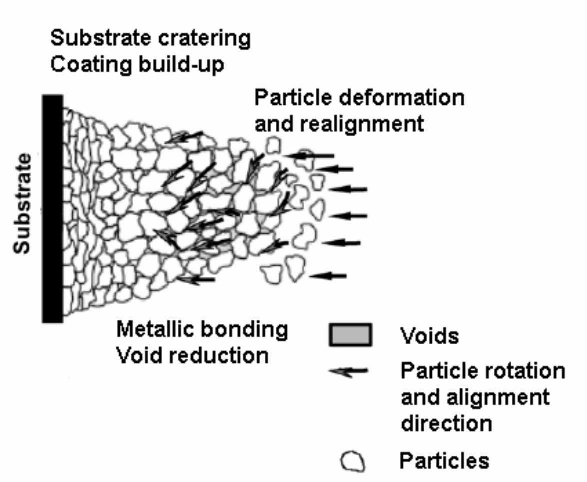

Figure 9. Schematic presentation of coating formation in cold spray process. Firstly, substrate cratering occurs together with first coating layer build-up. Secondly, at the same time, particles deform and realign together with resulting void reduction and metallic bonding between particles [23].

Typically, in the LPCS process, powder mixtures and powder blends are used as feedstock materials. Figure 10a presents the formation of the structure from powder mixture and the arrangement of particles of different-type powder materials during impacts. In addition, Fig. 10b shows schematic presentation of the mixture coating with particle alignments in the flow and in the structure [6,49]. Acceleration of particles in the high-velocity air flow is caused by drag forces [6]. According to Maev et al. [6] particles deform highly and inter-particle sliding occurs during particle interactions.

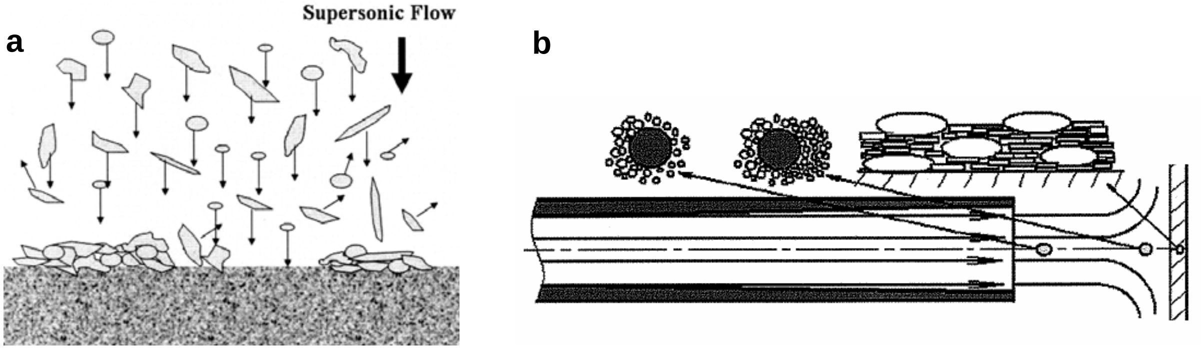

Figure 10. Schematic presentation of mixture coating formation in cold spray process: a) particle impacts [49] and b) particle alignment in the flow and in the coating structure [6].

The coating is formed by several particle collisions and thus, structure formation depends on the neighboring particles [23]. During powder particle impacts, high contact pressure forms on the particle-substrate interface. Pressure level generation during impact time is presented in Fig. 11. Obviously, the highest pressure point is formed at the connecting point of the particle and substrate impact [59].

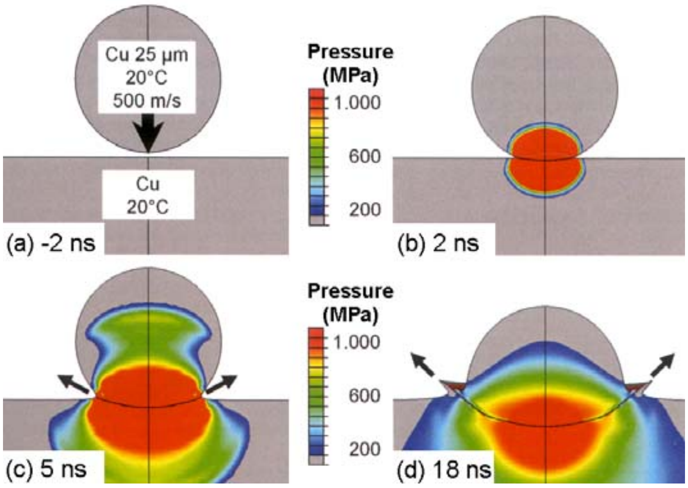

Figure 11. Impact of cold-sprayed Cu particle (25 µm) on Cu substrate a) before impact, b) after 2 ns, c) after 5 ns, and d) after 18 ns. Colors indicate pressure distribution during impact. Simulated condition, after Schmidt [59].

As previously known, the powder particle deforms plastically in the particle impact. A high strain level is achieved and is mostly concentrated on the particle-substrate or particle-particle interfaces on the impact surface. The strain distributions after 0.01 µs and 0.05 µs are presented in Figs. 12a and 12b, respectively. Jetting is caused by high straining [59] and thus, the highest strains are detected in the jetting regions [26]. In addition to the high pressure level and high strain, the temperature is increased on the impact surface during the particle impacts [9,59] and concentrated primarily on the jetting area. During impact time, the temperature rapidly decreases [59]. This is presented in Figs. 12c and 12d. In the adhesion and sticking of the particles, kinetic energy transforms into heat and strain energy [7,23]. The temperature and strain are inhomogeneously distributed, indicating localized deformation. Furthermore, the particle deformation is strong at the localized contact interfaces [25].

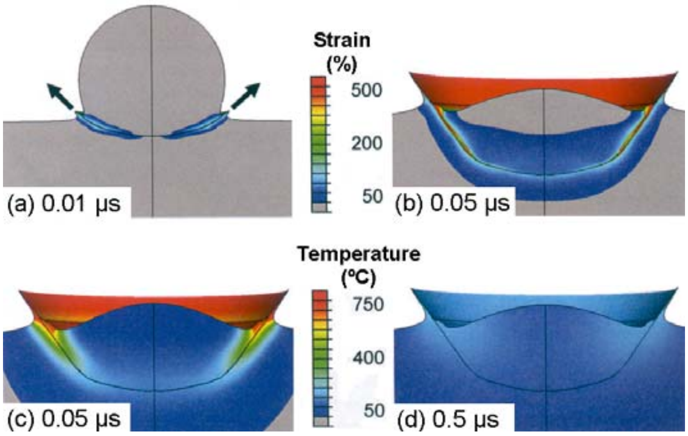

Figure 12. Impact of cold-sprayed Cu particle on Cu substrate. Strain distribution a) after 0.01 µs, formation of material jets started and b) formation state after 0.05 µs. Temperature distribution c) after 0.05 µs and d) after 0.5 µs. Colors indicate either strain or temperature distributions after impact. Simulated condition, after Schmidt et al. [40] and Schmidt [59].

3.1.1 Velocities

Numerous studies concern modeling and simulation of the cold spray processes, particle velocities, and related phenomena are analyzed elsewhere, e.g., in [6,24,31,60]. In this particular study, critical velocities are not modeled, calculated or measured. Instead of that, this study focused on characterization of the already formed coating structures. However, because of the importance of the particle velocity in order to form the coating, particle velocities and critical velocity are described here.

3.1.1.1 Critical velocity

As mentioned before, in the cold spray process, critical velocity of powder particles is required for the formation and build-up of the coating. Reportedly, critical velocity depends on the sprayed material. Furthermore, critical velocity is influenced by powder quality, particle size (not included in the equations), and particle impact temperature [24,31]. In addition, critical velocity depends on kinetic energy, material strength and heat generation [40]. Schmidt et al. [24] after Assadi et al. [31] have described simple expression for the critical velocity using the following equation (Eq. 1).

$$v_{crit} = 667 - 0.014\rho + 0.08(T_m - T_R) + 10^{-7}\sigma_u - 0.4(T_i - T_R) \qquad \text{(Eq. 1)}$$

ρ	Density	T_m	Melting point
σ_u	Yield strength	T_i	Impact temperature
		T_R	Reference temperature (293 K)

This equation is useful for materials similar to copper [24]. Densities of the particles affect the velocity; heavier particles have a lower critical velocity [31]. In addition to that, particle size can affect the velocity [24,61]. The effect of particle size on the particle impact velocity and critical impact velocity is presented in Fig. 13. Furthermore, particle velocity is said to be a function of its size [24] and thus, powder has a range of particle velocities [62].

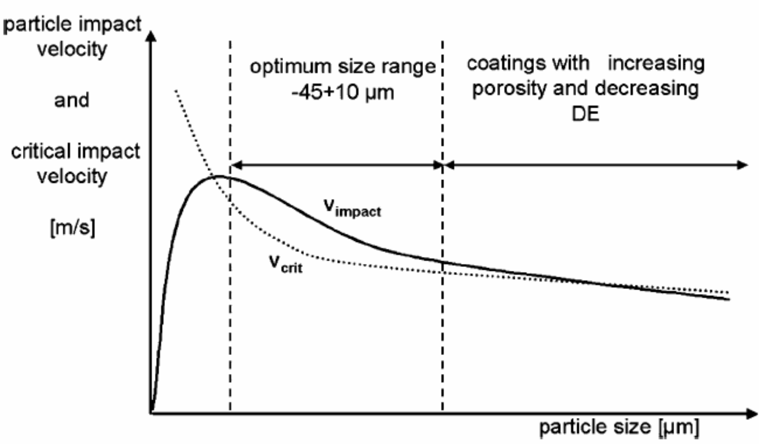

Figure 13. Schematic presentation of particle impact velocity and critical impact velocity as a function of particle size. After Schmidt et al. [24].

On the other hand, if the particle size distribution of the powder is wide, critical velocity is defined for the largest particles [24] due to the fact that smaller particles have higher velocity [24,60]. Critical velocities are mostly modeled values and in the evaluations, 90 % of plastic strain energy is assumed to be dissipated into heat [24]. One explanation for the heat transfer is the wave propagation [31]. In addition, Schmidt et al. [24] have presented an advanced equation for the critical velocity, $v_{crit}^{th,mech}$ which also takes specific heat, tensile strength, and mechanical and thermal calibration factors into account, Eq. 2. Calculated critical velocities for 25 µm particles for several metal materials calculated with Eq. 2, are shown in Fig. 14.

$$v_{crit}^{th,mech} = \sqrt{\frac{F_1 * 4 * \sigma_{TS} * \left(1 - \frac{T_i - T_R}{T_m - T_R}\right)}{\rho} + F_2 * c_p * (T_m - T_i)} \qquad \text{(Eq. 2)}$$

ρ	Density	T_m	Melting point
σ_{TS}	Tensile strength	T_i	Impact temperature
c_p	Specific heat	T_R	Reference temperature (293 K)
F_1	Mechanical calibration factor (for cold spray 1.2)		
F_2	Thermal calibration factor (for cold spray 0.3)		

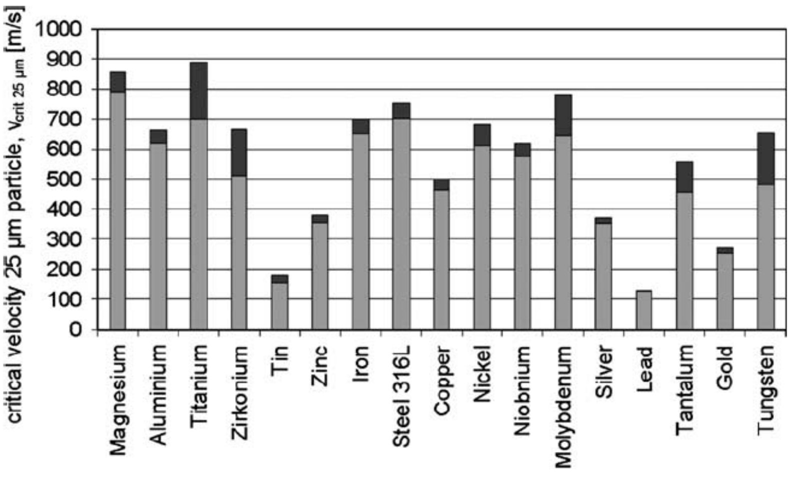

Figure 14. Critical impact velocities for several powder materials (Ø 25 µm) [24].

Particle size affects velocity by increasing it with decreasing particle size. Additionally, small particles have higher critical velocities due to the higher impurity content. Kang et al. [63] have reported that higher oxygen content of powder in as-received state increases critical velocity of the powder. On the other hand, critical velocity can be decreased by increasing temperature. Particles having a higher temperature are in the softer state and thus, less kinetic energy is needed for the plastic deformation. [24]

3.1.1.2 Particle velocity

Gas dynamics have an influence on the particle velocity and temperature on impact. The most important characteristics of gas flow are high-pressure shock wave layer formed near to the substrate, structure, and stability of the supersonic jet [6,27,64]. Bow shocks are observed with Schlieren imaging and are achieved in the supersonic velocity [28]. Velocity decreases in the shock wave (bow shock) layer, increasing gas mass density and therefore, increases drag forces on the particles [27]. In addition, bow shock decreases the gas velocity to subsonic velocity [65]. High pressure (as was already detected in Fig. 11), together with high density gas flow, generates formation of the shock wave layer near to the sprayed substrate, Fig. 15 [28,65,66]. This layer reduces the particle velocity and thus, particles should have enough velocity to go through the bow shock layer. In addition, shock wave increases gas pressure and temperature while gas velocity decreases [29]. The shock wave layer has more proper effect on the particle velocity of small particles [29,65,66]. Furthermore, bow shock is more evident with short spraying distances and could disappear with larger distances [28]. Moreover, a drag coefficient is lower with the spherical particles compared with the irregular particles [67,68]. Therefore, the irregular particles with high drag forces exhibit higher velocities [28].

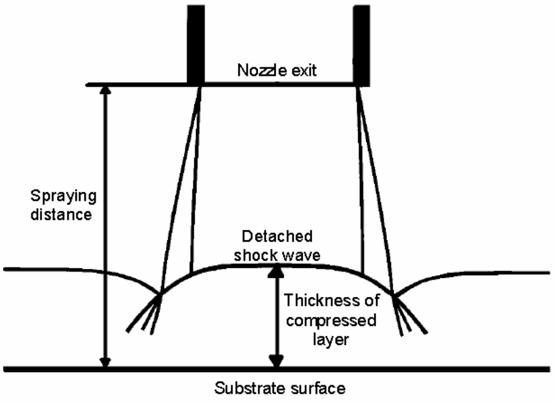

Figure 15. Schematic presentation of supersonic jet [66].

Particle impact velocity is also one of the crucial factors in the coating formation [69]. In cold spraying, solid particles impact on the sprayed surface with high velocities, 400-1200 m/s [24,40,70]. In the LPCS process, particle velocities are reported to be approximately from 350 to 700 m/s [71]. Obviously, particle size affects the particle velocity [70,72]. Large particles have lower velocity and also because of that, the degree of strain is slightly decreasing with increasing particle size [70]. Higher particle velocity, reportedly, improves coating quality [24,66]. In addition, the coating properties are improved by using higher preheating temperatures [39], resulting in higher particle temperature and hence, stronger deformability and adhesion [73]. Velocity increases in the throat of the nozzle and supersonic velocity is achieved in the divergent part of the nozzle. In the pressurized gas flow, powder particles reach the supersonic velocity as presented in Fig. 16. Due to the bow shock, particle velocity decreases in this area and thus, particles should have enough velocity and kinetic energy to go through the bow shock layer and to impact on the surface.

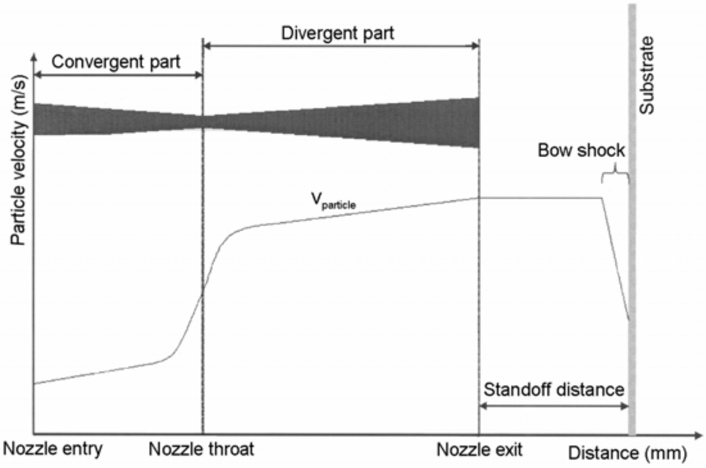

Figure 16. Schematic presentation of particle velocity behavior from nozzle entry to substrate surface. After Kairet [72].

Obviously, gas velocity also increases at the nozzle throat and in the diverging part of the nozzle. On the impact, the gas achieves higher velocities but lower temperatures than the particles [9]. The particle temperature increases near to the sprayed surface due to the bow shock formed near to the surface. The particle temperature from nozzle entry to the particle impact on the substrate is presented in Fig. 17. Temperatures of gas and particles are detected to have strong effect on the bonding between particles and particle-substrate [57]. On the other hand, the particle impact temperature can be increased by preheating the particles [40].

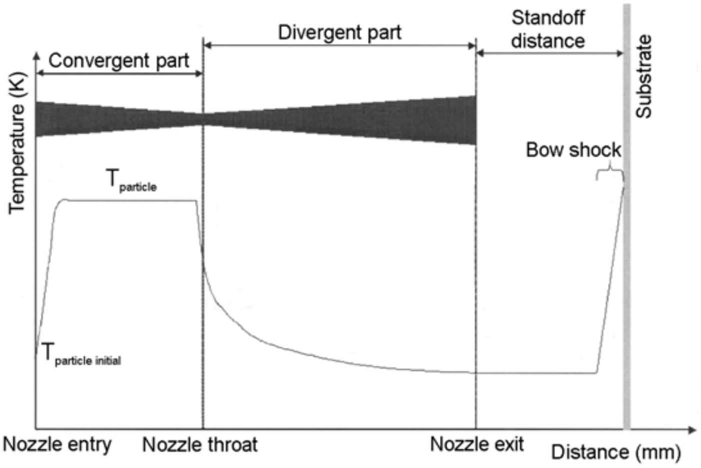

Figure 17. Schematic presentation of particle temperature behavior from nozzle entry to substrate surface. After Kairet [72].

As stated, the critical velocity is needed for the coating formation. However, if the velocity is too high, erosion occurs and coating is not formed [23]. Schmidt et al. [24] have presented a window of sprayability for the cold spraying, Fig. 18. Particle impact velocity should be higher than critical velocity v_{crit} and on the other hand, lower than erosion velocity $v_{erosion}$. In addition, v_{crit} and $v_{erosion}$ decrease with increasing particle impact temperature [24].

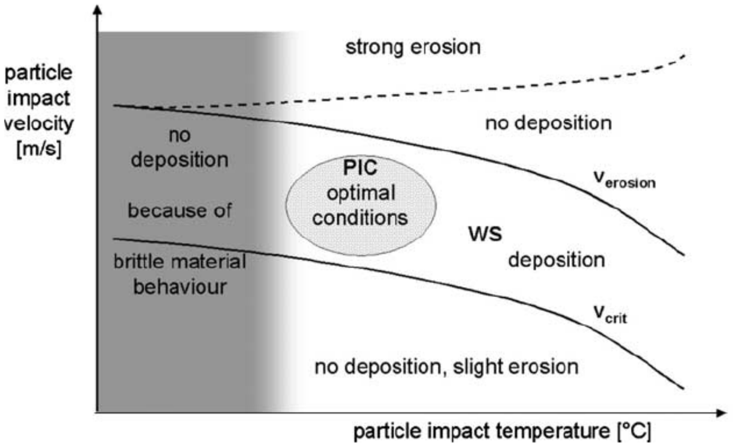

Figure 18. Window of sprayability (WS) and optimal impact conditions (PIC) for cold spraying as a function of particle impact velocity and particle impact temperature [24].

Particle velocity depends on particle size and density, gas pressure, gas temperature, gas molecular weight, and nozzle shape [4]. As stated, higher gas velocity generates higher particle velocity and for that purpose, gas is preheated in order to increase gas velocity and therefore, particle velocity [1,2,6]. In addition, lower molecular weight of the gas increases the velocity. [1,23] Typically, nitrogen, helium or air is used as a process gas. Molecular weights of N_2 and He are 28 and 4, respectively [74]. Lower weight increases the velocity. Ratio of specific heat for monatomic gas (He) is 1.66 and for diatomic gas (N_2, in addition, air is usually modeled as a diatomic gas (mixture of N_2 and O_2)), it is 1.4. Higher ratio of specific heat leads to higher velocity [4]. In addition, sonic velocity of air (80%N_2+20%O_2) is 343 m/s, of nitrogen 349 m/s and of helium 989 m/s, explaining the higher velocities produced by using helium as a process gas [1,75]. However, He is significantly more expensive gas which limits its use. The costs can be reduced by using a recycling system of He [1]. Moreover, the particle velocity increases with increasing temperature of the gas [65,76] and decreasing molecular weight of the gas [4]. Increasing pressure of the gas also increases particle velocity [76]; however, the effect of pressure is less significant than the effect of temperature [65]. Due to the lower molecular weight of He (4 versus 28), gas velocity of He is found to be twice as high as the velocity of N_2 exiting the nozzle, reflecting more acceleration effect of He on the particle velocity in the gas flow. In addition, larger particles have lower velocity than smaller ones [75].

3.1.2 Particle deformation

Due to the fact that coating formation depends on plastic deformation via particle impacts, particle deformation is an important factor in the coating deposition [5,6,9,23]. Particle deformation arising from plastic deformation, adiabatic shear instability, material jet formation, and adhesion of particle interfaces are discussed below.

3.1.2.1 Plastic deformation

Plastic deformation is a permanent phenomenon and is caused by e.g., dislocation motion. Dislocation movements are also called slipping and therefore, dislocation lines as slip planes. In addition, plastic deformation can cause twinning in the structures. [77] Schematic presentations of deformation by slip and by twinning are clarified in Fig. 19 [78]. There again, high strain-rate deformation generates slipping and formation of the twins [5,78]. Plastic deformation is originated from dislocation movements caused by critical shear stress. In principle, plastic deformation occurs in each grain in the individual powder particle which means that particle boundaries can restrict the deformation of some grains. This indicates different levels of plastic deformations in the inter-particle structure and hence, through the coating structure. [79]

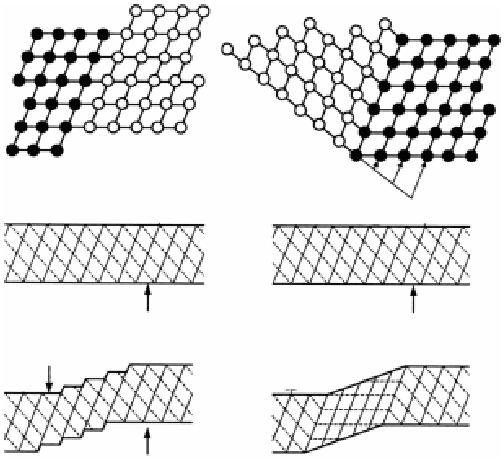

a) slip **b) twinning**

Figure 19. Schematic presentation of deformation a) by slip and b) by twinning [78].

In addition, coating structures' hardening mechanisms, work hardening and strain hardening, take place under high deformation [79]. Furthermore, hardness and strength of materials indicate their capability to resist this permanent deformation [77]. As it is known, in cold spraying, coating formation is based on plastic deformation. Plastic deformation is mostly concentrated on regions close to particle boundaries and therefore, material jets (of coating and substrate material) are formed in order to increase coating quality and adhesion [30]. On the other hand, generally, material properties depend on its microstructure which in turn, depends on grain structure and treatments. Typically, plastic deformation is detected from an etched microstructure of cold-sprayed coatings by a flattening degree of the particles. [79] Highly deformed particles have highly flattened shapes after impacts [80]. In turn, flattening degree depends, in addition to the deformation level, on the coating and substrate material combination. Flattening of the sprayed particle is higher on the impact on steel substrate compared with Cu substrate due to the higher hardness of steel substrate [31].

Particles deform more on impacts against hard substrates whereas on impacts against softer substrate, deformation of substrate material is stronger [81]. These effects are illustrated in Fig. 20 by the impacts of Al particles on Cu substrate (Fig. 20a) and Cu particles on Al substrate (Fig. 20b). During impact (increasing contact time), particle height-to-weight ratio obviously decreases together with increasing depth of cratering of substrate. However, it should be noticed that flattening of the particle is not so high in the case of Cu on Al than Al on Cu. It was assumed that differences are caused by larger kinetic energy of heavier Cu particles together with their higher strength. In addition, material jets are wider in the case of Cu impacts on Al compared with Al impacts on Cu. Interfacial instability is more pronounced on the impacts of Cu on Al, indicating also higher deposition efficiency (DE) for this situation. [82]

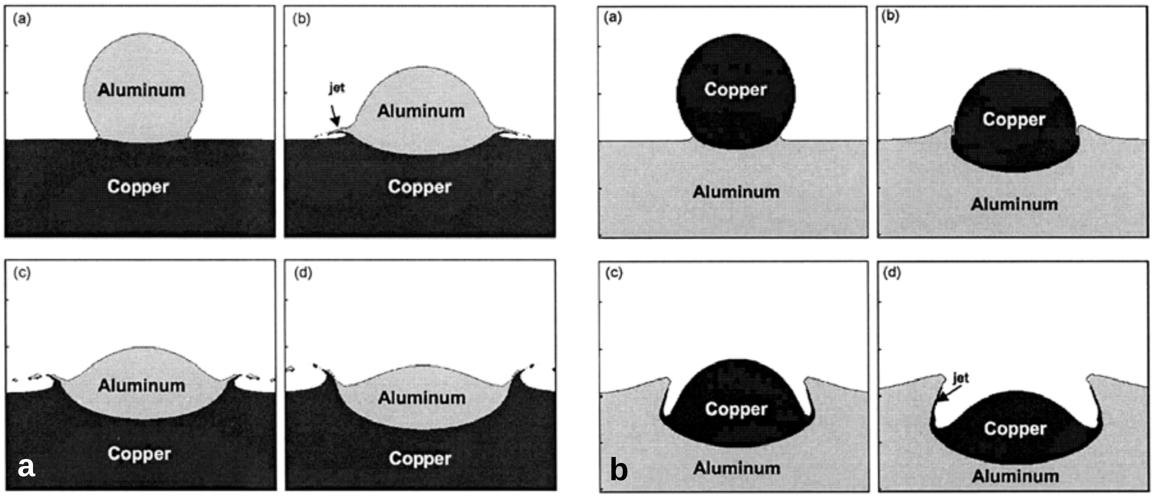

Figure 20. Particle impacts on the substrate at the velocity of 650 m/s: a) Al particle to the Cu substrate and b) Cu particle to the Al substrate as a function of impact time (a) 5 ns, (b) 20 ns, (c) 35 ns, and (d) 50 ns [82].

Plastic deformation under high strain rate conditions creates several microscopic features in the microstructure such as high amount of dislocations, dislocation wall formations, formation of elongated sub-grains, break-ups of sub-grains and recrystallization. At a solid state, under high strain rate, localized heating (material is still under melting point) generates adiabatic shearing instabilities at the interfaces, and then, formation of localized shear bands starts [26,67]. Borchers et al. [26] have illustrated microstructural defects such as vacancies and interstitials formed during or immediately after cold spray process. These defects are formed due to the temperature rises near melting point on the impacts and on the other hand, due to the strong deformation with very high strain rates. This, in turn, is caused by dislocations and their movements under high plastic deformation [26]. The structure with fine-sized grains without voids or oxide inclusions caused by dynamic recrystallization leads to a tight metal-metal bonding between particles [5,83]. Recrystallization due to high temperature during the collisions in the interfacial regions was observed [82].

3.1.2.2 Adiabatic shear instability and material jets

Adiabatic shear instability due to the thermal softening leads to successful bonding in cold spraying [38]. Powder particles impact on the sprayed surface with high velocity under high pressure. On the impact, strain load is generated by pressure gradient caused on both interfaces during the collision (Fig. 21a). The pressure distribution during particle impact is also detected in Fig. 11. Shear load causes localized shear straining whereas plastic deformation, strain hardening, and thermal softening generate shear localization [67] and formation of shear bands [6]. Under the high impact conditions, this shear straining causes adiabatic shear instability due to the thermal softening and the influence is strongest at the interface by leading the jetting and thus, formation of material jets (Fig. 21b) [5,24,31]. Localized heating on the impact zone in the deformation region due to the high strain rate causes the formation of adiabatic shear bands [26,67]. On the other hand, strain is more compressive in the middle of the particle-substrate interface marked with gray arrow in Fig. 21b [26]. Additionally, locally deformed grains inside the powder particle can concentrate into shear bands. On the other hand, shear bands are produced by local dislocation reorganization which can generate elongated dislocation-free regions [67].

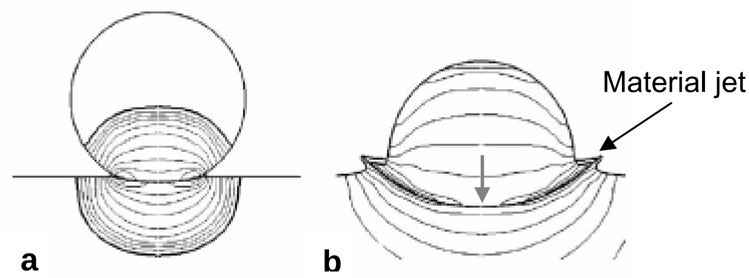

Figure 21. Particle impact: a) pressure distribution generation during particle impacts on the substrate and b) material jet formation [24].

Particle size is reported affecting the adiabatic shear instability behavior, attaining to the interface temperature, strain rate, and stress. Small particles have higher temperature gradients and thus, shear instability can be hindered by the high cooling rates. Additionally, smaller particles are more strain-rate hardened due to the high strain-rate. [24] Moreover, the effect of shock waves should be detected [28,66]. Localized heating near to the coating-substrate interface is clearly detected and it is the starting point for material jet formation. Moreover, higher particle velocities assist in the formation of higher material jets. [31]

High strain-rate deformation causes various microstructural details in the structure. Figure 22 shows these features of dynamic recrystallization. Randomly arranged dislocations (Fig. 22a) rearrange themselves to the dislocation cells (Fig. 22b) due to dynamic recovery. Then, severe deformation generates the formation of elongated subgrains (Fig. 22c). Furthermore, subgrains break-up (Fig. 22d) and finally, recrystallization of microstructure (Fig. 22e) takes place inside the structure [67].

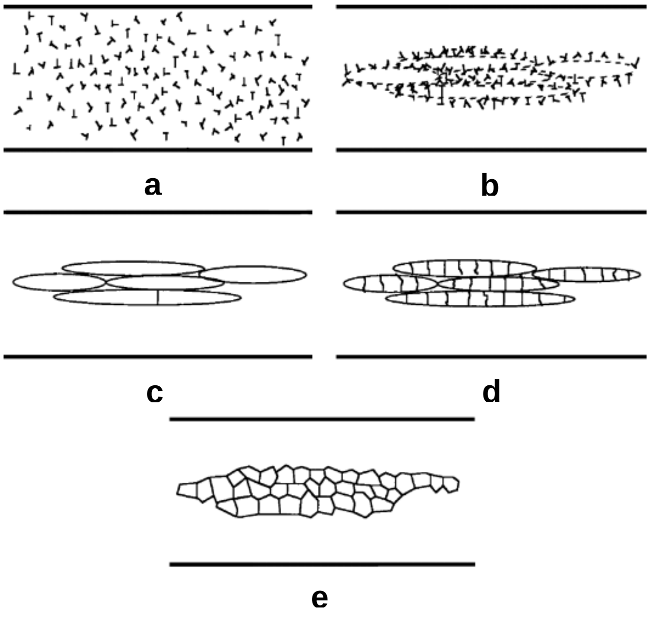

Figure 22. Microstructural details caused by high strain-rate deformation: a) randomly distributed dislocations, b) elongated dislocation cells, c) elongated subgrains, d) break-up of initial elongated subgrains, and e) recrystallized microstructure. After Meyers [67].

Generally speaking, several processes are able to occur during shearing. Meyers [67] has reported different mechanisms: *dynamic recovery, dynamic recrystallization, phase transformation, strain-induced precipitate dissolution, melting and resolidification, amorphization and crystallization*. Different processes can take place at the same time or separately. Structure inside the shear bands contains fine-sized and possibly recrystallized grains. [67] Borchers et al. [5] have shown recrystallized grain structure of the cold-sprayed Cu coating. In the cold spray process, dynamic recovery and recrystallization can play crucial roles in the shear localization caused by thermal softening in the case of metal materials. In turn, as for ceramic materials, localized shearing can occur due to particle breaking-up or comminuting [67]. Grain refinement of the cold-sprayed particles together with non-uniform and randomly orientated fine-sized grains in the inter-particle structures is detected by TEM analysis [84,85]. Fine inter-particle grain size resulted from high plastic deformation whereas coarser grains appear in less deformed places [84].

Under high adiabatic shear instability, material jets form in the particle interfaces. The formation of these material jets is crucial for good and adherent particle-substrate and particle-particle bonding [5,31]. In addition, these material jets clean the surface, revealing a metal surface and further, a metal-metal bonding. In cold spraying, a phenomenon of material jet formation is comparable to the explosive welding [81]. For a dense coating and tight bonds between the particles, the metal-metal bonding is required. This requires clean contact surfaces under high pressure conditions [17,30,82]. Material jet formation is also one of the requirements for successful and tight bonding on impacts [82]. Fukumoto et al. [86] have described that material jetting can define coating properties. For that purpose, oxide layers of powder particles should be destroyed and removed from the metal surface on the impacts [1,3,53]. This is due to high plastic deformation and materials jets [1,4,17,30,82]. Removal of oxide layer can be illustrated with an egg-cell-model (during impact, particles behave like an egg, hard cell (oxide) breaks down and soft inside (metal) deforms). After oxide layer is broken down, gas flow removes oxides away. [1] In addition, fracturing of these oxide layers requires high impact velocity of the particles [23]. On the other hand, ceramic particles mixed with metallic powder can remove the oxide layers from the surfaces of metallic particles by activation, occurring on the collision of hard particles on the metallic region of the surfaces [87].

3.1.2.3 Bonding

Particle-substrate and particle-particle bonding are compared with the explosive powder compaction where powder is loaded by strong shock waves with a high shock pressure. In the explosive powder compaction method, particles are welded and they form dense structure. Common for both methods is the highly localized interfacial deformation caused by material jets and also a highly elongated grain structure. [36] Reportedly, in the coating formation, the role of adhesive forces is not significant. After formation, however, these forces could have a role in the adhesion of the coating and the substrate. [23]

Adhesion caused by van der Waals and electrostatic forces is typically formed as sticking [57]. The adhesion depends on the size of interfacial area between particle and substrate [82]. In addition, one mechanism for the bonding is mechanical interlocking. It is usually present in the interfacial bonding [57]. Mechanical interlocking could be one bonding mechanism at the particle-substrate interface indicated by material jets and substrate deformation [86]. Interfacial instability is the driving force for the interlocking between coating and substrate [82]. Also, it should be noticed that repeated impacts have an influence on coating formation in cold spraying. This is also related to the activation by rebounded particles and, on the other hand, to the densifying effect of particles incoming next. In addition, sticking can become stronger during particle impacts and therefore, adhesion between particles is tighter [57]. On the contrary, adhesion by interlocking increases with increasing velocity and density of the sprayed particles. At the same time, increasing surface tension can degrade the adhesion [8]. In addition, oxide layers should be removed during impacts (by plastic deformation); revealing metal-metal contacts, pronounce metallic bonding between particles and substrate [86].

In cold spraying, bonding between particles and substrate and between particles can be said to be a combination of different bonding mechanisms. Localized metallurgical bonding was obtained and associated with impact fusion [88]. In addition, Hussain et al. [89] have reported that bonding is the combination of metallurgical bonding and interlocking. Furthermore, the bonding could be a combination of the metal-metal bonding, mechanical blocking, van der Waals adhesion, and diffusion. Diffusion was observed as a bonding mechanism between cold-sprayed Cu splats and Al substrate as the formation of intermetallic, nanocrystallized, thin layer at the interface [90]. In addition, Kairet [72] has found slight diffusion occurrence at Cu-Al interface. Furthermore, Guetta et al. [90] have suggested that local transient melting could occur in the high-pressure and high-temperature impacts of Cu particles on Al surface. However, according to Grujicic et al. [82] atomic diffusion at the particle-substrate interface is not a dominant bonding mechanism. Accordingly, bonding is strongly influenced by the powder material, powder-substrate material combination together with the spraying parameters and heat treatments. For instance, bonding is influenced by substrate softening during impacts on the soft substrate materials, e.g., Cu impacts on Al substrate, making the strong adhesion between coating and substrate [72].

Melting of Cu particles was not found in the cold-sprayed or kinetically-sprayed Cu coatings when comparing feedstock structure with coating structure [5,23]. The coatings have anisotropic nature, having a flattened shape in the cross-sectional direction [23]. On the other hand, some localized melting in the particle interfaces was found with materials with low melting point, such as Zn and Al-12Si when using relatively high gas temperatures. Additionally, low thermal conductivity of powder material assists in local melting occurrence [88].

3.2 Coating properties

Coating properties depend on various factors. One important factor is the powder. Firstly, the effect of powder characteristics on coating properties is discussed. Secondly, structural and mechanical properties are discussed and finally, corrosion properties and potential applications are presented.

3.2.1 Effect of powders

The powder has a very crucial role in the coating formation and coating properties in the cold spray process. Firstly, powder material should be deformable and ductile. Thus, only metallic powder materials can be used in cold spray process. Furthermore, powder mixtures can be sprayed when at least one component of the powder mixture is a metallic powder. Therefore, metallic-ceramic powder mixtures can be used [23,91,92]. As a general trend, these powders are mostly used in the LPCS process. In addition, metal-metal powder mixtures are used in order to modify the coating properties. Secondly, powder characteristics, e.g., particle size, particle size distribution, particle morphology, and purity level affect the coating quality. Microstructural details of the powder mainly determine the microstructure of the coating [72]. In the LPCS process, brittleness of ceramic particles in powder mixture is compensated with ductile metallic particles [6]. Reportedly, thin deposits of hardmetals, e.g., WC-Co, are produced by using cold spray process. Furthermore, nano-sized structure of WC-Co was detected in the coating structure as well as in the initial powder structure, indicating no phase transformation occurrence during the cold spray process. [93,94]

Ductility of metallic powder or at least one component in the powder mixtures is required for flattening of the particles by plastic deformation. Thus, suitable powder material for spraying should endure plastic flow without fracturing in order to produce dense coatings by cold spraying [24]. Furthermore, it should be noticed that in composite mixture coatings, deposition efficiencies can vary in different components of the powder due to the possible differences on the critical velocities. Therefore, composition of coating and powder can differ strongly, depending on the initial powder composition [39]. Particle size has reportedly effect on coating formation. Small particles (5 µm) undergo shear instability. However, if impact temperature increases, shear instability does not necessarily occur. This is due to the high heat transfer over the particle volume and thus, high cooling rates which can hinder the occurrence of shear instability [24]. According to Schmidt et al. [24] if cooling and heating rates are close to each other, shear instability can be hindered or prevented.

Particle velocity depends on particle size. Powder contains certain particle size distribution and hence, it can be said that velocity of powder is composed of different velocities, depending on particle size distribution. Optimal particle size distribution should be determined particularly for each powder material and composition [24]. Production method of powder particles affects the oxygen content of particles. Gas-atomized particles are dense and have low oxygen content whereas particles produced by direct reduction contain impurities in their structures. It is evident that coatings sprayed with higher oxygen content particles will have higher amount of oxygen in the coating structure as well. Trapped oxides have been found in the coating structures sprayed with higher oxygen content powder. [95] At the same time, flattening of Al particles was decreased with increased oxygen content of initial powder particles [63]. As known, particle velocity has strong effect on the coating formation. Higher velocities lead to higher coating quality. Therefore, powder characteristics affect the velocity and coating properties. Irregular particles have higher in-flight velocities compared with spherical particles. [69] However, it should be noted that irregular particles could contain higher amount of impurities in the as-received state due to the production method (water atomization or electrolytic production versus gas atomization).

For successful bonding, deposition conditions should be such that oxide layers on the particle surfaces are fractured during impact, revealing pure metallic contact [5,6]. In the optimal state, due to the highly strained interfaces, oxide cells are broken and clean metal surfaces are revealed for the tight bonding [24]. However, smaller particles typically contain more impurities arisen from higher surface area. This can lead to the higher critical velocities for smaller particles due to the fact that smaller particles have higher oxide content. Van Steenkiste et al. [23] have suggested that larger particles have more energy to fracture the oxide layers. In addition, more kinetic energy is required with increased thickness of oxide layers to remove oxides and for plastic deformation [63]. Moreover, inter-particle sliding can take place on the particle impacts during spraying [6].

Hard particles

Ceramic particles mixed with metallic powder affect the coating formation. Hard particles densify the metallic structure by assisting higher plastic deformation. Al_2O_3 particles mixed with e.g., Al powder have reportedly increased adhesion between coating and substrate, creating micro-asperities and increasing contact area [50]. Moreover, the addition of ceramic particles has been reported to improve the denseness of the LPCS Al coatings [96]. Coating properties depend on composite powder compositions [50]. On the other hand, metallic powder mixture can also increase plastic deformation. Maev et al. [97] have found out that Ni particles deform more intensively when they contain W particles in the initial powder mixture. One explanation can be higher kinetic energy of W particles due to their high density, when W particles impact on the Ni particles [97]. Ceramic particles embed in the soft metallic matrix or they can be fractured to small pieces in the structure during particle impacts [14,92]. Lee et al. [14] have reported no signs of cratering of soft Si substrate during impacts of hard ceramic WO_3 particles, in turn, ceramic particles embedded in the substrate and no erosion occurred.

The main function of the Al_2O_3 particle addition is to keep the nozzle of the gun clean. Furthermore, Al_2O_3 particles activate (clean and roughen) the sprayed surfaces, i.e., through activation the surface becomes cleaner and more adaptive to the sprayed particles, which then stick better to the surface. In addition to these, Al_2O_3 particles affect mechanically the coating by hammering the substrate/sprayed layers or by peening effect via particle impacts. [49] During particle impacts, collision of the ceramic particles also increases the deformation of the metallic particles (compacting effect) which in turn, affects the coating properties and deposition efficiency particularly in the LPCS process [51]. Papyrin et al. [55] have reported that hard particles (e.g., Al_2O_3) can affect the temperature (and thus, velocity) of soft metallic particles (e.g., Cu and Al) in the metallic-ceramic powder mixtures. Hard particles decrease the so-called critical temperature of metallic particles and therefore, also decrease critical velocity needed due to the activation of ceramic particles. This can explain the lower particle velocities in the LPCS process compared with the HPCS process [50,55].

3.2.2 Coating structure

Cold-sprayed coatings have a strongly deformed coating structure due to the high plastic deformation. Cold-sprayed coatings are reportedly dense without evidence of pores by microscopic analysis [9]. However, porosity level in the coatings depends strongly on sprayed materials as well as spraying parameters [18]. Rezaeian et al. [18] have shown porosity levels for cold-sprayed Ti, Ni, and Cu coatings: 9-21 %, 1-4 %, and 0-8 %, respectively. Due to the high plastic deformation, particle structure is flattened and become pancake-like with flattening ratio of 3:1 or 5:1 [23]. Etching reveals the flattening of the powder particles which is extensively high due to the high plastic deformation [88]. Borchers et al. [5,26] have presented dense particle interfaces between cold-sprayed Cu particles and furthermore, high dislocation density areas, elongated grains, twins, and recrystallized grain structures, indicating unequal and nonuniform microstructure. Moreover, Zou et al. [98] have studied microstructures of cold-sprayed Ni coatings with EBSD and found clearly inhomogeneous structure with equiaxed and elongated grains. Ultra-fine grains were observed in the particle-particle interfaces [98]. Moreover, Kairet et al. [76] have found that cold-sprayed Cu coatings sprayed using fine particles have higher dislocation density than larger ones. Furthermore, heat treatments have an influence on the coating structures, e.g., porosity of the HPCS Cu coating (air used as process gas, dendritic particles as feedstock) was slightly decreased [73]. Figure 23 shows typical microstructures of the cold-sprayed coatings, cross-section of cold-sprayed Cu coating without any defects is in Fig. 23a [99], faultless interface between the Ni coating and grit-blasted steel substrate in Fig. 23b, etched structure of the Cu coating with flattened particle shapes in Fig. 23c, and elongated grain structure with localized deformation of the Ni-20Cr coating in Fig. 23d [100]. Elongation of highly deformed grains inside the flattened particles was also observed [83].

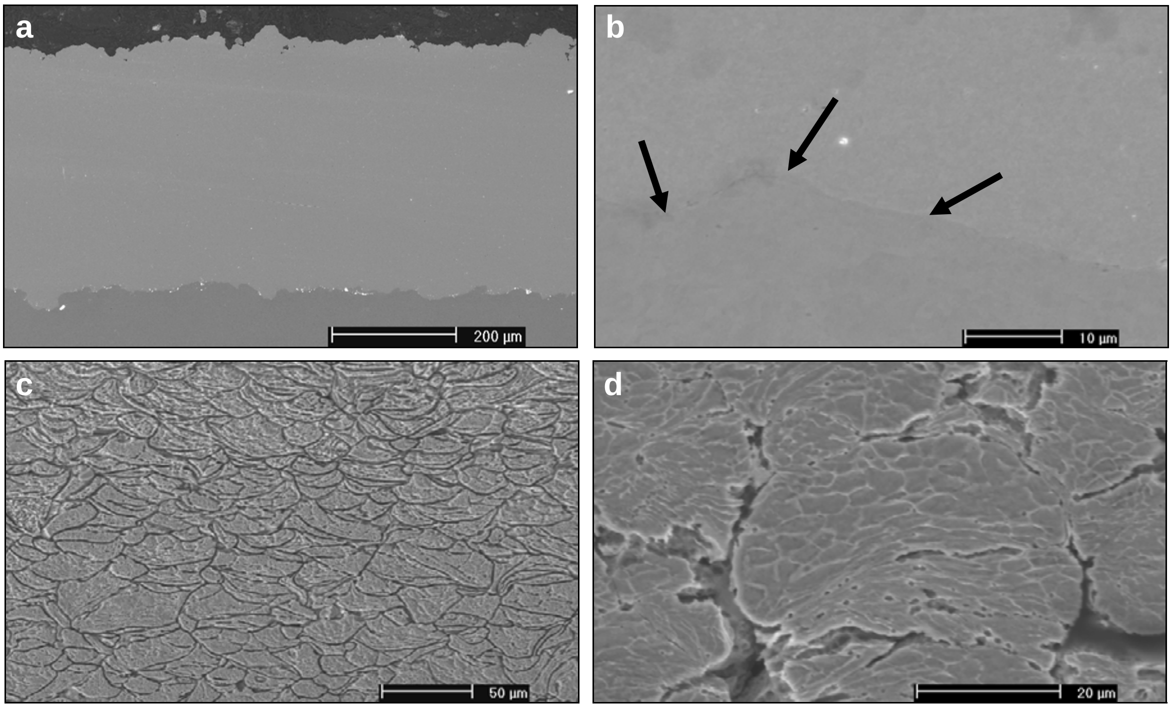

Figure 23. Cross-sectional structures of cold-sprayed coatings: a) Cu on grit-blasted steel substrate [99], b) interface (arrows) between Ni and grit-blasted steel substrate, c) etched Cu coating, and d) etched Ni-20Cr coating [100]. SEM images.

One advantage of cold spraying is to avoid the occurrence of oxidation and phase transformation caused by melting during spraying. This eliminates formation of undesirable phases and is material-dependent. However, interfacial boundaries of intermetallic phases (e.g., NiAl, $NiAl_3$, Ni_3Al) formed in the spraying of Al on Ni have been found [101]. In addition, Guetta et al. [90] have illustrated nanocrystallized phases, Al_2Cu and Al_4Cu_9 phases, in the interface between cold-sprayed Cu splats and Al substrate by using TEM.

Heat treatments affect microstructural details of the cold-sprayed coatings by several mechanisms depending on heat treatment temperatures. Recovery, recrystallization and grain growth [80] occur in different temperature regions [102]. Figure 24 shows changes in the microstructure as a function of temperature. Refinement of grain structures after heat treatment due to the recrystallization was found in several studies. In addition, fracture behavior mostly changes after heat treatments from the brittle (as-sprayed state) to ductile (heat-treated state). [103]

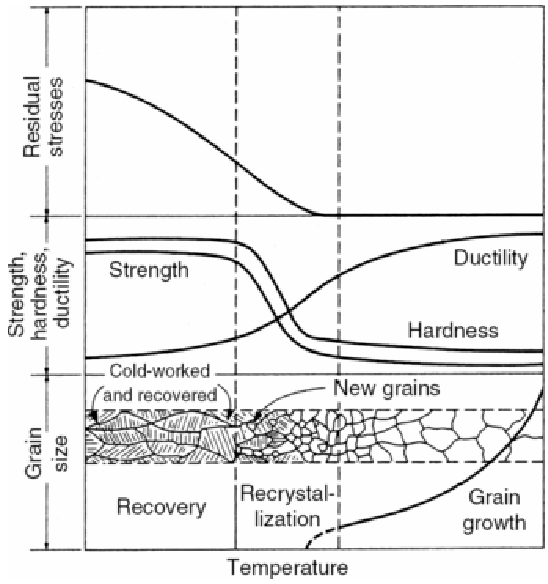

Figure 24. Cold-worked structure and properties. Effects of annealing temperature on recovery, recrystallization, and grain growth [102].

Shkodkin et al. [51] have reported increased bond strength and coating density with increasing ceramic particle addition. Amount of ceramic particles in the sprayed coating is low in comparison with the initial powder composition. Usually, coatings contain ceramic particles below 5 % from total amount of ceramic powder [51]. This indicates occurrence of erosion and activation by rebounded ceramic particles [51,104].

In addition, one way to improve the quality of LPCS $Cu+Al_2O_3$ coatings is to produce coatings with laser assistance. Laser-assisted low-pressure cold-sprayed (LALPCS) coatings have shown improved denseness. Nd:YAG and diode lasers were tested and they were installed to Dymet spraying gun [100,105]. Continuous laser irradiation with the LPCS spray spot preheated the substrate. Firstly, coating thicknesses were increased with increasing laser energy (temperatures measured using pyrometer). Secondly, the denseness improvement was detected with open-cell potential measurements and salt spray tests. The LALPCS $Cu+Al_2O_3$ coatings did not have through-porosity in their structures and results were similar with both lasers (diode and Nd:YAG). [105]

3.2.3 Mechanical properties

Cold-sprayed coatings have reportedly low residual stresses due to low heat input, rather high adhesion, and hardness normally higher than that of the corresponding bulk materials [2]. Mechanical properties of cold-sprayed coatings are shown here.

Hardness

Hardness is the property of a material to resist permanent indentation. During strain or work hardening, material becomes harder and stronger due to plastic deformation [77]. This explains the high hardness and thus, highly work-hardened structure of the cold-sprayed coatings. Higher velocity obtained with higher preheating temperature leads to higher hardness due to the higher level of plastic deformation and cold working. Additionally, hardness of the coating is somewhat higher that corresponding bulk material. [2,23] This is caused by high dislocation densities in the coating structure due to the high deformation occurrence on the high-velocity impacts [9]. Calla et al. [106] have reported that an increased particle velocity due to an increased driving pressure resulted in more cold working in the coating, leading to high hardness. Hardness values of the cold-sprayed Cu coatings are reportedly significantly higher than those of corresponding bulk material (160 versus 90 $HV_{0.2}$). This is explained by the high work hardening effect and in addition to that, compressive residual stresses assist to increase the hardness of the coatings. [107]

According to Calla et al. [35] the reason for the high hardness of the cold-sprayed coatings is the very fine grain size and the significant micro-straining in the as-sprayed deposits. Cold-sprayed coatings have relatively high hardness due to the work hardening; however, annealing decreases the hardness [9,26,107]. Decrement of the hardness values was observed e.g., in the Al, Cu, Ni, and Ni-20Cr coatings [108]. Annealing at elevated temperatures affects the properties of cold-sprayed coatings. At temperatures of 300ºC and above for Cu, the dislocations in the grains rearrange, and recrystallization and further grain growth occur, usually reflecting decrement in the hardness [35]. The effect of annealing of cold-worked material is presented in Fig. 24. Cold-sprayed coatings could be expected to behave similarly.

Bond strength

Cold-sprayed coatings possess high adherence to base materials [23]. Reportedly, the bond strengths of HPCS Cu coatings on Al substrates are in the range of 35-40 MPa [9] or 20-60 MPa [76,89] and on steel and Cu substrates in the range of 30-40 MPa [5,31]. Additionally, in the other studies bond strengths were between 10 and 20 MPa [107,109]. Furthermore, the bond strengths of the LPCS coatings are reported to be in the range of 10-30 MPa [17]. Adhesion of soft metal coating is usually stronger on soft substrate than on hard substrate [109]. Higher values are measured in the coatings sprayed with higher gas velocities and particle velocities [31]. Adhesion of single splats also increases with higher impact velocity [90].

Meanwhile, high tensile strengths (cohesive strengths) of HPCS coatings between 85 and 150 MPa for Cu, are demonstrated [24]. Differences between adhesive strengths and cohesive strengths reflect the anisotropy of the coatings. Additionally, adhesion decreases with the increase of coating thickness. Furthermore, Schmidt et al. [110] have illustrated improvements of tensile strengths of the HPCS Cu coatings from 50 MPa to as high as 250 MPa with nozzle and spraying equipment developments. This is caused by the presence of internal stresses [26]. Annealing is reported to have influence on the ultimate strength of the HPCS Cu coatings by decreasing it significantly with increasing annealing temperature. In addition, stress-strain curves have revealed ductility increment with annealing, similar behavior is observed with cold-worked materials shown in Fig. 24. In addition, the same effect was demonstrated by using He instead of N_2. The adhesion between Cu and steel was increased also when He was used as a process gas, 57 MPa in the as-sprayed state [83]. Furthermore, more ductile fracture behavior was seen in SEM analysis. Using He as a process gas, particles were more work-hardened because of higher particle velocities [80]. It is also known that coating formation and coating properties depend on the combination of the powder material and substrate material. The influence is detected mostly on adhesion of the coatings. The adhesion is reportedly higher on soft substrate (e.g., aluminium) compared with hard substrate (e.g., steel). The bond strength of the cold-sprayed Cu coating (as-sprayed, N_2) on Al was 40 MPa whereas on steel it was 10 MPa [83]. Moreover, adhesion can be affected by substrate pre-treatments, e.g., by grit-blasting. Additionally, the adhesive strengths are improved with annealing, the bond strength of Cu on Al after 200ºC/1h was 45 MPa and on steel after the same annealing 28 MPa [83]. Hussain et al. [89] have also reported increased adhesion of Cu coating on Al substrate after heat treatment (adhesion strength increased from 57 MPa to > 69 MPa).

Ductility

Cold-sprayed coatings are relatively brittle in the as-sprayed state [1]. However, ductility increases with annealing as a post-treatment [111]. Furthermore, ductility of the coating can increase with increasing preheating temperature of the process gas [23]. Schmidt et al. [110] have shown significant ductile increment in the as-sprayed state by using a developed nozzle and an advanced spraying system. At the previous development states, ductile fracture behavior was less than 15 % and nowadays, with the improved system, it can be as high as 85-90 % [110].

Coating properties, both structural and mechanical, can be modified with heat treatments as post-treatments. Three different processes can occur during annealing: recovery, recrystallization, and grain growth. Firstly, recovery relieves the strain energy and reduces amount of dislocations. Secondly, at higher temperature than in the case of recovery, recrystallization starts, forming new grains and rearranging grains inside the structure. Material becomes softer and more ductile during the recrystallization. After that at even higher temperature, grain growth takes place [77]. The effects of heat treatment on the mechanical and structural properties of cold-worked material are summarized in Fig. 24 [102].

Generally speaking, residual stresses start to release during recovery and are finally released during recrystallization. Furthermore, most significant differences between different properties occur during recrystallization. Hardness and strength decrease whereas ductility increases. Additionally, new grains are generated by recrystallization and further, in the grain growth region, grain size of these new grains is increased. Hardness and strength seemed to be relatively stable in the grain growth region whereas increment of ductility still continues. [102]

3.3 Corrosion resistance

Corrosion is defined as *an extractive metallurgy in reverse*. Corrosion is related to the chemical or electrochemical reaction between material (e.g., metal, coating) and its environment [112]. Therefore, one important technical issue is to manufacture corrosion resistant and protective materials and coatings with specific requirements, e.g., high reliability, quality, and low costs. Furthermore, corrosion resistance is necessary in several industries, in, e.g., chemical and process equipment, and energy production systems. Corrosion protection of metals is based on anodic protection by passivity or cathodic protection by sacrificial anode behavior. Therefore, metallic coatings can also give protection to the substrate in two ways: anodically or cathodically. Corrosion starts if protection fails or breaks down, making metal vulnerable to attacks of corrosion [113].

Corrosion can occur in different forms: e.g., uniform, pitting, crevice, and galvanic corrosion are typical forms of corrosion for coatings. The most common forms of localized corrosion are pitting and crevice corrosion in which corrosive conditions could penetrate relatively rapidly [112]. Pitting corrosion occurs if the passive layer of protecting material is locally damaged, pits form on the surface, and underlying metal is open for the attack [114]. Pitting corrosion causes highly localized damages [115]. For coatings, where structures are not totally adhering and uniform, pitting corrosion takes place quite easily. Porosity in the anodically protective coatings accelerates pitting type corrosion by opening the way for aqueous solution to penetrate inside the coating structure [116]. Crevice corrosion is said to be the one of the most damaging forms of corrosion. Crevice corrosion causes localized corrosion [117]. Galvanic corrosion occurs when two dissimilar metals form an electrical couple in the same electrolyte. In the electrical couple, corrosion starts in the less corrosion resistant material (more active) which becomes the anode whereas the more resistant material (nobler) will be cathode [118]. Metallographic structure and microstructural properties are also said to have an influence on corrosion [112].

In this study, corrosion resistance of cold-sprayed coatings is focused on anodically protective coating materials, i.e., Ta, Cu, Ni, Ni-Cu, and Ni-Cr coatings on steel substrates. Galvanic series of materials in seawater shows anodic-cathodic behavior of materials compared with each other. Galvanic series is presented in Table 3. The nobler the material, the higher it is on the order. Platinum is the noblest material. Cathodic materials protect less noble materials anodically whereas anodic materials give cathodic protection to the nobler material. Moreover, it is known that cathodic protection is based on sacrificial behavior of anodic material, e.g., Zn coating on steel substrate. In this study, nickel, nickel-30copper, and copper give anodic protection against the corrosion of steel substrate. [112] Nickel-chromium and tantalum are also nobler than steel [119].

Table 3. Galvanic series in seawater [112,119].

Cathodic (noble)
↑
Platinum
Gold
Graphite
Titanium
Silver
Zirconium
AISI Type 316, 317 Stainless steel (passive)
AISI Type 304 Stainless steel (passive)
AISI Type 430 Stainless steel (passive)
Nickel (passive)
Copper-Nickel (70-30)
Bronzes
Copper
Brasses
Tantalum [119]
Chromium [119]
Nickel (active)
Naval Brass
Tin
Lead
AISI Type 316, 317 stainless steel (active)
AISI Type 304 stainless steel (active)
Cast Iron
Steel or Iron
Aluminum alloy 2024
Cadmium
Aluminum alloy 1100
Zinc
Magnesium and Magnesium alloys
↓
Anodic (active)

Figure 25 shows the schematic presentation of the corrosion behavior in the cases of anodically protective coating (tin on steel) and cathodically protective coating (zinc on steel). Steel is more active than tin and thus, when a tin layer is broken, steel is attacked. In the other case, steel is nobler than zinc and damaged zinc acts as sacrificial anode and reforms the protective layer again [116]. Therefore, porosity is not critical with cathodically protective coatings whereas in the anodically protective coatings, impermeability of the coating and passive layer on its surface is critical for corrosion resistance.

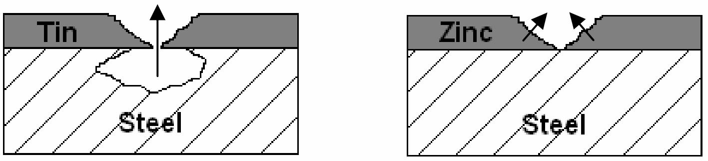

Figure 25. Corrosion behavior of a) anodically protective coating and b) cathodically protective coating in the case of galvanic corrosion at the damaged coatings. Steel is more active than tin and thus, steel corrodes strongly. Damaged zinc coating acts as a sacrificial anode and thus, steel does not corrode whereas zinc does due to the fact that steel is nobler than zinc. [116]

The best way to protect steel samples (active metal) is to deposit the protective coating on the steel surface [113]. For that purpose, cold spraying enables the production of dense coatings for corrosion resistance applications. In addition, denseness of the anodically protective coatings is the first criterion required for corrosion protection [120]. Common for all materials used in this study is that they give anodic protection to the steel substrate. Anodic protection is based on passivation of metals. Therefore, existing of passive film is the requirement for corrosion protection. [121] Passivation is based on a formation of thin, protective oxide layer, acting as a corrosion barrier film [112]. Some metals can form a protective film on their surface which inhibits interactions between metal and corrosive atmosphere due to passivation. Coverage of passive layer is crucial because if it is not or passive layer breaks down, corrosion can damage the structure. Metals' passivity is usually based on the formation of thin oxide layer typically in the air. It is very important to have a continuous and coherent oxide film. Nickel, nickel-chromium and copper are passivating metals. [113] Figure 26 presents anodic polarization curve where active, passive, and transpassive areas are observed. In passivated metals, passivation potential E_p indicates critical potential and above that corrosion rate of metal decreases. The area is called passivation range. Below E_p corrosion occurs at a higher rate. If the passive layer fractures, it opens the way for localized forms of corrosion [112]. Anodic polarization behavior shows material active-passive behavior and therefore, corrosion protection [115]. Furthermore, the passivity and protectiveness of metals can be studied from their active-passive-transpassive behavior in anodic polarization curves [112].

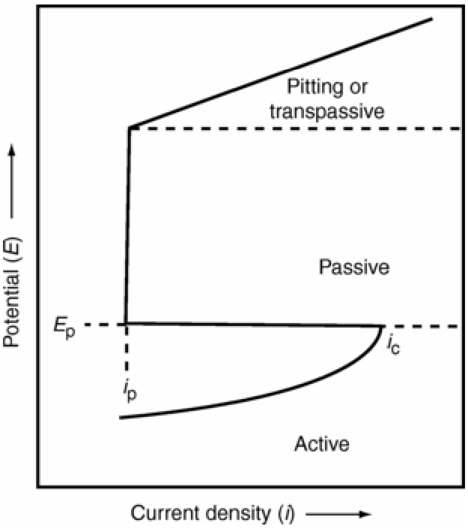

Figure 26. Example of anodic polarization curve. E_p is passivation potential, i_p passivation current density and i_c critical passivation current density [121].

Denseness, or in other words impermeability, is the criterion for good corrosion resistance [9]. Open-cell potential measurements and salt spray (fog) tests as wet corrosion tests are relevant methods to evaluate the denseness of coatings on corrodible substrate (e.g., carbon steel in saltwater conditions). Additionally, salt spray (fog) testing is a commonly used test method to evaluate the quality of various coatings. This particular test enables the use of different corrosive solutions and different test temperatures in a controlled test condition [122]. Corrosion protectiveness and corrosion rates can be estimated with polarization behavior of the coatings. Furthermore, active-passive behavior is clearly detected from anodic polarization measurements [115].

Figure 27 illustrates the potential behavior of coating, substrate and porous coating. If the coating contains interconnected porosity, potential behavior is composed of potentials of both coating and substrate which is seen as mixed potential. This is the basic idea for the open-cell potential measurements used in this study to evaluate existing interconnected porosity, in the other words, through-porosity or open-porosity.

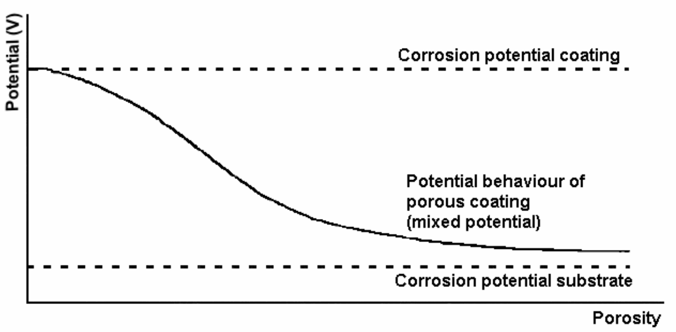

Figure 27. Potential behavior of the coating as a function of porosity [123].

Tantalum has extraordinary corrosion resistance [124] due to the formation of highly stable passivating layer [115]. Tantalum resists corrosion effectively in acids (not HF), salts, and organic chemicals even at elevated temperatures [124]. Furthermore, tantalum as a dense coating acts like corrosion barrier coating on a steel substrate, providing high corrosion resistance in many environments [112]. While, copper is a corrosion resistant material against seawater, waters, dilute sulfuric acid, phosphoric acid, acetic acid and other non-oxidizing acids and in addition, generally atmospheric exposure. Monel 400 (Ni-30Cu) has good corrosion resistance in sulfuric, hydrochloric, phosphoric, and hydrofluoric acids. In Monel alloy, Cu improves corrosion resistance better than pure Ni. [115] Usually, thermally-sprayed nickel-chromium alloy coatings are used for applications where corrosion and oxidation resistance is needed and additionally, for repairs and bond coats [125]. Protective Ta_2O_5 (tantalum pentoxide) layer forms on the surface of tantalum [115,124], protective Cu_2O layer, also called patina, forms on copper [115], and protective NiO layer on nickel surface [112].

Corrosion properties of the cold-sprayed coatings are reported rather briefly in other studies. These studies are more concentrated on the corrosion protection of materials which give cathodic protection based on sacrificial behavior, e.g., Zn and Al [126]. Blose et al. [126] have reported the corrosion protection of steel substrates with cold-sprayed Zn, Al, and Zn-Al coatings against wet corrosion. Furthermore, Karthikeyan et al. [53] have shown that corrosion resistance of the cold-sprayed Al coatings was higher than that of Al bulk material analyzed using polarization measurements. Repassivation was observed at higher potentials [53]. In addition, the cold-sprayed $Al+Al_2O_3$ coatings performed improved anti-corrosion ability compared with Al bulk material in the polarization measurements [127]. Furthermore, LPCS Al coatings act as sacrificial anode and protect the AA2024 substrate, reflecting possibility to be used for corrosion protection in atmospheric and seawater conditions [128].

3.4 Potential applications of cold-sprayed coatings

Corrosion resistance

There is high potential to use cold spray processes in the production of corrosion barrier coatings (low porosity) [2]. However, with some materials, optimization and improvement are still needed. The cold-sprayed Al and Zn coatings [6,129] and LPCS Zn/Al/Al_2O_3 coatings [49] are able to be used for corrosion protection. In addition, Zn, Ni, Ta, stainless steel, and brass coatings with low porosity in their structures are reported to have potential for corrosion resistance applications. In addition, Ta coatings could be optimal as chemical resistant materials in chemical industry and Ni coatings for replacing the electroplating. [130] It is also possible to use cold-sprayed coatings as anti-corrosion coatings on welds [57]. Additionally, cold-sprayed Ta, Zr, and Ti coatings are used to protect the substrates in the corrosion resistance applications [131].

Electrical and thermal conductivity

Based on high purity and oxide-free structures of the coatings, cold spraying can optionally be used in applications, where either electrical or thermal conductivity is needed [129]. Cold-sprayed Cu coatings can be used in connecting plates, Cu and Al coatings on heat sinks in electronics [6,130] and cooling devices [129]. Electrical conductivity of the cold-sprayed Cu coating can be as high as 95 % of the value of the bulk Cu [129]. In addition, one possibility is to use cold-sprayed coatings as thermal barrier coatings, e.g., in aluminum piston heads, disc brakes [6] or as electrically conducting or insulating coatings in applications in aerospace industry [57]. Again, one of the key properties of the cold-sprayed coatings is conductivity [6,11], thus, it is ideal for conductors and thermal management, e.g., as electric screening coatings on plastics or as conductive coatings on non-metal substrates [130].

Repairing

LPCS coatings can be used in metal restoration, repairing [17,48,51] and sealing, e.g., in engine blocks, castings, molds, and body repair [6,49] and repairing parts [57], e.g., pistons, bearing components, seals [2]. In addition, one advantage is the ability to repair Al structures by using HPCS Al coating for the reclamation purposes [53]. Additionally, cold spraying is reported to be used for repair parts by using Al, Cu, steel, Ni, and various alloy coatings [130,131]. Cast iron and steel substrates can be repaired by using LPCS Cu-W-Zn or Ni-TiC composite coatings [132] and damaged surfaces of chill cast by using HPCS coatings [129].

Functional coatings

In addition to the applications above, cold-sprayed coatings could be used as functional coatings where anti-stick and magnetic properties are required, in soldering of electronic components [6,49,129,130], and for implants [6]. With cold-sprayed coatings, strengthening and hardening can be added and near-net shapes and compact pieces, e.g., Ti and Ti-based coatings can be produced [1,2]. In addition, Ni coatings can be used as base or intermediate layers in sandwich structures [130]. Furthermore, Ni, pure Fe [129], and other magnetic materials are suitable for cooking applications for induction heating. Composite materials, powder mixtures with functional properties, e.g., layers for thermal management, wear protection, bearing or solder layers are reported. [130] Cold-sprayed ceramic and metal-matrix composite (Al_2O_3, Al_2O_3-Ti_2O, WO_3, Ta-MnO_2, Al-MnO_2) thin films (mostly particle penetrations) can be used as surface treatments for functional applications, e.g., catalytic coatings [12]. Cold-sprayed braze and Zn coatings can also be used for engraving surfaces in printing industry, and Ta, Nb, and TiMo coatings as sputtering targets [131].

4 AIM OF THE STUDY

The aim of this work was to characterize the microstructural and mechanical properties of cold-sprayed coatings and to find out affecting factors in order to produce overall dense coatings. Figure 28 shows the structure of the research topics and affecting factors. The research is focused on evaluation of the microscopic and macroscopic properties of high-pressure and low-pressure cold-sprayed coatings. The main goal was to find correlation between different properties including microstructure, grain structure, bonding, and mechanical properties, and the most important, denseness. In addition, corrosion resistance of overall dense coatings was investigated.

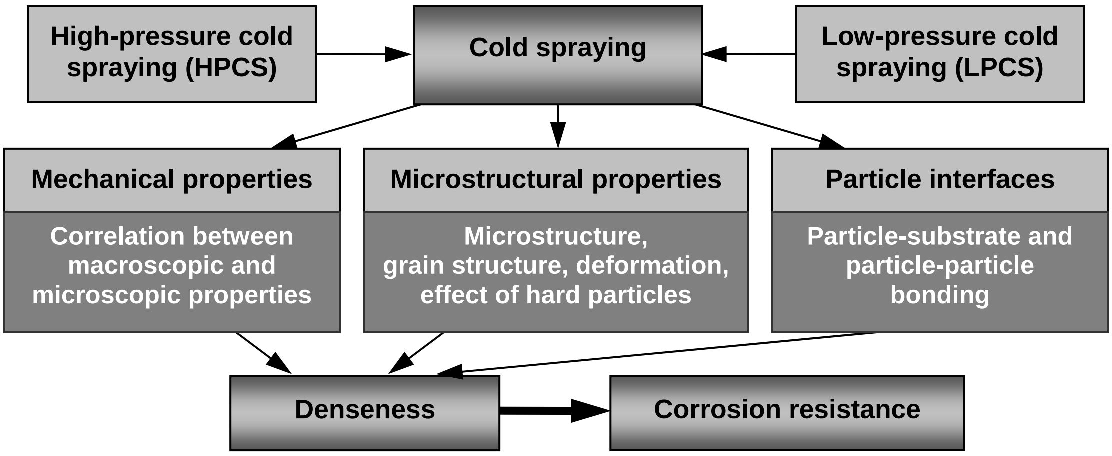

Figure 28. The structure of the research work.

The research was focused on the evaluation of powders, spraying parameters, substrates, post-treatments, and optimal combinations of these factors. Denseness of the coatings is a requirement for corrosion protection and for that, it was important to characterize microstructural details, denseness, and corrosion properties more specifically. This work is composed of the seven publications. The relationship between these publications is presented in Fig. 29.

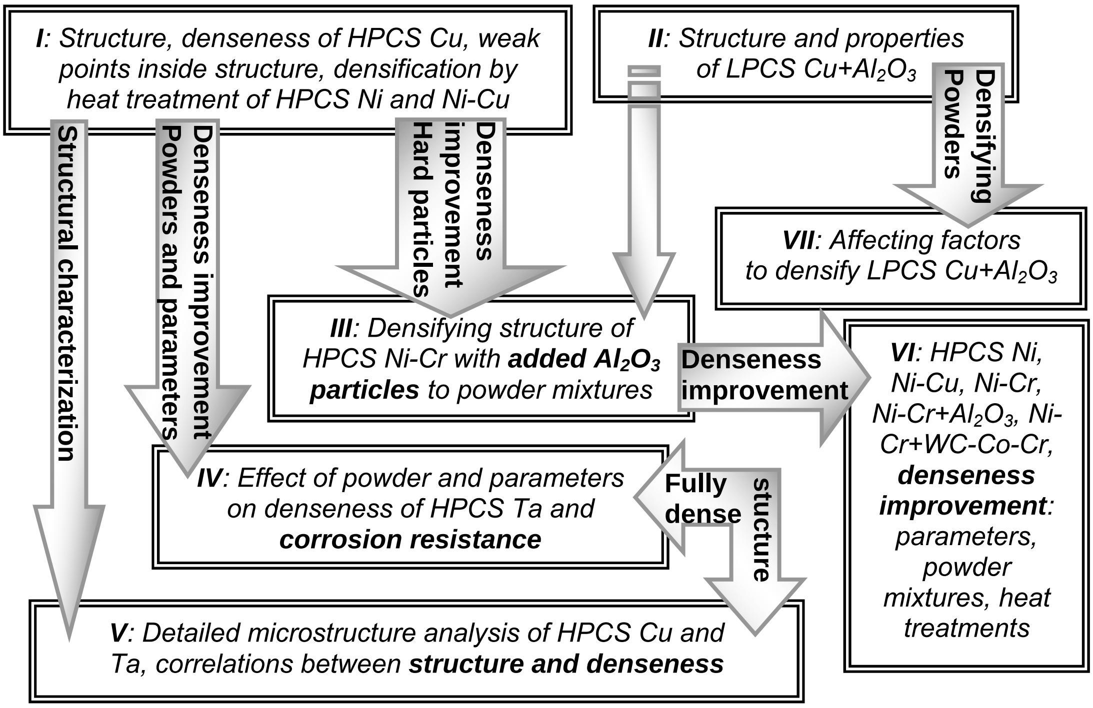

Figure 29. Relationship between research topics, main research results, and published papers (I-VII).

5 MATERIALS

Various powder materials were used. Metallic powders and metallic-ceramic powder mixtures were tested with different compositions and with different powder properties, e.g., particle size and particle morphology. Common feature for all these metallic materials is that they give anodic protection for the steel substrate. Copper was chosen as coating material due to its good electrical and thermal conductivity [133] and corrosion resistance in atmospheric conditions [115]. Nickel [134,135], nickel-chromium [135], nickel-copper [135] and tantalum [124] were chosen for their corrosion resistance in various corrosive environments.

5.1 Powder materials

Cu, Ta, Ni, Ni-20/30Cu, Ni-20Cr, Ni-20Cr+Al_2O_3, and Ni-20Cr+WC-10Co-4Cr coatings were manufactured using the HPCS system whereas Cu and Cu+Al_2O_3 coatings were produced using the LPCS system. Table 4 summarizes the powder characteristics. Spherical particles are produced by using gas atomization, dendritic particles by using electrolytical production method, and blocky-shaped particles by fusing and crushing. In Table 4, after each powder material also the publication where the particular powder was used is stated.

Table 4. Characteristics of powders used in HPCS and LPCS processes.

Powder material	Particle size (µm)	Morphology	Spraying process used
Cu[I]	-22+5	Spherical	HPCS
Cu[I]	-30+10	Spherical	HPCS
Cu[V]	-35+15	Spherical	HPCS
Cu[I]	-38+11	Spherical	HPCS
Cu[VII]	-25+5	Spherical	LPCS
Cu+ Al_2O_3[II, VII]	-	Dendritic Blocky	LPCS
Cu+ (10, 30, 50%)Al_2O_3[VII]	-25+5 -22+5	Spherical Blocky	LPCS
Cu+ (10, 30, 50%)Al_2O_3[VII]	< 63 -22+5	Dendritic Blocky	LPCS
Ni[I]	-25+5	Spherical	HPCS
Ni[VI]	-30+10	Spherical	HPCS
Ni-20Cr[I, III]	-22+5	Spherical	HPCS
Ni-20Cr[IV, VI]	-30+10	Spherical	HPCS
Ni-20Cr+ (30, 50%)Al_2O_3[III]	-22+5 -90+45, -45+22, -22+5	Spherical Blocky	HPCS
Ni-20Cr+ 50%Al_2O_3[VI]	-30+10 -90+45	Spherical Blocky	HPCS
Ni-20Cr+ 30%WC10Cr4Co[VI]	-30+10 -45+15	Spherical Blocky	HPCS
Ni-20Cu[VI]	-30+10	Spherical	HPCS
Ni-30Cu[I]	-38+16	Spherical	HPCS
Ta[IV, V]	-30+10	Blocky	HPCS
Ta[IV]	-38+10	Blocky	HPCS

5.2 Substrate materials

Grit-blasted (mesh 18 (HPCS) or mesh 24 (LPCS) Al_2O_3 grits) carbon steel, Fe52 (cold-rolled) and copper (cold-rolled) sheets were used as substrate materials. Coatings were sprayed on steel substrate for denseness evaluations.

6 METHODS

In this work, two different spraying systems were used. High-pressure cold spray systems were used at Linde AG Linde Gas Division (Unterschleissheim, Germany) whereas low-pressure cold spray system was used at Tampere University of Technology (Tampere, Finland). Spraying methods, characterization methods and post-treatments are described here.

6.1 Spraying methods

6.1.1 High-pressure cold spray system

HPCS coatings were prepared with Cold Gas Technology's (CGT) Kinetiks 3000 and Kinetiks 4000 spraying systems. Nitrogen was used as a process gas. Kinetiks 4000 is an advanced spraying system (Fig. 30) which enables the use of pressure of max. 40 bar and preheating temperature of max. 800ºC whereas for Kinetiks 3000, pressure max. 30 bar and preheating temperature max. 600ºC. In addition, two heating systems can be used with Kinetiks 4000. Kinetiks 3000 (in publications I and IV) and Kinetiks 4000 (in publications III, IV, V, and VI) with electrical power of 47 kW and a standard MOC-nozzle were used in this study. Spraying parameters used are presented in the following publications: Cu, Ni, and Ni-30Cu [I], Ni-20Cr and Ni-20Cr+Al_2O_3 [III], Ta [IV], Cu and Ta [V], Ni, Ni-20Cu, Ni-20Cr, Ni-20Cr+Al_2O_3, and Ni-20Cr+WC-10Co-4Cr [VI].

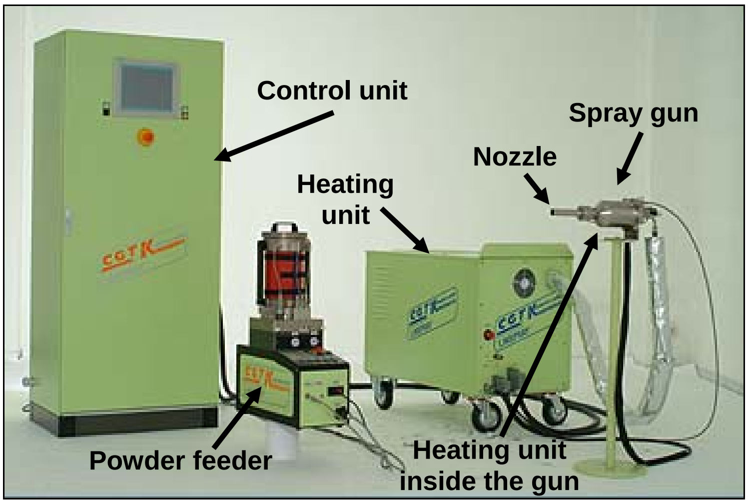

Figure 30. Cold Gas Technology GmbH (CGT) Kinetiks 4000 high-pressure cold spray system [136].

In both Kinetiks 3000 (20 kW) and Kinetiks 4000 systems, spraying conditions (e.g., powder feed, pressure, gas feed, and temperature) are controlled [137]. In Kinetiks 4000 equipment, 17 kW, 34 kW, and 47 kW heating power can be used. The system with 17 kW heating power is typically used with soft and low melting point materials, e.g., Al and Zn with maximum temperature of N_2 550ºC whereas 34 kW and 47 kW heating systems offer possibility to use preheating temperature of N_2 800ºC. These models are suitable for most of the materials used in cold spraying. In addition, for these two models, heating consists of two heating systems: a filament inside the nozzle and a separate heating unit with 17 kW or 30 kW power, depending on the model used [131].

6.1.2 Low-pressure cold spray system

LPCS coatings were prepared with a DYMET 304K equipment (Obninsk Center for Powder Spraying, OCPS). Compressed air was used as process gas. Maximum pressure is 9 bar and preheating temperature is 650ºC. Both round and tubular nozzles can be used. In this study, a round (Ø 5 mm) stainless steel nozzle was used. The DYMET 304K (Fig. 31) is a portable cold spray system, and it can be operated manually or with a robot or x-y manipulator. Spraying parameters used are presented in the following publications: Cu+Al_2O_3 [II], and Cu and Cu+Al_2O_3 [VII].

Figure 31. Obninsk Center for Powder Spraying (OCPS) DYMET 304K low-pressure cold spray system [56].

6.2 Characterization methods

Various characterization methods were used in order to find relationships between powders, spraying parameters, and post-treatments and structural characteristic and corrosion properties of the HPCS and LPCS coatings.

6.2.1 Microscopic techniques

Electron microscopes and a stereomicroscope were used in the characterization of the macro-, micro- and grain structures of the cold-sprayed coatings. Microscopes used are described below.

Scanning Electron Microscope (SEM)

Structures of the cold-sprayed coatings and powder morphologies were characterized using a scanning electron microscope (SEM, Philips XL30). Secondary (SE) and backscattering (BSE) detectors were used. The structures were analyzed from unetched and etched metallographic cross-sectional coating samples. Furthermore, cross-sectional analysis was performed after corrosion tests. HPCS coating samples were prepared by grinding them first with 600-4000 SiC papers and then by polishing with SiO polishing liquid (OP-U, Struers). LPCS coating samples were grinded with 600-1200 SiC papers, 5 µm Al_2O_3 paste and 1 µm Al_2O_3 liquid. Final polishing was done with SiO polishing liquid. Etching procedure is presented in publication [I].

Field-Emission Scanning Electron Microscope (FESEM)

The unetched microstructures and fracture surfaces were analyzed with an ultra high resolution field-emission scanning electron microscope (FESEM, Zeiss ULTRAplus). Metallographic cross-sectional samples were prepared with the same procedure as SEM samples. Coating samples were bent up to rupture for fracture surface analysis.

Transmission Electron Microscope (TEM)

The inter-particle structures were characterized using an analytical transmission electron microscope (TEM) with an energy dispersive X-ray spectrometer (EDS) (TEM (Jeol JEM 2010)+EDS (Noran Vantage)). In TEM characterization, samples were analyzed both from top-view and cross-section directions. Samples were either electrolytically prepared with twin jet electrolytical polisher (Struers Tenu-Pol-5) using a solution of nitric acid in methanol (1:2) or samples were prethinned by hand, then thinned with dimple grinder (Gatan Dimpler 656) and finally thinned with precision ion polishing system (Gatan PIPS 691).

Stereomicroscope (SM)

After corrosion tests, coating surfaces were analyzed with a stereomicroscope (SM, Leica MZ7.5). The coating samples were cleaned with water and ethanol prior to the surface analysis with stereomicroscope.

6.2.2 Corrosion tests

Denseness of the cold-sprayed coatings was evaluated with open-cell potential measurements and with salt spray tests. These tests reveal impermeability or existing through-porosity inside the coating structures. In addition, corrosion properties of the coatings were studied by using anodic polarization measurements. Corrosion tests used are presented below.

Open-cell potential measurements

The corrosion behavior and denseness, i.e., impermeability or existing through-porosity of the coatings, were tested with electrochemical open-cell potential measurements. The electrochemical cell used in the open-cell potential measurements consisted of a plastic tube of diameter 20 mm and volume 12 ml, glued on the surface of the coating specimen. A 3.5 wt.-% NaCl solution was placed in the tube for 9-, 18-, or 60-day measurements, taken with a Fluke 79 III true RMS multimeter. A silver/silver chloride electrode (Ag/AgCl) was used as a reference electrode. Bulk (cold-rolled metal sheets) materials were also tested as a reference.

Salt spray test

The salt spray tests were conducted according to the ASTM B117 standard. Substrates were masked with epoxy paint before testing in order to allow only the coating surfaces to be in contact with the corroding salt spray. A 5 wt.-% NaCl solution was used with an exposure time of 48, 96, or 240 h, a temperature of 35-40°C, a solution pH of 6.3, and a solution accumulation of 0.04 ml/cm^{2}h. The salt spray tests in publications I and II, were done at Tampere University of Technology whereas tests in publications III, IV, VI, and VII, were carried out at Technology Centre KETEK (Kokkola, Finland).

Anodic polarization measurements

Polarization measurements were carried out in order to evaluate the corrosion resistance of the cold-sprayed Ta coatings. Polarization behavior is usually studied in order to estimate corrosion protection and corrosion rates. Furthermore, active-passive behavior is clearly detected from anodic polarization measurements [115]. The anodic polarization tests were carried out adapting the standard ASTM G59. The polarization tests were run in a flat specimen cell with a rubber O-ring used as gasket. Tests were conducted in 3.5 wt.-% NaCl and 40 wt.-% H_2SO_4 water solutions at room temperature (RT) of 22ºC and at elevated temperature of 80ºC. Potential was scanned from 0.6 V below the resting potential (E_0) to potential of 3 V at a scanning rate of 2 mV/s. A saturated calomel electrode (SCE) was used for reference. The tests were done at Technology Centre KETEK (Kokkola, Finland).

6.2.3 Mechanical testing methods

Hardnesses and bond strengths of the cold-sprayed coatings were investigated in order to evaluate mechanical behavior and to find correlation between macroscopic properties and microscopic details.

Microhardness

Vickers hardness ($HV_{0.3}$) was measured as an average of ten measurements from the cross-sections of coatings with a Matsuzawa MMT-X7 hardness tester. The weight of the load was 300 g. In hardness measurements, the indentations were taken from the metallic coating areas of the coatings with hard particles to evaluate the mechanical behavior of the metallic particles.

Bond strength

Bond strength values were determined according to standard EN582 in a tensile pull test (Instron 1185 mechanical testing machine) as an average of three measurements. The coating samples were glued between two rods which were grit-blasted prior to gluing. The glue used was 3M Scott-Weld DP-460.

6.2.4 Other methods

In addition to the above methods, image analysis, particle size distribution measurements and chemical analysis were carried out.

Image analysis

The image analyses were done using ImageJ program. The hard particle fractions were calculated from cross-sectional samples of the coating using image analysis. In addition, the amount of corrosion spots on the coating surfaces after corrosion tests were calculated.

Particle size measurements

The particle size distributions of Ta powders were measured with Symantec Helos analysis in wet conditions (Sucell). Measurements are based on laser diffraction.

Chemical analysis

Oxygen contents of Ta powders (in publication IV) were measured with chemical analyzers (Leco TC-436DR and Leco TC-136) at Outotec Research, Pori, Finland.

6.3 Post-treatments

Heat treatments were done as post-treatments in order to densify the structures of HPCS Cu, Ni, Ni-20/30Cu, Ni-20Cr, Ni-20Cr+Al_2O_3, and Ni-20Cr+WC-10Co-4Cr coatings. In publication I, the heat treatments were done in a Carbolite 3-zone controlled atmosphere furnace using Ar as protective gas. Holding time at the annealing temperature was 5 hours and annealing temperatures were 200, 400, 600, 800, and 1000ºC, depending on the coating materials. In addition, in publication VI, heat treatments were done using a furnace in a protective (Ar-3%H_2) atmosphere with the holding time of 2 hours at 600ºC annealing temperature. In both heat treatment procedures, samples were under protective atmospheres during temperature rising, holding and cooling.

7 RESULTS AND DISCUSSION

The focus point of this study was to produce overall and fully dense cold-sprayed coatings and characterize the microscopic and macroscopic features of the coatings which affected the coating denseness. The denseness of the coatings strongly depends on powder characteristics together with spraying parameters. Microstructural properties (microstructure, grain structure, fracture surfaces, and particle bonding) were analyzed to gain the microstructure-denseness dependence. Corrosion properties and especially, impermeability were evaluated in order to estimate the capability of the coatings for corrosion protection.

7.1 Microscopic properties of cold-sprayed coatings

Structures of the cold-sprayed coatings as well as microstructures and grain structures of the dense coatings are shown here. It can be said that microstructure of the coatings defines their corrosion protection capability, denseness being the key factor.

7.1.1 Microstructure

Typically, the structure of cold-sprayed coatings is dense (without pores or with low porosity level) according to microscopic characterization. Figure 32a shows an example of the cross-sectional structure of HPCS Ta coating on grit-blasted steel substrate. This is the typical structure of a dense cold-sprayed metallic coating. In addition, the interface between the coating and substrate is clean and voidless. Furthermore, etching reveals the detailed microstructure of the coatings. Microscopic details; particle boundaries, partly inter-particle structure, particle deformation, and flattening are seen in the etched cross-sectional microstructure of HPCS Cu coating, Fig. 32b. Examples of slip planes caused by localized deformation are marked with arrows. Particles are highly flattened on the impacts due to the high level of plastic deformation. Furthermore, high deformation leads to high denseness [31]. The microstructures of HPCS Cu coatings are presented in [I, V], HPCS Ni in [I, VI], HPCS Ni-20/30Cu in [I, VI], HPCS Ni-20Cr and Ni-20Cr+Al_2O_3 [III, VI], HPCS Ni-20Cr+WC-10Co-4Cr [VI], and Ta in [IV, V].

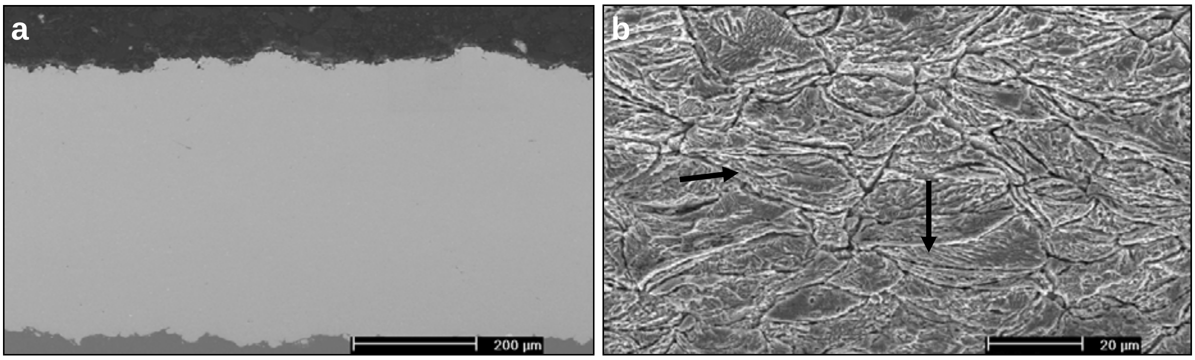

Figure 32. Cross-sectional structure of HPCS a) Ta coating on grit-blasted steel substrate, unetched [IV] and b) Cu coating, etched structure [I]. SEM images.

Metallic-ceramic powder mixtures are usually used in the LPCS process. Ceramic particles keep the nozzle clean, activate the sprayed surface, and densify the coating structures. Figure 33a shows the typical cross-sectional structure of LPCS Cu+Al_2O_3 coating. Black particles in the structure are Al_2O_3 particles arisen from an initial powder mixture. Coatings are visually dense, particles are plastically deformed; however, some oxidized particle boundaries are present, seen in Fig. 33b (SEM (BSE) image) as darker gray boundaries (arrows). Obviously, dendritic powder particles present relatively high number of oxidized particle boundaries due to the fact that primary particles contain irregular, dendritic structures. The etching reveals primary particle boundaries which are clearly visible in Fig. 33c. Powder particle boundaries are not detected in the structure and this is caused by break-down of powder particles on the high-velocity impact. In addition, the high level of plastic deformation of primary particles is detected in the etched microstructure as flattened particle shapes (Fig. 33c). The microstructures of LPCS Cu and Cu+Al_2O_3 coatings are presented in [II, VII].

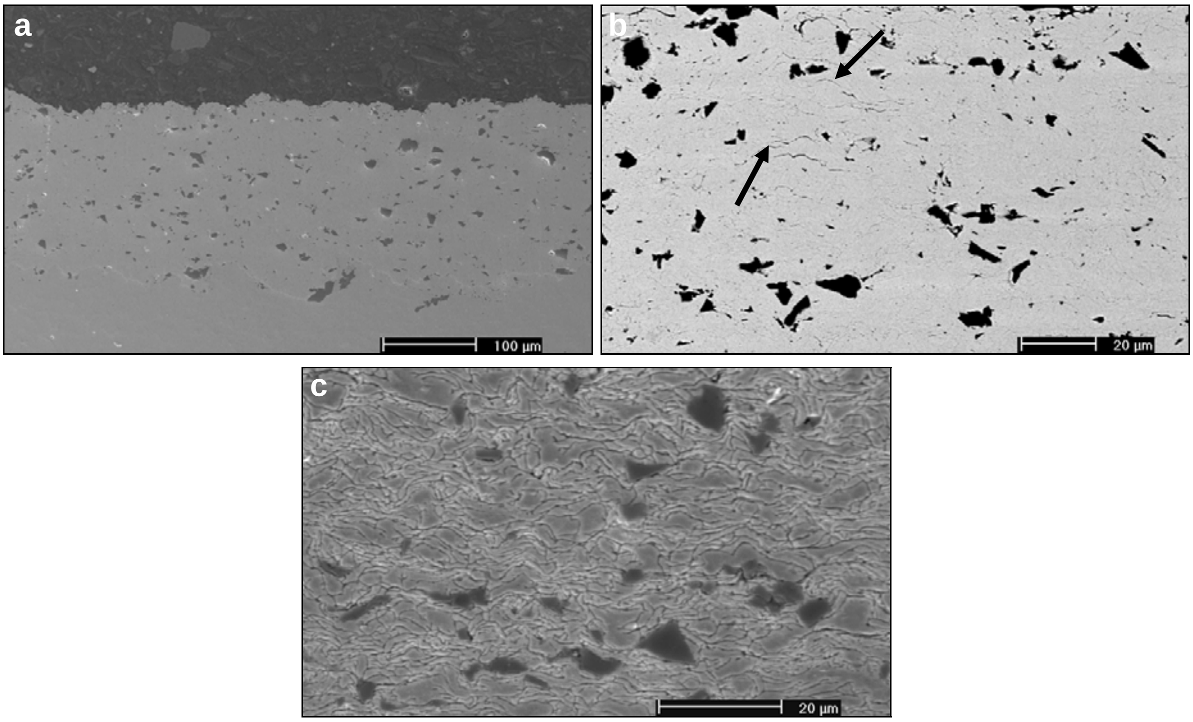

Figure 33. Cross-section of LPCS Cu+Al_2O_3 coating: a) unetched structure, coating on grit-blasted steel substrate (SE image), b) unetched microstructure (BSE image), oxidized particle boundaries are shown with arrows, and c) etched microstructure (SE image). SEM images. [II]

Powder characteristics have a strong influence on the coating formation and hence, the coating properties [1] also in the LPCS process. Two different types of Cu powders were studied in order to find affecting factors to densify the structures of LPCS Cu and Cu+Al_2O_3 coatings [VII]. An amount of 50% Al_2O_3 particles mixed with dendritic Cu powder showed the densest structure according to microscopic evaluation in the comparison between 0, 10, and 30% Al_2O_3 additions in the case of this powder. Figure 34 presents the cross-section of LPCS Cu+50Al_2O_3 prepared from Ecka dendritic powder. In this study, the highest amount of Al_2O_3 showed clearly decreased porosity and pores were mostly concentrated on the top of the coatings. However, some oxidized boundaries were still detected in the detailed structure (Fig. 34b), indicating that oxide layers of initial primary particles were not totally removed during impacts. Furthermore, the dendritic powder particles had large surface area due to the dendritic shape and thus, the high number of oxidized primary particle boundaries appears already in the as-sprayed state.

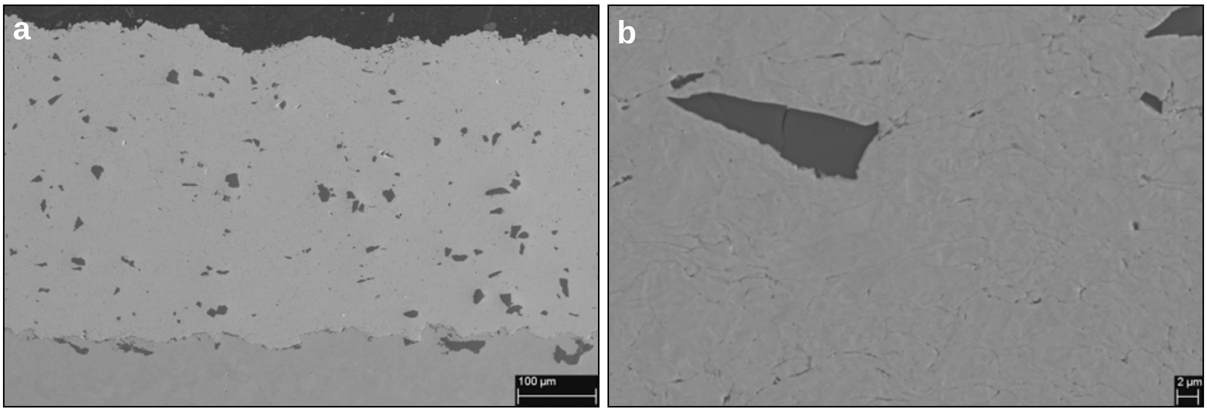

Figure 34. Cross-section of LPCS Cu+50%Al_2O_3 coating prepared from dendritic Cu powder particles (Ecka M15) mixed with Al_2O_3 particles: a) coating on grit-blasted steel substrate and b) unetched detailed microstructure. FESEM images. [VII]

On the other hand, one solution to decrease porosity and to increase denseness of the LPCS Cu coatings was gained by using spherical Cu particles. The spherical particles have lower number of particle boundaries compared with dendritic particles due to powder morphology and primary particle size. The relatively dense LPCS Cu coating without any hard particle addition was gained by using spherical Cu powder. In addition, 10% Al_2O_3 particle addition clearly densified the structure. Figure 35 shows the cross-section and detailed microstructure of LPCS Cu+10Al_2O_3 coating prepared from Osprey spherical powder. Only a few oxidized boundaries were detected in the structure. Additionally, the amount of these boundaries in this coating was lower than in other LPCS Cu and LPCS Cu+Al_2O_3 coatings.

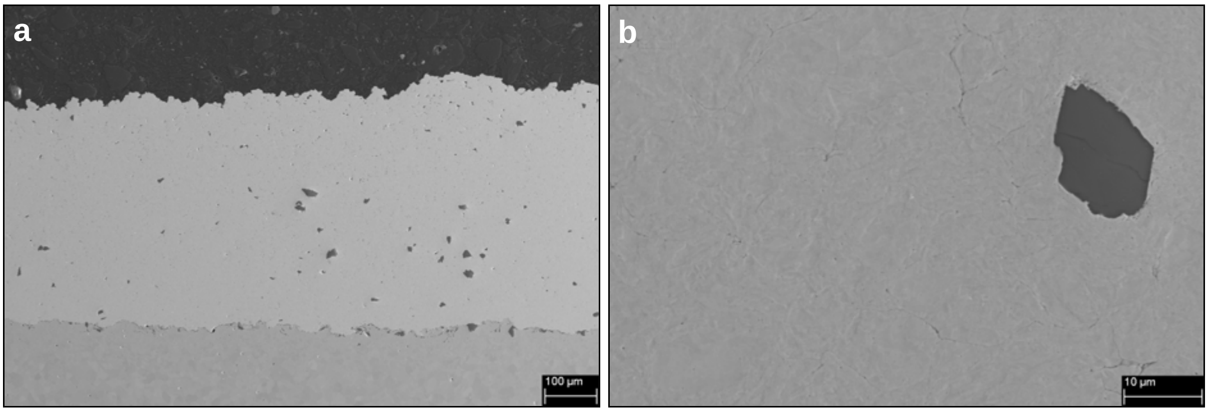

Figure 35. Cross-sectional structure of LPCS Cu+10%Al_2O_3 coating prepared from spherical Cu powder particles (Osprey) mixed with Al_2O_3 particles: a) coating on grit-blasted steel substrate and b) unetched detailed microstructure. FESEM images. [VII]

The hard particle addition has also shown its potential to densify the metallic structure of HPCS Ni-20Cr coatings. The cross-sections of HPCS Ni-20Cr+50Al_2O_3 and Ni-20Cr+30WC-10Co-4Cr are presented in Figs. 36a and 36b, respectively. The coating structures are visually dense without pores or other defects inside. Black particles in Fig. 36a are Al_2O_3 particles whereas light gray particles are WC-10Co-4Cr particles in Fig. 36b. The proportions of hard particles in the coatings are 5 % and 18 %, respectively. [VI]

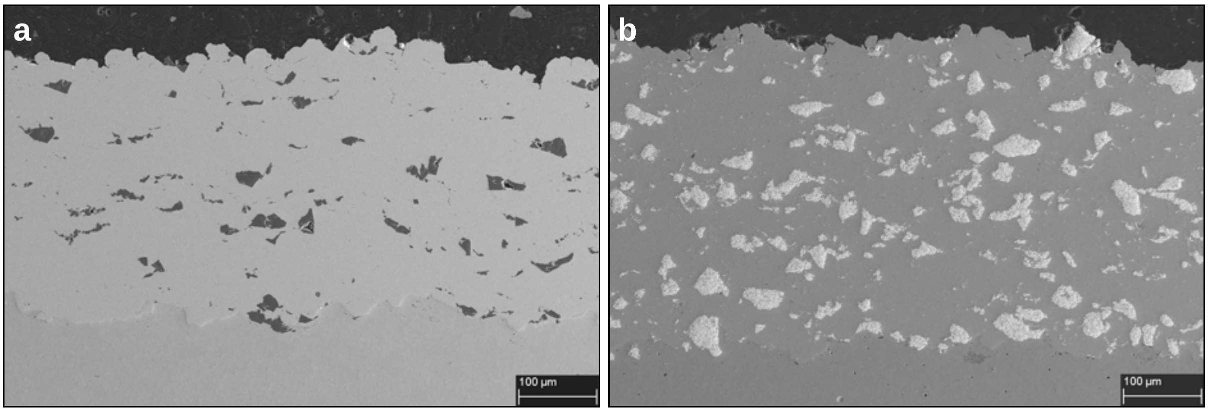

Figure 36. Cross-sectional structures of HPCS a) Ni-20Cr+50Al_2O_3 and b) Ni-20Cr+30WC-10Co-4Cr coatings on grit-blasted steel substrates. FESEM images. [VI]

As a summary, the microstructures of HPCS coatings are dense and oxide-free due to the highly plastically deformed structure caused by high-velocity particle impacts. For the dense structure formation, presence of pores, voids and other impurities should be eliminated. The high level of plastic deformation makes it possible to eliminate defects inside the structure by e.g., breaking down the oxide layers of initial powder particles. In addition, porosity is eliminated with high particle deformation. Typically, weak points in the cold-sprayed structures were concentrated on the particle boundaries at the connecting point of several particles. When particles are deformed enough, porosity is eliminated due to the localized deformation and formation of material jets.

With the HPCS Ta coatings, denseness improvement was detected with the optimal combination of powder (improved powder: particle size, particle size distribution, purity) and spraying conditions (advanced spray equipment). High preheating temperature affects coating quality [131] by increasing particle velocity and temperature which in turn, increases the particle deformation and forms a tighter structure [41]. The denseness improvement by optimal combination of powder and spraying parameters and its effect on particle deformation is schematically presented in Fig. 37, case 1. The optimal powder properties and further, spraying parameters are material-dependent. In the other case, denseness of the coatings was improved with the addition of hard particles. Firstly, it enables the use of higher process temperatures (without nozzle clogging) which in turn, improves coating quality [32,41]. Secondly, hard particles densify the structure due to hammering and tamping effects [49]. This is demonstrated in Fig. 37, case 2.

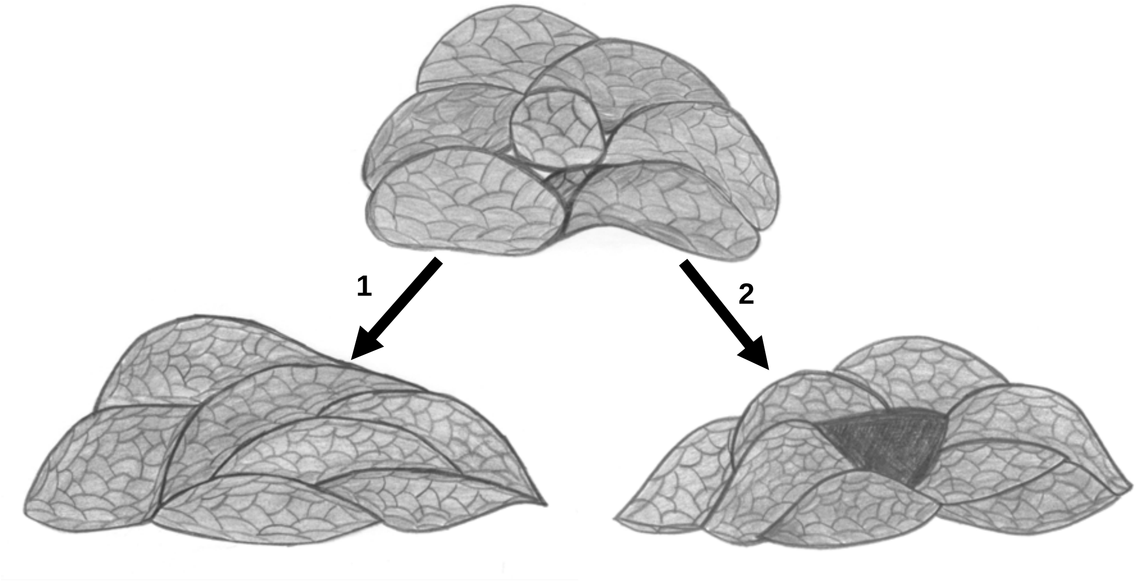

Figure 37. Schematic presentation of particle structure of coating with porosity and coatings with dense structure due to the high level of deformation. Number 1 indicates denseness improvement by choosing optimal combination of powder and spraying parameters and number 2 by adding hard particles to densify the metallic structure.

7.1.2 Grain structure

The FESEM characterization shows a dense structure and in addition to that, a grain structure with highly deformed grains. Tight bonding between the HPCS Ta particles as well as a metal-metal contact between particles is observed in Fig. 38. Metal-metal bonding is the requirement for tight bonds and therefore, overall dense coating structure. Figure 38a shows a very fine grain structure detected near to the particle-particle interface and additionally, elongated grains due to the high deformation. Furthermore, materials jets are reportedly crucial for the high coating quality [5,30,31,82]. Arrow shows material jet formed between two Ta particles (Fig. 38b). Powder characteristics together with optimized spraying parameters lead to the formation of highly dense coatings by cold spraying. In addition, purity of the powder is crucial for the metal-metal bonding, depending on oxide layer removal. Powder particles with high purity have thinner oxide layers on the particle surfaces, promoting tendency to get the metal-metal bonding on the impact. If the oxide layer is thick, removal of this layer is more difficult on the impacts and thus, there is possibility that oxides stay at particle boundaries in the structure and decrease the metal-metal bonding [1]. Localized deformation is due to the adiabatic shear instability and thermal softening [24,30,31]. High plastic deformation is needed to destroy oxide layers of the particles and thus, enabling the formation of the metal-metal bonding between particles.

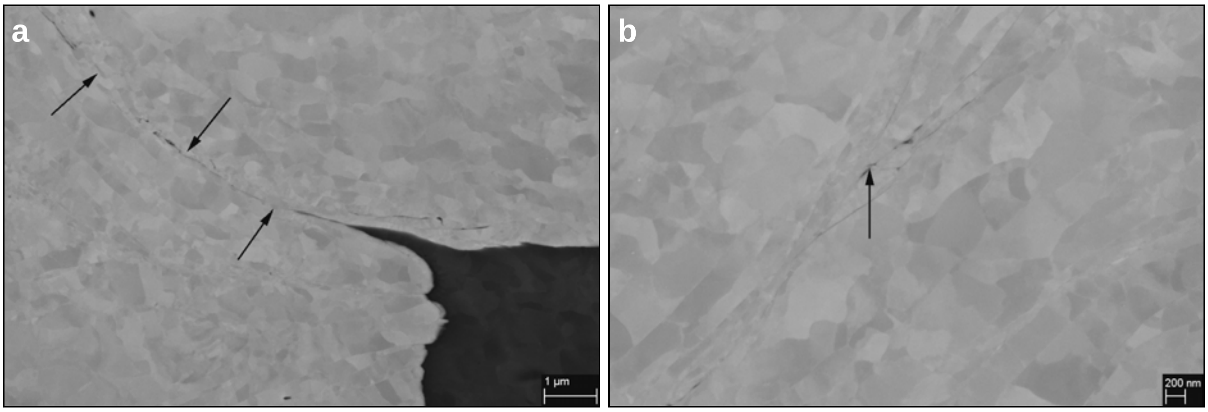

Figure 38. Cross-sectional microstructure of HPCS Ta coating: a) particle-particle and particle (gray area)-substrate (black area) interfaces (arrows indicate particle boundary) and b) metal-metal bonding between Ta particles (arrow indicates material jet). FESEM images. [V]

Plastic deformation is known to be related to dislocations (i.e., microstructural defects) in the structure. Under high strain, dislocation movement cause plastic flow and, hence permanent deformation. Even further, dislocation movement causes work hardening. In the microstructure, plastic flow can be seen in the presence of slip planes due the sliding [79] and of shear bands due to the adiabatic shear localization [67]. High dislocation density indicates high plastic strain and hence, high level of deformation [79]. In addition to the high dislocation density, twinning, i.e., formation of twins causes permanent deformation in the material.

High plastic deformation together with adiabatic localization is detected by microscopic characterization from the structure by various nanoscale features. In addition, the cold-sprayed Cu coatings had non-uniform structures [138] due to the localized deformation. Localization of the grain deformation inside the particle structure is strongly concentrated on the region near to the particle interfaces. The strongest deformation is due the adiabatic shearing and thus, the elongation of grains. Moreover, high dislocation density together with a formation of shear bands, slip planes, and twins causes different levels of deformation in different part of particles. Figure 39a reveals shear bands and twins, indicating localized grain deformation on the impacts. Deformation and inter-particle structure from top-view direction of Ta particles are shown in Fig. 39b. High dislocation density areas are observed in the TEM images. Figure 39b shows elongated grains with high dislocation density.

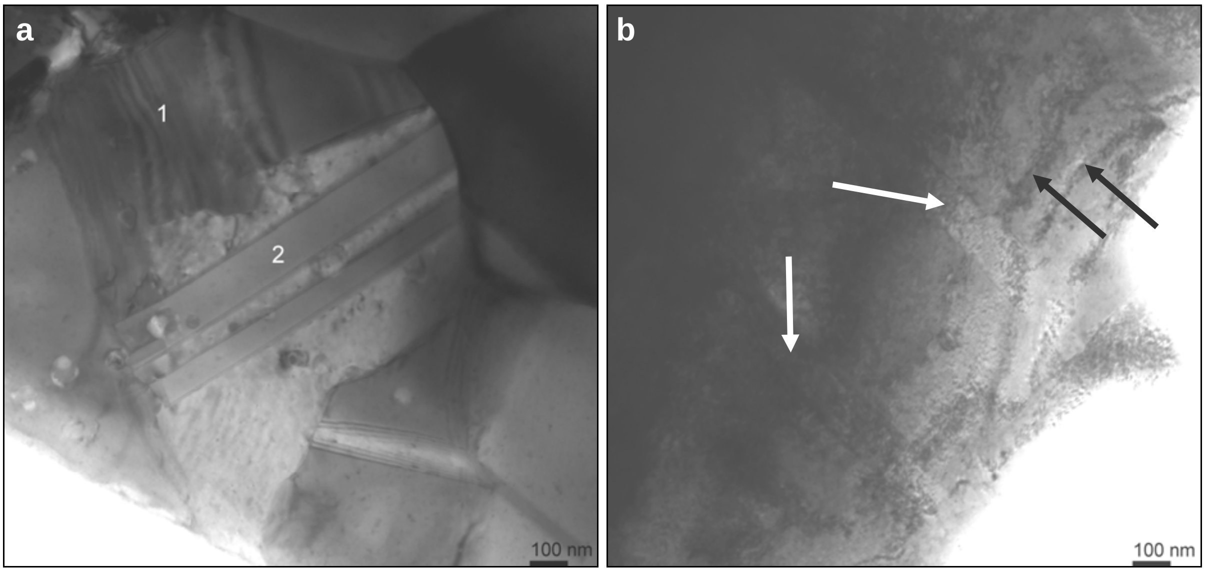

Figure 39. Inter-particle structure of HPCS a) Cu, 1 indicates shear bands and 2 twins, and b) Ta coatings with elongated grains (white arrows) and dislocation walls (black arrows). TEM images. [V]

7.2 Particle interfaces

In this work, also particle interfaces and bonding between metallic and metallic-ceramic particles were studied. Particle bonds are tight in the dense coating structure and metal-metal bonds are dominant in the metallic coatings. In addition, in the metallic-ceramic mixture coatings, ceramic particles reinforce the structure and mechanical bonding between metallic and ceramic particles has been observed.

7.2.1 Metal-metal particle bonding

As already mentioned, typical weak points in the cold-sprayed coating are concentrated on particle interfaces due to the weak particle boundaries. Weak bonds between particles caused by undeformed or only slightly deformed particle together with insufficiently removed oxide layers on the particle surfaces can compose porosity [85]. In addition, in some cases, e.g., in Ni-20Cr coatings, porous layer on the top of the coatings is formed due to the absence of tamping effect of next incoming particles [85,111]. Figure 40a shows porosity (black area) in the structure of HPCS Ni-20Cr coating and oxide layers between particles (darker gray areas, marked with arrows). Furthermore, open particle boundaries are observed in the structure of HPCS Ni-30Cu coating after salt spray test as shown in Fig. 40b, indicating a weak structure with local defects and thus, non-protective coating. In addition, the most critical areas in the particle bonding are the connection points between several particles. For tight bonding without weak bonds and local defects, metal-metal bonding is required and it is able to be attained with high particle deformation on the particle impacts by removing the oxides from the surfaces while gas flow removes them away.

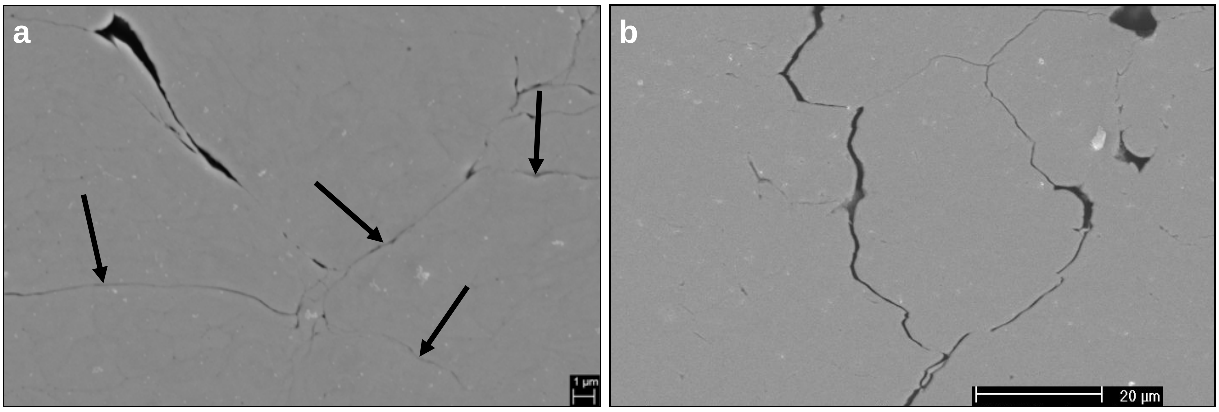

Figure 40. Cross-sectional structure of HPCS a) Ni-20Cr coating with weak particle boundaries (arrows indicate oxidized particle boundaries), FESEM image [VI] and b) Ni-30Cu coating after salt spray test, SEM image [I].

Examples of tight, dense, and oxide-free particle interfaces are presented in Fig. 41. Arrows indicate the connection points between particles: Ni-Ni and Cu-Cu, in Figs. 41a and 41b, respectively. In addition, randomly aligned grains are detected inside the structure of HPCS Cu coating (Fig. 41b).

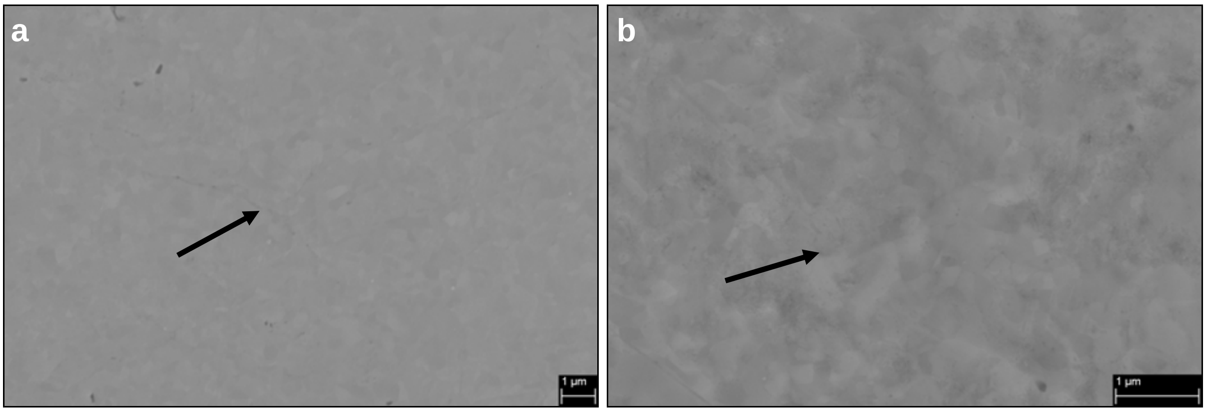

Figure 41. Cross-sectional microstructure of HPCS a) Ni [VI] and b) Cu [V] coatings. Dense coatings have tight particle bonds. Arrows indicate bonding between three particles. FESEM images.

Also TEM characterization reveals the tight particle bonds. Figure 42a shows the inter-particle structure and particle interface of HPCS Cu particle in the cross-sectional direction whereas the inter-particle structure of HPCS Ta particle from top-view direction is presented in Fig. 42b. In Fig. 42a, holes in the structure arisen from ion milling are designated as weaker particle boundaries whereas other parts of the boundaries were tight. In addition, removal of oxides from initial powder particle was observed with TEM+EDS analysis. The EDS analysis revealed the oxygen contents at the selected points in the structure of HPCS Cu: 1) 1.9 wt.-%, 2) 2.6 wt.-%, 3) 0.9 wt.-%, and 4) 0.5 wt.-%, as shown in Fig. 42a. These analyses show the oxygen contents at the selected points and they do not reflect to the total amount of oxygen in the structure. Values are given here in order to have comparison between different regions inside the coatings. The EDS analysis revealed that the oxygen content was lower inside the particle (points 3 and 4 in Fig. 42a) than at the particle boundary (points 1 and 2). Additionally, the oxygen content was lower at point 1 than at point 2, indicating tighter bonding region (point 1). On the other hand, it is possible that higher oxygen content in the open boundary (point 2) compared with the tight boundary (point 1) reflects to the fact that the oxide layers were not totally removed. As a conclusion, there are still some weak points in the structures of the dense HPCS Cu coating, however, tight bonds are dominant and thus, coating has impermeable cross-sectional structure. This was also verified with corrosion tests.

Figure 42b shows the microstructural details of HPCS Ta coating, e.g., tight particle bonds with shear bands (white arrows indicate particle boundaries whereas black arrow shows shear bands). The EDS analysis from selected points revealed low oxygen contents both at the particle boundary and in the inter-particle structure: 1) 0.7 wt.-%, 2) 0.7 wt.-%, 3) 0.5 wt.-%, and 4) 0.6 wt.-%, as shown in Fig. 42b. This indicates pure metal-metal bonding between the particles. The HPCS Ta coating had very dense and highly deformed structure with tight bonds. This coating contained a high amount of dislocations and especially dislocation walls. Moreover, the elongated grains indicate high plastic deformation and localized deformation due to the localized adiabatic shearing and thermal softening.

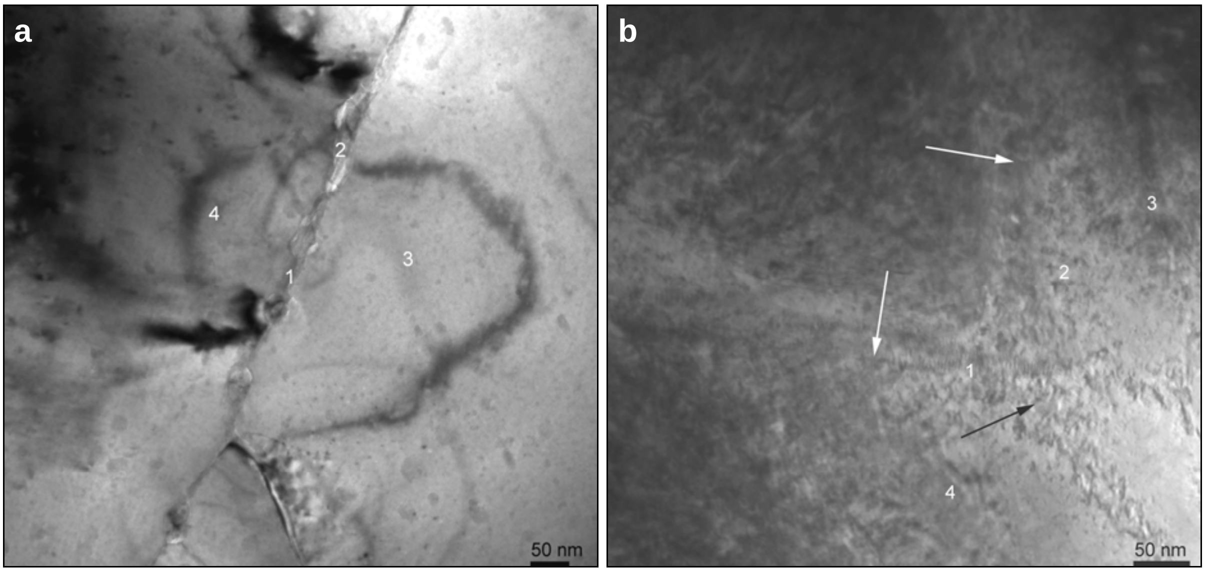

Figure 42. Particle boundaries between HPCS a) Cu particles (cross-sectional direction) and b) Ta particles (top-view direction). EDS analyses taken from places 1-4. Particle boundaries are indicated with white arrows and example of shear bands with black arrow. TEM images. [V]

7.2.2 Metal-ceramic particle bonding

One solution to densify the coating structure of HPCS metallic coating is to use metallic-ceramic powder mixtures. The experiments revealed technical spraying limitations when spraying Ni-20Cr powder. At higher temperature (600ºC/700ºC versus 500ºC) Ni-20Cr particles clogged the nozzle. This was possibly caused by the Ni-20Cr particles which were in softer state and thus, they stuck more easily to the surface of the nozzle [III]. To solve such problems, metallic powders were mixed with ceramic particles. Hard particles in the metallic powder have three functions: 1) to keep the nozzle clean, 2) to activate the sprayed surface, and 3) to densify the coating structure. Hard ceramic particles, Al_2O_3, were added into the metallic Ni-20Cr powder in order to improve coating quality and denseness together with possibility to use higher process temperature. Figure 43 shows bonding between Ni-20Cr and Al_2O_3 particles in the metallographic cross-section (Fig. 43a) and in the fracture surface (Fig. 43b). Al_2O_3 particles were mostly embedded into the softer metallic matrix and they were stuck to the surface. The particle interface seemed to be dense without visually detectable pores. In addition, the high level of plastic deformation of Ni-20Cr particle with material jets is observed from fracture surface in Fig. 43b. Hard particle hammers the previous particle, densifing the entire structure. In addition, Al_2O_3 particles were slightly fractured instead of deformation. It has been reported that fracturing of ceramic particles can be necessary for the coating formation [23,92].

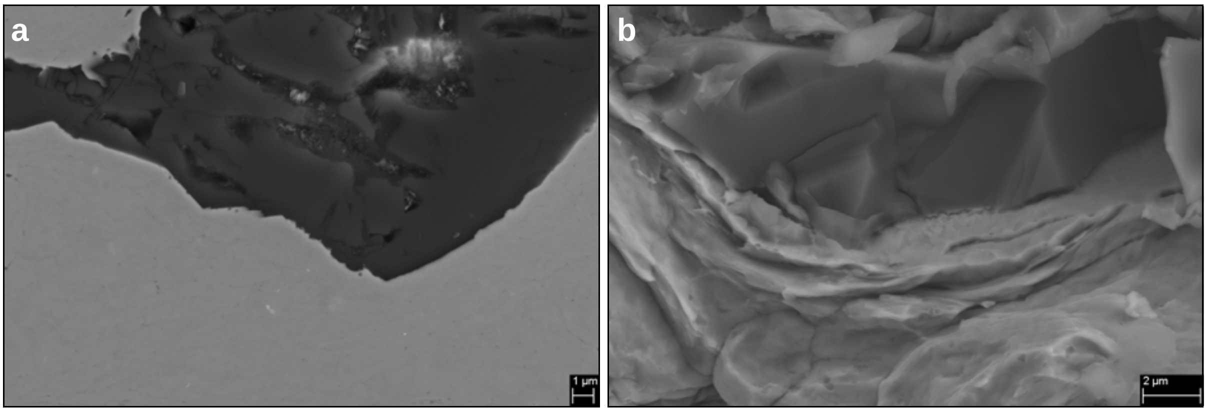

Figure 43. HPCS Ni-20Cr+50Al_2O_3 coating: a) cross-sectional structure and b) fracture surface. Bonding between Ni-20Cr (lighter gray) and Al_2O_3 (darker gray) particles. FESEM images. [VI]

In addition to the Al_2O_3 particle addition, hardmetal particle addition showed the denseness improvement in HPCS Ni-20Cr coatings. WC-10Co-4Cr particles were added into the Ni-20Cr powder. The cross-sectional structure of HPCS Ni-20Cr+WC-10Co-4Cr mixture coating is presented in Fig. 44a and fracture surface in Fig. 44b. WC-Co-Cr particles were broken down and scattered inside the structure on the particle impact and then, fragmented. The hammering effect of WC-Co-Cr particles on the deformation of Ni-20Cr particles was also noticeable.

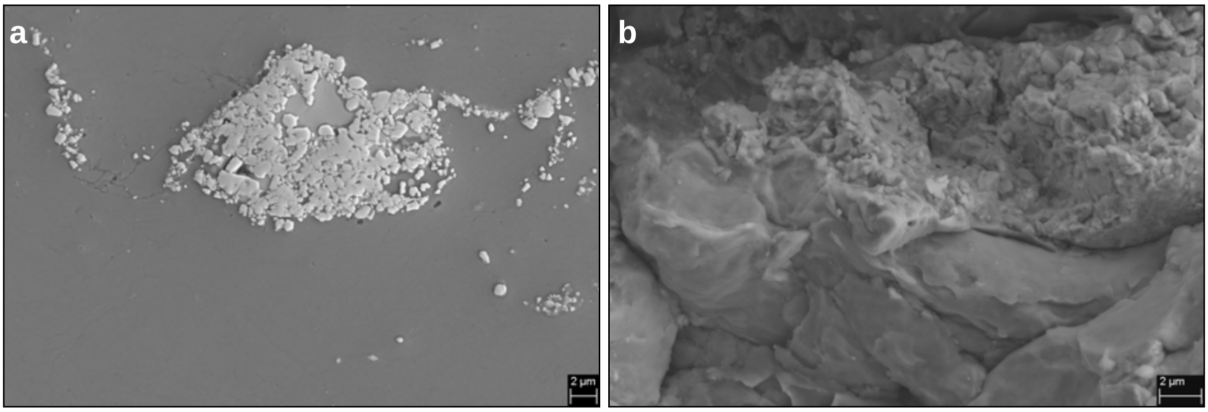

Figure 44. HPCS Ni-20Cr+30WC-10Co-4Cr coating: a) cross-sectional structure (heat-treated) and b) fracture surface. WC-Co-Cr particles broke down on the impact. FESEM images. [VI]

Bonding between dendritic Cu particles and hard Al_2O_3 particles is presented in fracture surface of LPCS Cu+Al_2O_3 coating in Fig. 45. Ceramic particles reinforced the structure by hammering and tamping the impacted surface and some of hard particles stuck to the surface. Localized deformation of Cu primary particles is observed in Fig. 45. However, also less deformed primary particles are detected in the structure of LPCS Cu+Al_2O_3 coating due to the fact that dendritic particles contain significantly finer primary particle size and thus, there are more particle boundaries for the deformation (more initial oxide layers to be removed). Moreover, powder particle boundaries were not clearly seen whereas primary particles were observed. [VII]

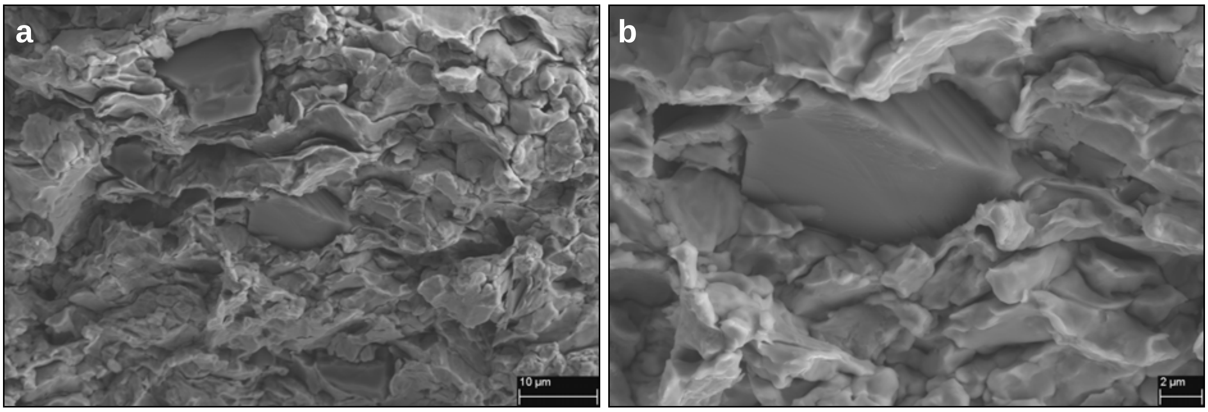

Figure 45. Fracture surfaces of LPCS Cu+Al_2O_3 coating: a) general overview and b) bonding between Cu and Al_2O_3 particles. FESEM images. [VII]

7.2.3 Particle deformation

In addition to the fracture behavior, fracture surface analysis reveals particle deformation. The dense coating structure contains highly deformed microstructure and inter-particle structures. The fracture surface of the fully dense HPCS Cu coating is presented in Fig. 46a. The fracture is partly brittle and partly ductile. In addition to the ductile behavior, due to the dynamic recrystallization [138] recrystallized grains are observed [V]. The HPCS Ta coating also had an overall dense structure. Figure 46b shows the high level of particle flattening due to the high deformation. However, grains inside differ from those inside the Cu particles; the Ta particles have columnar shapes. Material differences together with different powder types of Cu and Ta leads to different inter-particle behavior (recrystallized grains versus columnar grains).

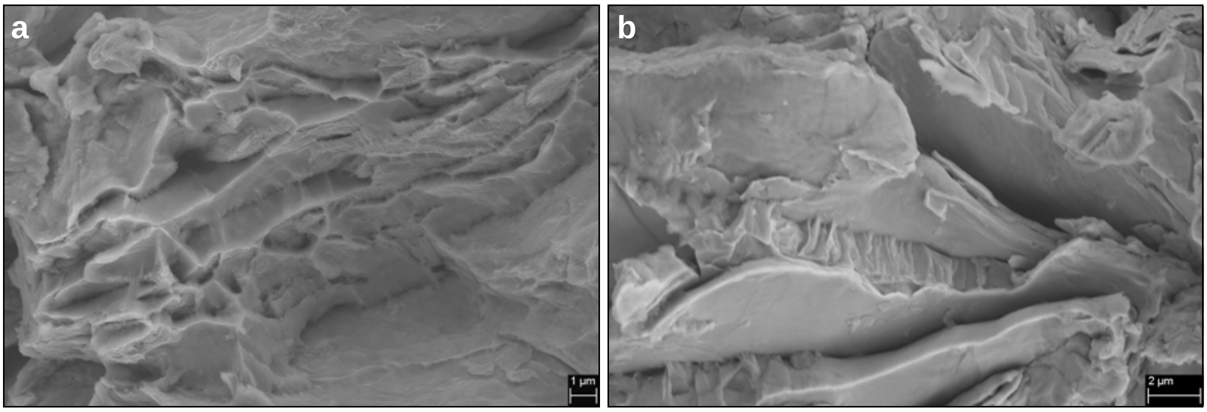

Figure 46. Fracture surfaces of HPCS a) Cu and b) Ta coatings. Highly deformed particles. FESEM images. [V]

The crossing points of HPCS Ni particles in as-sprayed and heat-treated state in the fracture surfaces are presented in Fig. 47. The structure became significantly more ductile after heat treatment due to recrystallization. Additionally, small-sized grains are detected in the fracture surface of heat-treated Ni coating, Fig. 47b. The same influence of heat treatment on the fracture behavior is observed in the case of Ni-20Cu coating, shown in Fig. 48. In the as-sprayed state, fracture is mostly brittle-type, whereas in the heat-treated state, it is mostly ductile-type (Fig. 48b). In addition, coating structure was densified during heat treatment due to the void reduction and recrystallization. [VI]

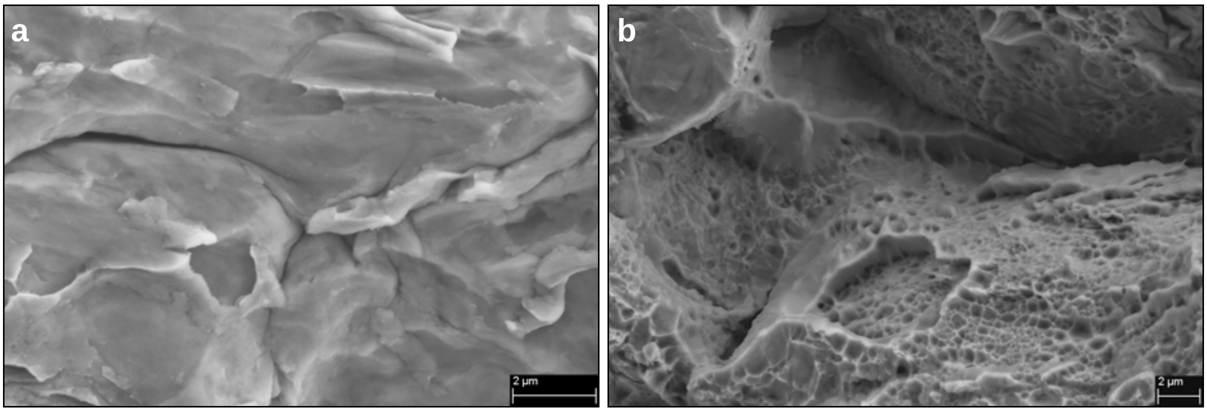

Figure 47. Fracture surface of HPCS Ni coating in a) as-sprayed and b) heat-treated state. Structure became more ductile during heat treatment. [VI]

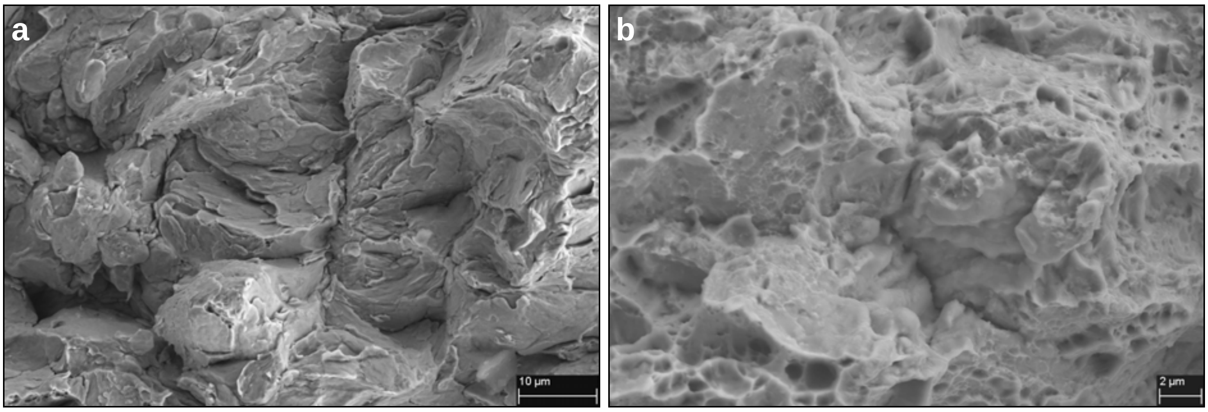

Figure 48. Fracture surface of HPCS Ni-20Cu coating in a) as-sprayed (mostly brittle-type fracture) and b) heat-treated (mostly ductile-type fracture) state. Structure is highly deformed. FESEM images. [VI]

Comparison between the coating structures of LPCS Cu coatings prepared from dendritic and spherical particles are shown in Figs. 49a and 49b, respectively. The fracture surface of dendritic Cu coating reveals the high number of primary particle boundaries and less deformed particles in the structure. Whereas spherical Cu particles are more deformed with flattened shapes and the coating contains less particle boundaries due to larger primary particle size. It should be noticed that these coatings are sprayed from pure Cu powders without Al_2O_3 addition. Furthermore, the hard particle addition leads to denser coating structure with higher deformation level of Cu particles due to the hammering effect of Al_2O_3 particles. The effect was stronger in the case of dendritic Cu particles than in the case of spherical Cu particles.

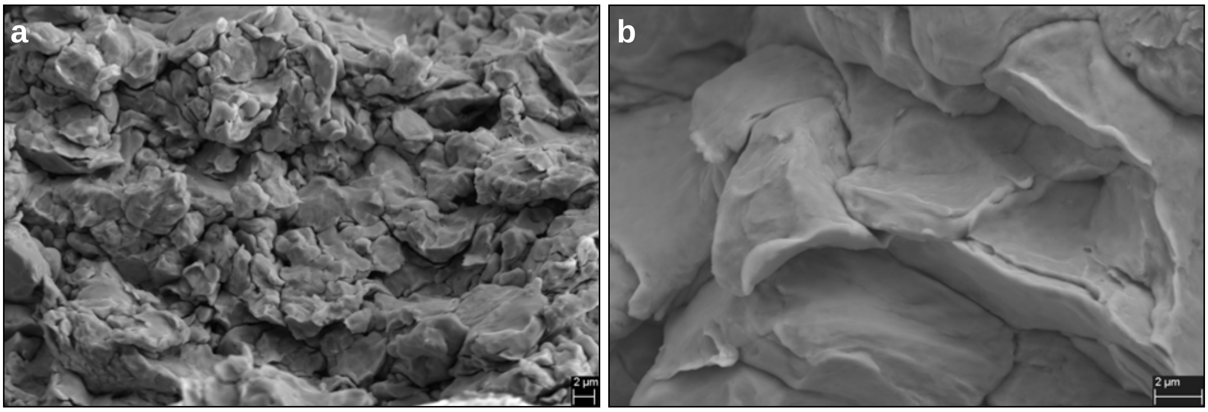

Figure 49. Fracture surfaces of LPCS Cu coatings a) prepared from dendritic Cu powder (Ecka) and b) prepared from spherical Cu powder (Osprey). FESEM images. [VII]

On particle impacts, particle deformation is a very crucial factor in order to produce dense coating structures. One important factor is the disruption and removal of continuous oxide layers from the particle surfaces. Adhesion between particles is tighter between metal-metal surfaces compared with the metal-oxide layer surfaces. Thus, metal-metal bonds should be dominant bonding mechanism for dense coatings. Oxide layers are removed from the surfaces in the gas flow, presuming the disruption of the layer. The TEM characterization proves a slight amount of oxygen (by EDS analysis) in some parts of the particle boundaries. However, pure metallic bonding was dominant and hence, the coating structure was tight and dense.

Metal-metal bonding performed tight and adherent particle boundaries. This is due to the localized particle and grain deformation. Adiabatic shear instability due to high contact pressure impact and thermal softening possesses formation of material jets to the connecting points of particle-substrate or particle-particle. In addition, material jets assist in the disruption of oxide layers from initial powder particle surfaces. Furthermore, one way to densify the metallic structure of cold-sprayed coatings was to add hard particles into the metallic powder. Densification was clearly detected both in the HPCS and LPCS coatings. Obviously, bonds between metallic particles are tighter than metallic-ceramic bonds; however, ceramic particles increase particle deformation of metallic particles by hammering the structure and by activating the sprayed surface. Due to the fact that the amount of ceramic particles is relatively low in the coating in comparison with the initial powder mixture, most of the ceramic particles rebound and do not adhere to the structure and thus, they activate the surface. Furthermore, attached hard particles are stuck to the metallic matrix of the coating. To sum up, low amount of parts of oxide layers and few embedded hard particles do not hinder the impermeability of the coating structure as long as the most dominant particle bonding is metal-metal bonding.

7.3 Macroscopic properties of cold-sprayed coatings

Here, mechanical properties, hardness, and bond strength, are presented. These macroscopic properties reflect to deformation level generated during spraying due to work and strain hardening and plastic deformation.

7.3.1 Microhardness

Highly deformed and tightly bonded structures of the HPCS Cu and Ta coatings were observed with FESEM and TEM characterizations. In addition to these, a high level of plastic deformation causes work hardening in the coating structure. While, high hardness indicates work hardening. Hardness of the HPCS Ta coating was 230 $HV_{0.3}$ and of Ta bulk material 100 $HV_{0.3}$ [139]. The same trend was detected also with the HPCS Cu compared with the Cu bulk material, 150 $HV_{0.3}$ versus 80 $HV_{0.3}$ [139]. In both coatings, increment of the coatings' hardness was significant, indicating strain hardening and work hardening resulted from plastic deformation. In hardened material, dislocation density increases, making connection between work hardening (increased hardness) and highly deformed microstructure (high dislocation density). [77]

For the HPCS Ni-20Cr coating, hardness was 240 $HV_{0.3}$ and between 320 - 340 $HV_{0.3}$ for the HPCS Ni-20Cr+Al_2O_3 coatings [III]. The Al_2O_3 particles affected the hardness by increasing its value; this effect arises from hardening and reinforcing by the hard particles. This effect was clearly detected. In hardness measurements, the indentations were taken from the metallic coating areas in order to evaluate the behavior of the metallic Ni-20Cr particles. High hardness of the Ni-20Cr+Al_2O_3 coatings can be reflected to their high work hardening level [106]. More hardening (compacting effect of Al_2O_3 particles) occurred at higher particle velocities [43] caused by high gas temperature. Comparison of the Ni-20Cr and Ni-20Cr+Al_2O_3 coatings revealed that, the Al_2O_3 particle addition together with a high gas temperature had a pronounced effect on microstructural properties and on hardness values.

Hardness of the Ni bulk material was 118 $HV_{0.3}$, of Ni-20Cr bulk material 202 $HV_{0.3}$, and of Ni-30Cu bulk material 147 $HV_{0.3}$. In every case, the HPCS coatings have significantly higher hardness, Table 5, compared with corresponding bulk materials, shown above. It should be noticed that the HPCS Ni-20Cr coating had not as high hardness increment than Ni and Ni-20Cu coatings had. However, with hard particle addition, hardness of metallic part increased due to the densifying effect of hard particles by hammering the structure for higher plastic deformation. As detected in the microstructural characterization, the Ni-20Cr coating contained porosity in its structure. In addition, the hardness of Ni and Ni-20Cu coatings was significantly decreased after heat treatment due to the fact that coatings were in a softer state caused by recovery and recrystallization. However, the hardness of Ni-20Cr, Ni-20Cr+50Al_2O_3, and Ni-20Cr+30WC-10Co-4Cr coatings were at the same level when comparing the as-sprayed and heat-treated coatings with each other. This is possibly caused by the oxygen content of the coatings resulting in weak points in the particle boundaries. The effect of oxidized areas was probably higher than recovery and thus, hardness was not decreased after heat treatments. Moreover, the hardness of Ni-20Cr with added hard particles was higher than that of pure Ni-20Cr (measurements were done from the metallic part of the coating), indicating the hardening by hard particles.

Table 5. Vickers hardness ($HV_{0.3}$) of HPCS Ni, Ni-20Cu, Ni-20Cr, Ni-20Cr+50Al_2O_3, and Ni-20Cr+30WC-10Co-4Cr coatings in as-sprayed and heat-treated states. [VI]

	Vickers hardness $HV_{0.3}$	
Coating	**As-sprayed**	**Heat-treated**
HPCS Ni	238	124
HPCS Ni-20Cu	266	185
HPCS Ni-20Cr	247	308
HPCS Ni-20Cr+50Al_2O_3	398	372
HPCS Ni-20Cr+30WC-10Co-4Cr	388	387

The powder type and composition have a strong effect on hardening of the powder particles in the LPCS process, Table 6. It should be noticed that an indentation was taken from a metallic area of the coating in order to analyze the behavior of metallic Cu particles and the effect of Al_2O_3 particles on it. The LPCS Cu coating prepared from dendritic Cu (E_Cu) particles has lower hardness than the coating sprayed from spherical Cu (O_Cu) particles. Furthermore, hardness increases with increasing amount of Al_2O_3 particle addition, indicating high deformation and thus, higher hardening effect. Denser powder particles with higher primary particle size can explain this effect due to the fact that spherical particles undergo higher level of plastic deformation. Thus, probability to have a lower number of weak particle boundaries is higher due to higher particle size.

Table 6. Vickers hardness ($HV_{0.3}$) of LPCS Cu and Cu+Al_2O_3 coatings. [VII]

Coating	**Vickers hardness $HV_{0.3}$**
E_Cu (dendritic)	83
E_Cu+10Al_2O_3	95
E_Cu+30Al_2O_3	96
E_Cu+50Al_2O_3	103
O_Cu (spherical)	106
O_Cu+10Al_2O_3	113
O_Cu+30Al_2O_3	127
O_Cu+50Al_2O_3	127

In cold spray processes, powder particles undergo relatively high level of plastic deformation which is reflected to the high hardness values of the coatings. The high hardness is proven with comparison between coatings and bulk materials. Also, the addition of hard particles increases the hardness of the metallic regions of the coatings by hammering and tamping the structure. This effect of hard particles on the hardness and thus, on work hardening and deformation level is clearly observed with all metallic-ceramic mixture coatings independently on the spraying process.

7.3.2 Bond strength

The bond strengths (adhesion strengths) of the Ni-20Cr+Al_2O_3 coatings were 25 - 38 MPa [III], and for Ni-20Cr, it was 31 MPa [99]. In all cases, failure occurred at the interface between coating and substrate, indicating the adhesive-type bond strengths. Because Al_2O_3 particle addition to the metallic Ni-20Cr powder only slightly affected the adhesion strength, it can be concluded that in all cases, with and without the addition of Al_2O_3 particles, the adhesion strengths between the Ni-20Cr coatings and substrates were acceptable, indicating a reasonable adhesion between coatings and substrates. Bond strength of HPCS Ni was 20 MPa, of Ni-20Cu, it was 25 MPa, and for Ni-20Cr+30WC-10Co-4Cr coating 32 MPa. In addition, the bond strength of the HPCS Ta coating was 32 MPa [120]. Meanwhile, the bond strengths of the HPCS Cu were 29-36 MPa on Cu substrate [99]. Also these bond strengths are reasonable, indicating rather good bonding between the coating and substrate. Furthermore, it should be noticed that failure occurred at the coating-substrate interfaces in the HPCS coatings, them being the weakest points in the coating-substrate combination. This indicates higher strength between particles (cohesive strength) than these adhesion strengths.

Bond strengths of the LPCS Cu and Cu+Al_2O_3 coatings were also reasonable and increased with the increasing amount of added Al_2O_3 particles. In addition, bond strengths of the Cu coatings prepared from spherical particles were higher than those of coatings sprayed with dendritic Cu powder. In addition, bond strengths were cohesive or cohesive/adhesive-type in dendritic coatings, whereas fractures occurred at the coating-substrate interface in the coatings prepared from spherical particles, indicating adhesive-type bond strength. Bond strength of LPCS Cu prepared from dendritic powder was 8 MPa and with 50% Al_2O_3 particle addition, 18 MPa. Meanwhile, bond strength of LPCS Cu prepared from spherical powder was 13 MPa and with 50% Al_2O_3 particle addition it was 32 MPa. Improvement of adhesion was significant and therefore, bond strengths of Cu+Al_2O_3 mixture coatings are reasonable, in the range of 20-30 MPa. [VII] The Al_2O_3 particle addition has activation effect, causing cratering of the substrate which in turn, helps to achieve higher adhesion between coating and substrate by increasing the impact surface [91].

7.4 Corrosion resistance of cold-sprayed coatings

Denseness is the first criterion for the corrosion resistance of coatings which are nobler than substrate material. In this study, all coating materials (Cu, Ta, Ni, Ni-Cu, and Ni-Cr) are nobler than steel substrate. Denseness means impermeability of the coatings, indicating coating structures without existing through-porosity. Denseness, or on the other hand, existing through-porosity, is identified by using corrosion tests. The open-cell potential measurements and salt spray (fog) tests were chosen for the denseness evaluations. Because coatings used in this study are not corroded by seawater whereas substrate material does [115], the open-cell potential measurements using salt solution and salt spray tests are good methods for testing coating's impermeability. In addition, anodic polarization measurements were carried out in order to indicate corrosion resistance and corrosion properties of the HPCS Ta coatings.

7.4.1 Denseness

Open-cell potential measurements show existence of through-porosity in the coating structures. If the open-cell potential value of the coating approaches the value of the corresponding bulk material, it indicates impermeable and dense coating structure. However, if the value of the coating approaches the value of the substrate material (here Fe52), it reflects the through-porosity in the coating structure. In such situation, testing liquid has an open access to penetrate from the surface of the coating to the interface between coating and substrate, it will corrode the substrate, and corrosion products will come up to the surface. Figure 50 indicates overall dense coating structures of the HPCS Cu (-35+15 µm) and Ta coatings, having a similar open-cell potential behavior with corresponding bulk materials. According to microscopic analysis and corrosion tests, the structure of these coatings is fully dense resulting from the optimal combination of powder and spraying parameters. The coatings remained stable in the long-time exposure, indicating their structural durability [V]. In addition, fully dense structures of HPCS Cu coatings prepared from two other powders (-38+11 µm and -30+10 µm) were also verified with open-cell potential measurements in [I]. In addition, salt spray tests showed an overall dense structure of HPCS Ta coating, no changes were detected on the coating surface after 240-h exposure [IV].

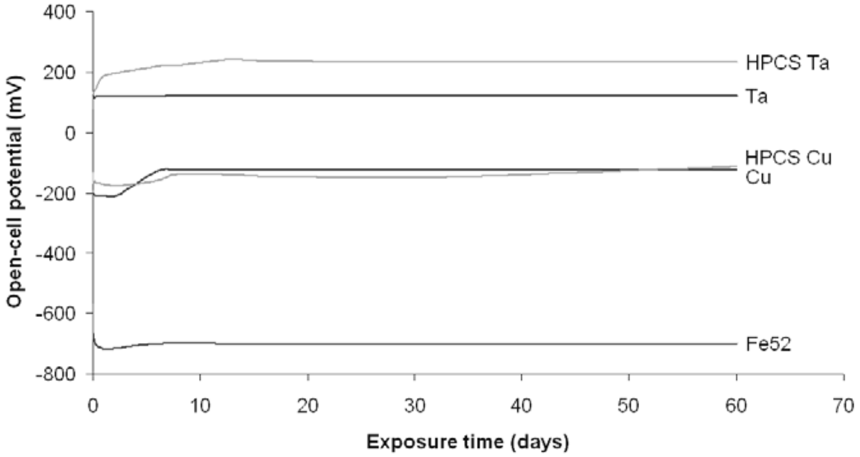

Figure 50. Open-cell potentials of HPCS Ta and Cu coatings, Ta and Cu bulk materials and Fe52 substrate material as a function of exposure time in 3.5%NaCl solution. Ag/AgCl reference electrode. [V]

Open-cell potentials of as-sprayed and heat-treated HPCS Ni and Ni-20Cu coatings are also closer to the bulk materials (Ni and Ni-30Cu) than to the substrate material (Fe52), Fig. 51. In addition, the denseness of these coatings was improved with heat treatments, which is also seen in the open-cell potential behavior; values of these coatings are even closer to the bulk materials. Heat treatment densified the coating structures due to recovery, recrystallization, and void reduction by the softening and rearrangement of grains [I, VI]. Number 2 indicates the optimized spraying parameters used. More information about effect of spraying parameters on the denseness of HPCS Ni and Ni-20Cu coatings can be found in [VI]. The denseness of HPCS Ni coatings was improved with right spraying parameters, more details in [VI]. With lower traverse speed together with higher beam distance (distance between two adjacent spray beads), the structure became denser due to the fact that this combination induced high particle deformation and thus, tight particle boundaries (without weak bonds) into the structures. In addition, the denseness improvement of HPCS Ni coating by heat treatment was detected [I].

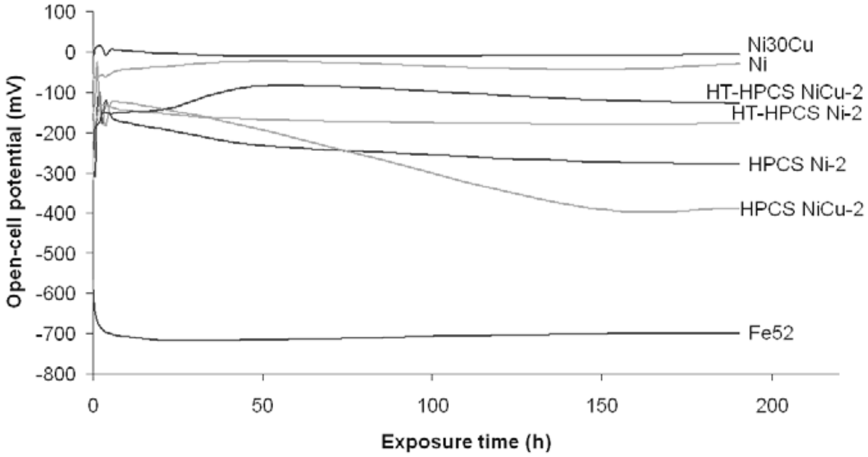

Figure 51. Open-cell potentials of as-sprayed and heat-treated HPCS Ni and Ni-20Cu coatings, Ni and Ni-30Cu bulk materials and Fe52 substrate material as a function of exposure time in 3.5%NaCl solution. Ag/AgCl reference electrode. [VI]

Nickel alloy coatings give protection against wet corrosion to steel substrate; however, due to their behavior as nobler material than steel, giving the anodic protection, dense coating structure is required. Figure 52 shows open-cell potentials of HPCS Ni-20Cr, Ni-20Cr+50Al_2O_3, and Ni-20Cr+30WC-10Co-4Cr coatings in the as-sprayed and heat-treated state. The HPCS Ni-20Cr coating contained through-porosity. Moreover, heat treatment did not densify the structure of the Ni-20Cr coating. Their open-cell potentials were close to that of Fe52 substrate material. One way to improve the denseness of the Ni-20Cr coating was to add hard particles into the metallic powder. Addition of Al_2O_3 and WC-10Co-4Cr particles showed significant improvement of denseness of the Ni-20Cr coatings. In addition, heat treatment increased the denseness of Ni-20Cr+Al_2O_3 coating whereas heat treatment did not affect the denseness of the Ni-20Cr+WC-10Co-4Cr coating, as seen in Fig. 52. [VI] WC-Co-Cr was chosen because of it has better corrosion resistance than WC-Co [140].

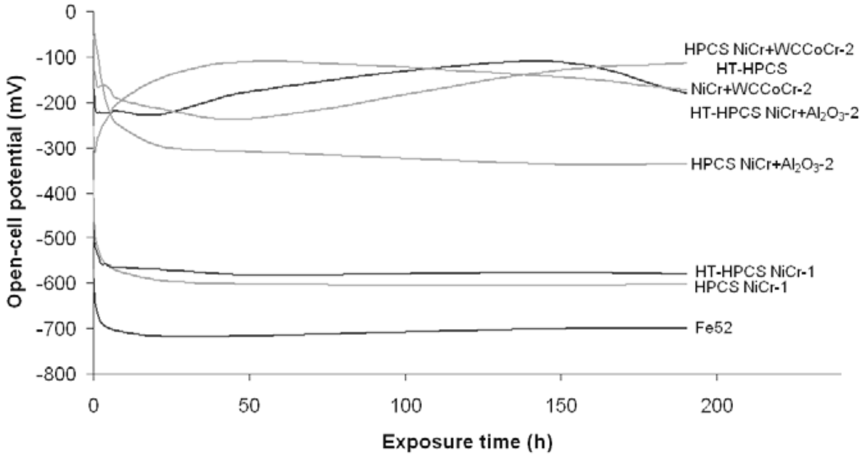

Figure 52. Open-cell potentials of as-sprayed and heat-treated HPCS Ni-20Cr+30WC-10Co-4Cr, Ni-20Cr+50Al_2O_3 and NiCr coatings and Fe52 substrate material as a function of exposure time in 3.5%NaCl solution. Ag/AgCl reference electrode. [VI]

Salt spray test is the complementary test to evaluate existing through-porosity in the coating structures. As was observed in the open-cell potential measurements [III], Ni-20Cr coating contained through-porosity. On the other hand, densifying effect of Al_2O_3 particle addition was noticeable after salt spray test. Figure 53 shows the coating surfaces of Ni-20Cr and Ni-20Cr+50Al_2O_3 coatings after 48-h salt spray test [III]. The amount of corrosion spots on the surface was significantly decreased with Ni-20Cr+Al_2O_3 mixture coating from 45.5% (Ni-20Cr) to 0.8% (Ni-20Cr+50Al_2O_3, -90+45 μm) [III].

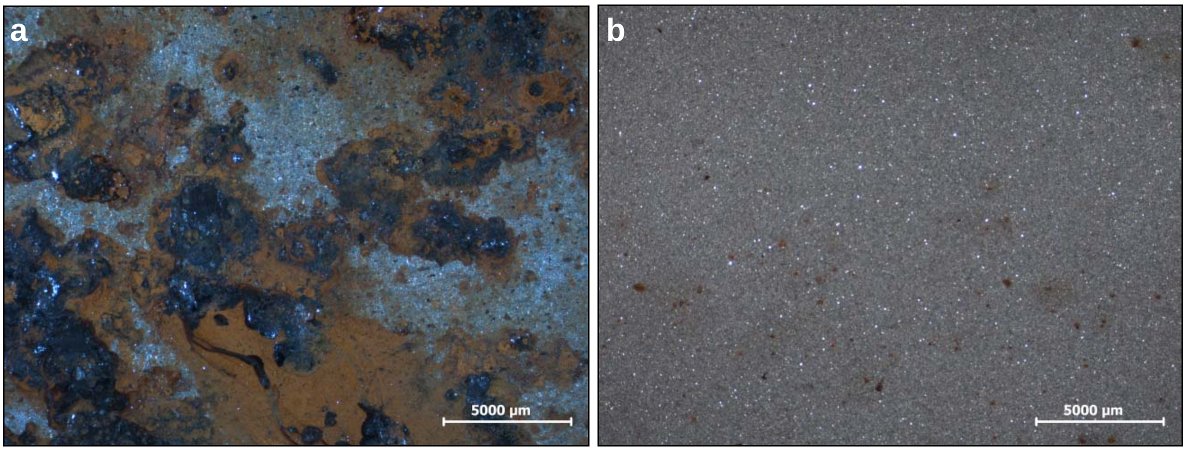

Figure 53. Coating surfaces of HPCS a) Ni-20Cr and b) Ni-20Cr+50Al_2O_3 coatings after 48-h salt spray test. SM images. [III]

The HPCS Ni coating was dense according to salt spray test, having very low amount of corrosion spots on its surface whereas Ni-20Cu coating became denser after heat treatment. The amounts of corrosion spots on the coating surfaces after 96-h salt spray test by image analysis (ImageJ) are summarized in Table 7. The HPCS Ni-20Cr coating was totally corroded; however, densifing effect of hard particles was clearly observed with Al_2O_3 particle addition.

Heat treatment densified the structure of HPCS Ni, Ni-20Cu, and Ni-20Cr+50Al_2O_3 coatings which is detected in the amount of corrosion spots on the surfaces after salt spray tests. The HPCS Ni-20Cr coatings contained over-amount defects in their structures and thus, not even heat treatment was able to densify the structure. Heat treatment did not densified the HPCS Ni-20Cr+WC-Co-Cr coatings whereas process parameters had strong influence on denseness of these coatings (is shown in publication VI). The denseness (through-porosity) behavior of HPCS Ni-20Cr+30WC-Co-Cr coatings after heat treatments needs further investigations to explain different behavior compared with Ni-20Cr coatings with the addition of Al_2O_3 particles.

Table 7. Amount (%) of corrosion spots on the surface of the HPCS Ni, Ni-20Cu, Ni-20Cr, Ni-20Cr+50Al_2O_3, and Ni-20Cr+30WC-10Co-4Cr coatings after 96-h salt spray test by image analysis. [VI]

	Corrosion spots (%)	
HPCS coating	**As-sprayed**	**Heat-treated**
Ni	0.8	0.1
Ni-20Cu	34.7	11.3
Ni-20Cr	98.5	98.9
Ni-20Cr+50Al_2O_3	12.7	8.5
Ni-20Cr+30WC-10Co-4Cr	24.7	30.0

Summing up, the HPCS Ni coating has a highly dense structure and it was further densified by heat treatments. Also in the case of HPCS Ni-20Cu coating, heat treatment significantly densified the structure. However, the structure still contains some weak points which can be explained by oxidized particle boundaries, in other words, some parts were not deformed enough in order to remove oxide layers from initial powder particles. In spite of that, the denseness improvement was remarkable. In addition, the hard particle addition mixed with Ni-20Cr powder showed notable denseness improvement as analyzed by corrosion tests. [VI]

The open-cell potential measurements and salt spray tests showed that the LPCS Cu and Cu+Al_2O_3 coatings contained through-porosity in their structures. Open-cell potentials of the coatings were close to the values of Fe52 substrate material [II, VII]. Regardless, in the LPCS process, powder type and composition had strong influence on the denseness of the Cu and Cu+Al_2O_3 coatings. Denseness of the coatings was improved with Al_2O_3 particle addition. Table 8 summarizes the amounts of corrosion spots after salt spray test on the coating surfaces analyzed by image analysis (ImageJ). In the E_Cu and E_Cu+Al_2O_3 coatings, denritic Cu particles were used, whereas spherical Cu particles were used in O_Cu and O_Cu+Al_2O_3 coatings. The LPCS Cu coatings prepared from spherical feedstock had a denser structure compared with coatings prepared from dendritic feedstock. These results indicate that bonds between particles were tighter in these O_Cu coatings than in E_Cu coatings. Moreover, the denseness was improved most with 10 vol.-% Al_2O_3 particle addition to the spherical powder and with 30 vol.-% Al_2O_3 particle addition to the dendritic powder. This indicates that optimal composition of metallic and ceramic particles in the powder mixture depends on sprayed material combination and powder type of metallic particles.

Table 8. Amount (%) of corrosion spots on the surface of the LPCS Cu and Cu+Al_2O_3 coatings after 96-h salt spray test by image analysis. [VII]

Sample	Corrosion spots (%)
E_Cu (dendritic)	94.5
E_Cu+10 vol.%Al_2O_3	73.0
E_Cu+30 vol.%Al_2O_3	59.4
E_Cu+50 vol.%Al_2O_3	68.5
O_Cu (spherical)	38.9
O_Cu+10 vol.%Al_2O_3	19.2
O_Cu+30 vol.%Al_2O_3	32.1
O_Cu+50 vol.%Al_2O_3	31.3

7.4.2 Corrosion properties

The anodic polarization measurements were performed in order to characterize the polarization behavior of the HPCS Ta coating in comparison with Ta bulk material. Open-cell potential measurements and salt spray fog tests already confirmed an overall dense structure of the HPCS Ta coating (CS Ta2 [IV]). The CS Ta1 coating with through-porosity was also tested for a comparison between dense coating (CS Ta2) and coating (CS Ta1) with through-porosity. Figure 54 shows polarization behavior in 3.5% NaCl and Fig. 55 in 40%H_2SO_4 solutions.

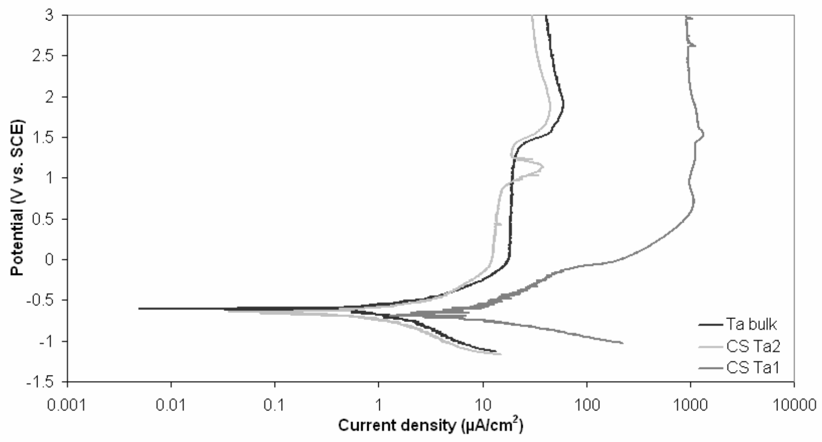

Figure 54. Polarization behavior of tantalum bulk material and HPCS Ta coatings in 3.5-wt.% NaCl solution at 22ºC. CS Ta2 is an improved coating and CS Ta1 a standard coating. [IV]

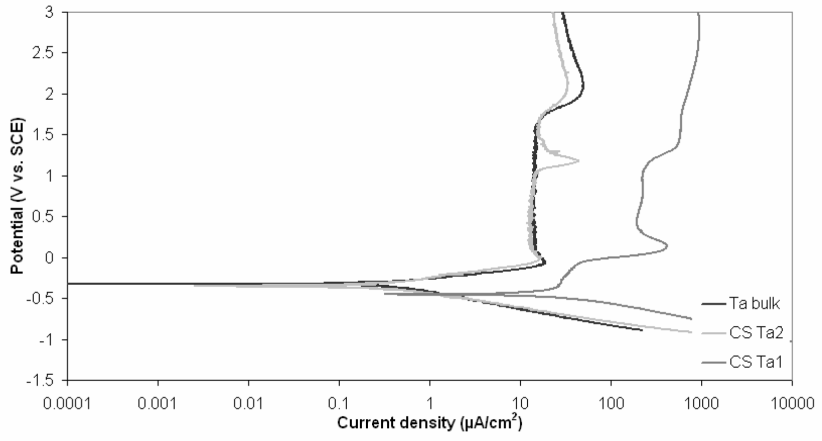

Figure 55. Polarization behavior of tantalum bulk material and HPCS Ta coatings in 40-wt.% H_2SO_4 solution at 22ºC. CS Ta2 is an improved coating and CS Ta1 a standard coating. [IV]

Tantalum gets passivated rapidly, as shown by its polarization curves in NaCl and H_2SO_4 solutions, transforming linearly and quickly from active to passive with increasing potential, indicating material stability. The CS Ta2 coating behaved like the bulk material. However, the CS Ta1 coating did not behave in a stable manner because of its through-porosity. Test solution reacted the steel substrate, thus anodic polarization was resulted from combination of behavior of steel substrate and CS Ta1 coating. This indicates possible instability of the passivation layer and thus, provides poor corrosion protection. Ta bulk material and dense HPCS Ta coating got passivated rapidly, and above their passivation potential, corrosion rate falls to very low value in the passive area due to the stable passive layer [112].

Tafel extrapolation was done to determine the corrosion potential E_{corr}, passivation potential E_{pp}, corrosion current density i_{corr}, and the passivation current density i_{pp} of the tantalum bulk material and the HPCS Ta (CS Ta2) coating in both NaCl and H_2SO_4 solutions at 22ºC and at 80ºC. Results are shown in Table 9.

Table 9. Corrosion potential E_{corr}, corrosion current density i_{corr}, passivation potential E_{pp}, and passivation current density i_{pp} of tantalum bulk material and CS coatings in 3.5-wt.% NaCl and 40-wt.% H_2SO_4 solutions analyzed by Tafel extrapolation. [IV]

Sample	Solution	T (ºC)	E_{corr} (V)	i_{corr} (µA/cm^2)	E_{pp} (V)	i_{pp} (µA/cm^2)
Ta bulk	NaCl	22	-0.66	1.1	0	16
HPCS Ta	NaCl	22	-0.67	1.1	0.05	11
Ta bulk	NaCl	80	-0.68	0.5	-0.25	20
HPCS Ta	NaCl	80	-0.66	0.6	0.05	13
Ta bulk	H_2SO_4	22	-0.32	0.4	0.08	12
HPCS Ta	H_2SO_4	22	-0.33	0.3	0.10	12
Ta bulk	H_2SO_4	80	-0.34	0.8	0.04	15
HPCS Ta	H_2SO_4	80	-0.30	2.0	0.05	15

The HPCS Ta coating, prepared from improved powder with advanced spraying equipment, behaved like bulk tantalum, indicating resistance to corrosion. The HPCS Ta coating and bulk material showed wide-ranging passivation, characteristic of stable passive behavior [141]. According to the polarization curves in both NaCl and H_2SO_4 solutions at room temperature and elevated temperature, the passivation of dense HPCS Ta coating was first linear, then curving slightly (possibly because of pit corrosion), followed by another stretch of linear passivation at higher potential (passive layer formation). This is due to the materials' ability to be repassivated. A pit may result from a failure in the passive layer [112,115], but when pits are insignificant, reparation or repassivation and thus, re-protection may occur in the protective passive layer [115]. At a high potential of about 1.2 V, coating (CS Ta2) showed unstable passivation; however, at an even higher potential the coating got repassivated. Balani et al. [37] have reported similar repassivation of cold-sprayed aluminum coatings. In fact, pitting corrosion may occur also in a transpassive area [141], and impurities may cause breaks in the passive layer [113]. With some metals, passivation depends on pH and the potential [113], but the highly protective oxide layer of tantalum remains stable at all pH and potential values [112].

In summary, overall and fully dense and impermeable Ta coatings can be produced by using the HPCS system. This will be a major advantage for corrosion resistance. The HPCS Ta coatings act like real corrosion barrier coatings and can thus, be used in applications where corrosion protection is needed.

8 CONCLUDING REMARKS AND SUGGESTIONS FOR FUTURE WORK

Cold spraying enables the production of overall dense coatings with porosity-free and pure (without oxidation) coating structures. Cold-sprayed coatings with impermeable structures have high potential to be used in corrosion protection. In this work, denseness improvement was performed in three ways: 1) by optimized powder-spraying parameters combination (Cu, Ta, Ni), 2) by adding hard particles to metallic powder (Ni-20Cr+Al_2O_3, Ni-20Cr+WC-10Co-4Cr, Cu+Al_2O_3), and 3) by heat treatments (Ni-20Cu). High plastic deformation together with metal-metal bonding is required for the denseness of cold-sprayed coatings. Although structure appears dense by microscopic evaluation, corrosion tests reveal impermeability, showing the existence/absence of through-porosity. Impermeability of the coatings is crucial and therefore, it could be said that microstructure defines corrosion protection capability of the cold-sprayed coatings. As a conclusion, cold-sprayed coatings have dense structures, high hardness due to the work hardening and reasonable bond strengths. Furthermore, it is worth noticing that hard particle addition affects in addition to structure, also the mechanical properties by increasing hardness of the metallic parts of the coatings and by improving bond strengths.

1) Optimized powder-spraying parameters combination

The HPCS Cu and Ta coatings possessed fully dense and overall impermeable coating structures according to both microstructural characterization and corrosion tests. In addition, the HPCS Ni coating had a dense structure. These are significant advantages, having possibility to use them in applications where corrosion resistance is needed. Powder characteristics had a very strong influence on the coating formation and hence, on the coating structure. The overall dense coating structure requires high level of plastic deformation, adiabatic shear instability conditions on the impacts and thus, material jet formation. In addition, tight bonds between particles and metal-metal bonding are required for the production of dense coatings and furthermore, acting as real corrosion barrier coatings. The optimal combination is material-dependent and process-dependent and it should be optimized separately for each case depending on the desired properties and functions of the coatings. In addition to the corrosion protectiveness, HPCS Ta coating behaved like the tantalum bulk material in the anodic polarization tests with rapid passivation and high passivation range, indicative of its corrosion resistance. Generally, Ta is typically used when extreme corrosion resistance is required and for that, denseness of the coatings is the first criterion for real corrosion protection. Therefore, it can be said that high-pressure cold spraying proves its potential in the production of uniformly dense and corrosion protective coatings. On the other hand, cold-sprayed Cu coatings are typically used in applications where electrical or thermal conductivity is needed. For applications of this kind, high purity and denseness of the coatings are advantageous properties.

Due to the fact that coating properties, especially denseness, depend strongly on powders and process parameters, the further development will focus on continuing optimization. The key words in future work are tailored powders with advanced methods. The powder development is going towards high purity and narrow particle size distribution whereas the development of the process itself is going towards even higher process temperatures and effectiveness (e.g., the latest development stage: Kinetiks 8000 with 1000ºC preheating temperature of N_2 [136]). Future work will concentrate on finding new materials and powders from which it is possible to produce fully dense cold-sprayed coatings with the optimal powder-spraying parameters combinations. In addition, the corrosion research of the cold-sprayed coatings and testing with more aggressive environments would be one of next steps.

2) Hard particle addition

The structures of the HPCS Ni-20Cr coatings showed prevalent through-porosity, as demonstrated by corrosion tests. The solution for that was to add hard particles into the Ni-20Cr powder. The hard particle addition (Al_2O_3 and WC-10Co-4Cr particles) into the metallic powder showed significant denseness improvement. Generally, the composition of the powder depends on the desired properties required for the coating. Addition of ceramic particles affected the properties of the coating deposited by HPCS process. On the other hand, Al_2O_3 particles mixed with metal alloy powder also had a spraying technical effect on the process parameters, enabling the use of higher gas temperatures without nozzle clogging. Hard particle addition has three functions: 1) to keep the nozzle clean, 2) to activate the sprayed surface, and 3) to reinforce the sprayed coating structure. Moreover, it was found that Al_2O_3 particles embedded into the structure of Ni-20Cr coatings whereas WC-Co-Cr particles broke down and stuck into the structure. However, both particle additions made the structure of the HPCS Ni-20Cr coating denser due to the fact that higher gas temperature could be used and due to the hammering and tamping the coating structure.

The LPCS process is a relevant method of preparing Cu and Cu+Al_2O_3 coatings. Also in here, powder characteristics and compositions affected the denseness. LPCS Cu and Cu+Al_2O_3 coatings prepared from spherical Cu particles contained less through-porosity in their structures compared with coatings prepared from dendritic particles, indicating denser coating structures. The dendritic particles have more boundaries in their structures, increasing the probability of weak bonds between the particles. Denser powder particles with higher primary particle size can be explained with the higher level of plastic deformation of the spherical particles. Thus, probability to have a lower number of weak particle boundaries is higher due to higher particle size. Moreover, it was also possible to produce pure Cu coatings from both spherical and dendritic feedstock by using the LPCS process. All in all, with the hard particle addition coating quality can be improved. This work clearly showed more deformed and denser coating structure of the LPCS Cu+Al_2O_3 coatings compared with the LPCS Cu coatings.

As stated, it is not always possible to manufacture overall dense microstructures of pure metallic coatings by using cold spraying. One solution to improve denseness is to add hard particles or to use powder mixtures in order to improve the quality of the coatings. In future, research will focus on finding new material compositions and powder mixtures for the production of composite coatings with optimal properties. In addition, powder and material mixing can open new possibilities with combined properties from all components.

3) Heat treatments

Cold spraying has proven to be an optimal thermal spray method in order to prepare fully dense or low-porosity coatings from metallic or metallic-ceramic composite mixture powder feedstock. In an optimal situation, fully dense coating structures can be manufactured with the optimal combination of powder and spraying parameters. In the contrast to this, if the optimal combination is not achieved, structural details could be improved with post-treatments. Denseness of HPCS Ni and Ni-20Cu coatings was improved with heat treatments. Heat-treated Ni and Ni-20Cu coatings were in a softer state due to void reduction, recovery and recrystallization. In addition, the degree of through-porosity was significantly reduced after heat treatments. Densification and denseness improvement by heat treatments were illustrated with the corrosion tests. Next, a possibility to improve the denseness of LPCS coatings with heat treatments will be investigated.

REFERENCES

[1] V. Champagne, Ed., 2007, *The Cold Spray Materials Deposition Process: Fundamentals and Applications*, Woodhead Publishing Ltd., Cambridge, England, 362 p

[2] A. Papyrin, V. Kosarev, S. Klinkov, A. Alkimov, V. Fomin, 2007 *Cold Spray Technology*, 1st ed., Elsevier, printed in the Netherlands, 328 p

[3] M. Grujicic, C. Zhao, C. Tong, W. DeRosset, D. Helfritch, Analysis of the impact velocity of powder particles in the cold-gas dynamic-spray process, *Mat. Sci. Eng. A*, 368, 2004, p 222-230

[4] R. Dykhuizen, M. Smith, Gas Dynamic Principles of Cold Spray, *J. Therm. Spray Technol.*, 7(2), 1998, p 205- 212

[5] C. Borchers, F. Gärtner, T. Stoltenhoff, H. Assadi, H. Kreye, Microstructural and Macroscopic Properties of Cold Sprayed Copper Coatings, *J. Appl. Phys.*, 93(12), 2003, p 10064-10070

[6] R. Maev, V. Leshchynsky, Air Gas Dynamic Spraying of Powder Mixtures: Theory and Application, *J. Therm. Spray Technol.*, 15(2), 2006, p 198-205

[7] T. Van Steenkiste, J. Smith, R. Teets, J. Moleski, D. Gorkiewicz, R. Tison, D. Marantz, K. Kowalsky, W. Riggs, II, P. Zajchowski, B. Pilsner, R. McCune, K. Barnett, Kinetic spray coatings, *Surf. Coat. Technol.*, 111, 1999, p 62-71

[8] V. Sobolev, J. Guilemany, J. Nutting, 2004, *High Velocity Oxy-Fuel Spraying, Theory, Structure-Property Relationships and Applications*, Maney Publishing, London, UK, 397 p

[9] T. Stoltenhoff, H. Kreye, H. Richter, An Analysis of the Cold Spray Process and its Coatings, *J. Therm. Spray Technol.*, 11(4), 2001, p 542-550

[10] Cordon England, website, http://www.gordonengland.co.uk/tsc.htm, referred 2009.

[11] L. Pawlowski, 1995, *The Science and Engineering of Thermal Spray Coatings*, John Wiley & Sons Ltd., New York, USA, 414 p

[12] S. Veräjänkorva, J. Lagerbom, P. Vuoristo, Influence of Powder Type and Properties on Ceramic Layer Deposition by Cold Spraying, *Thermal Spray 2006: Building on 100 Years of Success*, B. Marple, M. Hyland, Y.-C. Lau, R. Lima, J. Voyer (Eds.), May 15-18 (Seattle, Washington, USA), ASM International, 6 p

[13] J. Vlcek, L. Gimeno, H. Huber, A Systematic Approach to Material Eligibility for the Cold Spray Process, *Thermal Spray 2003: Advancing the Science & Applying the Technology*, C. Moreau, B. Marple (Eds.), May 5-8, (Orlando, Florida; USA), ASM International, p 37-44

[14] H.-Y. Lee, Y-H. Yu, Y.-C. Lee, Y.-P. Hong, K.-H. Ko, Interfacial studies between cold-sprayed WO_3, Y_2O_3 films and Si substrate, *Appl. Surf. Sci.*, 227, 2004, p 244-249

[15] C.-J. Li, G.-J. Yang, X.-C. Huang, W.-Y. Li, A. Ohmori, Formation of TiO_2 photocatalyst through cold spraying, *Thermal Spray 2004: Advances in Technology and Application*, May 10-12 (Osaka, Japan), ASM International

[16] Y. Ichikawa, K. Sakaguchi, K. Ogawa, T. Shoji, S. Barradas, M. Jeandin, M. Boustie, Deposition Mechanisms of Cold Gas Dynamic Sprayed MCrAlY Coatings, *Thermal Spray 2007: Global Coating Solutions*, B. Marple, M. Hyland, Y. Lau, C.-J. Li, R. Lima, G. Montavon (Eds.), May 14-16 (Beijing, China), ASM International, p 54-59

[17] R. Maev, V. Leshchynsky, 2008, *Introduction to Low Pressure Gas Dynamic Spray, Physics & Technology*, Wiley-VCH Verlag GmbH&Co, KGaA, Weinheim, Germany, 328 p

[18] A. Rezaeain, R. Chromik, S. Yue, E. Irissou, J.-G. Legoux, Characterization of cold-sprayed Ni, Ti and Cu coating properties for their optimizations, *Thermal Spray 2008: Thermal Spray Crossing Borders*, E. Lugscheider (Ed.), June 2-4 (Maastricht, The Netherlands), DVS, p 854-860

[19] L. Pawlowski, 2008, *The Science and Engineering of Thermal Spray Coatings*, 2nd edition, John Wiley & Sons Ltd., New York, USA, 656 p

[20] J. Davis (Ed.), 2004, *Handbook of Thermal Spray Technology*, ASM International, printed in the United States of America, 346 p

[21] A. Alkhimov, A. Papyrin, V. Kosarev, N. Nesterovich, M. Shushpanov, Gas-Dynamic Spray Method for Applying a Coating, U.S. Patent 5 302 414, 12 April 1994

[22] A. Alkhimov, A. Papyrin, V. Kosarev, N. Nesterovich, M. Shushpanov, Method and Device for Coating, European Patent 0 484 533 B1, 25 January 1995

[23] T. Van Steenkiste, J. Smith, R. Teets, Aluminum Coatings via Kinetic Spray with Relatively Large Powder Particles, *Surf. Coat. Technol.*, 154, 2002, p 237-252

[24] T. Schmidt, F. Gärtner, H. Assadi, H. Kreye, Development of a generalized parameter window for cold spray deposition, *Acta Mater.*, 54, 2006, p 729-742

[25] C.-J. Li, W.-Y. Li, Examination of the critical velocity for deposition of particles in cold spraying, *Thermal Spray 2005: Explore its surfacing potential!*, ASM International, May 2-4, 2005 (Basel, Switzerland), ASM International, p 217-224

[26] C. Borchers, F. Gärtner, T. Stoltenhoff, H. Kreye, Formation of persistent dislocation loops by ultra-high strain-rate deformation during cold spraying, *Acta Mater.*, 53, 2005, p 2991-3000

[27] B. Jodoin, Effects of Shock Waves on Impact Velocity of Cold Spray Particles, *Thermal Spray 2001: New Surfaces for a New Millennium*, C. Berndt, K. Khor, E. Lugscheider (Eds.), May 28-30 (Singapore), ASM International, p 399-407

[28] J. Pattison, S. Celotto, A. Khan, W. O'Neill, Standoff distance and bow shock phenomena in the Cold Spray process, *Surf. Coat. Technol.*, 202, 2008, p 1443-1454

[29] D. Helfritch, V. Champagne, Optimal Particle Size for the Cold Spray Process, *Thermal Spray 2006: Building on 100 Years of Success*, B. Marple, M. Hyland, Y.-C. Lau, R. Lima, J. Voyer (Eds.), May 15-18 (Seattle, Washington, USA), ASM International

[30] M. Grujicic, C.L. Zhao, W.S. DeRosset, D. Helfritch, Adiabatic shear instability based mechanism for particles/substrate bonding in the cold-gas dynamic-spray process, *Mater. Design*, 25, 2004, p 681-688

[31] H. Assadi, F. Gärtner, T. Stoltenhoff, H. Kreye, Bonding mechanism in cold gas spraying, *Acta Mater.*, 51, 2003, p 4379-4394

[32] P. Richter, H. Höll, Latest Technology for Commercially Available Cold Spray Systems, *Thermal Spray 2006: Building on 100 Years of Success*, B. Marple, M. Hyland, Y.-C. Lau, R. Lima, J. Voyer (Eds.), May 15-18 (Seattle, Washington, USA), ASM International

[33] T. Van Steenkiste, D. Gorkiewicz, Analysis of Tantalum Coatings Produced by the Kinetic Spray Process, *J. Therm. Spray Technol.*, 13(2), 2004, p 265-273

[34] T. Price, P. Shipway, D. McCartney, E. Calla, D. Zhang, A Method for Characterizing the Degree of Inter-particle Bond Formation in Cold Sprayed Coatings, *J. Therm. Spray Technol.*, 16(4), 2007, p 566-570

[35] E. Calla, D. McGartney, P. Shipway, Effect of Heat Treatment on the Structure and Properties of Cold Sprayed Copper, *Thermal Spray 2005: Explore its surfacing potential!*, , May 2-4 (Basel, Switzerland), ASM International

[36] T. Schmidt, F. Gärtner, H. Kreye, High Strain Rate Deformation Phenomena in Explosive Powder Compaction and Cold Gas Spraying, *Thermal Spray 2003: Advancing the Science & Applying the Technology*, C. Moreau, B. Marple (Eds.), May 5-8 (Orlando, Florida, USA), ASM International, p 9-18

[37] K. Balani, T. Laha, A. Agarwal, J. Karthikeyan, N. Munroe, Effect of Carrier Gases on Microstructural and Electrochemical Behavior of Cold-sprayed 1100 Aluminum Coating, *Surf. Coat. Technol.*, 195, 2005, p 272-279

[38] F. Gärtner, C. Borchers, T. Stoltenhoff, H. Kreye, H. Assadi, Numerical and Microstructural Investigations of the Bonding Mechanisms in Cold Spraying, *Thermal Spray 2003: Advancing the Science & Applying the Technology*, C. Moreau, B. Marple (Eds.), May 5-8 (Orlando, Florida, USA), ASM International, p 1-8

[39] S. Shin, S. Yoon, Y. Kim, C. Lee, Effect of particle parameters on the deposition characteristics of a hard/soft-particles composite in kinetic spraying, *Surf. Coat. Technol.*, 201, 2006, p 3457-3461

[40] T. Schmidt, H. Assadi, F. Gärtner, H. Richter, T. Stoltenhoff, H. Kreye, T. Klassen, From Particle Acceleration to Impact and Bonding in Cold Spraying, *J. Therm. Spray Technol.*, 18(5-6), 2009, p 794-808

[41] H. Kreye, T. Schmidt, F. Gärtner, T. Stoltenhoff, The Cold Spray Process and Its Optimization, *Thermal Spray 2006: Building on 100 Years of Success*, B. Marple, M. Hyland, Y.-C. Lau, R. Lima, J. Voyer (Eds.), May 15-18 (Seattle, Washington, USA), ASM International

[42] F. Gärtner, T. Stoltenhoff, T. Schmidt, H. Kreye, The Cold Spray Process and Its Potential for Industrial Applications, *J. Therm. Spray Technol.*, 15(2), 2006, p 223-232

[43] T. Schmidt, F. Gärtner, H. Kreye, New Developments in Cold Spray Based on Higher Gas- and Particle Temperatures, *J. Therm. Spray Technol.*, 15(4), 2006, p 488-494

[44] K. Sakaki, T. Tajima, H. Li, S. Shinkai, Y. Shimizu, Influence of Substrate Conditions and Traverse Speed on Cold Sprayed Coatings, *Thermal Spray 2004: Advances in Technology and Application*, May 10-12 (Osaka, Japan), ASM International

[45] J. Legoux, E. Irissou, C. Moreau, Effect of Substrate Temperature on the Formation Mechanism of Cold Sprayed Aluminum, Zinc and Tin Coatings, *Thermal Spray 2007: Global Coating Solutions*, B. Marple, M. Hyland, Y. Lau, C.-J. Li, R. Lima, G. Montavon (Eds.), May 14-16 (Beijing, China), ASM International, p 48-53

[46] Ktech Corp. website, http://www.ktech.com/Advanced_Manufacturing/Design_Build/Cold_Spray_System.html, referred 2009.

[47] http://www.cmit.csiro.au/innovation/2003-08/cold_spray.cfm, referred 2004.

[48] A. Kashirin, O. Klyuev, T. Buzdygar, A. Shkodkin, DYMET Technology Evolution and Application, *Thermal Spray 2007: Global Coating Solutions*, B. Marple, M. Hyland, Y. Lau, C.-J. Li, R. Lima, G. Montavon (Eds.), May 14-16 (Beijing, China), ASM International, p 141-145

[49] B. Djordjevic, R. Maev, SIMAT^{TM} Application for Aerospace Corrosion Protection and Structural Repair, *Thermal Spray 2006: Building on 100 Years of Success*, B. Marple, M. Hyland, Y.-C. Lau, R. Lima, J. Voyer (Eds.), May 15-18 (Seattle, Washington, USA), ASM International

[50] A. Sova, A. Papyrin, I. Smurov, Influence of Ceramic Powder Size on Process of Cermet Coating Formation by Cold Spray, *J. Therm. Spray Technol.*, 18(4), 2009, p 633-641

[51] A. Shkodkin, A. Kashirin, O. Klyuev, T. Buzdygar, The Basic Principles of DYMET Technology, *Thermal Spray 2006: Building on 100 Years of Success*, B. Marple, M. Hyland, Y.-C. Lau, R. Lima, J. Voyer (Eds.), May 15-18 (Seattle, Washington, USA), ASM International

[52] A. Shkodkin, A. Kashirin, Determination of the parameters of the process of gas-dynamic deposition of metallic coatings, *Weld. Internat.*, 20(2), 2006, p 161-164

[53] J. Karthikeyan, T. Laha, A. Agarwal, N. Munroe, Microstructural and Electrochemical Characterization of Cold-Sprayed 1100 Aluminum Coating, *Thermal Spray 2004: Advances in Technology and Application*, May 10-12 (Osaka, Japan), ASM International

[54] H. Weinert, E. Maeva, E. Leshchynsky, Low Pressure Gas Dynamic Spray Forming Near-net Shape Parts, *Thermal Spray 2006: Building on 100 Years of Success*, B. Marple, M. Hyland, Y.-C. Lau, R. Lima, J. Voyer (Eds.), May 15-18 (Seattle, Washington, USA), ASM International

[55] A. Papyrin, V. Kosarev, S. Klinkov, A. Sova, I. Smurov, P. Bertrand, Investigation of composites: metal - ceramics and metal - metal coatings produced with cold spray equipment with ejector, *Thermal Spray 2008: Thermal Spray Crossing Borders*, E. Lugscheider (Ed.), June 2-4 (Maastricht, The Netherlands), DVS, p 611-615

[56] Obninsk Center for Powder Spraying (OCPS, Russia) website, http://dymet.amazonit.ru/eindex.html, referred 2009.

[57] S. Klinkov, V. Kosarev, M. Rein, Cold spray deposition: Significance of particle impact phenomena, *Aerospace Sci. Technol.*, 9, 2005, p 582-591

[58] A. Papyrin, S. Klinkov, V. Kosarev, Effect of the substrate surface activation on the process of cold spray coating formation, *Thermal Spray 2005: Explore its surfacing potential!*, May 2-4 (Basel, Switzerland), ASM International, p 145-150

[59] T. Schmidt, Kaltgasspritzen, Eine Analyse des Materialverhaltens beim Partikelaufprall und die daraus abgeleitete Prozessoptimierung, Werkstofftechnik, Shaker Verlag, Hamburg, Germany, 2007, in Germany

[60] H. Katanoda, M. Fukuhara, N. Iino, Numerical Study of Combination Parameters for Particle Impact Velocity and Temperature in Cold Spray, *J. Therm. Spray Technol.*, 16(5-6), 2007, p 627-633

[61] A. Papyrin, S. Klinkov, V. Kosarev, Modelling of particle-substrate adhesive interaction under the cold spray process, *Thermal Spray 2003: Advancing the Science & Applying the Technology*, C. Moreau, B. Marple (Eds.), May 5-8 (Orlando, Florida, USA), ASM International, p. 27-?

[62] F. Raletz, M. Vardelle, G. Ezo'o, Critical particle velocity under cold spray conditions, *Surf. Coat. Technol.*, 201, 2006, p 1942-1947

[63] K. Kang, S. Yoon, Y. Ji, C. Lee, Oxidation Effects on the Critical Velocity of Pure Al Feedstock Deposition in the Kinetic Spraying Process, *Thermal Spray 2007: Global Coating Solutions*, B. Marple, M. Hyland, Y. Lau, C.-J. Li, R. Lima, G. Montavon (Eds.), May 14-16 (Beijing, China), ASM International, p 66-71

[64] V. Kosarev, S. Klinkov, A. Alkhimov, A. Papyrin, On Some Aspects of Gas Dynamics of the Cold Spray Process, *J. Therm. Spray Technol.*, 12(2), 2003, p 265-281

[65] T. Han, Z. Zhao, B. Gillispie, J. Smith, A fundamental study of the kinetic spray process, *Thermal Spray 2004: Advances in Technology and Application*, May 10-12 (Osaka, Japan), ASM International

[66] A. Alkhimov, V. Kosarev, S. Klinkov, The Features of Cold Spray Nozzle Design, *J. Therm. Spray Technol.*, 10(2), 2001, p 375-381

[67] M. Meyers, Plasticity: Adiabatic Shear Localization, *Encyclop. Mat.: Sci. Technol.*, p 7093-7103

[68] B. Jodoin, L. Ajdelsztajn, E. Sansoucy, A.Zúñiga, P. Richter, E. Lavernia, Effect of particle size, morphology, and hardness on cold gas dynamic sprayed aluminum alloy coatings, *Surf. Coat. Technol.*, 201, 2006, p 3422-3429

[69] H. Fukanuma, N. Ohno, B. Sun, R. Huang, The Influence of Particle Morphology on In-flight Particle Velocity in Cold Spray, *Thermal Spray 2006: Building on 100 Years of Success*, B. Marple, M. Hyland, Y.-C. Lau, R. Lima, J. Voyer (Eds.), May 15-18 (Seattle, Washington, USA), ASM International

[70] A. Alkhimov, S. Klinkov, V. Kosarev, Experimental Study of Deformation and Attachment of Microparticles to an Obstacle upon High-Rate Impact, *J. Appl. Mech. Techn. Phys.*, 41(2), 2000, p 245-250

[71] X.-J. Ning, X-J., J.-H. Jang, H.-J. Kim, C.-J. Li, C. Lee, Cold Spraying of Al-Sn Binary Alloy: Coating Characteristics and Particle Bonding Features, *Surf. Coat. Technol.*, 202(9), 2008, p 1681-1687

[72] T. Kairet, A contribution to the study of cold gas dynamic spraying of copper: Influence of the powder characteristics on the mechanical properties of the coating, Doctoral Thesis, Université Libre de Bruxelles, Belgium, 2007

[73] P. Sudharshan Phani, D. Srinivasa Rao, S. Joshl, G. Sundararajan, Effect of Process Parameters and Heat Treatments on Properties of Cold Sprayed Copper Coatings, *J. Therm. Spray Technol.*, 16(3), 2007, p 425-434

[74] S. Zumdahl, 1998, *Chemical Principles*, 3rd ed., Houghton Mifflin Company, Boston, New York, USA, 1040 p

[75] X.-J. Ning, J.-H. Jang, H.-J. Kim, The Effects of Powder Properties on In-Flight Particle Velocity and Deposition Process during Low Pressure Cold Spray Process, *Appl. Surf. Sci.*, 253(18), 2007, p 7449-7455

[76] T. Kairet, G. Di Stefano, M. Degrez, F. Campana, J.-P. Janssen, Comparison Between Coatings from two Different Copper Powders: Mechanical Properties, Hardness and Bond

Strength, *Thermal Spray 2006: Building on 100 Years of Success*, B. Marple, M. Hyland, Y.-C. Lau, R. Lima, J. Voyer (Eds.), May 15-18 (Seattle, Washington, USA), ASM International

[77] W. Callister, Jr., 2000, *Materials science and engineering, an introduction*, 5th ed., John Wiley &Sons Inc., printed in United State of America, 871 p

[78] ASM Metals Handbook, Vol. 14A, Metalworking: Bulk Forming, Plastic Deformation Structures, Plastic Deformation in Crystals, ASM international, 2005, p 539-551

[79] T. H. Courtney, 2000, *Mechanical Behavior of Materials*, McGrae-Hill Publishing Company, 2nd ed., (Singapore), 733 p

[80] F. Gärtner, T. Stoltenhoff, J. Voyer, H. Kreye, S. Riekehr, M. Kocak, Mechanical properties of cold-sprayed and thermally sprayed copper coatings, *Surf. Coat. Technol.*, 200, 2006, p 6770-6782

[81] D. Zhang, P. Shipway, D. McCartney, Particle-Substrate Interactions in Cold Gas Dynamic Spraying, *Thermal Spray 2003: Advancing the Science & Applying the Technology*, C. Moreau, B. Marple (Eds.), May 5-8 (Orlando, Florida, USA), ASM International, p 45-52

[82] M. Grujicic, J. Saylor, D. Beasley, W. DeRosset, D. Helfritch, Computational analysis of the interfacial bonding between feed-powder particles and the substrate in the cold-gas dynamic-spray process, *Appl. Surf. Sci.*, 219, 2003, p 211-227

[83] T. Stoltenhoff, C. Borchers, F. Gärtner, H. Kreye, Microstructures and key properties of cold-sprayed and thermally sprayed copper coatings, *Surf. Coat. Technol.*, 200, 2006, p 4947-4960

[84] P. Richter, A.Zúñiga, M. Yandouzi, B. Jodoin, CoNiCrAlY microstructural changes induced during Cold Gas Dynamic Spraying, *Surf. Coat. Technol.*, 203(3-4), 2008, p 364-371

[85] L. Ajdelsztajn, B. Jodoin, J. Schoenung, Synthesis and mechanical properties of nanocrystallize Ni coatings produced by cold gas dynamic spraying, *Surf. Coat. Technol.*, 201(3-4), 2006, p 1166-1172

[86] M. Fukumoto, M. Mashiko, M. Yamada, E. Yamaguchi, Deposition Behavior of Copper Particles onto Flat Substrate Surface in Cold Spraying, *Thermal Spray 2009: Expanding Thermal Spray Performance to New Markets and Applications*, B. Marple, M. Hyland, Y.-C. Lau, C.-J. Li, R. Lima, G. Montavon (Eds.), May 4-7 (Las Vegas, Nevada, USA), ASM International, p 273-278

[87] S. Klinkov, V. Kosarev, A. Sova, I. Smurov, Calculation of Particle Parameters for Cold Spray Spraying of Metal-Ceramic Mixtures, *J. Therm. Spray Technol.*, 18(5-6), 2009, p 944-956

[88] W.-Y. Li, C. Zhang, X. Guo, C.-J. Li, H. Liao, C. Coddet, Study on impact fusion at particle interfaces and its effect on coating microstructure in cold spraying, *Appl. Surf. Sci.*, 254, 2007, p 517-526

[89] T. Hussain, D. McCartney, P. Shipway, D. Zhang, Bonding Mechanisms in Cold Spraying: The Contributions of Metallurgical and Mechanical Components, *J. Therm. Spray Technol.*, 18(3), 2009, p 364-379

[90] S. Guetta, M. Berger, F. Borit, V. Guipont, M. Jeandin, M. Boustie, Y. Ichikawa, K. Sakaguchi, K. Ogawa, Influence of Particle Velocity on Adhesion of Cold-Sprayed Splats, *J. Therm. Spray Technol.*, 18(3), 2009, p 331-342

[91] H. Lee, S. Jung, S. Lee, Y. You, K. Ko, Correlation between Al_2O_3 particles and interface of Al-Al_2O_3 coatings by cold spray, *Appl. Surf. Sci.*, 252, 2005, p 1891-1898

[92] H. Lee, Y. Yu, Y. Lee, Y. Hong, K. Ko, Cold Spray of SiC and Al_2O_3 With Soft Metal Incorporation: A Technical Contribution, *J. Therm. Spray Technol.*, 13(2), 2004, p 184-189

[93] R. Lima, J. Karthikeyan, C. Kay, J. Lindemann, C. Berndt, Microstructural characteristics of cold-sprayed nanostructured WC-Co coatings, *Thin Solid Films*, 416, 2002, p 129-135

[94] H.-J. Kim, C.-H. Lee, S.-Y. Hwang, Fabrication of WC-Co coatings by cold spray deposition, *Surf. Coat. Technol.*, 191, 2005, p 335-340

[95] R. McCune, W. Donlon, O. Popoola, E. Cartwright, Characterization of Copper Layers Produced by Cold Gas-Dynamic Spraying, *J. Therm. Spray Technol.*, 9(1), 2000, p 73-82

[96] E. Irissou, J.-G. Legoux, B. Arsenault, C. Moreau, Investigation of Al-Al_2O_3 Cold Spray Coating Formation and Properties, *J. Therm. Spray Technol.*, 16(5-6), 2007, p 661-668

[97] R. Maev, V. Leshchynsky, A. Papyrin, Structure Formation of Ni-based Composite Coatings during Low Pressure Gas Dynamic Spraying, *Thermal Spray 2006: Building on 100 Years Success*, B. Marple, M. Hyland, Y. Lau, R. Lima, J. Voyer (Eds.), May 15-18 (Seattle, Washington, USA), ASM International

[98] Y. Zou, W. Qin, E. Irissou, J.-G. Legoux, S. Yue, J. Szpunar, Dynamic recrystallization in the particle/particle interfacial region of cold-sprayed nickel coating: Electron backscatter diffraction characterization, *Scripta Mater.*, 61, 2009, p 899-902

[99] H. Mäkinen, J. Lagerbom, P. Vuoristo, Adhesion of cold sprayed coatings: effect of powder, substrate, and heat treatment, T*hermal Spray 2007: Global Coating Solutions*, B. Marple, M. Hyland, Y.-C. Lau, C.-J. Li, R. Lima, G. Montavon (Eds.), May 14-16 (Beijing, China), ASM International, p 31-36

[100] H. Koivuluoto, M. Kulmala, P. Vuoristo, Structural Properties of High-Pressure Cold-Sprayed and Low-Pressure Cold-Sprayed Coatings, *Surface Modification Technologies XXII*, T. Sudarshan, P Nylen (Eds.),September 22-24,2008, (Trollhättan, Sweden), p 65-72

[101] A. Bolesta, V. Fomin, M. Sharafutdinov, B. Tolochko, Investigation of interface boundary occurring during cold gas-dynamic spraying of metallic particles, *Nuclear Instrum. Methods in Phys. Research A*, 470, 2001, p 249-252

[102] S. Semiatin, Recovery, Recrystallization, and Grain-Growth Structures, Metalworking: Bulk Forming, Vol.14A, ASM Handbook, ASM International, 2005, p 552-562

[103] M. Decker, R. Neiser, D. Gilmore, H. Tran, Microstructure and Properties of Cold Spray Nickel, *Thermal Spray 2001: New Surfaces for a New Millennium*, C. Berndt, K. Khor, E. Lugscheider (Eds.), May 28-30 (Singapore), ASM International, p 433-439

[104] A. Shkodkin, A. Kashirin, O. Klyuev, T. Buzdygar, Metal Particle Deposition Stimulation by Surface Abrasive Treatment in Gas Dynamic Spraying, *J. Therm. Spray Technol.*, 15(3), 2006, p 382-386

[105] M. Kulmala, H. Koivuluoto, P. Vuoristo, Influence of laser irradiation on formation of low-pressure cold sprayed coatings, *Thermal Spray 2008: Thermal Spray Crossing Borders*, E. Lugscheider (Ed.), June 2-4 (Maastricht, The Netherlands), DVS, p 950-955

[106] E. Calla, D. McCartney, P. Shipway, Deposition of Copper by Cold Gas Dynamic Spraying: an Investigation of Dependence of Microstructure and Properties of the Deposits on the Spraying Conditions, *Thermal Spray 2004: Advances in Technology and Application*, May 10-12 (Osaka, Japan), ASM International

[107] T. Xiong, Z. Bao, T. Li, Z. Li, Study on cold-sprayed copper coating's properties and optimizing parameters for spraying process, *Thermal Spray 2005: Explore its surfacing potential!*, May 2-4 (Basel, Switzerland), ASM International, p 178-183

[108] J. Lagerbom, H. Mäkinen, P. Vuoristo, Effect of heat treatment on properties of cold sprayed coatings, *Thermal Spray 2005: Explore its surfacing potential!*, May 2-4 (Basel, Switzerland), ASM International, p 240-244

[109] H. Fukanuma, N. Ohno, Study of Adhesive Strength of Cold Spray Coatings, T*hermal Spray 2004: Advances in Technology and Application*, May 10-12 (Osaka, Japan), ASM International

[110] T. Schmidt, F. Gärtner, H. Kreye, T. Klassen, Correlation of impact conditions and coating properties in cold spraying, *Thermal Spray 2008: Thermal Spray Crossing Borders*, E. Lugscheider (Ed.), June 2-4 (Maastricht, The Netherlands), DVS, p 724-731

[111] H. Mäkinen, J. Lagerbom, P. Vuoristo, Mechanical properties and corrosion resistance of cold sprayed coatings, *Thermal Spray 2006: Building on 100 Years of Success*, B. Marple, M. Hyland, Y.-C. Lau, R. Lima, J. Voyer (Eds.), May 15-18 (Seattle, Washington, USA), ASM International

[112] D. Jones, 1996, *Principles and Prevention of Corrosion*, Prentice-Hall, Upper Saddle River, NJ, 2nd ed., 572 p

[113] D. Talbot, J. Talbot, 1998, *Corrosion Science and Technology*, CRC Press LLC, 390 p

[114] G. Frankel, Pitting corrosion, Corrosion Fundamentals, Testing, and Protection, ASM Handbook, Volume 13A, ASM International, 2003, p. 236-241

[115] P.A. Schweitzer, Ed., 1996, *Corrosion Engineering Handbook*, Marcel Dekker, 736 p

[116] U. Chatterjee, S. Bose, S. Roy, 2001, *Environmental degradation of metals*, Marcel Dekker Inc., New York, USA, 498 p

[117] R. Kelly, Crevice corrosion, Corrosion Fundamentals, Testing, and Protection, ASM Handbook, Volume 13A, ASM International, 2003, p. 242-247

[118] R. Baboian, Galvanic corrosion, Corrosion Fundamentals, Testing, and Protection, ASM Handbook, Volume 13A, ASM International, 2003, p. 210-213

[119] L. Erb, Corrosion Control - Galvanic Table, Army Missile Command Report RS-TR-67-11, Practical Galvanic Series, 1997

[120] H. Koivuluoto, J. Näkki, P. Vuoristo, Structure and Corrosion Behavior of Cold-Sprayed Tantalum Coatings, *Thermal Spray 2009: Expanding Thermal Spray Performance to New Markets and Applications,* B. Marple, M. Hyland, Y.-C. Lau, C.-J. Li, R. Lima, G. Montavon (Eds.), May 4-7 (Las Vegas, Nevada, USA), ASM International, p 314-319

[121] ASM Handbooks Online, Volume 13A, Corrosion: Fundamentals, Testing, and Protection, Passivity, General Aspects.

[122] “Standard Test Method of Salt Spray (Fog) Testing,” B117-90, *Annual Book of ASTM Standards*, ASTM, p 19-25

[123] M. Vreijling, 1998, *Electrochemical characterization of metallic thermally sprayed coatings*, printed in the Netherlands, 143 p

[124] ASM Metals Handbook Online, vol. 13B, Corrosion: Materials, Corrosion of nonferrous Alloys and Speciality Products, Corrosion of Tantalum and Tantalum Alloys

[125] H.C. Starck, Amperit and Amperweld Homepage, Amperit Thermal Spray Powder Procedure, Available from http://www.amperit.info, referred 2008

[126] R. Blose, D. Vasquez, W. Kratochvil, Metal Passivation to Resist Corrosion using the Cold Spray Process, *Thermal Spray 2005: Explore its surfacing potential!*, May 2-4 (Basel, Switzerland), ASM International

[127] T. Xiong, Y. Tao, C. Sun, H. Jin, H. Du, T. Li, Study on Corrosion Behavior of Cold Sprayed $Al/\alpha\text{-}Al_2O_3$ Deposit on AZ91D Alloy, *Thermal Spray 2009: Expanding Thermal Spray Performance to New Markets and Applications*, B. Marple, M. Hyland, Y.-C. Lau, C.-J. Li, R. Lima, G. Montavon (Eds.), May 4-7 (Las Vegas, Nevada, USA), ASM International, p 669-672

[128] J. Villafuerte, D. Dzhurinskiy, R. Ramirez, E. Maeva, V. Leshchynsky, R. Maev, Corrosion Behavior and Microstructure of the $Al\text{-}Al_2O_3$ Coatings Produced by Low Pressure Cold Spraying, *Thermal Spray 2009: Expanding Thermal Spray Performance to New Markets and Applications*, B. Marple, M. Hyland, Y.-C. Lau, C.-J. Li, R. Lima, G. Montavon (Eds.), May 4-7 (Las Vegas, Nevada, USA), ASM International, p 908-913

[129] W. Kroemmer, P. Heinrich, Cold spraying - Potential and New Application Ideas, *Thermal Spray 2006: Building on 100 Years of Success*, B. Marple, M. Hyland, Y.-C. Lau, R. Lima, J. Voyer (Eds.), May 15-18 (Seattle, Washington, USA), ASM International

[130] S. Marx, A. Paul, A. Köhler, G. Hüttl, Cold spraying - innovative layers for new applications, *Thermal Spray 2005: Explore its surfacing potential!*, May 2-4 (Basel, Switzerland), ASM International, p 209-215

[131] H. Hoell, P. Richter, KINETIKS® 4000 - new perspective with cold spraying, *Thermal Spray 2008: Thermal Spray Crossing Borders*, E. Lugscheider (Ed.), June 2-4 (Maastricht, The Netherlands), DVS, p 479-480

[132] M. Beneteau, W. Birtch, J. Villafuerte, J. Paille, M. Petrocik, R. Maev, E. Strumban, V. Leshchynsky, Gas Dynamic Spray Composite Coatings for Iron and Steel Castings, *Thermal Spray 2006: Building on 100 Years of Success*, B. Marple, M. Hyland, Y.-C. Lau, R. Lima, J. Voyer (Eds.), May 15-18 (Seattle, Washington, USA), ASM International

[133] R. Caron, J. Staley, Effects of Composition, Processing, and Structure on Properties of Nonferrous Alloys, Copper and Copper Alloys, ASM Handbooks Online, 20, Materials Selection and Design, ASM International, 1997

[134] R. Caron, J. Staley, Effects of Composition, Processing, and Structure on Properties of Nonferrous Alloys, Nickel and Nickel Alloys, ASM Handbooks Online, 20, Materials Selection and Design, ASM International, 1997

[135] ASM handbooks online, Volume 13B, Corrosion Materials, Corrosion of Nickel and Nickel-Base Alloys

[136] Cold Gas Technology GmbH, website: http://www.cgt-gmbh.com/, referred 2009.

[137] W. Krömmer, P. Heinrich, P. Richter, Cold Spraying - Equipment and Application Trends, *Thermal Spray 2003: Advancing the Science & Applying the Technology*, C. Moreau, B. Marple (Eds.), May 28-30 (Orlando, Florida, USA), ASM International, p 97-102

[138] C. Borchers, F. Gärtner, T. Stoltenhoff, H. Kreye, Microstructural bonding features of cold sprayed face centered cubic metals, *J. Appl. Phys.*, 8(96), 2004, p 4288-4292

[139] H. Koivuluoto, M. Kotilainen, P. Vuoristo, Overview of Structure and Properties of High-Pressure and Low-Pressure Cold-Sprayed Coatings, *Weld. Cutt.*, 2, 2009, p 98-104

[140] L.-M. Berger, P. Ettmayer, P. Vuoristo, T. Mäntylä, W. Kunert, Microstructure and Properties of WC-10%-4%Cr Spray Powders and Coatings: Part 1. Powder Characterization, *J. Therm. Spray Technol.*, 10(2), 2001, p 311-325

[141] W. Tait, 1994, *An Introduction to Electrochemical Corrosion Testing for Practicing Engineers and Scientists*, Pair O Docs Publications, Racine, WI, 138 p

Publication I

Heli Koivuluoto, Juha Lagerbom and Petri Vuoristo

Microstructural Studies of Cold Sprayed Copper, Nickel, and Nickel-30%Copper Coatings

Journal of Thermal Spray Technology, 16 (4) 2007, p. 488-497

Reprinted from Journal of Thermal Spray Technology with permission of ASM International.
Copyright (2007) ASM International.

JTTEE5 16:488–497
DOI: 10.1007/s11666-007-9060-5
1059-9630/$19.00 © ASM International

Microstructural Studies of Cold Sprayed Copper, Nickel, and Nickel-30% Copper Coatings

Heli Koivuluoto, Juha Lagerbom, and Petri Vuoristo

(Submitted November 2, 2006; in revised form April 23, 2007)

Cold spraying enables to produce metallic coatings with low porosity level and low oxygen content. Several material properties such as electrical conductivity and corrosion resistance rely on these properties. Aim of this study was to characterize microstructural properties of cold sprayed copper, nickel, and nickel-30%copper coatings. Microstructures, denseness, and deformation of particles were investigated. SEM analysis and corrosion tests were done to get information of through-porosity. Open porosity has an important role on protectiveness of anodically protective coatings, such coating materials like copper and nickel. In this study, cold-sprayed Cu coating was fully dense. However, cold-sprayed Ni and Ni-30%Cu coatings seemed to be microstructurally dense but some porosity in some areas of the coatings especially in some parts of particle boundaries was noticed after corrosion tests. Furthermore, effect of annealing to microstructure and corrosion test behavior was studied. Cold sprayed Ni coating became denser during heat treatment.

Keywords cold gas dynamic spraying, corrosion test, copper nickel, microstructure, nickel-30% copper

1. Introduction

In the cold spray process, a gas is accelerated to supersonic velocity by a converging-diverging de Laval type nozzle (Ref 1). Formation of a cold-sprayed coating depends on the velocity of powder particles. Each material has a specific critical velocity v_{cr}. Above v_{cr} the particles adhere to the substrate causing plastic deformation and formation of the coating. At velocities lower than v_{cr} only erosion and particle rebounding occur with no coating building up (Ref 1, 2). In cold spraying, several parameters such as the particle size (typically 5-25 μm), particle temperature, substrate material, and the properties of the coating material have a remarkable influence on the formation and the deposition efficiency (Ref 1, 3, 4). Good bonding between the cold sprayed powder particles needs heavy plastic deformation during the particle impact (Ref 2, 4). Upon impact the solid particles deform and bond together, forming a coating (Ref 2). For successful bonding, deposition conditions in which oxide layers on the particle surfaces are destroyed during impact should be created (Ref 4). The powder particles impinge on the substrate in solid form, well below the powder melting temperature (Ref 2). Wide range of coating and substrate materials, e.g., pure metals, metal alloys, polymers, and composites, can be used in cold spraying (Ref 3). As a materials processing method, cold spraying is kept very similar to an explosive welding (Ref 5).

Cold spraying enables production of metallic coatings with very low porosity level and low oxygen content. Cold spraying is also an effective method to deposit dense and pure coatings (Ref 6). This is regarded as an advantage for several important material properties such as electrical conductivity and corrosion resistance (Ref 1). According to Stoltenhoff et al. (Ref 1) electrical conductivity of the cold sprayed copper is about 90% of the value of pure copper. Published studies on corrosion resistance of cold sprayed coatings are so far very rare, and have been reported only for Zn, Al, or Zn-Al composite coatings. Recently Blose et al. (Ref 7) reported that such coatings can protect steel substrates from wet corrosion. Sacrificial corrosion of Al in the cold sprayed Al coating and formation of thin $ZnCl_2$ layer through cathodic protection in the cold sprayed Zn coatings was found to protect steel in a chloride environment. Salt spray (fog) testing is a commonly used test method to evaluate the quality of various coatings. This particular test enables using different corrosive solutions and different test temperatures in a controlled test condition (Ref 8). In the present work, the studies are more focused on corrosion properties of anodically protective coatings instead of cathodically protective coatings.

It is known that cold sprayed coatings have hardnesses somewhat higher than in corresponding bulk materials, due to high degree of work hardening. The coatings possess also high adherence to base materials and low thermal stresses due to low particle temperatures (Ref 2). According to

Heli Koivuluoto, Juha Lagerbom, and **Petri Vuoristo,** Laboratory of Surface Engineering, Institute of Materials Science, Tampere University of Technology, PO Box 589, 33101 Tampere, Finland. Contact e-mail: heli.koivuluoto@tut.fi.

Calla et al. (Ref 5), the reason to high hardness of the cold sprayed coatings is the very fine grain size and the significant microstrain in the as-sprayed deposits. Annealing at elevated temperatures affects the properties of cold sprayed coatings. At temperatures of 300 °C and above for Cu, the dislocations in the grains rearrange, and recrystallization and further grain growth occur. A decrease in the hardness is usually the result (Ref 5).

In the present study characteristics of the cold sprayed copper, nickel, and nickel-30%copper (Monel 400) coatings were investigated. Aim of this study was to investigate the microstructure and degree of impermeability of coatings prepared by cold spraying. Denseness of the cold sprayed coatings was evaluated by wet corrosion testing, which is able to detect the existing through-porosity (open-porosity) in the coatings. The corrosion tests used were open cell potential measurements and salt spray fog testing. The structural integrity is important for several coating properties. Cold sprayed copper was chosen because of its interesting conductivity properties for electrical and heat conductivity applications. Nickel and nickel-30%copper coatings were chosen because of their potential in applications requiring good corrosion resistances. The substrate material used in the study was carbon steel. The effect of heat treatment to the different properties was also studied.

2. Experimental Procedure

2.1 Spraying Parameters

The cold sprayed coatings were prepared at Linde AG Linde Gas Division (Unterschleissheim, Germany). The cold spray system used was Kinetiks 3000 M with a standard gun nozzle (Cold Gas Technology GmbH, CGT, Germany). Nitrogen, helium, or mixture of them can be used as the process gas in the equipment. The gas pressure can be controlled in the range of 15-40 bar and the gas pre-heating temperature at 200-800 °C. The summary of the cold spraying parameters used in the present work is presented in Table 1. In this study, nitrogen was used as the process gas. Reference samples were HVOF sprayed with a Sulzer Metco Diamond Jet Hydrid 2700 gun. The HVOF spray parameters were oxygen flow rate of 202 l/min for Cu and 215 l/min for Ni and Ni-30%Cu, propane flow rate of 74 l/min, air flow rate of 391 l/min, powder feed rate of 60 g/min, surface velocity of 183 m/min, spraying distance 230 mm, and 48 spray layers with a rotating sample holder. Coating thickness of HVOF Cu, Ni, and Ni-30%Cu sprayed coatings was 320, 570, 285 μm, respectively.

2.2 Powders

The powders used in this study were copper, nickel, and nickel-30%copper alloy (Monel 400), see Table 2. Three different copper powders were used. They were purchased from two different suppliers and had three different particle sizes. The Ni and Ni-30%Cu powders selected were typical powders with good sprayability in the cold spray process. All powders were manufactured by gas atomization. Powders used for the reference samples were Cu (Sulzer Metco, Metco Diamalloy 1007, −88 + 31 μm), Ni (Sulzer Metco 56F NS, −45 + 10 μm), and Ni-30%Cu (Sandvik Osprey, −38 + 16 μm).

The three Cu, Ni, and Ni-30%Cu powders were sprayed onto grit blasted (18 mesh) steel substrates. Figure 1 shows the morphology of the BSA Cu (−22 + 5 μm) powder. Morphologies of the BSA Cu (−38 + 11 μm) and the Osprey Cu (−30 + 10 μm) are presented in Figs. 2 and 3, respectively. The particle size distribution of the Osprey Cu powder was smaller than the distribution of the BSA powders. Moreover, powders produced by BSA include smaller particles more than the Osprey Cu powder. Ni particles were spherical in shape, with few agglomerates also present (Fig. 4). Ni-30%Cu powder contained a lot of agglomerates (satellites) and also significantly more very small particles as compared to the nominal particle size given by the powder producer. Thus, the particle size distribution was relatively large (Fig. 5).

2.3 Sample Preparation

Samples had to be etched in order to see the real microstructures of the cold sprayed coatings. Table 3 presents the etching conditions for each coating material. The Ni coating was etched in a boiling solution.

2.4 Characterization of the Cold Sprayed Coatings

Microstructures of the cold sprayed coatings were investigated with a Philips XL30 scanning electron microscope (SEM). Microstructures of the cold sprayed coatings were studied from unetched and etched cross-sectional coating samples. Corrosion behavior and especially the through-porosity (impermeability) of the cold sprayed coatings were tested with open cell potential measurements and salt spray (fog) testing. Two plastic tubes were glued on the surface of the coating sample for the open cell potential measurements. The diameter of tube was 20 mm. An amount of 12 ml of 3.5 wt%

Table 1 Cold spray parameters and coating thicknesses

Material	Pressure (bar)	Total N_2 flow rate (m^3/h)	Temperature (°C)	Coating thickness (μm)
Cu (BSA −22 + 5)	28	70	320	520
Cu (BSA −38 + 11)	28	73	420	430
Cu (Osprey −30 + 10)	28	80	400	440
Ni	28	61	500	320
Ni-30%Cu	28, 30	64, 70	450, 525	150, 510

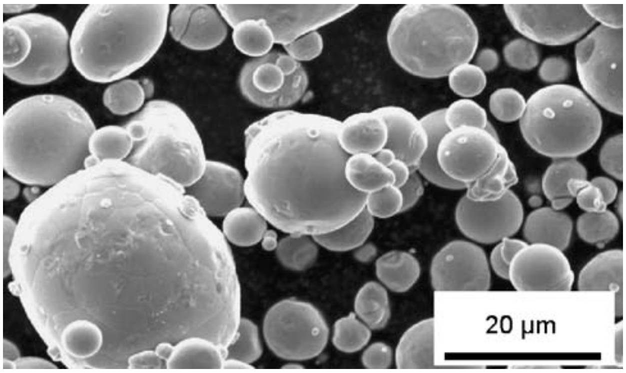

Fig. 1 Morphology of Cu powder (BSA −22 + 5 µm)

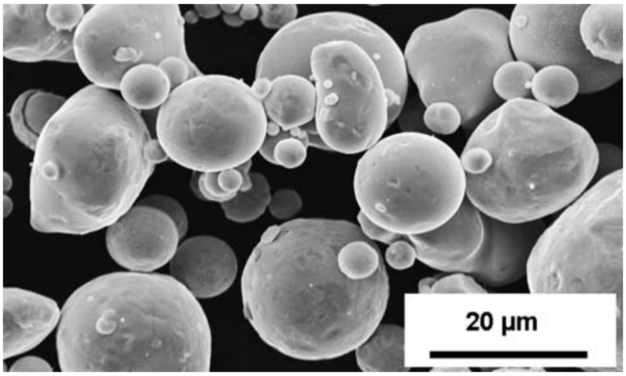

Fig. 2 Morphology of Cu powder (BSA −38 + 11 µm)

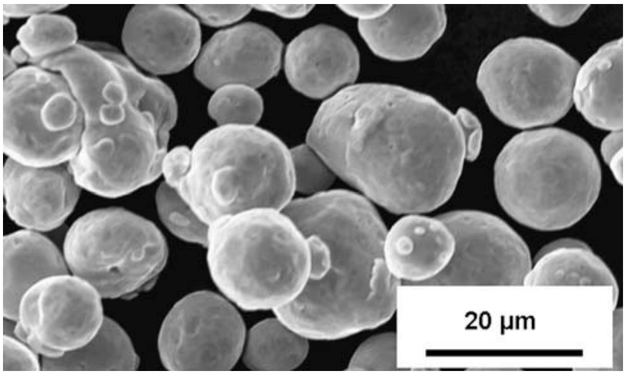

Fig. 3 Morphology of Cu powder (Osprey −30 + 10 µm)

Table 2 Spray powders used in cold spraying

Material	Particle size (µm)	Producer	Production Method
Cu	−22 + 5	BSA Metals	Gas atomized
Cu	−38 + 11	BSA Metals	Gas atomized
Cu	−30 + 10	Sandvik Osprey	Gas atomized
Ni	−25 + 5	H. C. Starck	Gas atomized
Ni-30%Cu	−38 + 16	Sandvik Osprey	Gas atomized

All particle sizes are nominal values given by the producer

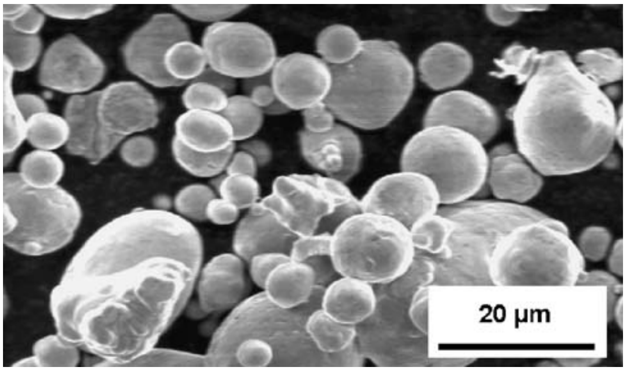

Fig. 4 Morphology of Ni powder

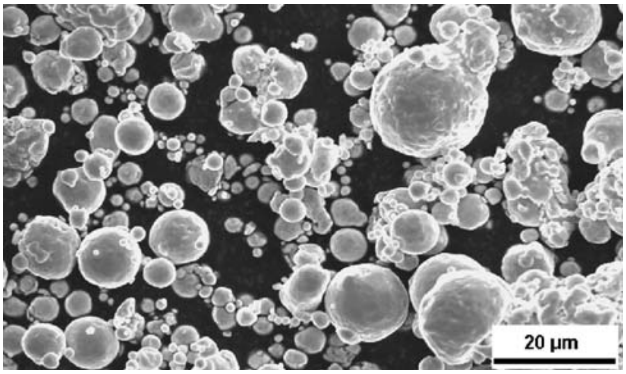

Fig. 5 Morphology of Ni-30%Cu powder

Table 3 Etching conditions for cold sprayed coatings

Material	Etching solution	Time (s)	Boiling solution
Cu	95 ml ethanol 5 g $FeCl_3$ 2 ml HCl	90	No
Ni	10 ml glycerol 5 ml HNO_3 15 ml HCl	3	Yes
Ni-30%Cu	99 ml ethanol 5 g $FeCl_3$ 2 ml HCl	40	No

NaCl-solution was filled into the tubes. Measurement period was 9 days. Open cell measurements were done with Fluke 79 III true RMS-multimeter. Silver/silver chloride electrode was used as a reference electrode. Salt spray (fog) testing was done by following the ASTM B117 standard. 5 wt% NaCl-solution was used and exposure time was 96 h. Temperature was 35-40 °C, pH of the salt solution was 6.3 and accumulation of solution was 0.04 ml/cm^2 h during exposure. The samples were examined visually before, during and after exposure. Also cross-sectional SEM studies after corrosion test were performed. The effect of heat treatments on properties of the cold sprayed coatings was studied. Heat treatments were done in a

Carbolite 3-zone controlled atmosphere furnace using argon as the protective gas. Holding time at the annealing temperature was 5 h.

3. Results

3.1 Microstructure of Cold Sprayed Coatings

Microstructures of the as-sprayed and the heat-treated cold sprayed coatings on steel substrates are presented in Figs. 6-11. Figure 6 presents the microstructure of cold sprayed Cu coating sprayed from the fine size BSA powder with the particle size of −22 + 5 μm. The unetched microstructure of the coating is shown in Fig. 6a. Cu coatings sprayed from the two other powders had similar

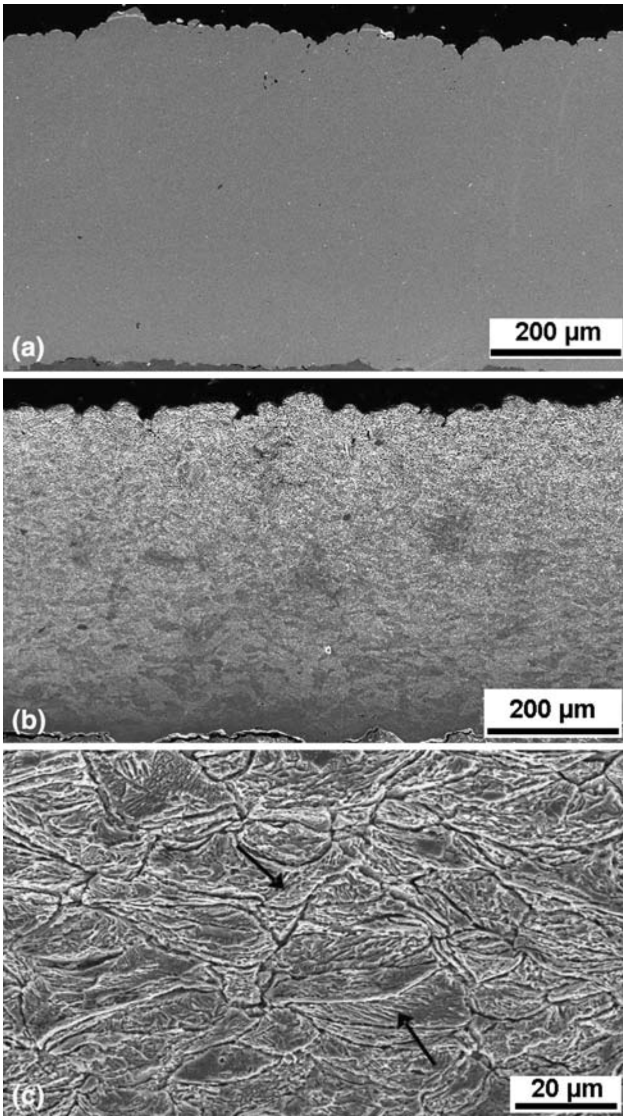

Fig. 6 Cold sprayed Cu coating (BSA −22 + 5 μm) on grit blasted steel (a) unetched, (b), and (c) etched. The arrows indicate the slip bands

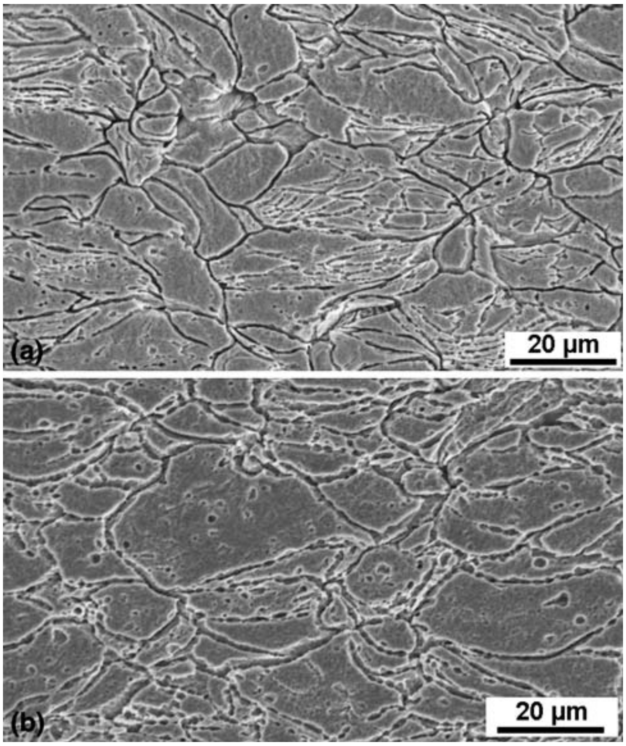

Fig. 7 Etched cold sprayed Cu coating (BSA −22 + 5 μm), at (a) 200 °C and (b) 400 °C heat-treated (5 h)

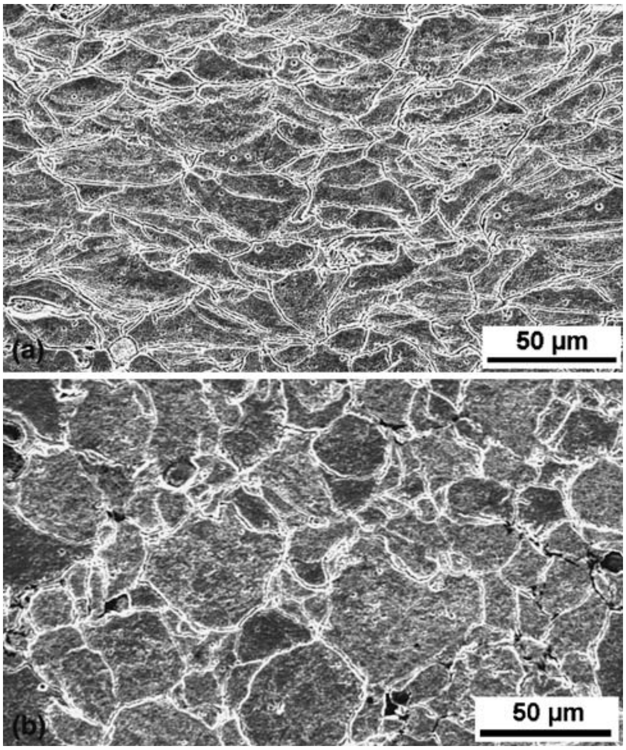

Fig. 8 Cold sprayed Cu coating (BSA −38 + 11 μm) (a) etched cross-sectional and (b) etched top-view microstructure

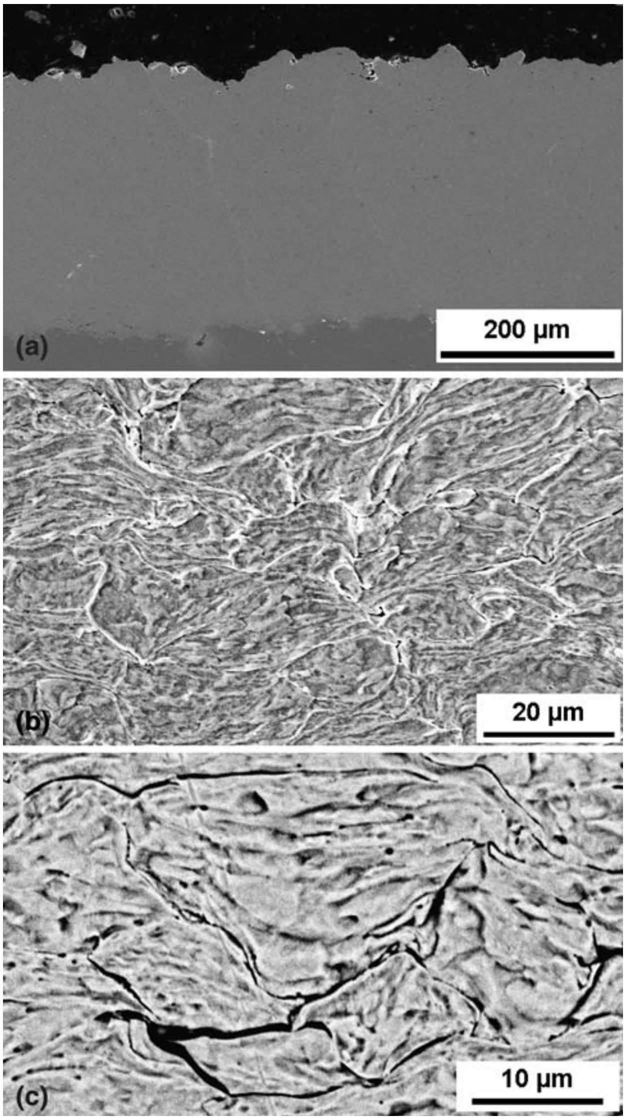

Fig. 9 Cold sprayed Ni coating on grit blasted steel (a) unetched, (b) etched, and (c) etched BSE image

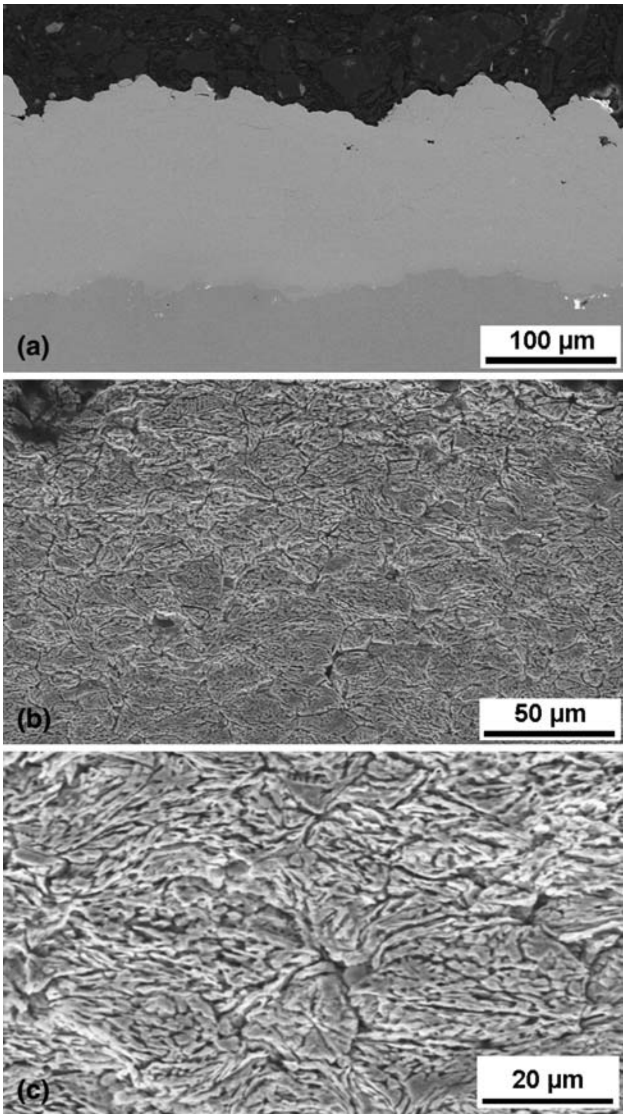

Fig. 10 Cold sprayed Ni-30%Cu coating on grit blasted steel (a) unetched, (b), and (c) etched

microstructures as that shown in Fig. 6a. All cold sprayed Cu coatings were found to be dense showing no signs of porosity or voids. Figures 6b and c present the etched microstructures of the cold sprayed Cu coating prepared from the fine size BSA powder. The particle boundaries and deformation present in the form of slip bands in the coating particles are seen in the etched microstructure. The actual grain size within the particles is not clearly seen. The sprayed particles show high degree of flattening when impacting the substrate or previously sprayed coating layer. Figure 7 presents the microstructure of a heat-treated cold sprayed Cu (BSA −22 + 5 μm) coating. The microstructures of cold sprayed Cu coatings heat-treated at 200 °C and 400 °C for 5 h are presented in Figs. 7a and b, respectively. At 200 °C some recrystallization has possibly taken place. This is seen as a noticeably lower amount of slip bands. The cold sprayed Cu coating heat-treated at 400 °C seems to have even less slip bands. Also the primary spray particles seem to be slightly larger. However, this needs to be verified with other characterization methods.

An etched microstructure of the cold sprayed Cu coating prepared from the slightly coarser BSA powder (BSA −38 + 10 μm) is presented in Fig. 8. Sample preparation from two different directions, i.e., from cross-section and from top of the coating, was also conducted. Shapes of particle splats in the etched cross-section sample were compared to the polished and etched top-view sample. Cross-sectional microstructure is presented in Fig. 8a and the top-view microstructure in Fig. 8b. Obviously, the shapes of the flattened and deformed particles are only seen from the cross-sectional view and not directly from the top-view.

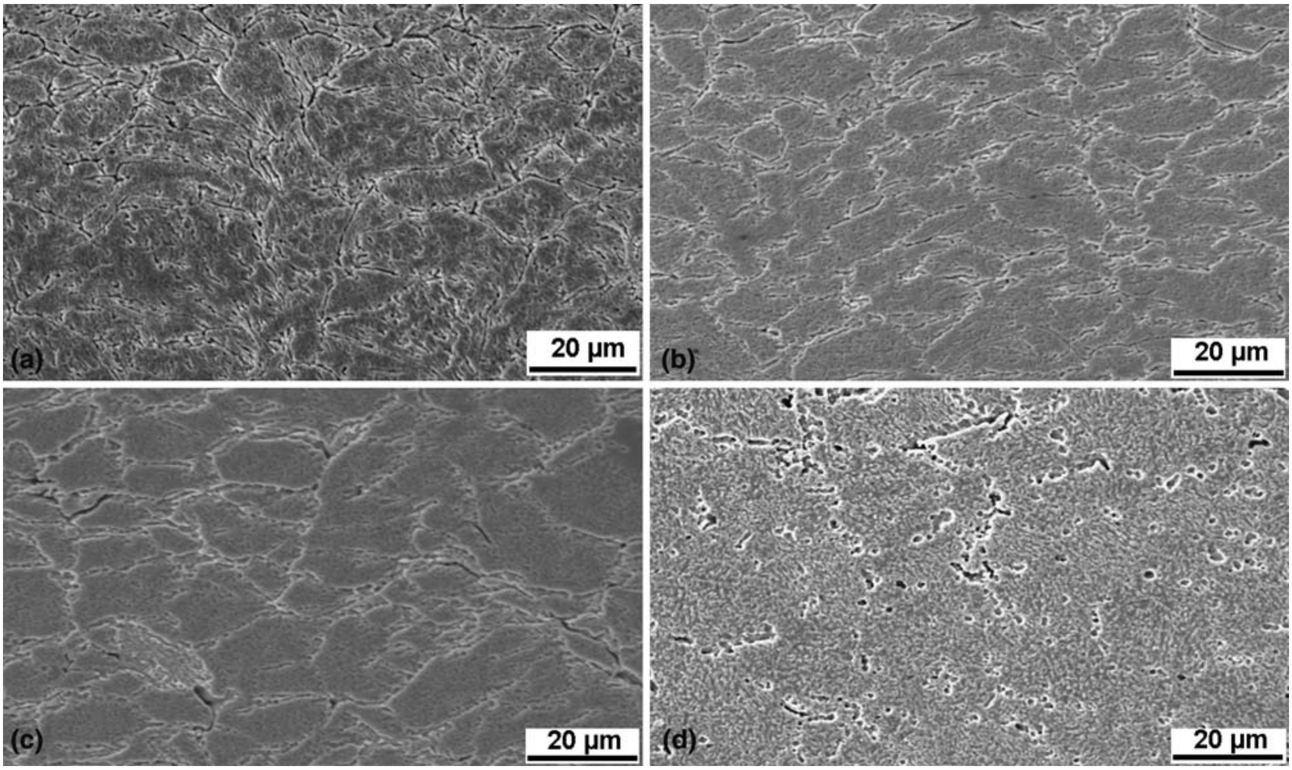

Fig. 11 Etched cold sprayed Ni-30%Cu coating, heat-treated (5 h) at (a) 400, (b) 600, (c) 800, and (d) 1000 °C

Microstructures of the cold sprayed Ni coating on grit blasted steel substrates are presented in Fig. 9. The cold sprayed Ni coating is microstructurally dense as studied by SEM. Very low amount of pores are seen in the coating microstructure, see Fig. 9a. An etched microstructure of the cold sprayed Ni coating is shown in Fig. 9b. Some particle boundaries and also grain boundaries due to the deformed material are also seen in the microstructure. The interface between the coating and the substrate was found to be mainly faultless and clean. Backscattering electron (BSE) image taken from an etched cold sprayed Ni coating is shown in Fig. 9c. The better contrast in the etched microstructure as compared to the secondary electron (SE) image (Fig. 9b) is apparently caused by the imaging method used.

The cold sprayed Ni-30%Cu coating on grit blasted steel substrate (unetched and etched microstructure) is presented in Fig. 10. This coating is also very dense with low amount of detectable pores and voids based on studies with SEM. The interface between the coating and the substrate is also mainly faultless. Some particle boundaries and also some microstructural details, possibly for example grain boundaries, are also seen in the etched specimen. Microstructures of the heat-treated cold sprayed Ni-30%Cu coatings are presented in Fig. 11. The heat treatment temperatures were 400, 600, 800, and 1000 °C. The duration of the heat treatment was 5 h. All coating specimen were etched under similar conditions, i.e., same time and etching solution. Particle boundaries were not so clearly seen with increasing heat treatment temperature. This may be a consequence of a denser cold sprayed coating with a low amount of inter-particle voids.

3.2 Denseness and Corrosion Characteristics of Cold Sprayed Coatings

More exact information about the denseness and especially about the through-porosity (open porosity) of the coatings was obtained by testing the corrosion behavior of the cold sprayed coatings. Cu, Ni and Ni-30%Cu coatings are known to give anodic protection to steel. Therefore, the open porosity has an important role on the protectiveness of such coatings on steel. The corrosion tests used in this work i.e., open cell potential measurements and salt spray (fog) testing, showed some through-porosity in the cold sprayed Ni and Ni-30%Cu coatings. These cold sprayed coatings had several areas in which the surfaces were uncorroded, which shows their potential as corrosion resistant coatings. However, both cold sprayed Ni and Ni-30%Cu coatings had several weak-points, which resulted local corrosion in the tests used in this work. Figure 12 presents the cross-sectional microstructure of the cold sprayed Ni-30%Cu coating after open cell potential measurements. The corrosion tests showed the local weak areas in the cold sprayed coatings. This coating area was chosen after corrosion test to indicate structural defects in the coating. A path for the electrolyte (3.5% NaCl solution) to penetrate into the coating and to the coating/substrate interface is partly seen in the centre of the SEM micrograph. With such imperfections the corrosive salt solution is able to penetrate through the particle boundaries from the surface to the interface causing corrosion attack in the substrate material. Some areas at the interface between the coating and the substrate are clearly open possibly due to corrosion of substrate or imperfections on the interface. Corrosion products including iron oxides were found also on the surface of the coating.

The open cell potentials of the cold sprayed Cu coatings prepared from two coarse powders were similar to open cell potential of Cu bulk. The open cell potential of the cold sprayed Cu coating (BSA −22 + 5 μm) was closer to the potential of bulk Cu than that of the HVOF sprayed Cu coating. The open cell potential results were as follows: cold sprayed (CS) Cu coating −280 mV, HVOF sprayed Cu coating −500 mV, and wrought Cu −125 mV. Figure 13 presents the open cell potential behavior as a function of the exposure time for the Cu coatings and bulk material. The open cell potential of steel grade Fe52 was −700 mV. Open cell potential of different cold sprayed Cu coatings as compared to wrought Cu and Fe52 as a reference. Open cell potential of the coatings was quite close to the curve of Cu bulk material.

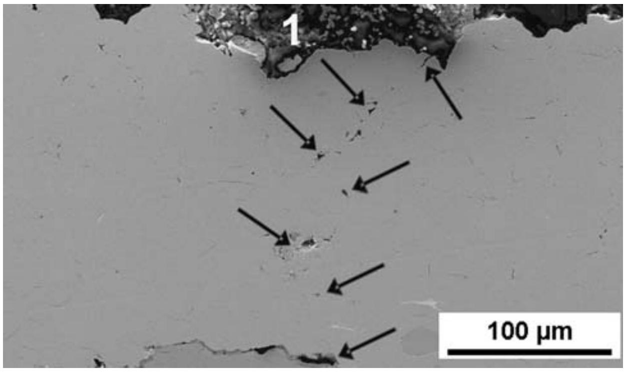

Fig. 12 Cold sprayed Ni-30%Cu coating after open cell potential measurements. Arrows indicate the possible penetrating bath. Interface seemed to be open and corrosion products (1) was seen on the top surface

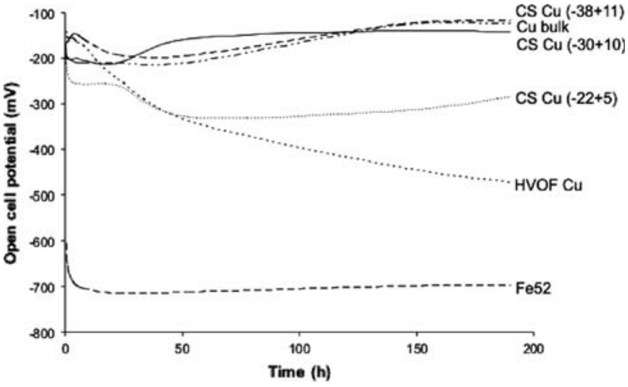

Fig. 13 Open cell potential of Cu bulk, reference Fe52, HVOF sprayed Cu, cold sprayed Cu (BSA −22 + 5 μm), cold sprayed Cu (BSA −38 + 11 μm), and cold sprayed Cu (Osprey −30 + 10 μm) as a function of exposure time

Through-porosity was found with the open cell potential measurements in the both Ni coatings. The open cell potential of the cold sprayed Ni coating was −520 mV and the HVOF sprayed Ni coating −400 mV. Electrolytically deposited standard Ni coating was chosen as a reference instead of bulk Ni and its potential was −260 mV. Open cell potential of heat-treated (400 °C and 5 h) cold sprayed Ni coating was close to the open cell potential of electrolytically deposited Ni coating (Fig. 14). The open cell potential of the as-sprayed cold sprayed Ni-30%Cu coating was −560 mV and the HVOF sprayed −260 mV, see Fig. 15. Open cell potential of the cold sprayed Ni-30%Cu coatings was near to same value after heat treatment (400 °C and 5 h) also.

Table 4 presents the summary of the visual examination of the cold sprayed and HVOF sprayed coatings on steel substrate after salt spray fog testing. Cold sprayed Cu coating was sprayed with the BSA (−22 + 5 μm) powder. The first changes detected on the coating surface during the test and the final state after exposure is shown in the table. According to the salt spray tests, the reference

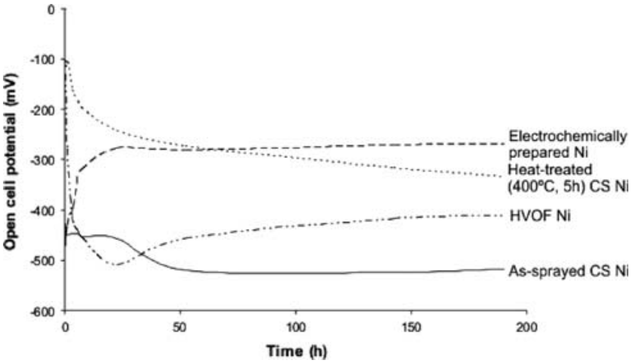

Fig. 14 Open cell potential of cold sprayed Ni coatings as-sprayed and heat-treated (400 °C and 5 h) and electrolytically prepared Ni coating as a function of exposure time

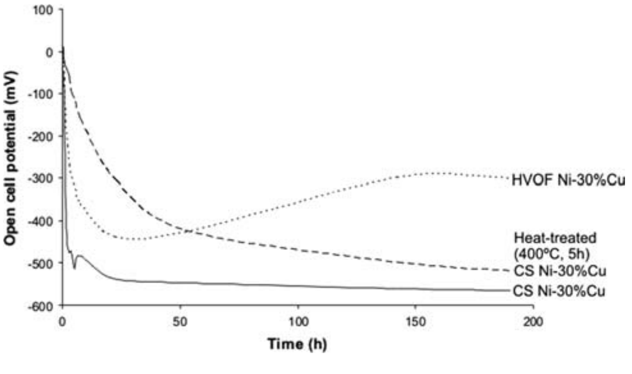

Fig. 15 Open cell potential of cold sprayed Ni-30%Cu coatings as-sprayed and heat-treated (400 °C and 5 h) and HVOF sprayed Ni-30%Cu coating as a function of exposure time

Table 4 Summary of coatings performance in salt spray fog testing

Coating	Time to first change	Final state (96 h)	Comment (96 h)
CS Cu	6 h, several corrosion spots	Pit-type corrosion	Strong rust areas
HVOF Cu	24 h, several corrosion spots	Pit-type corrosion	Strong rust areas
CS Ni	48 h, some local corrosion spots	Pit-type corrosion	Partly clean and rust areas
HVOF Ni	No changes	No corrosion products	···
CS Ni-30%Cu	6 h, several corrosion spots	Pit-type corrosion	Partly clean and rust areas
HVOF Ni-30%Cu	96 h, some local corrosion spots	Few rust areas	Local rusty areas

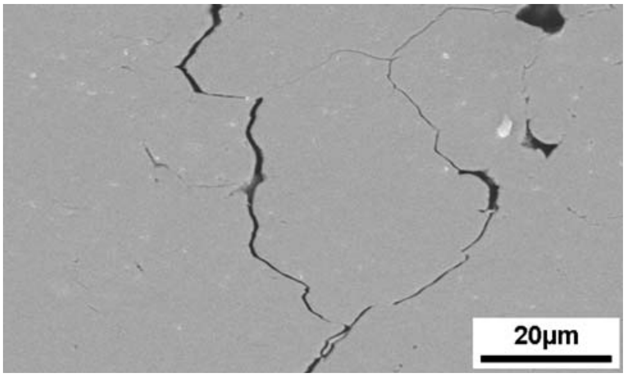

Fig. 16 Cold sprayed Ni-30%Cu coating after salt spray testing. Particle boundaries seemed to be open in some parts of the coating

HVOF coatings were found to have slightly better corrosion resistance than the cold sprayed coatings. Figure 16 presents the microstructure of the cold sprayed Ni-30%Cu coating after the salt spray test. Inter-particle boundaries seem to be also more open in the some areas of the coating than in the as-sprayed coating.

The salt spray corrosion tests showed clearly that all cold sprayed coatings were not fully protective and the coatings seemed to contain a varying amount of local defects. These areas acted as routes along which the salt solution was able to penetrate to the coating-substrate interface. It was also found that the surfaces of the cold sprayed coatings could typically have both areas with corrosion products but also areas free of these. It is apparent that the clean areas with no corrosion products reflect dense coatings with nearly perfect microstructures. Despite of the dense microstructures, as observed by SEM, the cold sprayed Ni and Ni-30%Cu coatings seemed not to be fully protective and perfect corrosion barriers due to some through-porosity present in the coatings. It is evident that more coating improvement and optimization is needed in order to produce fully protecting corrosions barriers. The HVOF sprayed coatings were found to be dense or to contain through-porosity, depending on the coating, see Table 4.

4. Discussions

4.1 Microstructure of Cold Sprayed Coatings

The cold sprayed coatings seemed to be dense according to microstructural studies of unetched coating specimens by SEM, see Figs. 6a, 9a and 10a. Pores, other voids or inter-particle boundaries were not detectable unless the coatings specimens were chemically etched. Therefore, more detailed information about the real microstructure could be obtained only from etched specimens, see Figs. 6c, 8a, 9b and 10c. Only chemical etching could reveal the inter-particle boundaries, microstructure inside the spray particles, more detailed characteristics such as slip bands or grain boundaries, and degree of deformation of the sprayed powder particles. In the cross-sectional specimen, the sprayed particles were strongly flattened due to high impact velocities of the sprayed powder particles. Deformation during cold spraying presents in the form of slip bands in the coating particles are seen to some extent in the etched microstructures. However, the actual grain size within the particles is not clearly seen. Calla et al. (Ref 5) have reported that notably degrees of grain refinement in cold spraying as compared to the original Cu powder can occur. Etching of the coating microstructure has also been reported to show highly localized particle deformation (Ref 9). Our studies showed that the interface between the coating and the substrate seemed to be almost faultless, which is known to be typical to cold sprayed coatings, see e.g., Fig. 10a. This clearly proves that the sprayed powder particles adhere well to the surface of the substrate. Moreover, the cold sprayed Ni-30%Cu coating appeared to be dense, because all particle boundaries are not clearly seen in the etched specimen.

Chemical etching of the cross-sectional coating specimen was found to be very challenging because of the different coating and substrate materials. Different nobleness of the coatings and the substrates affects the etching behavior in the cross-sectional specimen. Galvanic couples tend to form between the coating and the substrate in the presence of the chemical etching electrolyte. The steel substrate behaved sacrificially as compared to the cold sprayed Cu coating influencing that the coating did not become etched uniformly equally all around the cross-section, see Fig. 6b. Furthermore, the cold sprayed Cu coating tends to become etched more on the top of the coating as compared to the interface between the coating and the substrate. This influence in different etching behavior was eliminated in the polished specimen with top view of the coating, but obviously the microstructures are very different due to different viewing directions. The shapes of the flattened and deformed particles are only seen from the cross-sectional view and not directly from the top-view. However, the top-view examination of the cold sprayed coating particles gives a better possibility to evaluate the microstructure inside the particles as well as gives some useful information about adhesion and voids present between the sprayed particles or splats. Such voids can be detrimental to the protectiveness of the coating in corrosive environments.

Heat treatment affects microstructures and properties of the cold sprayed coatings. Heat treatment affected coating properties through the well-known by recovery, recrystallization and grain growth mechanisms. After a heat treatment at 200 °C for cold sprayed Cu coating, some recrystallization has possibly taken place showing signs of noticeably lower amount of slip bands, see Fig. 7a. Moreover, even less slip bands are observed in a cold sprayed Cu coating heat-treated at 400 °C, Fig. 7b. In the case of cold sprayed Ni-30%Cu coatings the effect of heat treatment on the microstructure appeared as different chemical etching behavior under similar etching conditions. Degrees of etching of cold sprayed Ni-30%Cu coating decreased significantly with increased heat treatment temperature, which indicates denser coating with a lower amount of inter-particle voids. Recovering is known to restore work hardening and the mechanism prevailing is the reduction of internal energy by dislocation rearrangement. After recovery the grains are still in a relatively high strain energy state. Recrystallization further decreases internal energy. Metals become softer and more ductile during recrystallization; the properties then depend on both the time and the temperature of the heat treatment. The degree of recrystallization is known to increase with time (Ref 10). At the heat treatment temperatures 200-300 °C for cold sprayed Cu coating, hardness was found to decrease and correlating with the recrystallization and thus softening of the coating material (Ref 11). Moreover, recrystallization is also seen in the microstructures of heat-treated cold sprayed coatings by different etching degrees. The heat treatment temperature 200 °C for cold sprayed Cu coating has been indicated to cause recrystallization according to Stoltenhoff et al. (Ref 9). Also they have reported that recrystallization is mainly focused at the temperature of 200 °C on strongly deformed areas. Recrystallization tends to occur more rapidly in pure metals than in metal alloys, i.e., alloying tends to raise the recrystallization temperatures (Ref 10).

4.2 Denseness and Corrosion Characteristics of Cold Sprayed Coatings

The aim of the corrosion tests was to investigate the denseness and especially the presence of through-porosity of the cold sprayed coatings. Through-porosity is critical to Cu, Ni, and Ni alloy coatings because these coatings are known to protect anodically the steel substrates against the potential corrosion attack. Production of fully dense coatings plays an important role in creating corrosion resistant and protective coatings. In this work, possibly existing through-porosity and local weak areas in the cold sprayed coatings was revealed by corrosion testing. Measurement of the open cell potentials with time of immersion could show the existing through-porosity by comparison of the potentials of coatings on substrates and reference materials, i.e., the corresponding bulk/wrought material and the carbon steel substrate. Another methods used was conventional salt spray fog testing. In this test the surfaces were studied by visual inspection of the corrosion products originating from the substrate at the interface of the coating and the substrate.

According to the open cell potential measurements cold sprayed Cu coatings prepared from slightly coarser powders, i.e., BSA −38 + 11 μm and Osprey −30 + 10 μm, were fully dense and no defects or voids were observed. Open cell potentials of these cold sprayed Cu coatings were found to be similar with the values of bulk Cu, as is presented in Fig. 13. Obviously, the powder characteristics can affect the impermeability of cold sprayed Cu coatings. The cold sprayed Cu coatings prepared from the coarser powders were dense also according to the open cell potential measurements. The cold sprayed Cu coating prepared from the finer powder (BSA −22 + 5 μm) behaved somewhat weaker than the other cold sprayed Cu coatings. Some through-porosity was found to be in this cold sprayed Cu coating. However, it should be noticed that this cold sprayed Cu (−22 + 5 μm) coating performed still better than HVOF sprayed Cu coating, although as well as the other cold sprayed Cu coatings. The cold sprayed Cu coating (−22 + 5 μm) seemed to contain some local defects according to both corrosion tests. Apparently the salt spray solution could easily found a way to penetrate to the substrate surface and corrosions products were noticed to be present on the surface of the coating. To summarize the results, fully dense Cu coating can be cold sprayed with optimum size spray powder, in this work with the coarser powder, and also with the warmer cold spraying parameters, i.e., a higher gas preheating temperature. It is possible that lower preheating temperature with finer Osprey Cu powder had an influence to the results of the corrosion tests. Process temperature can affect to the particle velocity meaning lower velocity with lower temperature. The temperature can have an influence to the denseness of the coating in the cold spraying process. Microstructure can be denser spraying with warmer parameters affecting better results during corrosion tests.

Also cold sprayed Ni and Ni-30%Cu coatings seemed to be dense according to the SEM analysis. Although the coatings appeared to be microstructurally dense, the cold sprayed Ni and Ni-30%Cu coatings showed through-porosity in the some parts of the coatings according to the corrosion tests. Some weak-points were between weakly bonded particle interfaces (pores); all particles were not well enough deformed and adhered to result in the most perfect coatings, see Figs. 12 and 16. The cold sprayed coatings contained through-porosity in the some parts of the coatings and inter-particle boundaries seemed to be more open in the some areas of the coating (Fig. 16). The bonding between the particles is stronger in the more closed areas of the particle boundaries than in the open boundaries. Pit-type corrosion areas were found to be typical to cold sprayed coatings on the coating by the surface examination during and after the corrosion tests. Reference HVOF sprayed coatings were noticed to be dense like HOVF Ni coating or to contain through-porosity like HVOF Cu and

Ni-30%Cu coatings. Some cold sprayed coating areas did not leak (clean and corrosion product-free surfaces) giving a potential to develop also even fully dense Ni and Ni-30%Cu coatings by cold spraying. This is assumed to be able to be reached by powder development and by substrate-coating pairs character balance. Effect of heat treatment to denseness was also tested with cold sprayed Ni and cold sprayed Ni-30%Cu coatings. In open cell potential measurement, cold sprayed Ni coating became denser after heat treatment because of recrystallization and softening possible due to that rearrangement of grains close the pores. Open cell potential of cold sprayed Ni coating was near to value of electrolytically deposited Ni coating indicating denser microstructure. In the case of heat-treated (400 °C) cold sprayed Ni-30%Cu coating, open cell potential (Fig. 15) did not change needing more research and development.

5. Conclusions

This study concentrated in microstructural studies of cold sprayed copper, nickel, and nickel-30%copper coatings. SEM analysis and corrosion tests were done to get more information about denseness of the coatings and characteristics of the spray particle boundaries. The cold sprayed coating seemed to be dense by microstructural examination. The interface between the coating and the substrate seemed to be fairly faultless. To reveal the real microstructure, coatings had to be etched to see the particle boundaries, deformation and microstructure inside the sprayed particles. Cold sprayed Cu coatings (coarser particle size) were dense according to SEM analysis and open cell potential measurements, indicating fully dense Cu coatings producible by cold spraying. Cold sprayed Ni and Ni-30%Cu coatings seemed also to be dense according to the SEM studies. However, corrosion tests showed some through-porosity in the cold sprayed Ni and Ni-30%Cu coatings. It was noticed that the weak-points were on the particle boundaries where the bonding is not strong and uniform enough between the particles. Areas with corrosion products and clean uncorroded surface areas after corrosion tests were found to be typical for the cold sprayed coatings. Moreover, those clean areas showed that the possibility to produce fully dense Ni and Ni-30%Cu coatings by cold spraying. Furthermore, cold sprayed Ni coating became denser after heat treatment (400 °C, 5 h) because of pores closuring by rearrangement of grains and softening. Further research should be focussed to development and optimization of the spray powders as well as in optimization of the cold spray parameters and process to produce microstructurally fully dense coatings. Such examinations should also include SEM analysis and corrosion tests to be able to detect the real protectiveness of the coatings.

Acknowledgments

The authors would like to thank Mr. Werner Krömmer from Linde AG Gas for spraying coatings and for valuable discussions. The work in which this study was done was funded by The National Technology Agency of Finland (Tekes) and some Finnish industrial companies.

References

1. T. Stoltenhoff, H. Kreye, and H.J. Richter, An Analysis of the Cold Spray Process and its Coatings, *J. Therm. Spray Technol.*, 2001, **11**(4), p 542-550
2. T.H. Van Steenkiste, J.R. Smith, and R.E. Teets, Aluminum Coatings via Kinetic Spray with Relatively Large Powder Particles, *Surf. Coat. Technol.*, 2002, **154**, p 237-252
3. R.C. Dykhuizen and M.F. Smith, Gas Dynamic Principles of Cold Spray, *J. Therm. Spray Technol.*, 1998, **7**(2), p 205-212
4. C. Borchers, F. Gärtner, T. Stoltenhoff, H. Assadi, and H. Kreye, Microstructural and Macroscopic Properties of Cold Sprayed Copper Coatings, *J. Appl. Phys.*, 2003, **93**(12), p 10064-10070
5. E. Calla, D. G. McGartney, and P.H. Shipway, Effect of Heat Treatment on the Structure and Properties of Cold Sprayed Copper, *Thermal Spray 2005: Explore its Surfacing Potential!*, ASM International, May 2-4, 2005 (Basel, Switzerland), ASM International, 2005
6. K. Balani, T. Laha, A. Agarwal, J. Karthikeyan, and N. Munroe, Effect of Carrier Gases on Microstructural and Electrochemical Behavior of Cold-sprayed 1100 Aluminum Coating, *Surf. Coat. Technol.*, 2005, **195**, p 272-279
7. R. E. Blose, D. Vasquez, and W. Kratochvil, Metal Passivation to Resist Corrosion using the Cold Spray Process, *Thermal Spray 2005: Explore Its Surfacing Potential!*, ASM International, May 2-4, 2005 (Basel, Switzerland), ASM International, 2005
8. "Standard Test Method of Salt Spray (Fog) Testing," B117-90, Annual Book of ASTM Standards, ASTM, p 19-25
9. T. Stoltenhoff, C. Borchers, F. Gärtner, and H. Kreye, Microstructures and Key Properties of Cold-sprayed and Thermally Sprayed Copper Coatings, *Surf. Coat. Technol.*, 2006, **200**, p 4947-4960
10. W. D. Callister, *Materials Science and Engineering*, 5th ed, John Wiley & Sons, Inc. 2000, 871 p
11. J. Lagerbom, H. Mäkinen, and P. Vuoristo, Effect of Heat Treatment on Properties of Cold Sprayed Coatings, *Thermal Spray 2005: Explore Its Surfacing Potential!*, ASM International, May 2-4, 2005 (Basel, Switzerland), ASM International, 2005

Publication II

Heli Koivuluoto, Juha Lagerbom, Mikko Kylmälahti and Petri Vuoristo

Microstructure and Mechanical Properties of Low-Pressure Cold-Sprayed (LPCS) Coatings

Journal of Thermal Spray Technology, 17 (5-6) 2008, p. 721-727

Reprinted from Journal of Thermal Spray Technology with permission of ASM International.
Copyright (2008) ASM International.

JTTEE5 17:721–727
DOI: 10.1007/s11666-008-9245-6
1059-9630/$19.00 © ASM International

Peer Reviewed

Microstructure and Mechanical Properties of Low-Pressure Cold-Sprayed (LPCS) Coatings

Heli Koivuluoto, Juha Lagerbom, Mikko Kylmälahti, and Petri Vuoristo

(Submitted May 7, 2008; in revised form September 9, 2008)

In low-pressure cold spraying, compressed air is used as a process gas. The most important process parameters are temperature and pressure. In the Low-Pressure Cold Spraying (LPCS) system in this study, the maximum preheating temperature is 650 °C and pressure is 9 bar. Powders used in LPCS process contain alumina with metallic powders; therefore LPCS is the method to spray soft metallic coatings with ceramic hard phase for different application areas, e.g., thick coatings and coatings for electrical and thermal conduction and corrosion protection applications. The aim of this study was to investigate microstructure, denseness, and mechanical properties of LPCS Cu, Ni, and Zn coatings. LPCS coatings seemed to be dense according to Scanning Electron Microscope (SEM) studies but corrosion tests were needed to identify the existence of porosity. Through-porosity was observed in structures of the LPCS coatings. Bond strengths of LPCS Cu and Zn coatings were found to be 20-30 MPa, and hardness was high indicating reinforcement and work hardening.

Keywords copper, low-pressure cold spraying, mechanical properties, microstructure, nickel, zinc

1. Introduction

Cold spraying was developed in the former Soviet Union in the 1980s. Cold spraying is regarded as the latest development in the thermal spray techniques. The process is based on the utilization of significantly lower process temperatures with high particle velocities than those in other thermal spray methods. A coating is formed when powder particles impact at high velocities (high kinetic energy) on the substrate, deform, and adhere to substrate or to other particles. Moreover, good bonding between the cold-sprayed powder particles needs a high degree of plastic deformation upon the particle impact (Ref 1, 2). In low-pressure cold spraying (LPCS), preheating temperatures of the process gas (air) are between room temperature (RT) and 650 °C, and pressures are between 5 and 9 bar. Typically, compressed air is used in this method as the process gas to spray powder mixtures (Ref 3). Particle velocities are reported to be approximately from 350 to 700 m/s in the low-pressure cold spray process (Ref 4). Irissou et al. (Ref 5) have reported particle velocities of 580 m/s for Al_2O_3 particles (mean size 25.5 μm). In addition, Ning et al. (Ref 6) have updated mean particle velocities of 450 m/s for Cu particles (30 μm) (sprayed with helium). Furthermore, irregular particles have reportedly higher in-flight velocities compared to spherical particles (Ref 6) possibly explaining the utilization of dendritic particles in the some cases (e.g., Cu and Ni) in LPCS process.

Low-Pressure Cold-Sprayed (LPCS) is the method to spray metallic powders (e.g., Cu, Al, Ni, Zn) with an addition of ceramic powder in the blended spray powder. Different substrate materials, e.g., metals, ceramics, and plastics, can be used. The main functions of the ceramic addition are the activation of the sprayed surfaces and the cleaning of the nozzle of the gun. In addition to these, ceramic particles are affected by mechanical hammering of the substrate/sprayed layers or by the so-called shot peening via particle impacts (Ref 7). Ceramic addition in the powder also has a compacting effect during the impact, indicating influences on coating properties and improved deposition efficiency (Ref 8). Shkodkin et al. (Ref 8) have reported increased bond strength and coating density with increasing ceramic addition. The amount of ceramic particles in the sprayed coating is low compared to initial powder composition. Usually, coatings contain ceramic particles below 5% of the total amount of ceramic powder (Ref 8). This indicates the erosion occurrence of and also activation by ceramic particles (Ref 8, 9). A hard phase

---

This article is an invited paper selected from presentations at the 2008 International Thermal Spray Conference and has been expanded from the original presentation. It is simultaneously published in *Thermal Spray Crossing Borders, Proceedings of the 2008 International Thermal Spray Conference*, Maastricht, The Netherlands, June 2-4, 2008, Basil R. Marple, Margaret M. Hyland, Yuk-Chiu Lau, Chang-Jiu Li, Rogerio S. Lima, and Ghislain Montavon, Ed., ASM International, Materials Park, OH, 2008.

Heli Koivuluoto, Juha Lagerbom, Mikko Kylmälahti, and **Petri Vuoristo**, Department of Materials Science, Tampere University of Technology, P.O. Box 589, 33101 Tampere, Finland. Contact e-mail: heli.koivuluoto@tut.fi.

can be used for the purpose of reinforcement to strengthen the metallic matrix in LPCS process (Ref 10). Low-pressure cold spraying has many advantageous features, e.g., possibility to produce thick coatings, use in repair and shape modification of molds (Ref 3, 8). Low-pressure cold spraying or radial injection gas dynamic spray (RIGDS) reportedly have applications in the fields of aerospace, automotive, and rebuild industries (Ref 2).

Copper has good electrical and thermal conductivity (Ref 11); therefore it has been used often as a well-conducting coating material. Furthermore, nickel has good corrosion-resistance in many corrosion environments (Ref 12). Zinc is also a good corrosion resistant material for applications in which corrosion protection is provided by cathodic protection of steels. Zinc coatings act as a sacrificial anode protection (Ref 13). Zinc coatings are, therefore, mostly used only for corrosion protection, e.g., in car industry (Ref 3).

The aim of this study was to characterize microstructures of LPCS Cu, Ni, and Zn coatings and to get more information about the denseness of these coatings by corrosion studies. Moreover, mechanical properties (hardness and bond strength) on grit-blasted steel and copper substrates were investigated to get more information about coatings, and, as well as the influences of hard, ceramic phase on the coating properties.

2. Experimental Procedure

In this study, LPCS Cu, Ni, and Zn coatings were prepared at Tampere University of Technology with a DYMET 304 K equipment. Compressed air was used as a process gas. Spraying parameters are summarized in Table 1. DYMET equipment was installed into an x-y manipulator. A round (Ø 5 mm) tubular nozzle was used in this study. Substrates were grit-blasted (mesh 24, Al_2O_3 grits) steel and copper plates with the dimensions of 100 × 50 × 5 mm.

Three commercial powders were tested in LPCS process. Figure 1 shows the morphologies of copper powder K-01-01 ($Cu + 50vol.\text{-}\%Al_2O_3$), nickel powder K32 ($Ni + 50vol.\text{-}\%Al_2O_3$), and zinc powder K-0011 ($Zn + 50vol.\text{-}\% Al_2O_3$) from OCPS (Obninsk Center for Powder Spraying). Copper and nickel powders were electrolytically prepared, having a dendritic structure, whereas zinc powder was atomized and possessed a spherical shape. With all these powder mixtures, the ceramic particles in the metal/ceramic powder blends were a fused and crushed alumina (Al_2O_3), having a blocky and irregular shape.

LPCS coatings were characterized using a Philips XL30 Scanning Electron Microscope (SEM). The microstructures of LPCS coatings were studied from metallographic cross sections (unetched and etched structures). LPCS Cu coating was etched with an etching solution of 95 mL ethanol, 5 g $FeCl_3$ and 2 mL HCl. Denseness, and especially through-porosity of the LPCS coatings, was tested with corrosion tests, open-cell electrochemical potential measurements, and salt spray (fog) test. The electrochemical cell used in the open-cell potential measurements consisted of a tube, of diameter 20 mm and volume 12 mL, glued on the surface of the coating specimen. A 3.5 wt.% NaCl solution was poured into the tubes for

Table 1 Spraying parameters of LPCS coatings. Beam distance stands for distance between two adjacent spray beads

Spraying parameter	LPCS Cu	LPCS Ni	LPCS Zn
Pressure, bar	6	6	6
Preheating temperature, °C	540	540	440
Powder feed, g/min	20	15	24
Traverse speed, m/min	6	6	6
Beam distance, mm	1	1	1
Spraying distance, mm	10	10	10
Number of layers	2	7	2

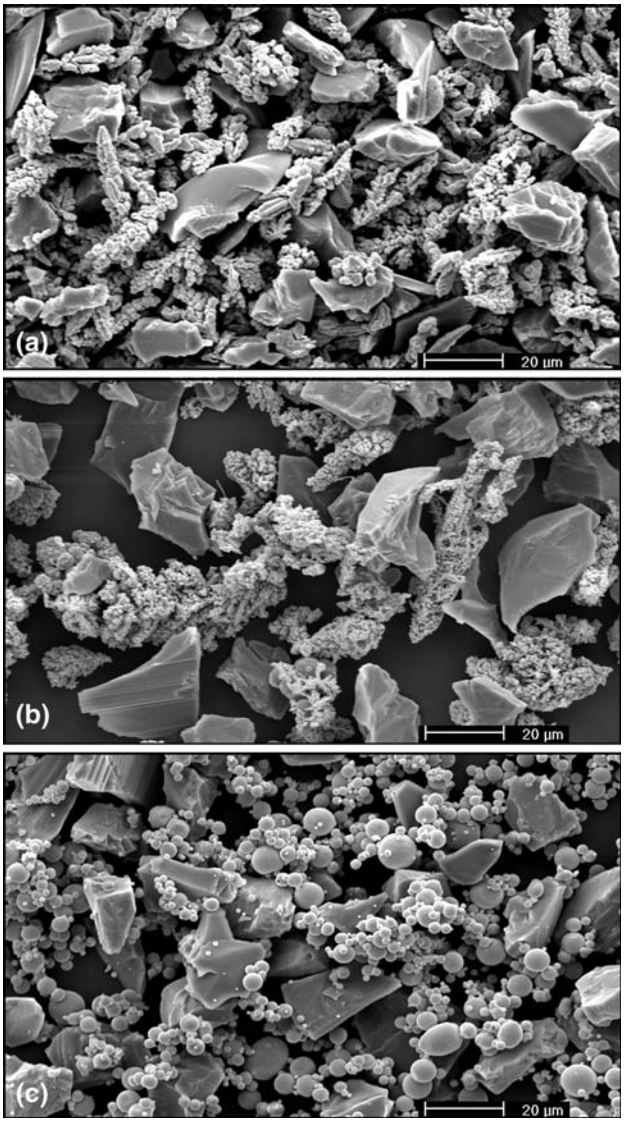

Fig. 1 Morphologies of powders (a) $Cu + Al_2O_3$, (b) $Ni + Al_2O_3$, and (c) $Zn + Al_2O_3$ used in LPCS process

nine-day measurements. Open-cell potential measurements were done with a Fluke 79 III true RMS multimeter. A silver/silver chloride (Ag/AgCl) electrode was used as a reference electrode. Salt spray fog test was done according to the ASTM B117 standard. A 5-wt.% NaCl solution was used with an exposure of 96 h, a temperature of 35-40 °C, a solution pH of 6.3, and a solution accumulation of 0.04 mL/cm^2 h. Samples were visually examined before, during, and after exposure.

Mechanical properties, hardness, and bond strength were also tested. Vickers hardness ($HV_{0.3}$) was measured as an average of ten measurements with a Matsuzawa MMT-X7 hardness tester. Bond strength values were determined according to the standard EN582 in a tensile pull test (Instron 1185 mechanical testing machine). Three measurements were carried out to calculate the average values of bond strength or in this case cohesive strength because of fracture planes (more details later).

3. Results and Discussion

The microstructural details, i.e., microstructure and denseness (existence of through-porosity) were investigated in this study. In addition, mechanical properties, hardness and bond strength, were obtained to gain more information about coating properties.

3.1 Microstructure of LPCS Coatings

Microstructures of LPCS Cu, Ni, and Zn coatings on grit-blasted steel substrates were investigated with SEM (SE and BSE images) analysis (Fig. 2, 3, and 4, respectively). In the microstructures of LPCS Cu, Ni, and Zn coatings, the detected black particles are Al_2O_3, arising from the powder mixture. The thickness of LPCS Cu coating was 200 μm. According to visual examination, LPCS Cu coating seemed to be dense without any noticeable pores (Fig. 2a). However, some oxidized areas (dark gray areas) between particle boundaries are detected in the coating structure (Fig. 2b, BSE image). LPCS Cu coating was etched to reveal the real cross-sectional microstructure. Powder particle boundaries cannot be noticed in the microstructure but the primary particle boundaries can be observed from the etched microstructure (Fig. 2c). It is possible that powder particle with dendritic structure breaks down during the particle impact on the surface of substrate or other particles. Moreover, flattened shape of primary particles indicates that high degree of plastic deformation occurred during spraying.

Figure 3(a) presents the microstructure of LPCS Ni coatings. The thickness of LPCS Ni coating was 290 μm. LPCS Ni coating was relatively dense according to visual observation. However, some open boundaries can be detected near the coating surface and some oxidized boundaries can be observed in the coating structure (Fig. 3b). Oxidation was mostly concentrated in the primary particle boundaries in the structure of LPCS Cu and Ni coatings, which is shown in Fig. 2(b) and 3(b). As-received powder particles had an oxidized layer on the surface caused by the electrolytic production method of the powder. Dendritic particles have large surface areas and, hence, more oxidized areas than on the surface of, e.g., atomized spherical particles. In addition, it is possible that powder particles oxidized during spraying because air was used as a process gas. Thus, oxidized boundaries in the coating structure were possibly originated both from oxidized layers in the powder particles and from oxidation during spraying (both during in-flight and on the substrate).

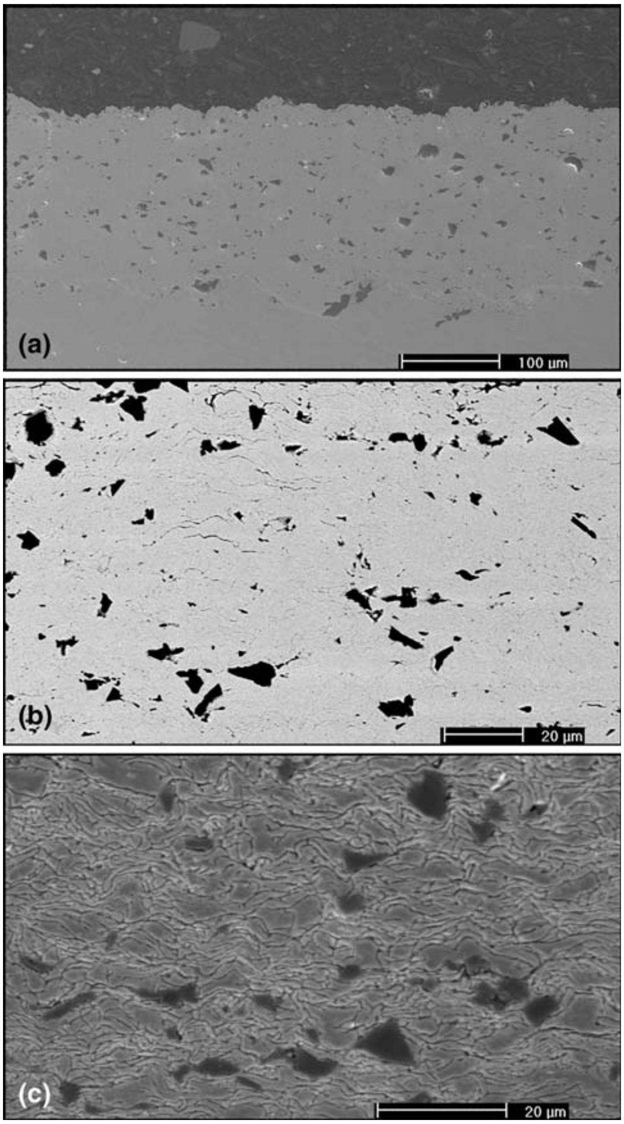

Fig. 2 LPCS Cu coating on grit-blasted steel substrate (a) SE image, (b) BSE image, and (c) SE image, etched microstructure

The detected black particles in the LPCS Zn coating also were Al_2O_3 particles on the gray metallic matrix (Fig. 4). The thickness of LPCS Zn coating was 150 μm. The structure of LPCS Zn coating by BSE image (SEM) differs from the structure of LPCS Cu and Ni coatings because of the different types (shape, production method)

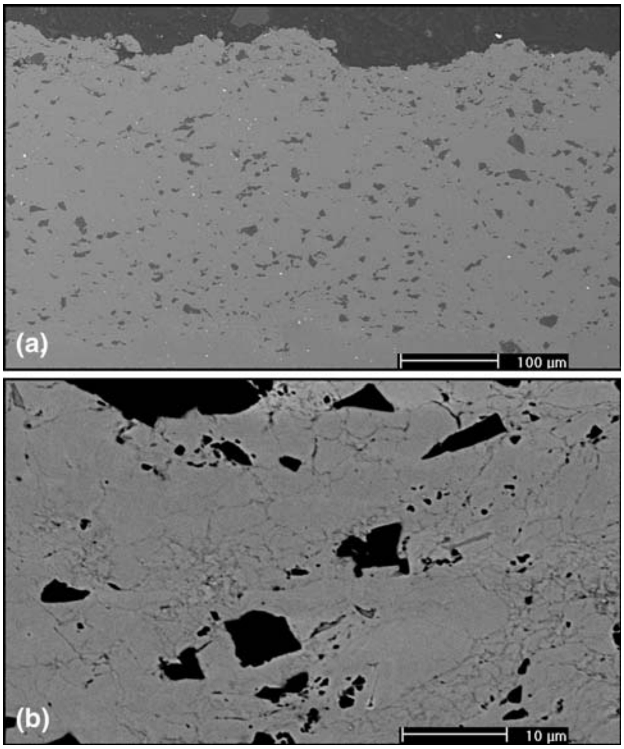

Fig. 3 LPCS Ni coating on grit-blasted steel substrate (a) SE image and (b) BSE image

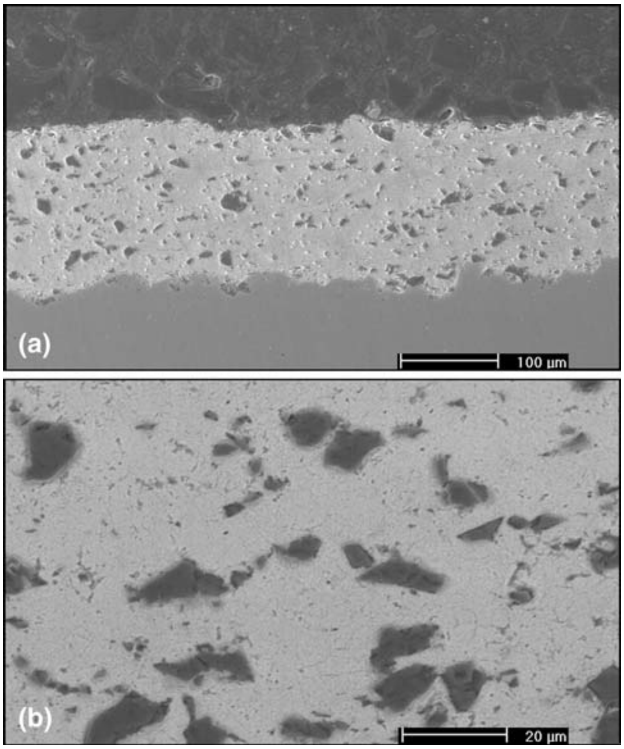

Fig. 4 LPCS Zn coating on grit-blasted steel substrate (a) SE image and (b) BSE image

of powders. Zinc powders were atomized, whereas nickel and copper were electrically prepared. Particle boundaries (initial state spherical particle shape) were imperceptible from unetched structure, indicating visually dense microstructure (Fig. 4b). Besides, it should be noticed that low amount of porosity in zinc coatings can be allowed because the steel substrate is in any case protected cathodically by the zinc coating. In summary, LPCS Cu, Ni, and Zn coatings were dense according to visual evaluation by SEM. Noticeable pores were not observed in the coating structures; nevertheless, some oxidized areas or boundaries can be detected especially in the LPCS Ni coating.

3.2 Denseness of LPCS Coatings

LPCS coatings were found to be quite dense according to SEM examinations. Furthermore, denseness was investigated with corrosion tests to get more information about existing through-porosity (open-porosity). The corrosion tests used were open-cell potential measurement and salt spray fog test.

Open-cell potentials of LPCS Cu and Ni coatings are presented in Fig. 5 and 6 as a function of exposure time. During the exposure, the behavior of the LPCS Cu coating was compared to the behavior of bulk Cu plate and

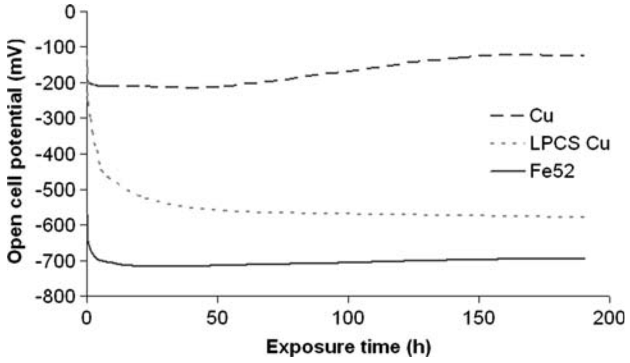

Fig. 5 Open-cell potential of Cu bulk material, LPCS Cu coating, and Fe52 substrate material as a function of exposure time (Ag/AgCl reference electrode)

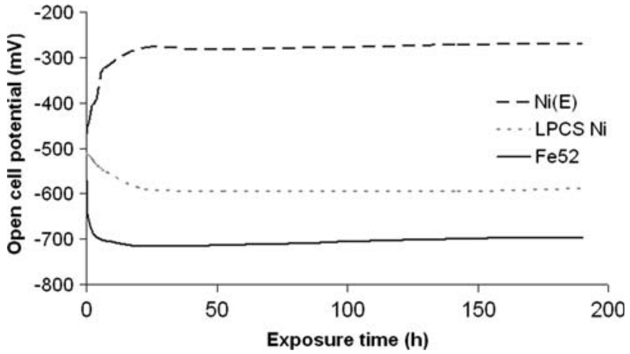

Fig. 6 Open-cell potential of electrolytically prepared Ni coating (Ni(E)), LPCS Ni coating, and Fe52 substrate material as a function of exposure time (Ag/AgCl reference electrode)

substrate material Fe52 plate to find out existing porosity. When open-cell potential curve of the coating is close to the curve of bulk material, it indicates denseness (impermeability) of the coating. However, if the value of the coating is closer to the substrate material, it reflects through-porosity, indicating the open way for exposure solution (NaCl in this study) from the coating surface to interface between coating and substrate. LPCS Cu coating was not fully dense because of existing through-porosity (Fig. 5). The LPCS Ni coating showed similar behavior as the LPCS Cu coating in the open-cell potential measurements. LPCS Ni coating contained also through-porosity (Fig. 6). Electrolytically prepared Ni coating was chosen as a reference sample in this study. In addition, corrosion products from the substrate material (iron oxide) were found by visual examination on the surfaces of LPCS Cu and Ni coatings after exposure. Open-cell potential of LPCS Zn coating was stabilized to the value of −1020 mV. Typically, zinc coating gives cathodic protection to steel substrate, behaving like a sacrificial anode. Because of cathodic protection, denseness (overall dense structure) is not critical for corrosion resistance in the case of zinc coatings.

In addition, denseness of LPCS Cu, Ni, and Zn coatings were tested with salt spray fog test. After exposure, coatings were visually examined. According to visual analysis, corrosion products from substrate material (iron oxide, rust) were detected on the surface of LPCS Cu and Ni coatings, indicating existence of through-porosity. Moreover, only white rust (corrosion product of zinc) was observed on the surface of LPCS Zn coating, indicating sacrificial behavior and at the same time corrosion protection.

According to corrosion tests (open-cell potential measurements and salt spray fog test) LPCS Cu and Ni coatings contained through-porosity. However, steel substrate was protected cathodically by LPCS Zn coating. The addition of ceramic particles has been reported to have an influence on the denseness of the LPCS Al coatings, indicating the possibility of spraying dense coatings with low-pressure cold spray equipment (Ref 5). This will need optimization of powder mixtures and spraying parameters for other coating materials to produce dense coatings with LPCS process.

3.3 Mechanical Properties of LPCS Coatings

3.3.1 Hardness of LPCS Coatings. Hardness of LPCS Cu, Ni, and Zn coatings on both steel and copper substrates is summarized in Table 2. Increased hardness of coatings indicates work hardening due to particle impacts. Somewhat higher hardness values of the LPCS coatings indicated a high level of plastic deformation and strain hardening. Moreover, it should be noticed that Al_2O_3 addition can also have influence on the hardness by increasing the values. The hard phase in the powder mixture was found to have an activation effect of the surface and also a hardening effect, which is seen in the hardness values. Substrate material did not have remarkable influence on the hardness of LPCS Cu, Ni, or Zn coatings.

The hardness of LPCS Cu coating was higher as compared to bulk material than in the cases of LPCS Ni coating. This clearly indicates a higher degree of plastic deformation. The impact may be much stronger in the case of LPCS Cu coating. The hardness of bulk Cu is reported in earlier studies to be $HV_{0.3}$ 90 (Ref 14), which is lower than the value of the LPCS Cu coating. The hardness of high-pressure cold-sprayed (HPCS) Cu and Ni coatings are $HV_{0.1}$ 147 and 238, respectively (Ref 14). The hardness of Ni and Zn bulk materials was $HV_{0.3}$ 111 (stand. dev. 9.0) and 43 (stand. dev. 1.8), respectively. HPCS coatings had higher hardness possibly arising from higher level of plastic deformation. However, it should be noticed that the production method of metallic powder is different and is therefore possibly affecting the hardness values as well. The hardness of LPCS Cu was closer to the value of HPCS Cu than LPCS Ni compared to HPCS Ni coating. This indicates higher level of deformation and more work hardening due to impacts in the case of LPCS Cu particles. In addition, high values of standard deviations (Table 2, stand. dev.) in the hardness measurements of LPCS Ni coatings reflect poor coating quality and very heterogeneous structure.

3.3.2 Bond Strength of LPCS Coatings. The bond strengths of LPCS Cu, Ni, and Zn coatings on both steel and copper substrates were measured with tensile pull tests. Fracture planes were inside the coating, meaning cohesive type fracture. In all the cases, the fracture was found nearer to the interface between coating and substrate but still inside the coating (Table 3).

LPCS Zn coating has significantly high bond strength on both steel and copper substrates, indicating good bonding between coating and substrate, and also between the sprayed particles. Adhesion of LPCS Zn was significantly higher compared to HPCS Zn coating, 13 MPa (Ref 14) on steel substrate arising from the reinforcement effect of Al_2O_3. In this study, all LPCS coatings had the weakest point in the coating. It can be supposed that

Table 2 Hardness ($HV_{0.3}$) of LPCS coatings

Coating	Substrate	Hardness, $HV_{0.3}$	Stand. dev.
Cu	Steel	105	5.3
Cu	Cu	104	3.6
Ni	Steel	119	21.4
Ni	Cu	124	31.7
Zn	Steel	57	0.8
Zn	Cu	57	1.1

Table 3 Bond strength of LPCS coatings

Coating	Substrate	Bond strength, MPa	Stand. dev.
Cu	Steel	20	3.6
Cu	Cu	23	4.1
Ni	Steel	8	3.6
Ni	Cu	9	0.5
Zn	Steel	33	4.7
Zn	Cu	38	0.7

adhesion between coating and substrate was at least the value of the bond (cohesive type) strengths. The bond strength of LPCS Cu coating was also reasonable, 20-23 MPa, and higher than the value of HPCS Cu coating (process gas N_2) on steel substrate (8 MPa) (Ref 14). In the case of LPCS Ni coating, the bond strength was very low, indicating poor bonding between powder particles. Moderate values of bond strengths of LPCS coatings are caused by defects (e.g., pores and imperfect interparticle contacts) and also thin oxide layers between particles (Ref 15), which were also noticed in this study, especially with the LPCS Ni coating. LPCS Ni particles did not undergo as high a plastic deformation as LPCS Cu particles, and thus, the bonds between particles were very moderate due to the possibly stronger oxide layers of powder particles, making even weaker bonding without destroying the oxide layer during impact. On the other hand, ceramic phase has been reported elsewhere to affect adhesion between particles and substrates by increasing it (Ref 5). Lee et al. (Ref 16) have reported that ceramic addition in the powder increased the adhesion of cold-sprayed $Al\text{-}Al_2O_3$ coatings compared to pure Al coating. High adhesion is due to the size of craters between coating and substrate (like activation) (Ref 16). Cohesive type fracture after tensile tests can be explained by poor adhesion between metallic and ceramic particles (Ref 5).

4. Summary

LPCS Cu and Ni coatings were dense according to SEM analysis, whereas through-porosity was observed in the corrosion tests. Some oxidized boundaries and other microscale defects were detected as the weak points in the microstructure, indicating poor bonding and existence of small interparticle porosity. Although the hard phase (Al_2O_3) had a reinforcing effect, it apparently did not hammer the metallic matrix enough to form a dense coating structure (e.g., destroy oxide layers in the powder particle and primary particle boundaries). At least, visually dense and thick coatings can be sprayed with low-pressure cold spraying for applications where corrosion resistance is not crucial (e.g., for electrical and thermal conduction applications). Moreover, LPCS Zn coating was also visually dense and the open-cell potential was electronegative, indicating corrosion resistance behaving like sacrificial anode for the protection of steel substrates.

In this study, mechanical properties were reasonable instead of the bond strength of LPCS Ni coating. High hardness values measured indicated work hardening occurring during spraying. On the other hand, ceramic addition can affect the values. The weak points were at the bonding between particles, indicating cohesive failure type fracture. Therefore, adhesion between particles and substrates was not the most critical point (similar to thermally sprayed coatings).

Optimization of powders, substrates, their combinations, and, moreover, substrate pretreatments and hard phase addition will be investigated in future to produce dense and well-adhered coatings with low-pressure cold spray process.

Acknowledgments

The research was funded by Finnish Funding Agency for Technology and Innovation (TEKES) and a group of Finnish industrial companies.

References

1. C. Borchers, F. Gärtner, T. Stoltenhoff, H. Assadi, and H. Kreye, Microstructural and Macroscopic Properties of Cold Sprayed Copper Coatings, *J. Appl. Phys.*, 2003, **93**(12), p 10064-10070
2. R.G. Maev and V. Leshchynsky, Air Gas Dynamic Spraying of Powder Mixtures: Theory and Application, *J. Therm. Spray Tech.*, 2006, **15**(2), p 198-205
3. A. Kashirin, O. Klyuev, T. Buzdygar, and A. Shkodkin, DYMET Technology Evolution and Application, *Global Coating Solutions: Proceedings of the 2007 International Thermal Spray Conference*, B.R. Marple, M.M. Hyland, Y.C. Lau, C.-J. Li, R.S. Lima, and G. Montavon, Eds., May 14-16, 2007 (Beijing, China), ASM International, p 141-145
4. X.-J. Ning, J.-H. Jang, H.-J. Kim, C.-J. Li, and C. Lee, Cold Spraying of Al-Sn Binary Alloy: Coating Characteristics and Particle Bonding Features. *Surf. Coat. Technol.*, 2008, **202**(9), p 1681-1687
5. E. Irissou, J.-G. Legoux, B. Arsenault, and C. Moreau, Investigation of $Al\text{-}Al_2O_3$ Cold Spray Coating Formation and Properties, *J. Therm. Spray Tech.*, 2007, **16**(5-6), p 661-668
6. X.-J. Ning, J.-H. Jang, and H.-J. Kim, The Effects of Powder Properties on In-Flight Particle Velocity and Deposition Process during Low Pressure Cold Spray Process, *Appl. Surf. Sci.*, 2007, **253**(18), p 7449-7455
7. B.B. Djordjevic and R.G. Maev, SIMAT^{TM} Application for Aerospace Corrosion Protection and Structural Repair, *Building on 100 Years Success: Proceedings of the 2006 International Thermal Spray Conference*, B.R. Marple, M.M. Hyland, Y.C. Lau, R.S. Lima, and J. Voyer, Eds., May 15-18, 2006 (Seattle, Washington, USA), ASM International, 2006
8. A. Shkodkin, A. Kashirin, O. Klyuev, and T. Buzdygar, The Basic Principles of DYMET Technology, *Building on 100 Years Success: Proceedings of the 2006 International Thermal Spray Conference*, B.R. Marple, M.M. Hyland, Y.C. Lau, R.S. Lima, and J. Voyer, Eds., May 15-18, 2006 (Seattle, Washington, USA), ASM International, 2006
9. A. Shkodkin, A. Kashirin, O. Klyuev, and T. Buzdygar, Metal Particle Deposition Stimulation by Surface Abrasive Treatment in Gas Dynamic Spraying, *J. Therm. Spray Tech.*, 2006, **15**(3), p 382-386
10. H. Weinert, E. Maeva, and E. Leshchynsky, Low Pressure Gas Dynamic Spray Forming Near-net Shape Parts, *Building on 100 Years Success: Proceedings of the 2006 International Thermal Spray Conference*, B.R. Marple, M.M. Hyland, Y.C. Lau, R.S. Lima, and J. Voyer, Eds., May 15-18, 2006 (Seattle, Washington, USA), ASM International, 2006
11. R.N. Caron and J.T. Staley, Effects of Composition, Processing, and Structure on Properties of Nonferrous Alloys, Copper and Copper Alloys, *ASM Handbooks Online*, 20, Materials Selection and Design, ASM International, 1997
12. R.N. Caron and J.T. Staley, Effects of Composition, Processing, and Structure on Properties of Nonferrous Alloys, Nickel and Nickel Alloys, *ASM Handbooks Online*, 20, Materials Selection and Design, ASM International, 1997
13. R.N. Caron and J.T. Staley, Effects of Composition, Processing, and Structure on Properties of Nonferrous Alloys, Zinc and Zinc Alloys, *ASM Handbooks Online*, 20, Materials Selection and Design, ASM International, 1997

14. H. Mäkinen (Koivuluoto), J. Lagerbom, and P. Vuoristo, Mechanical Properties and Corrosion Resistance of Cold Sprayed Coatings, *Building on 100 Years Success: Proceedings of the 2006 International Thermal Spray Conference*, B.R. Marple, M.M. Hyland, Y.C. Lau, R.S. Lima, and J. Voyer, Eds., May 15-18, 2006 (Seattle, Washington, USA), ASM International, 2006
15. M. Beneteau, W. Birtch, J. Villafuerte, J. Paille, M. Petrocik, R.G. Maev, E. Strumban, and V. Leshchynsky, Gas Dynamic Spray Composite Coatings for Iron and Steel Castings, *Building on 100 Years Success: Proceedings of the 2006 International Thermal Spray Conference*, B.R. Marple, M.M. Hyland, Y.C. Lau, R.S. Lima, and J. Voyer, Eds., May 15-18, 2006 (Seattle, Washington, USA), ASM International, 2006
16. H.Y. Lee, S.J. Jung, S.Y. Lee, Y.H. You, and K.H. Ko, Correlation between Al_2O_3 Particles and Interface of Al-Al_2O_3 Coatings by Cold Spraying, *Appl. Surf. Sci.*, 2005, **252**, p 2892-2898

Publication III

Heli Koivuluoto and Petri Vuoristo

Effect of Ceramic Particles on Properties of Cold-Sprayed Ni-20Cr+Al_2O_3 Coatings

Journal of Thermal Spray Technology, 18 (4) 2009, p. 555-562

Reprinted from Journal of Thermal Spray Technology with permission of ASM International.
Copyright (2009) ASM International.

JTTEE5 18:555–562
DOI: 10.1007/s11666-009-9345-y
1059-9630/$19.00 © ASM International

Effect of Ceramic Particles on Properties of Cold-Sprayed Ni-20Cr+Al_2O_3 Coatings

Heli Koivuluoto and Petri Vuoristo

(Submitted January 5, 2009; in revised form May 20, 2009)

Cold spraying is a thermal spray process enabling the production of metallic and metal-ceramic coatings with low porosity and low oxygen content, capable of, e.g., resisting corrosion. The aim of this study was to characterize the microstructural and mechanical properties of cold-sprayed Ni-20Cr+Al_2O_3 coatings and to clarify the effect of the hard particles on different coating properties. Accordingly, the research focused on the microstructure, denseness (impermeability), adhesion strength, and hardness of the coatings. Scanning electron microscopy (SEM) analysis and corrosion tests were run to gain information on the through-porosity. Ceramic addition in cold-sprayed Ni-20Cr+Al_2O_3 coatings improved their quality by lowering their porosity. Moreover, hardness was slightly higher than those of cold-sprayed Ni-20Cr coating, indicating a hardening effect by the ceramic particles. The addition of Al_2O_3 also made it possible to use high gas temperatures without nozzle clogging, which affects coating properties, such as coating thickness, denseness, and hardness.

Keywords coating structure, cold spraying, denseness, mechanical properties, Ni-20Cr+Al_2O_3

1. Introduction

Cold spraying, one of the latest thermal spray techniques, developed in the former Soviet Union in the 1980s, is based on lower gas temperatures and higher particle velocities than those encountered in other thermal spray methods (Ref 1). In the cold spray (CS) process, a gas is accelerated to supersonic velocity by a converging-diverging de Laval type nozzle (Ref 2). A coating is formed when powder particles at high velocities (high kinetic energy) impact on the substrate, deform, and adhere to it or to other particles. In addition, good bonding between CS powder particles requires a high plastic deformation during particle impact (Ref 3-5). Powder particles adhere to the substrate in solid form well below the powder melting temperature, and on impact deform and bond together, forming a coating (Ref 3). For successful bonding, deposition conditions should be such that oxide layers on the particle surfaces are fractured during impact (Ref 4). Cold spraying can make use of a wide range of coating and substrate materials, e.g., pure metals, metal alloys, polymers, and composites (Ref 6).

Usually, thermal-sprayed nickel alloy coatings, e.g., nickel chromium alloys, are used for applications requiring resistance to corrosion and oxidation and for repairs and bond coats (Ref 7). Thus, nickel chromium alloy coatings are of high interest to CS because the technique enables the production of metallic and metal-ceramic coatings with low porosity and low oxygen content. In these coatings, denseness (impermeability) is the criterion for good corrosion resistance (Ref 2). CS coatings also show low residual stresses, rather high adhesion, and hardness normally higher than that of the corresponding bulk materials. High hardness is caused by significant work hardening of the sprayed particles (Ref 3). Calla et al. (Ref 8) reported that an increased particle velocity due to an increased driving pressure resulted in more cold working in the coating, leading to high hardness. High velocities also result in a high impact deformation at the interface of both substrate and coating and between particles. Furthermore, gas temperature affects significantly the quality of the CS coatings. A high temperature leads to high velocity and, therefore, to strong impacts. Moreover, because deposition efficiency (DE) depends on the temperature of the gas, DE is reportedly improved at high gas temperatures (Ref 9). The gas temperature affects the gas and particle velocity, meaning higher velocity at higher temperature. Reportedly, increased particle temperature also improves the coating quality in the CS process (Ref 10, 11).

This study sought to investigate the effect of the Al_2O_3 particles on the properties of CS Ni-20Cr+Al_2O_3 coatings. It was found out experimentally some technical spraying limitations to spray Ni-20Cr powder due to the fact that high gas temperatures can cause nozzle clogging with Ni-20Cr particles. To solve such problems, a metallic powder was mixed with a ceramic powder to eliminate clogging and, consequently, to make it possible to use higher gas temperatures. The main function of the Al_2O_3 addition is to keep the nozzle of the gun clean. Furthermore, Al_2O_3 particles activate (clean and roughen) the sprayed surfaces, i.e., through activation the surface becomes cleaner and more adaptive to the sprayed

---

Heli Koivuluoto and **Petri Vuoristo**, Department of Materials Science, Tampere University of Technology, P.O. Box 589, 33101 Tampere, Finland. Contact e-mail: heli.koivuluoto@tut.fi.

particles, which then stick better to the surface. In addition to these, Al_2O_3 particles mechanically affect the coating by hammering of the substrate/sprayed layers or by the so-called shot peening effect via particle impacts (Ref 12). During the particle impacts, collision of the ceramic particles also increases the deformation of the metallic particles (compacting effect), which affects the coating properties and DE particularly in the low-pressure CS process (Ref 13). In this study, the properties of microstructure, denseness, adhesion strength, and hardness were investigated and three different particle sizes of Al_2O_3 powders and two different compositions of each particle size were tested. The aim of this work was to prepare CS Ni-20Cr+Al_2O_3 coatings with improved properties using higher gas temperatures, which were made possible by spraying Ni-20Cr with a simultaneous Al_2O_3 injection.

2. Experimental Techniques

Ni-20Cr powder was cold-sprayed with different parameters: gas temperatures of 500 °C for Ni-20Cr and 700 °C for Ni-20Cr+Al_2O_3, and with six different metal alloy-ceramic powder mixtures. A gas-atomized, spherical Ni-20Cr powder having a particle size of $-22.5+10$ μm, supplied by H.C. Starck, and as the ceramic addition fused and crushed, irregular, blocky Al_2O_3 powders, also from H.C. Starck were used in this study. Three different particle sizes of Al_2O_3 were tested, $-90+45$ μm, $-45+22$ μm, and $-22+5$ μm, in two different compositions, 50 and 30 vol.%. Grit-blasted (1 mm Al_2O_3) carbon steel sheets (50 × 100 × 1.5 mm) were used as substrates.

CS coatings were prepared at Linde AG Linde Gas Division (Unterschleissheim, Germany) with a CGT Kinetiks 4000 CS system (high-pressure CS equipment). Spraying parameters for the CS Ni-20Cr+Al_2O_3 and Ni-20Cr coatings are shown in Table 1. All Ni-20Cr+Al_2O_3 powders were sprayed using the same parameters. The CS Ni-20Cr without added Al_2O_3 particles could not be sprayed at high temperature, i.e., at 700 and 600 °C, because powder clogged the nozzle, therefore, the temperature had to be dropped to 500 °C. This is the reason the Ni-20Cr coating was sprayed at 500 °C whereas Ni-20Cr+Al_2O_3 coatings at 700 °C (Al_2O_3 particles made it possible to use higher gas temperature). Furthermore, the reason for the use of the higher gas temperature with the Ni-20Cr+Al_2O_3 powders was that reportedly high temperatures improve the coating quality (Ref 11).

The coatings were characterized using a Philips XL30 scanning electron microscope (SEM). Microstructures of the coatings were studied from unetched metallographic cross section samples, and surfaces were analyzed with a Leica MZ7.5 stereomicroscope (SM). Al_2O_3 fractions were calculated from the coating cross sections using image analysis (ImageJ). Coating thicknesses were measured from cross sections of the coatings as an average of eight measurements, whereas the coating denseness and especially the through-porosity were studied using spray tests and open-cell electrochemical potential measurements. The salt spray test was done according to the ASTM B117 standard. Substrates were masked with epoxy paint before testing in order to allow the coating surfaces to be in contact only with the corroding salt spray. A 5 wt.% NaCl solution was used with an exposure time of 48 h, a temperature of 35-40 °C, a solution pH of 6.3, and a solution accumulation of 0.04 mL/cm^2 h. Surfaces of the coatings were analyzed visually and amounts (%) of corrosion spots were characterized using image analysis (ImageJ). The electrochemical cell used in the open-cell potential measurements consisted of a plastic tube, of diameter 20 mm and volume 12 mL, glued on the surface of the coating specimen. A 3.5 wt.% NaCl solution was placed in the tube for nine-day measurements. Open-cell potential measurements were taken with a Fluke 79 III true RMS multimeter. A silver/silver chloride (Ag/AgCl) electrode was used as a reference electrode. Adhesion strength (standard EN-582) was measured in a tensile test (Instron 1185 mechanical testing machine) as an average of three measurements. Vickers hardness ($HV_{0.3}$) was measured as an average of ten measurements with a Matsuzawa hardness tester.

3. Results and Discussion

Nickel alloys are known for their good corrosion resistance. Furthermore, nickel alloy coatings give protection against wet corrosion to steel substrates that require a fully dense (overall dense) coating. The effect on the coating properties (denseness and mechanical properties) of added Al_2O_3 particles in the Ni-20Cr powder were investigated. The addition of Al_2O_3 powder was studied to decrease the coating porosity and to enable the use of higher gas temperatures.

3.1 Microstructure

The microstructure of a Ni-20Cr coating is shown in Fig. 1. Some pores and defects appear in the coating

Table 1 Spraying parameters of CS Ni-20Cr+Al_2O_3 and CS Ni-20Cr coatings

CS coating	Process gas	Pressure, bar	Gas temperature, °C	N_2 flow rate, m^3/h	Traverse speed, m/min	Number of layers
Ni-20Cr+Al_2O_3	N_2	37	700	82	20	3
Ni-20Cr	N_2	36	500	95	20	3

Spraying distance was 40 mm. Distance between two adjacent spray beads was 1.5 mm

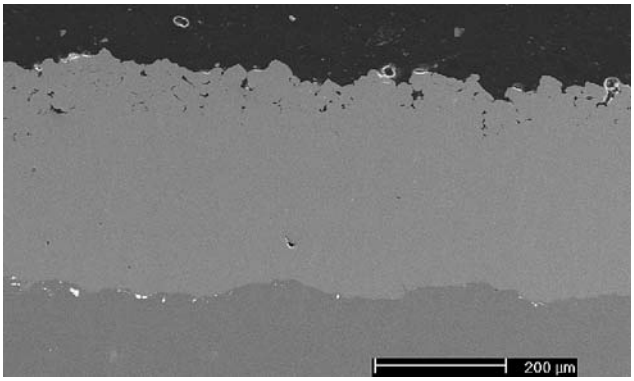

Fig. 1 Microstructure of CS Ni-20Cr coating on grit-blasted steel substrate, SEM image

structure mostly near its surface. It is worth noting that the Ni-20Cr coating without an Al_2O_3 addition was sprayed at a low gas temperature (500 °C). At higher temperatures (600 and 700 °C), the Ni-20Cr powder clogged the nozzle; therefore, 500 °C was the highest gas temperature which could be used in this study without nozzle clogging. At higher temperatures, Ni-20Cr particles were possibly in a soft-state because of thermal softening and thus, easily stuck to the surface of the nozzle whereas the Al_2O_3 particles mixed with Ni-20Cr particles apparently kept the nozzle clean and eliminated clogging. In the powder (metallic-ceramic particle mixture)—gas flow, ceramic particles can prevent metallic particles from sticking inside the nozzle wall at higher preheating temperatures. This arises from the durability of ceramic particles (high hardness and high melting point). Therefore, this study shows the comparison between Ni-20Cr and Ni-20Cr+Al_2O_3 coatings sprayed with the optimal gas temperatures for these coating materials (Ni-20Cr: 500 °C and Ni-20Cr+Al_2O_3: 700 °C).

Figure 2 shows microstructures of Ni-20Cr+Al_2O_3 coatings with Fig. 2(a) and (d) corresponding to an Al_2O_3 particle size of -90 +45 µm, Fig. 2(b) and (e) to a particle size $-45+22$ µm, and Fig. 2(c) and (f) to $-22+5$ µm with both compositions of 50% and 30%, respectively. In the microstructures, the detected dark particles are Al_2O_3. Clearly in the coating, the number of Al_2O_3 particles decreased with the lower Al_2O_3 composition (30%). Furthermore, the coating thickness was greater for the 30% Al_2O_3 composition (see Fig. 3). Table 2 summarizes the comparison between Al_2O_3 fractions in the powder and in the coating using image analysis on the coating cross sections in Fig. 2(a) to (f). The finer the Al_2O_3 particles, the better their chance of developing a velocity high enough to impact on a substrate and stick to its surface or to other particles (Ref 14). However, in some cases though fine particles may have high acceleration velocity, they also rapidly lose it after the nozzle because of bow shock waves (Ref 14). This is a possible reason that the Ni-20Cr+Al_2O_3 ($-22+5$ µm) coating contained lower amount of Al_2O_3 particles in its structure than Ni-20Cr+Al_2O_3 ($-45+22$ µm) coating. In addition, spraying materials have specific ranges of particle size (fine to coarse) at critical velocity (Ref 14). Adding Al_2O_3 particles to the metallic powder could extend the spraying conditions (possibility to use high gas temperature) to improve coating properties (e.g., microstructural properties).

Figure 3 summarizes the thicknesses of the CS Ni-20Cr+Al_2O_3 and Ni-20Cr coatings. Clearly, a higher coating thickness was achieved with less Al_2O_3 (30% instead of 50%) arisen from the initial powder composition. An Al_2O_3 addition improved the metallic deposition buildup (comparison between coating thicknesses and volume amount of metallic particles (100%, 70%, or 50%) in the powder mixtures), suggesting a compacting and peening effect of the hard particles together with an influence of higher gas temperature. This result was achieved with all the metal-ceramic powder mixtures; the best result was obtained with the 30% Al_2O_3 composition. Metallic particles have higher capability to build up the deposition (due to the capability to undergo plastic deformation during impact) than ceramic particles. Thus, powder with higher amount of Ni-20Cr particles (lower amount Al_2O_3) has higher deposition buildup. Moreover, coating thicknesses increased slightly as the Al_2O_3 particles increased in size. This is possible due to the highest compacting effect of Al_2O_3 particles during spraying.

Figure 4 compares the cross section regions near to the surfaces of Ni-20Cr and Ni-20Cr+50Al_2O_3 ($-90+45$ µm) coatings. In Fig. 4(a), the dark areas are pores and in Fig. 4(b) they are mainly Al_2O_3 particles. The Ni-20Cr coating had a porous layer with more open particle boundaries on top, whereas the Ni-20Cr+50Al_2O_3 coating was dense with only a few pores, indicating a densifing effect by the use of Al_2O_3 particles and higher gas temperature.

Adding Al_2O_3 particles to the metallic Ni-20Cr powder was observed to affect the coating's microstructure and thickness. In this study, the most important function of the Al_2O_3 powder was the possibility to use a high gas temperature to obtain a high deposition buildup. Furthermore, the porosity of the Ni-20Cr+Al_2O_3 coatings decreased with a Al_2O_3 addition, as confirmed by SEM examinations. The sprayed surfaces (substrate or previous coating layers) were activated and hammered by Al_2O_3 particles and higher gas temperatures were made possible due to the barrel cleaning action of the Al_2O_3 particles producing a denser coating structure (noticed also in corrosion studies, in Section 3.2).

3.2 Coating Denseness

A salt spray test was run to analyze the denseness of the coatings and the effect of the added Al_2O_3 particles on the protective behavior of Ni-20Cr+Al_2O_3 coatings. A pure Ni-20Cr coating was also tested for reference. Figure 5 shows a SM image of the Ni-20Cr coating surface after a 48-h exposure in a salt spray chamber. The surface was strongly corroded because corrosion products from the substrate could openly diffuse from the coating interface to its surface (through-porosity; *brown areas* in Fig. 5).

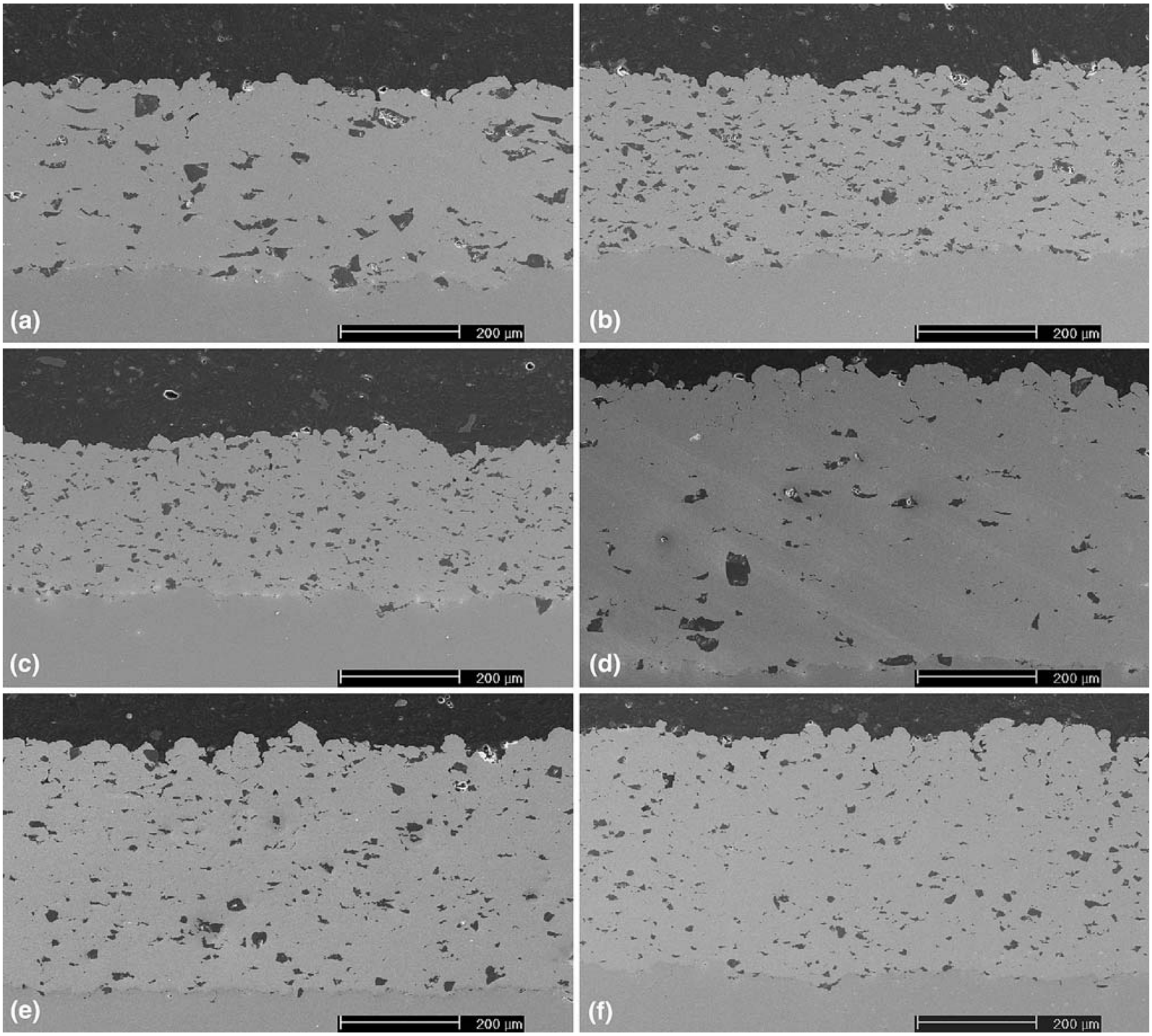

Fig. 2 Microstructure of CS (a) Ni-20Cr+50Al_2O_3 (−90 + 45 μm), (b) Ni-20Cr+50Al_2O_3 (−45 + 22 μm), (c) Ni-20Cr+50Al_2O_3 (−22 + 5 μm), (d) Ni-20Cr+30Al_2O_3 (−90 + 45 μm), (e) Ni-20Cr+30Al_2O_3 (−45 + 22 μm), and (f) Ni-20Cr+30Al_2O_3 (−22 + 5 μm) coatings on grit-blasted steel substrate, SEM images

After 48 h in the salt spray chamber, the Ni-20Cr+Al_2O_3 coatings showed spots of pit corrosion by visual quantification. SM images of Ni-20Cr+Al_2O_3 coating surfaces are shown in Fig. 6. In addition, the Ni-20Cr+30Al_2O_3 exhibited more corrosion spots than the corresponding Ni-20Cr+50Al_2O_3, a behavior observed with all particle sizes of Al_2O_3 powders. A quantitative analysis (%) of corrosion spots on the surfaces of the Ni-20Cr and Ni-20Cr+Al_2O_3 coatings were characterized from Fig. 5 and 6(a) to (f). Results of amount of corrosion areas are 45.5% (Ni-20Cr), 0.8% (Ni-20Cr+50Al_2O_3, −90 + 45 μm), 1.9% (Ni-20Cr+50Al_2O_3, −45 + 22 μm), 3.3% (Ni-20Cr+50Al_2O_3, −22 + 5 μm), 1.7% (Ni-20Cr+30Al_2O_3, −90 + 45 μm), 2.2% (Ni-20Cr+30Al_2O_3, −45 + 22 μm), and 5.2% (Ni-20Cr+30Al_2O_3, −22 + 5 μm). The Ni-20Cr+Al_2O_3 coatings contained less through-porosity than the pure Ni-20Cr coating indicating higher denseness of the Ni-20Cr+Al_2O_3 coating. The through-porosity of the Ni-20Cr+Al_2O_3 coatings decreased with an increasing size of Al_2O_3 particles. On the other hand, the through-porosity of the Ni-20Cr+50Al_2O_3 dropped below that of the 30% composition.

CS coatings were slightly porous (contained through-porosity), a fact that was already shown already in previous corrosion results (Ref 15, 16). Existing porosity (especially through-porosity) is very detrimental to corrosion resistance especially in wet conditions. Salt spray tests and open-cell potential measurements as auxiliary

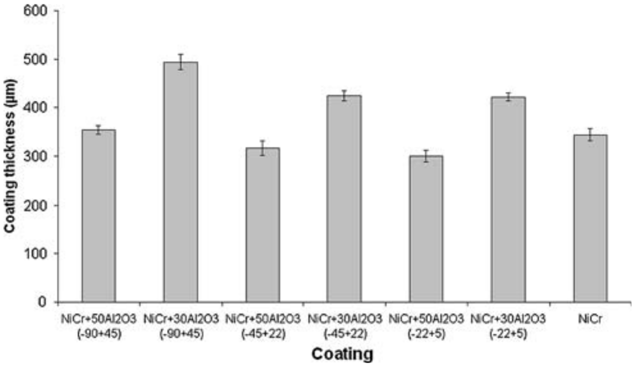

Fig. 3 Thickness (and standard deviations) of CS Ni-20Cr+Al_2O_3 coatings with 30% or 50% Al_2O_3 (Al_2O_3 particle sizes: $-90+45$ µm, $-45+22$ µm, and $-22+5$ µm) and Ni-20Cr coating

Table 2 Fractions of Al_2O_3 particles in the powder and in the CS Ni-20Cr+Al_2O_3 coatings analyzed from cross sections of the coatings by image analysis

Powder/coating	Fraction of Al_2O_3 in the powder, vol.%	Fraction of Al_2O_3 in the coating, vol.%
Ni-20Cr+50Al_2O_3 ($-90+45$ µm)	50	8.2
Ni-20Cr+50Al_2O_3 ($-45+22$ µm)	50	11.2
Ni-20Cr+50Al_2O_3 ($-22+5$ µm)	50	10.1
Ni-20Cr+30Al_2O_3 ($-90+45$ µm)	30	3.6
Ni-20Cr+30Al_2O_3 ($-45+22$ µm)	30	6.4
Ni-20Cr+30Al_2O_3 ($-22+5$ µm)	30	5.2

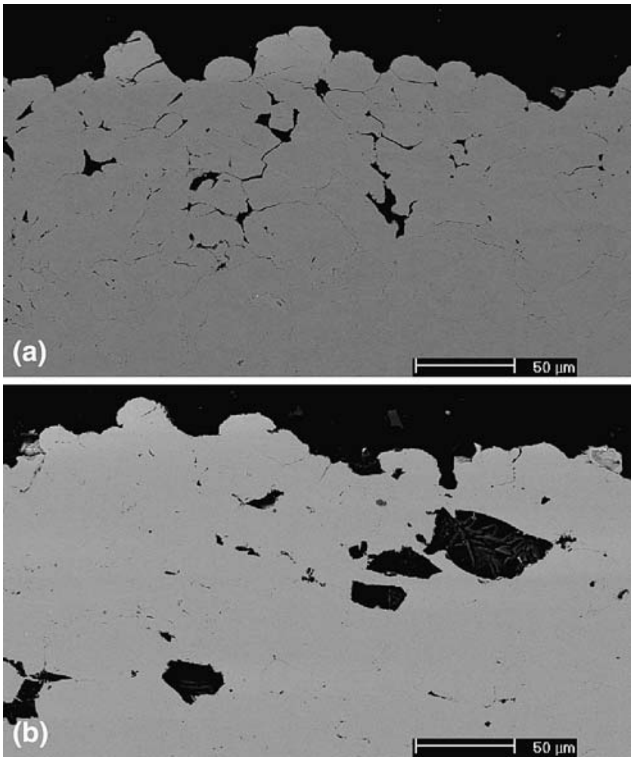

Fig. 4 Coating structure near the surface of CS (a) Ni-20Cr and (b) Ni-20Cr+50Al_2O_3 ($-90+45$ µm) coatings, BSE images (SEM)

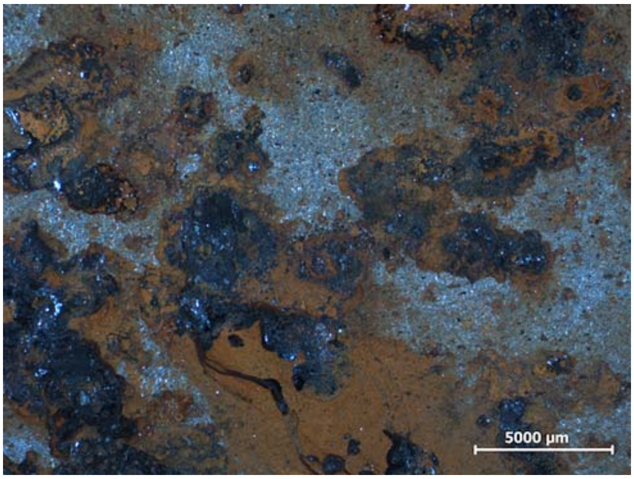

Fig. 5 Strongly corroded surface of CS Ni-20Cr coating after 48-h salt spray test, SM image

tests were useful and fast methods to analyze the existing through-porosity in the coating structures. Open-cell potential measurements were taken to identify the existing through-porosity in the Ni-20Cr+Al_2O_3 coatings. The open-cell potential of the substrate material (Fe52) was −700 mV (Ref 16). When open-cell potential of a coating approaches the open-cell potential of the substrate, a salt solution has open access to penetrate from the coating surface into the interface of the coating and the substrate. The effect of an Al_2O_3 addition on the Ni-20Cr+Al_2O_3 coating denseness was tested with open-cell potential measurements. Results are presented in Fig. 7. The open-cell potential of the Ni-20Cr was not measured because of its weak protection in the salt spray test, the two methods being complementary. The open-cell potential measurements showed existing through-porosity in the coatings. Nevertheless, the Ni-20Cr+50Al_2O_3 ($-90+45$ µm) coating showed the fewest weak points after the salt spray test (Fig. 6a) and a slightly higher open-cell potential than the other coatings, indicating a somewhat lower through-porosity.

According to SEM analysis (Figs. 1 and 4a) and the salt spray test (Fig. 5), the Ni-20Cr coating had several weak points and in addition, the salt spray test showed through-porosity in the coating structure. After the salt spray test, the coating surface was mostly corroded (iron oxide), and the salt solution had penetrated into the interface between the coating and the substrate, indicating an existing through-porosity. In addition, pores and especially a porous layer near the surface were evident in the SEM images. Compared to the Ni-20Cr coating, the

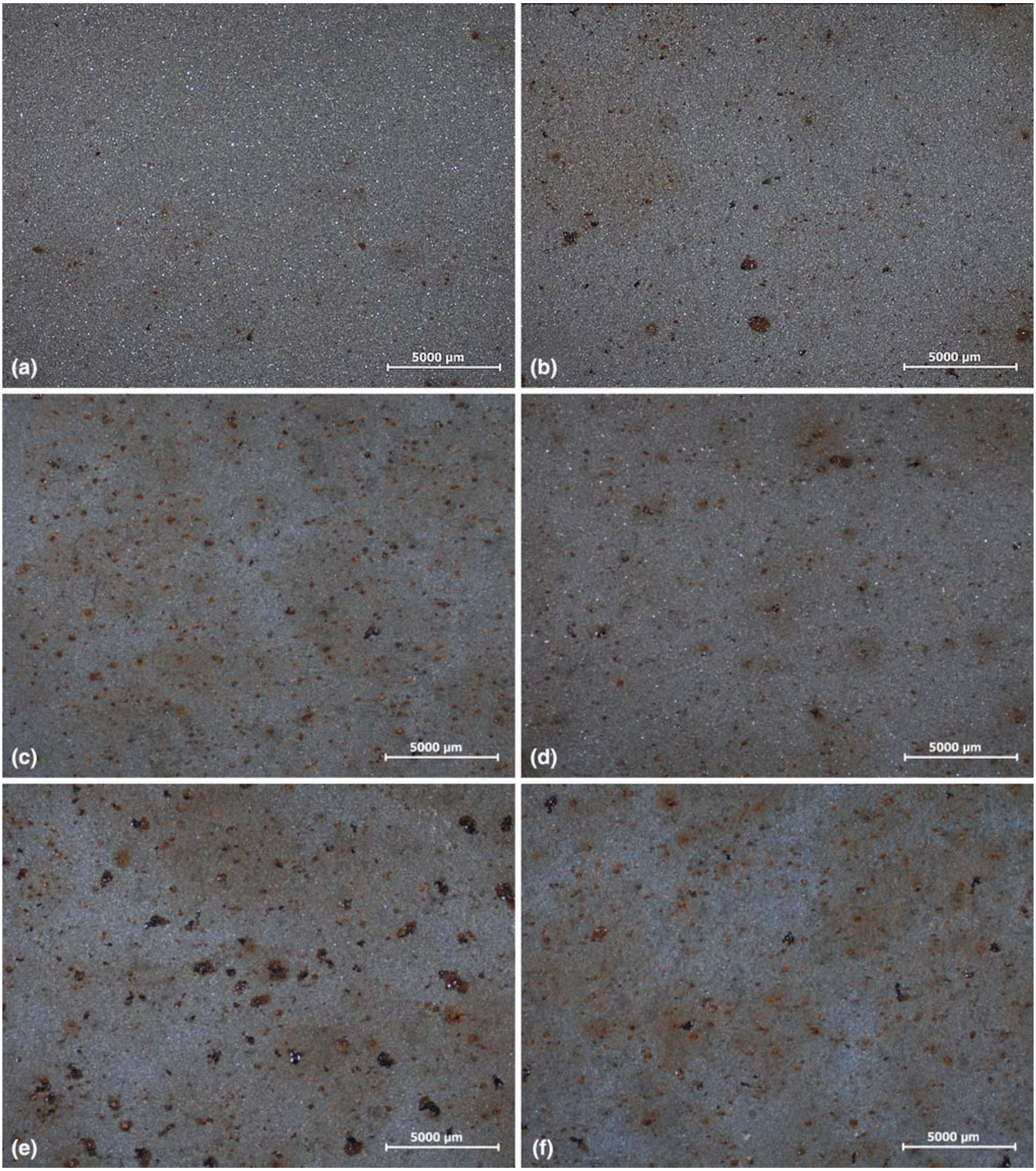

Fig. 6 Surface of CS (a) Ni-20Cr+50Al_2O_3 (−90 + 45 μm), (b) Ni-20Cr+50Al_2O_3 (−45 + 22 μm), (c) Ni-20Cr+50Al_2O_3 (−22 + 5 μm), (d) Ni-20Cr+30Al_2O_3 (−90 + 45 μm), (e) Ni-20Cr+30Al_2O_3 (−45 + 22 μm), and (f) Ni-20Cr+30Al_2O_3 (−22 + 5 μm) coatings after 48-h salt spray test, SM images

microstructural properties of the Ni-20Cr+Al_2O_3 coatings improved with the addition of Al_2O_3 particles together with high gas temperature. Their denseness improved noticeably with all compositions and particle sizes of Al_2O_3. However, because of a few weak spots, they lacked a fully dense microstructure. In this study, the Ni20-Cr+50Al_2O_3 (−90 + 45 μm) coating, though not even fully dense, was the most protective with the best impermeability with only a few pit-type corrosion spots detected on its surface.

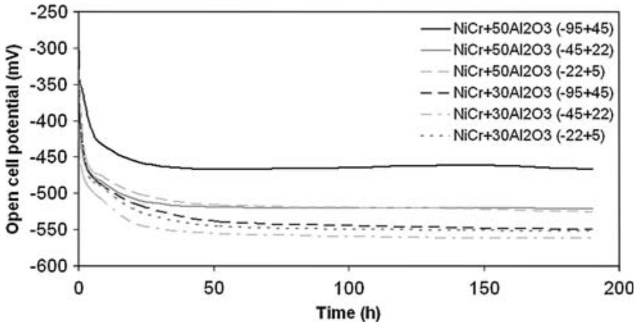

Fig. 7 Open-cell potential (vs. Ag/AgCl) of CS Ni-20Cr+Al_2O_3 coatings with 30% or 50% Al_2O_3 (Al_2O_3 particle sizes: $-90+45$ µm, $-45+22$ µm, and $-22+5$ µm) as a function of exposure time

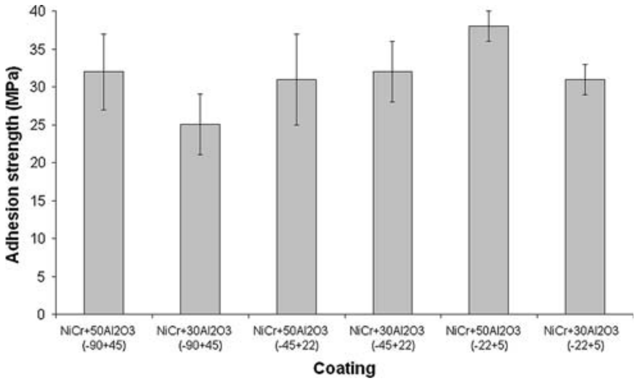

Fig. 8 Adhesion strengths (and standard deviations) of CS Ni-20Cr+Al_2O_3 coatings with 30% or 50% Al_2O_3 (Al_2O_3 particle sizes: $-90+45$ µm, $-45+22$ µm, and $-22+5$ µm)

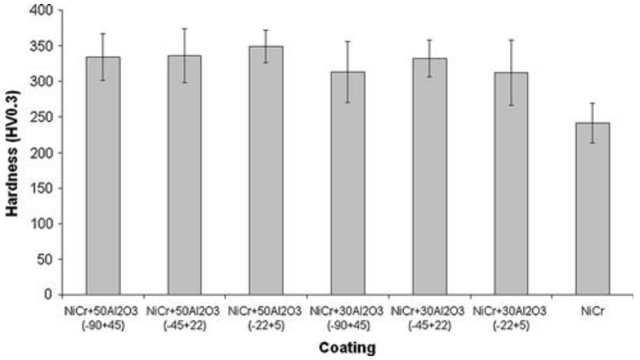

Fig. 9 Vickers hardness $HV_{0.3}$ (and standard deviations) of CS Ni-20Cr+Al_2O_3 coatings with 30% or 50% Al_2O_3 (Al_2O_3 particle sizes: $-90+45$ µm, $-45+22$ µm, and $-22+5$ µm) and CS Ni-20Cr coating

3.3 Mechanical Properties

The Ni-20Cr+Al_2O_3 coatings were tested for adhesion strength and hardness to obtain information on the effect of the Al_2O_3 particles on some mechanical properties. In a previous study (Ref 17), the adhesion strength of a Ni-20Cr coating on a steel substrate was 31 MPa, which was used as a reference in this study. The adhesion strength of Ni-20Cr+Al_2O_3 coatings is shown in Fig. 8. In the all cases, failure occurred at the interface between coating and substrate. The Ni-20Cr+Al_2O_3 coatings showed an adhesion strength of 25-38 MPa, whereas the Ni-20Cr+50Al_2O_3 ($-22+5$ µm) coating obtained the highest adhesion strength. The adhesion strengths of the Ni-20Cr+Al_2O_3 coatings were slightly higher than that of the Ni-20Cr coating depending on the composition. Because adding Al_2O_3 particles to the metallic Ni-20Cr powder only slightly affected the adhesion strength, it can conclude that in all cases, with and without an Al_2O_3 particles mixing, the adhesion strengths between the Ni-20Cr coatings and substrates were acceptable, indicating a reasonable adhesion between coatings and substrates.

Figure 9 shows the Vickers hardness ($HV_{0.3}$) of Ni-20Cr+Al_2O_3 and Ni-20Cr coatings. For the Ni-20Cr coating, it was 240 $HV_{0.3}$ and between 320 and 340 $HV_{0.3}$ for the Ni-20Cr+Al_2O_3 coatings. The Al_2O_3 particles affected the hardness by increasing its value, the effect arising from hardening by the hard particles. In addition to the effect of Al_2O_3 particles, high gas temperature affected the properties of coatings deposited. The effect of the Al_2O_3 addition on hardness was noticeable. In the hardness measurements, the indentations were taken in the metallic coating areas to evaluate the behavior of the metallic Ni-20Cr particles. The high hardness of the Ni-20Cr+Al_2O_3 coatings was reflected in their high work hardening (Ref 8). More hardening (compacting effect of Al_2O_3 particles) occurred at higher particle velocities (Ref 9) caused by the high gas temperature. Comparison of the Ni-20Cr and Ni-20Cr+Al_2O_3 coatings revealed that, the Al_2O_3 addition together with a high gas temperature had a pronounced effect on microstructural properties and on hardness values. A high hardness was caused by the work hardening of the particles together with high plastic deformation during impacts. On the other hand, the Al_2O_3 particles may also have reinforced the structure and thereby increased the hardness. In this study, the particle size and composition of Al_2O_3 had no clear effect on hardness.

4. Conclusions

Adding ceramic particles, in this study Al_2O_3, affected the properties of coating deposited by CS process. On the other hand, Al_2O_3 particles mixed with a metal alloy powder also had a technical spraying effect on the process parameters: they enabled the use of a higher gas temperature (700 °C) without clogging the nozzle. Adding Al_2O_3 powder affected mostly the microstructure. With the Al_2O_3 particles (high gas temperature) and compared to the Ni-20Cr coating, the metallic deposition buildup (coating thickness) of the Ni-20Cr+Al_2O_3 coatings increased. Their coating thickness increased with an increasing particle size and a decreasing composition of

Al_2O_3. The Ni-20Cr coating showed prevalent through-porosity, as demonstrated by corrosion products from the substrate on its surface after a salt spray test. The Al_2O_3 addition markedly affected the denseness of the Ni-20Cr+Al_2O_3 coatings with only a few pit-type corrosion spots visible on their surface. Obviously, the coatings did not have a fully, evenly dense structure, but they showed clear improvement. Moreover, adding Al_2O_3 particles decreased also the coatings' porosity in comparison with Ni-20Cr. The Al_2O_3 addition had a minor effect on the coatings' mechanical properties. The Ni-20Cr and Ni-20Cr+Al_2O_3 coatings showed reasonable adhesion strengths of about 30 MPa. The Al_2O_3 addition affected more the hardness of the coating's metallic part by increasing it, indicating reinforcement and high plastic deformation of the Ni-20Cr particles due to the high gas temperature.

Though high-pressure CS process uses mostly metallic powders, this study shows that metal alloy-ceramic powder blends could also be used. Generally, the composition of the powder depends on the properties desired for the coating. However, coating properties can be improved and spraying parameters extended by adding Al_2O_3 particles to Ni-20Cr powder. Furthermore, for pure Ni-20Cr coating, the powder must be optimized to make full use of a high gas temperature. The results of this study are promising, but for CS coatings, optimization of the powders and parameters is needed to produce fully, evenly dense coatings.

Acknowledgments

The authors like to thank Mr. Werner Krömmer of Linde AG Gas for the spray coatings and for his valuable advice. The project was funded by Finnish Funding Agency for Technology and Innovation (TEKES) and a group of Finnish industrial companies.

References

1. A. Papyrin, V. Kosarev, S. Klinkov, A. Alkimov, and V. Fomin, *Cold Spray Technology*, 1st ed., Elsevier, the Netherlands, 2007, p 328
2. T. Stoltenhoff, H. Kreye, and H.J. Richter, An Analysis of the Cold Spray Process and Its Coatings, *J. Therm. Spray Technol.*, 2001, **11**(4), p 542-550
3. T.H. Van Steenkiste, J.R. Smith, and R.E. Teets, Aluminum Coatings Via Kinetic Spray with Relatively Large Powder Particles, *Surf. Coat. Technol.*, 2002, **154**, p 237-252
4. C. Borchers, F. Gärtner, T. Stoltenhoff, H. Assadi, and H. Kreye, Microstructural and Macroscopic Properties of Cold Sprayed Copper Coatings, *J. Appl. Phys.*, 2003, **93**(12), p 10064-10070
5. R.G. Maev and V. Leshchynsky, Air Gas Dynamic Spraying of Powder Mixtures: Theory and Application, *J. Therm. Spray Technol.*, 2006, **15**(2), p 198-205
6. R.C. Dykhuizen and M.F. Smith, Gas Dynamic Principles of Cold Spray, *J. Therm. Spray Technol.*, 1998, **7**(2), p 205-212
7. H.C. Starck, Amperit and Amperweld Homepage, Amperit Thermal Spray Powders Procure. Available from http://www.amperit.info/index.php?page_id=2029
8. E. Calla, D.G. McCartney, and P.H. Shipway, Deposition of Copper by Cold Gas Dynamic Spraying: An Investigation of Dependence of Microstructure and Properties of the Deposits on the Spraying Conditions, *Thermal Spray 2004: Advances in Technology and Application*, 10-12 May, 2004 (Osaka, Japan), ASM International, p 6
9. T. Schmidt, F. Gärtner, and H. Kreye, New Developments in Cold Spray Based on Higher Gas- and Particle Temperatures, *J. Therm. Spray Technol.*, 2006, **15**(4), p 488-494
10. P. Richter and H. Höll, Latest Technology for Commercially Available Cold Spray Systems, *Thermal Spray 2006: Building on 100 Years of Success*, B.R. Marple, M.M. Hyland, Y.-C. Lau, R.S. Lima, and J. Voyer, Ed., May 15-18, 2006 (Seattle, Washington, USA), ASM International, p 3
11. H. Kreye, T. Schmidt, F. Gärtner, and T. Stoltenhoff, The Cold Spray Process and Its Optimization, *Thermal Spray 2006: Building on 100 Years of Success*, B.R. Marple, M.M. Hyland, Y.-C. Lau, R.S. Lima, and J. Voyer, Ed., May 15-18, 2006 (Seattle, Washington, USA), ASM International, p 5
12. B.B. Djordjevic and R.G. Maev, SIMAT™ Application for Aerospace Corrosion Protection and Structural Repair, *Thermal Spray 2006: Building on 100 Years Success*, B.R. Marple, M.M. Hyland, Y.C. Lau, R.S. Lima, and J. Voyer, Ed., May 15-18, 2006 (Seattle, Washington, USA), ASM International, p 5
13. A. Shkodkin, A. Kashirin, O. Klyuev, and T. Buzdygar, The Basic Principles of DYMET Technology, *Thermal Spray 2006: Building on 100 Years Success*, B.R. Marple, M.M. Hyland, Y.C. Lau, R.S. Lima, and J. Voyer, Ed., May 15-18, 2006 (Seattle, Washington, USA), ASM International, p 3
14. D. Helfritch, and V. Champagne, Optimal Particle Size for the Cold Spray Process, *Thermal Spray 2006: Building on 100 Years of Success*, B.R. Marple, M.M. Hyland, Y.-C. Lau, R.S. Lima, and J. Voyer, Ed., May 15-18, 2006 (Seattle, Washington, USA), ASM International, p 5
15. H. Mäkinen (Koivuluoto), J. Lagerbom, and P. Vuoristo, Mechanical Properties and Corrosion Resistance of Cold Sprayed Coatings, *Thermal Spray 2006: Building on 100 Years of Success*, B.R. Marple, M.M. Hyland, Y.-C. Lau, R.S. Lima, and J. Voyer, Ed., May 15-18, 2006 (Seattle, Washington, USA), ASM International, p 6
16. H. Koivuluoto, J. Lagerbom, and P. Vuoristo, Microstructural Studies of Cold Sprayed Copper, Nickel, and Nickel-30%Copper Coatings, *J. Therm. Spray Technol.*, 2007, **16**(4), p 488-497
17. H. Mäkinen (Koivuluoto), J. Lagerbom, and P. Vuoristo, Adhesion of Cold Sprayed Coatings: Effect of Powder, Substrate, and Heat Treatment, *Thermal Spray 2007: Global Coating Solutions*, B.R. Marple, M.M. Hyland, Y.-C. Lau, C.-J. Li, R.S. Lima, and G. Montavon, Ed., May 14-16, 2007 (Beijing, China), ASM International, p 31-36

Publication IV

Heli Koivuluoto, Jonne Näkki and Petri Vuoristo

Corrosion Properties of Cold-Sprayed Tantalum Coatings

Journal of Thermal Spray Technology, 18 (1) 2009, p. 75-82

Reprinted from Journal of Thermal Spray Technology with permission of ASM International.
Copyright (2009) ASM International.

JTTEE5 18:75–82
DOI: 10.1007/s11666-008-9281-2
1059-9630/$19.00 © ASM International

Corrosion Properties of Cold-Sprayed Tantalum Coatings

Heli Koivuluoto, Jonne Näkki, and Petri Vuoristo

(Submitted May 30, 2008; in revised form October 10, 2008)

Cold spraying enables the production of pure and dense metallic coatings. Denseness (impermeability) plays an important role in the corrosion resistance of coatings, and good corrosion resistance is based on the formation of a protective oxide layer in case of passivating metals and metal alloys. The aim of this study was to investigate the microstructural details, denseness, and corrosion resistance of two cold-sprayed tantalum coatings with a scanning electron microscope and corrosion tests. Polarization measurements were taken to gain information on the corrosion properties of the coatings in 3.5 wt.% NaCl and 40 wt.% H_2SO_4 solutions at room temperature and temperature of 80 °C. Standard and improved tantalum powders were tested with different spraying conditions. The cold-sprayed tantalum coating prepared from improved tantalum powder with advanced cold spray system showed excellent corrosion resistance: in microstructural analysis, it showed a uniformly dense microstructure, and, in addition, performed well in all corrosion tests.

Keywords cold spraying, corrosion properties, microstructure, tantalum

1. Introduction

Cold spraying, the latest thermal spray technique, developed in the former Soviet Union in the 1980s, is based on the use of significantly lower process temperatures with high particle velocities than those in other thermal spray techniques. A coating is formed when powder particles at high velocities (high kinetic energy) impact on the substrate, deform and adhere to substrate or other particles. In addition, good bonding between cold-sprayed powder particles requires high plastic deformation on particle impact (Ref 1-3). In cold spraying, several parameters such as particle size, particle temperature, substrate material, and the properties of the coating material affect greatly the coating formation and deposition efficiency (Ref 1, 4, 5). Because the sprayed material undergoes neither phase transformations nor melting during the spraying process (solid state process), cold spraying enables in principle the production of highly dense and pure metallic coatings (Ref 3, 6).

Chemical reactions between a material (e.g., metal, coating) and its environments can cause corrosion (Ref 7). Therefore, one important technical issue is to manufacture corrosion resistance/protective materials and coatings with specific requirements (high reliability, quality, and low costs). Corrosion resistance is necessary in several industries, in, e.g., chemical and process equipment, paper machines, and energy production systems. In many cases, protective surface coating is reportedly the best way to control corrosion, e.g., on steel products (Ref 8). Usually, the corrosion protection of many corrosion-resistant materials is based on their passivity, i.e., on the formation of a thin and protective oxide film. The passivity and protection of metals can be studied from their active-passive-transpassive behavior in anodic polarization curves (Ref 7).

Tantalum is a heavy refractory metal (atomic weight 180.948, density 16.6 g/cm^3) (Ref 9) and thus evidently suitable for cold spraying. It is also a very expensive material and therefore used only for extreme corrosion resistance. Tantalum resists corrosion effectively in acids (not HF), salts, and organic chemicals even at elevated temperatures. For example, it is highly resistant to corrosion by H_2SO_4 at a temperature of up to 200 °C. Used in chemical processing equipment and electronic devices, its corrosion resistance and inertness are based on the formation of a very thin, dense, adherent, and protective oxide layer (usually tantalum pentoxide Ta_2O_5) (Ref 10), which is a very stable compound (Ref 7). Moreover, tantalum has a low ductile-to-brittle transition temperature and a high melting temperature (2996 °C). Because ductility decreases with increasing amount of impurities (Ref 9), it should be taken into account when developing high-purity tantalum powders for cold spraying.

Tantalum coatings prepared with electrodeposition (Ref 11) and PVD (Ref 12) deposition techniques for corrosion resistance applications and with plasma spraying (Ref 13) have been reported elsewhere. Tantalum as a dense coating acts like a corrosion barrier coating on a steel substrate, providing high corrosion resistance in many environments (Ref 7). PVD (magnetron-sputtered)

Heli Koivuluoto and **Petri Vuoristo**, Department of Materials Science, Tampere University of Technology, P.O. Box 589, 33101 Tampere, Finland; and **Jonne Näkki** and **Petri Vuoristo**, Technology Centre KETEK Oy, Korpintie 8, 67100 Kokkola, Finland. Contact e-mail: heli.koivuluoto@tut.fi.

tantalum coatings have reportedly a corrosion performance equal to bulk tantalum foil (Ref 12). However, impurities and defects in the metallic coating can affect its corrosion behavior in that corrosion may arise locally from existing defects (Ref 12). Tantalum is also used as an alloying element (e.g., Ti-Ta alloys) to improve corrosion protection in sulfuric acid solutions (Ref 14). However, plasma-sprayed tantalum coatings have been shown to lack a fully dense structure in order to requirements for sealing or fusing post treatment (Ref 13).

This study sought to investigate the corrosion resistance of cold-sprayed (CS) tantalum coatings. Two different powders, standard and improved, were sprayed using different spraying parameters with two different spraying systems. The denseness of the cold-sprayed tantalum coatings was examined from scanning electron microscope (SEM) images and in corrosion tests: open-cell potential measurements and a salt spray fog test were run to assess through-porosity and polarization measurements to yield the corrosion properties of these coatings.

2. Experiments

Cold-sprayed tantalum coatings were prepared at Linde AG Linde Gas Division (Unterschleissheim, Germany). Two as-received tantalum powders from H.C. Starck GmbH (Goslar, Germany) (P1: Amperit 150.090 and P2: Amperit 151.065) were used in this study (more information on the powders in Section 3.1). The cold spray systems used were the Kinetiks 3000 and Kinetiks 4000 (Cold Gas Technology GmbH, CGT, Ampfing, Germany) high-pressure cold spray equipment with nitrogen as process gas. Kinetiks 4000 equipment is the advanced cold spray system in which can be used powder preheating, higher process temperatures and pressures, affecting particle velocities and therefore coating properties (Ref 15). In this study, CS Ta1 and CS Ta2 coatings represent two different development stages of cold-sprayed tantalum coatings. The parameters used here for cold spraying are shown in Table 1. Grit-blasted (mesh 18) carbon steel (Fe52) sheets (50 × 100 × 2 mm) were used as substrates. The reference material was a bulk tantalum sheet, supplied by Harald Pihl Ab, Sweden (ASTM B708-98 RO5200 annealed).

Microstructures of the cold-sprayed tantalum coatings were characterized using a Philips XL30 SEM. The structures were studied in unetched cross-sectional coating samples. Corrosion behavior and denseness (impermeability), i.e., the existing through-porosity of the cold-sprayed tantalum coatings, were tested with electrochemical open-cell potential measurement and a salt spray fog test. The electrochemical cell used in the open-cell potential measurements consisted of a plastic tube, of diameter 20 mm and volume 12 mL, glued on the surface of the coating specimen. A 3.5 wt.% NaCl solution was placed in the tube for 420-h measurements, taken with a Fluke 79 III true RMS multimeter. A silver/silver chloride electrode (Ag/AgCl) was used as a reference electrode. The salt spray fog test was done by following the ASTM B117 standard. Substrates were masked with epoxy paint before test in order to allow the coating surfaces only to be contact with the corroding salt spray fog. A 5 wt.% NaCl solution was used with an exposure of 240 h, a temperature of 35-40 °C, a solution pH of 6.3, and a solution accumulation of 0.04 mL/cm^2 h. The samples were characterized visually before and after exposure. Polarization measurements were taken to gain information on the corrosion resistance of the tantalum coatings. Anodic polarization tests were run adapting the standard ASTM G59. Polarization tests were run in a flat specimen cell with a rubber O-ring used as gasket. Tests were conducted in 3.5 wt.% NaCl and 40 wt.% H_2SO_4 water solutions at a room temperature (RT) of 22 °C and an elevated temperature of 80 °C. Potential was scanned from 0.6 V below the resting potential (E_0) to a potential of 3 V at a scanning rate of 2 mV/s. A saturated calomel electrode (SCE) was used for reference.

3. Results and Discussion

We investigated the microstructures and denseness of cold-sprayed tantalum coatings by SEM analysis. In addition, we evaluated the coatings' denseness and corrosion behavior with corrosion tests. Because coating denseness is important for a corrosion-resistant material such as tantalum, the first requirement is that the coating structure be of even, overall coverage.

3.1 Tantalum Powder Characteristics

We used two tantalum powders from H.C. Starck. Powder P1 was standard powder, of particle size $-38+10$ µm, as given by the producer, sprayed with a Kinetiks 3000 system (Fig. 1a). Powder P2 was improved powder, of particle size $-30+10$ µm, as given by the producer, sprayed with a Kinetiks 4000 (Fig. 1b). Figure 2 shows cumulative particle size distributions measured by laser diffraction (Sympatec Helos). Powder P2 had a finer particle size and narrower particle size distribution than powder P1. The oxygen content of P1 and P2 was 0.188 and 0.045%, respectively, measured as an average of measurements with Leco TC-436DR and Leco TC-136 chemical analyzers (Outotec Research Oy, Pori, Finland).

Table 1 Cold spray parameters and coating thicknesses

CS coating	Powder	Spray equipment	Pressure, bar	N_2 flow rate, m^3/h	Gas temperature, °C	Coating thickness, µm
CS Ta1	P1	Kinetiks 3000	32	73	530	470 (8 layers)
CS Ta2	P2	Kinetiks 4000	38	82	800	450 (3 layers)

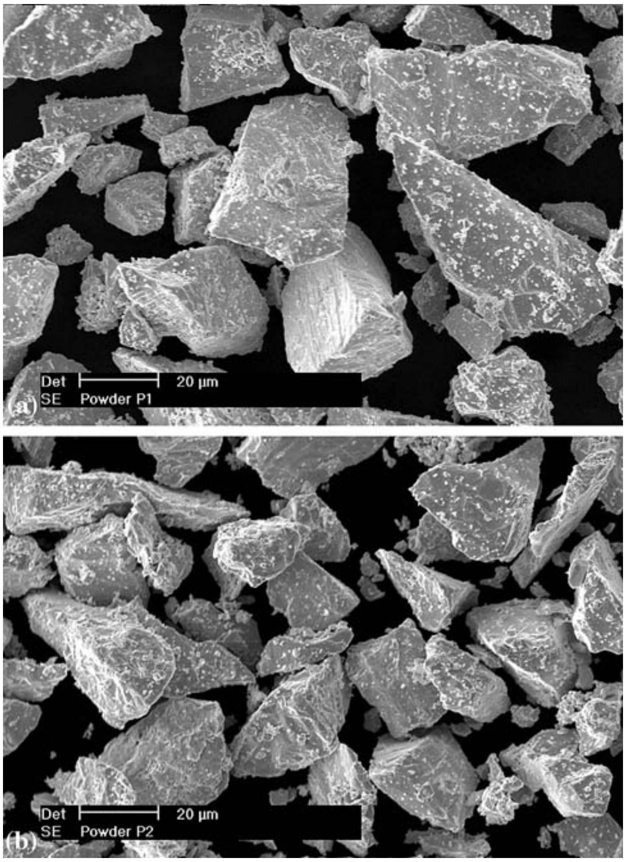

Fig. 1 Morphology of tantalum powders: (a) P1 (standard), nominal particle size −38 + 10 µm and (b) P2 (improved), nominal particle size −30 + 10 µm

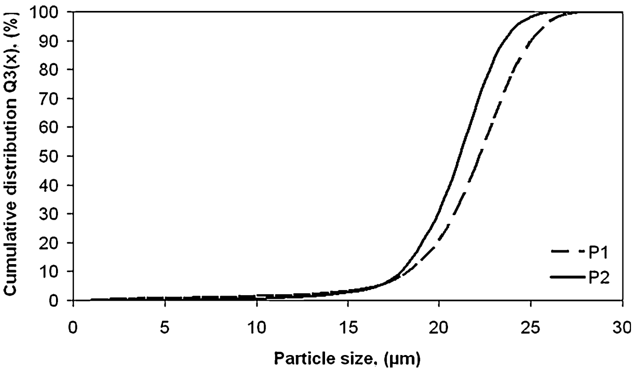

Fig. 2 Cumulative particle size distribution of powders P1 (standard) and P2 (improved) measured by laser diffraction

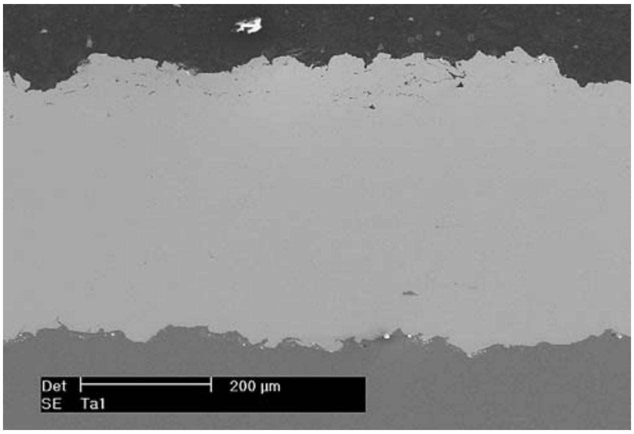

Fig. 3 Cold-sprayed tantalum coating (CS Ta1) on grit-blasted steel substrate (P1, standard)

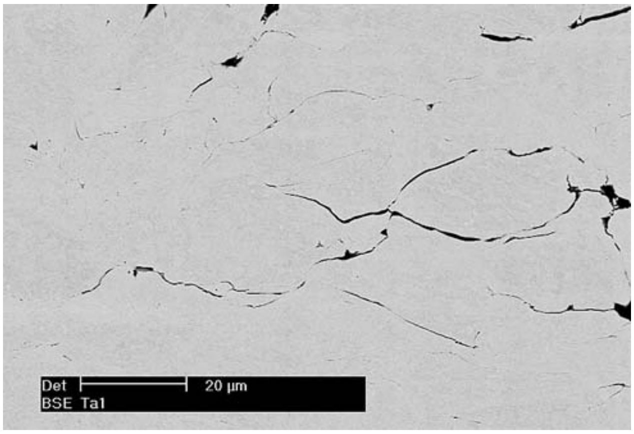

Fig. 4 Internal structure of cold-sprayed tantalum coating (CS Ta1), unetched, BSE image

3.2 Microstructure of Cold-Sprayed Tantalum Coatings

Figure 3 shows a cold-sprayed tantalum coating (CS Ta1) prepared from P1 with a Kinetiks 3000 system on a grit-blasted steel substrate. Some porosity is evident in the coating structure mostly near the surface, and some defects appear in the structure (internal structure, unetched, shown in Fig. 4, a BSE image with high magnification). Defects, pores, and open boundaries (dark areas in Fig. 4) were observed, which are conceivable to cause poor corrosion resistance. Weak points were found in particle boundaries, reflecting locally poor adhesion between particles, and apparently oxide layers on particle surfaces not destroyed during particle impact and deformation.

Figure 5 shows the microstructure of the tantalum coating CS Ta2 prepared from improved powder P2 with a Kinetiks 4000 system on a grit-blasted steel substrate. The coating seems dense without noticeable pores. Figure 6 shows the internal structure as dense (without defects) and the interface between coating and substrate as faultless, thus testifying to a uniformly dense coating microstructure.

According to SEM analysis, CS Ta2, prepared from improved powder with advanced spraying system (Kinetiks 4000), was dense whereas CS Ta1, prepared from standard powder, contained some porosity, as evident in the SEM images (Fig. 3 and 4). These two coatings differ in their powder characteristics and spraying conditions

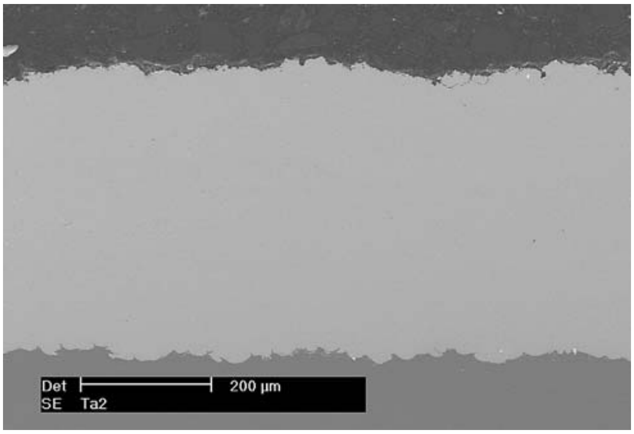

Fig. 5 Cold-sprayed tantalum coating (CS Ta2) on grit-blasted steel substrate (P2, improved)

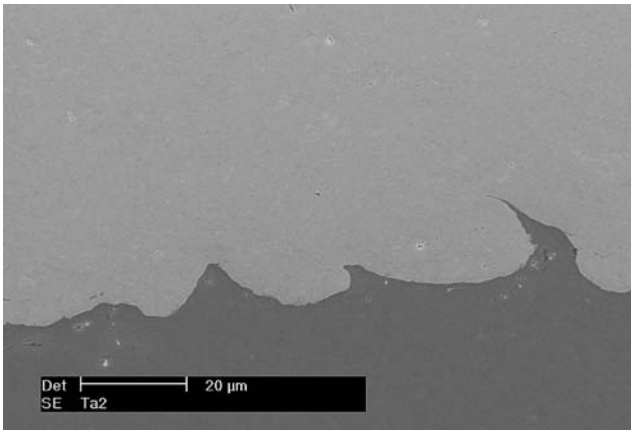

Fig. 6 Interface between cold-sprayed tantalum coating (CS Ta2) and grit-blasted steel substrate

(spraying equipment) and therefore represent tantalum coatings from two development stages. The improvement in the coating structure can be explained by an optimal combination of the powder and spray conditions. The optimal particle size for tantalum powder was −30 + 10 µm, which was slightly finer than that of the standard powder (−38 + 10 µm). Moreover, in the improved powder, the particle size distribution was slightly narrower and its purity higher than in the standard powder. Schmidt et al. (Ref 16) have reported that particle size affects on particles' impact velocities; finer particles have higher impact velocities which provide good bonds and adherence between particles and particle-substrate. On the other hand, high-purity powder particles have thinner oxide layers on the particle surfaces, promoting more tendency to get metal-metal bonding on the impact. Comparison of the microstructures of CS Ta1 (standard powder) and CS Ta2 (improved powder) reveals a significant improvement in the denseness of the cold-sprayed tantalum coating (Fig. 4 and 6).

High preheating temperatures of the process gas in the Kinetiks 4000 equipment (CGT) affect coating quality (Ref 15). First, deposition efficiency (DE) depends on gas temperature and reportedly improves at high temperature (Ref 4, 16). Second, process temperature affects the gas and particle velocity, meaning high velocity at high temperature. In addition, increased particle temperature has been reported to improve coating quality in the cold spray process (Ref 17, 18). In this study, a comparison of coating thicknesses and the number of layers sprayed revealed that DE was notably higher when the powder was sprayed with higher gas temperature (improved powder). The thickness of a single layer of CS Ta1 coating (standard, 32 bar, 540 °C) was about 60 µm and that of CS Ta2 (improved, 38 bar, 800 °C) about 150 µm. Van Steenkiste et al. (Ref 19) have also reported increased coating thickness of kinetic-sprayed tantalum coating at increased gas temperatures. On the other hand, high temperature leads to high particle velocity, which again affects coating porosity, which can increase at low particle velocity because of low kinetic energy together with less plastic deformation (Ref 19, 20). Therefore, heavy plastic deformation during particle impact (Ref 20) is crucial for efficient bonding of cold-sprayed powder particles into a dense microstructure.

3.3 Corrosion Characteristics of Cold-Sprayed Tantalum Coatings

The corrosion resistance of the cold-sprayed tantalum coatings was studied with open-cell potential measurements and a salt spray fog test to assess any existing through-porosity in the coating structure. In addition, the corrosion behavior of the coatings was compared with that of bulk tantalum in two different (3.5 wt.% NaCl and 40 wt.% H_2SO_4) testing environments (room temperature and elevated temperature) using anodic polarization measurements.

3.3.1 Open-Cell Potential Measurement. As stated before (Ref 21), open-cell potential measurement is a good method to assess any existing through-porosity (or open-porosity) in a coating structure. Because coatings are sprayed on a steel substrate, any through-porosity (allowing the test solution to penetrate the coating into the interface of coating and substrate) makes the open-cell potential of the coating approach that of the substrate. On the other hand, if the coating is dense (no existing through-porosity), the open-cell potential of the coating approaches that of the corresponding bulk material. In this study, the bulk material was a tantalum sheet and the substrate carbon steel (Fe52). Figure 7 shows the open-cell potential (reference electrode Ag/AgCl) of the tantalum bulk material (120 mV), the Fe52 bulk material (−700 mV), and CS Ta1 sprayed with standard powder (100 mV) and CS Ta2 sprayed with improved powder (−580 mV).

CS Ta2, prepared from improved powder, was structurally dense without existing through-porosity because it behaved similar like bulk tantalum during the open-cell potential measurements. In contrast, CS Ta1, prepared from standard powder, was not consistently dense because

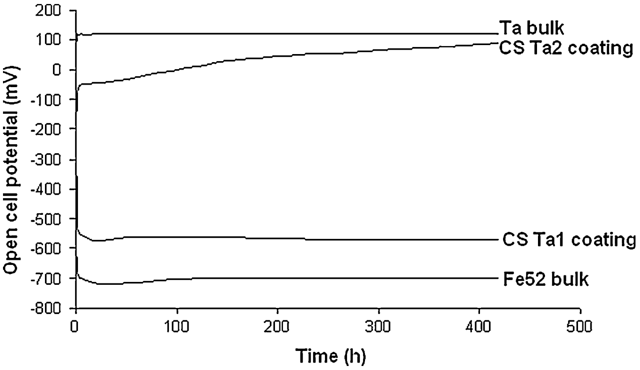

Fig. 7 Open-cell potential of tantalum (bulk material), Fe52 (substrate material), CS Ta1 (P1, standard), and CS Ta2 coating (P2, improved) as a function of exposure time with Ag/AgCl as reference electrode

its open-cell potential behavior approached that of the substrate material, suggesting existing through-porosity.

3.3.2 Salt Spray Fog Test. According to open-cell potential measurements, the CS Ta2 coating was dense; thus a salt spray fog test was run for more information about its denseness. The CS Ta1 coating was not tested because it leaked already in the open-cell potential measurements. No changes were detected on the CS Ta2 surface during exposure, indicating a uniformly dense microstructure. Figure 8 shows the surfaces of this coating taken with a digital camera before (Fig. 8a) and after a 240-h (Fig. 8b) salt spray fog test.

Open-cell potential measurement and the salt spray fog test as an auxiliary test were useful and fast methods to analyze existing through-porosity in the metallic coating structures. The salt spray fog test is a commonly used method to evaluate the quality of various coatings (Ref 22). Because tantalum is not attacked by seawater (Ref 23), these are good tests of a coating's impermeability. Because CS Ta1 showed through-porosity in corrosion tests and existing porosity in SEM studies, the key result remained the uniform denseness of the through-porosity-free CS Ta2 coatings, testifying to cold spraying's potential to produce dense, good-quality coatings. In this study, higher process temperature (CS Ta2) leads to porosity-free structure, indicating formation of tight bonds between particles and thus overall dense coating. In the cold spray process, gas preheating temperature is one of the most important spraying parameters. This study shows the effect of spraying parameters on denseness. Furthermore, strength and electrical conductivity of CS Cu coatings are reportedly improved with higher gas temperatures (Ref 16).

3.3.3 Polarization Behavior. Anodic polarization measurements were used to characterize the polarization behavior of the tantalum bulk material and the CS Ta2 and CS Ta1 coatings in two different test solutions, 3.5 wt.% NaCl and 40 wt.% H_2SO_4, at room temperature (22 °C) and at an elevated temperature (80 °C). The open-cell potential measurement and salt spray fog test already confirmed CS Ta2's overall dense structure; now its corrosion behavior and corrosion resistance were assessed with polarization behavior tests. The tantalum bulk material was tested for reference. The CS Ta1 coating was also tested in both solutions at room temperature for a comparison between dense structure coating (CS Ta2) and coating (CS Ta1) with through-porosity.

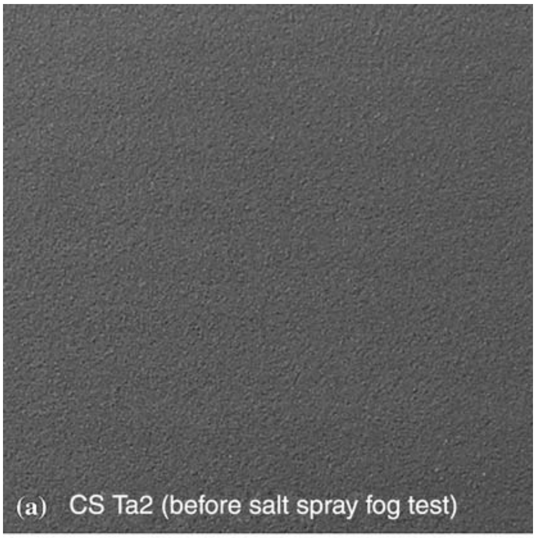
(a) CS Ta2 (before salt spray fog test)

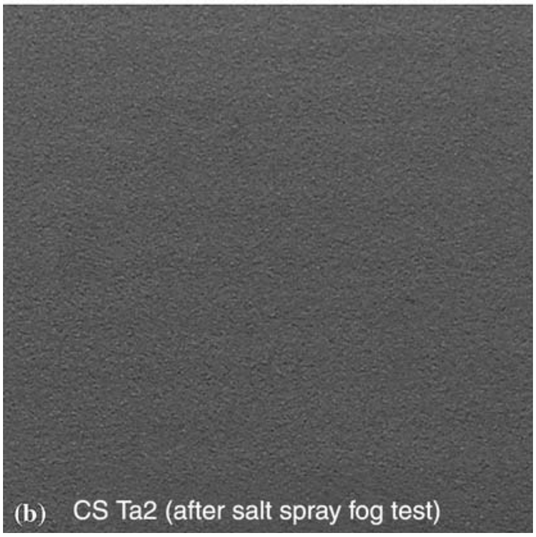
(b) CS Ta2 (after salt spray fog test)

Fig. 8 Surface of CS Ta2 coating (a) before and (b) after 240-h salt spray fog test. No changes during exposure indicate dense coating structure

Figure 9 shows the anodic polarization of the tantalum bulk material and the CS Ta2 and CS Ta1 coatings in 3.5 wt.% NaCl solutions at room temperature. Tantalum gets passivated rapidly, as shown by its polarization curves in the NaCl solution, transforming linearly and quickly from active to passive with increasing potential, indicative of material stability. The CS Ta2 coating behaved like the bulk material. However, the CS Ta1 coating did not behave in a stable manner because of its through-porosity. Test solution reached with steel substrate, thus anodic polarization was a result from combination of behavior of steel substrate and CS Ta1 coating. This indicates possible instability of the passivation layer and thus provides poor

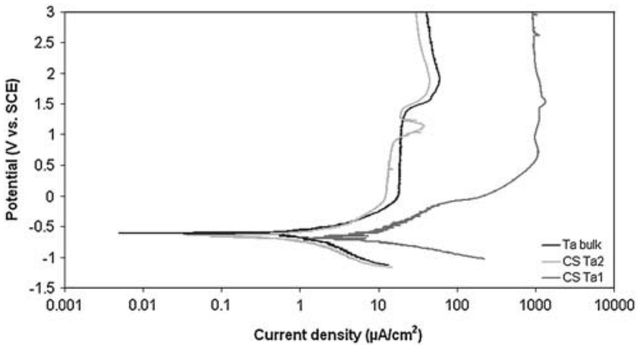

Fig. 9 Polarization behavior of tantalum bulk material, CS Ta2 (improved), and CS Ta1 (standard) coatings in 3.5 wt.% NaCl solution at 22 °C

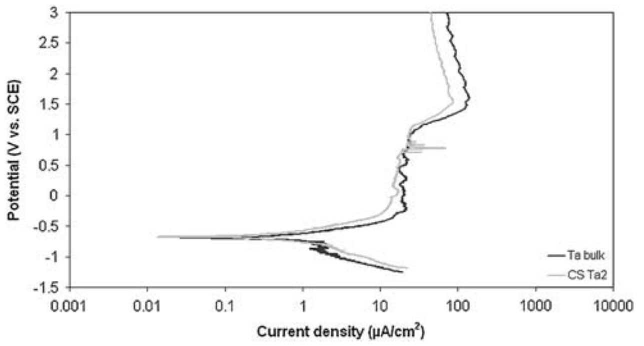

Fig. 10 Polarization behavior of tantalum bulk material and CS Ta2 (improved) coating in 3.5 wt.% NaCl solution at 80 °C

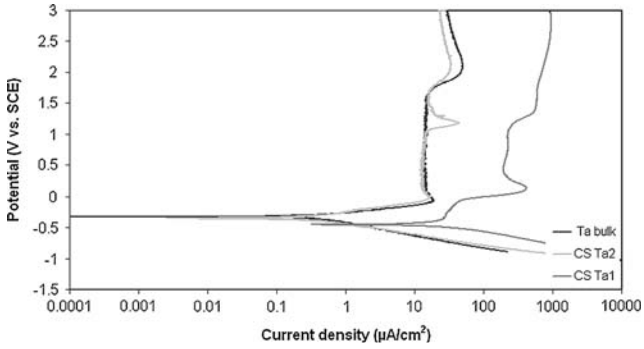

Fig. 11 Polarization behavior of tantalum bulk material, CS Ta2 (improved) and CS Ta1 (standard) coatings in 40 wt.% H_2SO_4 solution at 22 °C

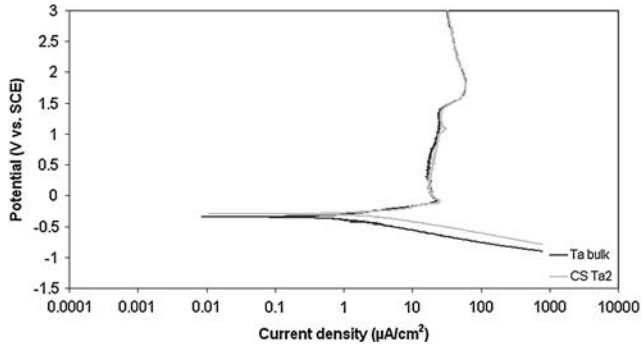

Fig. 12 Polarization behavior of tantalum bulk material, CS Ta2 (improved) coating in 40 wt.% H_2SO_4 solution at 80 °C

Table 2 Corrosion potential E_{corr}, corrosion current density i_{corr}, passivation potential E_{pp}, and passivation current density i_{pp} of tantalum bulk material, CS Ta2 and CS Ta1 coatings in 3.5 wt.% NaCl by Tafel extrapolation

Sample	Solution	T, °C	E_{corr}, V	i_{corr}, μA/cm²	E_{pp}, V	i_{pp}, μA/cm²
Ta bulk	NaCl	22	−0.66	1.1	0	16
CS Ta2	NaCl	22	−0.67	1.1	0.05	11
CS Ta1	NaCl	22	−0.68	7.1	…	…
Ta bulk	NaCl	80	−0.68	0.5	−0.25	20
CS Ta2	NaCl	80	−0.66	0.6	0.05	13

corrosion protection. The polarization behavior of the tantalum bulk material and the CS Ta2 coating was tested also in a 3.5 wt.% NaCl solution at an elevated 80 °C (Fig. 10). The CS Ta1 coating was not tested because of its results of existing porosity. For the results, a low current can cause some noise in the curves. The tantalum bulk material and the CS Ta2 coating showed similar polarization behavior also at the elevated temperature.

Tafel extrapolation was done from the polarization curves (Fig. 9 and 10) to determine the corrosion potential E_{corr}, passivation potential E_{pp}, corrosion current density i_{corr}, and the passivation current density i_{pp} of the tantalum bulk material and the CS Ta2 and CS Ta1 coatings (results shown in Table 2). At room temperature, CS Ta1, which lacked impermeability, showed a higher corrosion current density than the tantalum bulk and CS Ta2. The tantalum bulk and CS Ta2 got passivated rapidly, and above their passivation potential, a stable passive layer testified to a very low corrosion rate in the passive area (Ref 7).

The polarization behavior of tantalum was also investigated in an H_2SO_4 solution. Tantalum protects well against corrosion by sulfuric acid (Ref 23). Figure 11 shows the polarization curve of the tantalum bulk and CS Ta2 and CS Ta1 coatings at room temperature. As in the NaCl solution, CS Ta2 behaved here like the bulk material. However, CS Ta1 did not behave in a stable manner. At 80 °C, CS Ta2 behaved again like the bulk material, indicating capability to protect against corrosion (Fig. 12).

Table 3 summarizes the corrosion potential E_{corr}, passivation potential E_{pp}, corrosion current density i_{corr}, and passivation current density i_{pp} determined from the polarization curves (Fig. 11 and 12) by Tafel extrapolation. Also, here the corrosion current density of CS Ta1 exceeded that of the tantalum bulk and CS Ta2.

In summary of the polarization measurements, the CS Ta1 coating, prepared from standard powder, showed

Table 3 Corrosion potential E_{corr}, corrosion current density i_{corr}, passivation potential E_{pp} and passivation current density i_{pp} of tantalum bulk material, CS Ta2 and CS Ta1 coatings in 40 wt.% H_2SO_4 solution by Tafel extrapolation

Sample	Solution	T, °C	E_{corr}, V	i_{corr}, μA/cm^2	E_{pp}, V	i_{pp}, μA/cm^2
Ta bulk	H_2SO_4	22	−0.32	0.4	0.08	12
CS Ta2	H_2SO_4	22	−0.33	0.3	0.10	12
CS Ta1	H_2SO_4	22	−0.43	13	…	…
Ta bulk	H_2SO_4	80	−0.34	0.8	0.04	15
CS Ta2	H_2SO_4	80	−0.30	2.0	0.05	15

higher corrosion current density but no stability in its porous microstructure, whereas CS Ta2, prepared from improved powder, behaved like bulk tantalum, indicating resistance to corrosion. The latter two showed wide-ranging passivation, characteristic of stable passive behavior (Ref 24). General and pitting corrosion may occur in active areas (Ref 24). According to the polarization curves, in both NaCl and H_2SO_4 solutions, CS Ta2 passivation was first linear, then curving slightly (possibly because of pit corrosion), followed by another stretch of linear passivation at higher potential (passive layer formation). A pit may result from a failure in the passive layer (Ref 7, 23), but when pits are insignificant, reparation or repassivation and thus re-protection may occur in the protective passive layer (Ref 23). At a high potential of about 1.2 V, CS Ta2 showed unstable passivation; however, at an even higher potential the coating got repassivated. Balani et al. (Ref 6) have reported similar repassivation of cold-sprayed aluminum coatings. In fact, pitting corrosion may occur also in a transpassive area (Ref 24), and impurities may cause breaks in the passive layer (Ref 8). With some metals, passivation depends on pH and the potential (Ref 8), but the highly protective oxide layer of tantalum remains stable at all pH and potential values (Ref 7).

4. Conclusions

Cold spraying is a spraying technique capable of producing uniform dense metallic coatings by solid-state particle impacts. Because of no oxidation or melting during spraying, the coatings turn out pure and dense. In this study, we characterized two different cold-sprayed tantalum coatings (CS Ta1 and CS Ta2 from different development stages). This study reveals the importance of process parameters together with the powder type in the cold spraying. First, parameters have a very important role in the production of high-quality cold-sprayed coatings. High preheating temperature leads to high particle velocities and temperatures and further particle softening and therefore more plastic deformation occurring during impact. As is observed, process temperature affects the gas and particle velocity (Ref 4, 16). Moreover, increased particle temperature during impact reportedly improves coating quality in the cold spray process (Ref 17, 18), a fact corroborated in this study by denseness improvement. Secondly, improved tantalum powder properties were found to be the particle size and purity level. Particle size affects particle velocity and thus level of plastic deformation and coating formation. On the other hand, because tantalum is a very sensitive material to become oxidized, purity of powder particle is critical for formation of bonds between particles without micro scale defects on the boundaries. For high-pressure cold spraying, optimal tantalum powder is fused and crushed with irregular, blocky particles ($-30+10$ μm) and narrow particle size distribution. As a summary, we can notice that overall dense tantalum coating requires optimal combination of parameters and powder (particle size and purity). We suggest that gas preheating temperature is the most effective parameter, especially in the case of refractory materials with high melting temperatures. High temperature causes softening of particles and thereby tight bonds by plastic deformation.

In this study, the cold-sprayed Ta2 coating, prepared from improved powder with advanced spraying equipment (Kinetiks 4000, CGT), was microstructurally dense without noticeable pores or defects whereas the cold-sprayed Ta1 coating, prepared from standard powder (Kinetiks 3000, CGT), contained pores and weak particle boundaries. In this study, denseness was tested with corrosion tests, open-cell potential measurement, and a salt spray fog test. The results showed that CS Ta2 was impermeable with no pores in its structure. In addition, the tantalum bulk material and the coatings were tested in NaCl and H_2SO_4 solutions for their polarization behavior. CS Ta2 behaved like the tantalum bulk with rapid passivation and a high passivation range, indicative of its corrosion protection. On the other hand, CS Ta1 was not uniformly dense and thus less corrosion resistant.

High-pressure cold spraying proves its potential in the production of uniformly dense coatings. However, the powder micro- and grain structure should be studied in detail for more information on the deformation and adhesion of particles and other factors affecting dense structure formation. In future, corrosion tests will be run in more aggressive environments.

Acknowledgments

We thank Mr. Werner Krömmer, of Linde AG Gas, for the spray coatings and for his valuable advice. We also thank Dr. Karri Osara, of Outotec Research Oy, for organizing chemical analysis of the powders. This study was funded by Finnish Funding Agency for Technology and Innovation (TEKES) and a group of Finnish industrial companies.

References

1. C. Borchers, F. Gärtner, T. Stoltenhoff, H. Assadi, and H. Kreye, Microstructural and Macroscopic Properties of Cold Sprayed Copper Coatings, *J. Appl. Phys.*, 2003, **93**(12), p 10064-10070

2. R.G. Maev and V. Leshchynsky, Air Gas Dynamic Spraying of Powder Mixtures: Theory and Application, *J. Therm. Spray Technol.*, 2006, **15**(2), p 198-205
3. V.K. Champagne, *The Cold Spray Materials Deposition Process: Fundamentals and Applications*, Woodhead Publishing Limited, Cambridge, 2007, p 362
4. T. Stoltenhoff, H. Kreye, and H.J. Richter, An Analysis of the Cold Spray Process and its Coatings, *J. Therm. Spray Technol.*, 2002, **11**(4), p 542-550
5. R.C. Dykhuizen and M.F. Smith, Gas Dynamic Principles of Cold Spray, *J. Therm. Spray Technol.*, 1998, **7**(2), p 205-212
6. K. Balani, T. Laha, A. Agarwal, J. Karthikeyan, and N. Munroe, Effect of Carrier Gases on Microstructural and Electrochemical Behavior of Cold-Sprayed 1100 Aluminum Coating, *Surf. Coat. Technol.*, 2005, **195**, p 272-279
7. D.A. Jones, *Principles and Prevention of Corrosion*, 2nd ed., Prentice-Hall, Upper Saddle River, NJ, 1996, p 572
8. D.E.J. Talbot and J.D.R. Talbot, *Corrosion Science and Technology*, CRC Press LLC, 1998, p 390
9. ASM Metals Handbook Online Volume 2, *Properties and Selection: Nonferrous Alloys and Special-Purpose Materials, Pure Metals, Properties of Pure Metals, Tantalum*
10. ASM Metals Handbook Online Volume 13B, *Corrosion: Materials, Corrosion of nonferrous Alloys and Speciality Products, Corrosion of Tantalum and Tantalum Alloys*
11. S. Zein El Abedin, U. Welz-Biermann, and F. Endres, A Study on the Electrodeposition of Tantalum on NiTi Alloy in an Ionic Liquid and Corrosion Behaviour of the Coated Alloy, *Electrochem. Commun.*, 2005, **7**, p 941-946
12. S. Maeng, L. Axe, T.A. Tyson, L. Gladczuk, and M. Sosnowski, Corrosion Behaviour of Magnetron Sputtered α- and β-Ta Coatings on AISI 4340 Steel as a Function of Coating Thickness, *Corros. Sci.*, 2006, **48**, p 2154-2171
13. T. Kinos, S.L. Chen, P. Siitonen, and P. Kettunen, Densification of Plasma-Sprayed Titanium and Tantalum Coatings, *J. Therm. Spray Technol.*, 1996, **5**(4), p 439-444
14. K.A. de Souza and A. Robin, Influence of Concentration and Temperature on the Corrosion Behavior of Titanium, Titanium-20 and 40% Tantalum Alloys and Tantalum in Sulfuric Acid Solutions, *Mater. Chem. Phys.*, 2007, **103**, p 351-360
15. H. Hoell and P. Richter, KINETIKS® 4000 – New Perspective with Cold Spraying, *Thermal Spray 2008: Thermal Spray Crossing Borders*, DVS, June 2-4, 2008 (Maastricht, The Netherlands), p 2
16. T. Schmidt, F. Gärtner, and H. Kreye, New Developments in Cold Spray Based on Higher Gas- and Particle Temperatures, *J. Therm. Spray Technol.*, 2006, **15**(4), p 488-494
17. P. Richter and H. Höll, Latest Technology for Commercially Available Cold Spray Systems, *Thermal Spray 2006: Building on 100 Years of Success*, B.R. Marple, M.M. Hyland, Y.-C. Lau, R.S. Lima, and J. Voyer, Eds., May 15-18 (Seattle, Washington, USA), ASM International, p 3
18. H. Kreye, T. Schmidt, F. Gärtner, and T. Stoltenhoff, The Cold Spray Process and Its Optimization, *Thermal Spray 2006: Building on 100 Years of Success*, B.R. Marple, M.M. Hyland, Y.-C. Lau, R.S. Lima, and J. Voyer, Eds., May 15-18 (Seattle, Washington, USA), ASM International, p 5
19. T. Van Steenkiste and D.W. Gorkiewicz, Analysis of Tantalum Coatings Produced by the Kinetic Spray Process, *J. Therm. Spray Technol.*, 2004, **13**(2), p 265-273
20. T.H. Van Steenkiste, J.R. Smith, and R.E. Teets, Aluminum Coatings Via Kinetic Spray with Relatively Large Powder Particles, *Surf. Coat. Technol.*, 2002, **154**, p 237-252
21. H. Koivuluoto, J. Lagerbom, and P. Vuoristo, Microstructural Studies of Cold Sprayed Copper, Nickel, and Copper-30% Nickel Coatings, *J. Therm. Spray Technol.*, 2007, **16**(4), p 488-497
22. Standard Test Method of Salt Spray (Fog) Testing, B117-90, *Annual Book of ASTM Standards*, ASTM, p 19-25
23. P.A. Schweitzer, Ed., *Corrosion Engineering Handbook*, Marcel Dekker, 1996, p 736
24. W.S. Tait, *An Introduction to Electrochemical Corrosion Testing for Practicing Engineers and Scientists*, Pair O Docs Publications, Racine, WI, 1994, p 138

Publication V

Heli Koivuluoto, Mari Honkanen and Petri Vuoristo

Cold-sprayed copper and tantalum coatings – Detailed FESEM and TEM analysis

Surface & Coatings Technology, 204 (15) 2010, p. 2353-2361

Reprinted from Surface & Coatings Technology with permission of Elsevier B.V.
Copyright (2010) Elsevier B.V.

Surface & Coatings Technology 204 (2010) 2353–2361

Contents lists available at ScienceDirect

Surface & Coatings Technology

journal homepage: www.elsevier.com/locate/surfcoat

Cold-sprayed copper and tantalum coatings — Detailed FESEM and TEM analysis

Heli Koivuluoto *, Mari Honkanen, Petri Vuoristo

Tampere University of Technology, Department of Materials Science P.O. Box 589, 33101 Tampere, Finland

ARTICLE INFO

Article history:
Received 3 November 2009
Accepted in revised form 4 January 2010
Available online 11 January 2010

Keywords:
Cold spraying
Copper coating
Tantalum coating
Microstructure
FESEM
TEM

ABSTRACT

In cold spraying, a high level of plastic deformation and adiabatic shear instability are required for the tight bonding between powder particles and thus, formation of a dense microstructure. Cold-sprayed copper and tantalum coatings have fully dense structures according to microscopic evaluations and corrosion tests, indicating coatings' impermeability. Actually, denseness, i.e., existing through-porosity is a crucial coating characteristic which is reflected to the structural properties. In this study, the microstructure and fracture behavior are characterized using a field-emission scanning electron microscope (FESEM) and the inter-particle structures with a transmission electron microscope (TEM). Furthermore, a long-time impermeable behavior of these coatings was performed with open-cell potential measurements. Cold-sprayed copper and tantalum coatings possessed highly and localized deformed micro- and grain structures with high amount of dislocations and shear bands in their structures. Additionally, metal–metal particle bonds were attained as an important factor in the tight particle bonding. Moreover, partly ductile fracture behavior and material jets due to the thermal softening were observed from the fracture surfaces.

© 2010 Elsevier B.V. All rights reserved.

1. Introduction

Cold spraying is a potential thermal spraying technique to produce dense coatings with impermeable structures. Our previous study [1] showed clearly the denseness of the cold-sprayed Cu coatings. In addition, the dense and impermeable structure of the cold-sprayed Ta coating was proven [2,3]. Formation of a dense and impermeable coating structure is based on high-velocity particle impacts together with high level of plastic deformation [4]. On the impact, powder particles deform plastically and adhere to substrate surface or to other particles and build-up the coating [5]. A critical particle impact velocity is required to attain successful bonding between particles and thus, sticking [4,6]. Furthermore, in the gas flow, compressed layer takes form near to the impact surface and leads formation of shock waves (bow shock) near to the sprayed surface. Shock layer decreases particle velocity and increases particle temperature [5,7]. Particles should go through the shock layer and hence, high velocity and high kinetic energy are required. At the same time, thermal softening and adiabatic shear instability play a very important role in the particle–particle and particle–substrate in the cold spray process [4,8,9].

Denseness or in the other words impermeability depends strongly on spraying process conditions and cold spray equipment technology, powder characteristics, powder material, and in addition to these, mostly on the combination of these affecting factors [2]. Additionally, a coating quality relies on the spraying conditions; higher velocity leads stronger deformation and furthermore, coating structure become denser and mechanical properties improve [10,11]. The preheating temperature of the process gas reportedly has the influence on the coating quality. Higher process temperature together with higher pressure promotes denser coating structure precisely due to the thermal softening and local shear instability [9]. Moreover, in the particle interfaces, temperature is increased due to the adiabatic localization [8].

As is known, in cold spraying, coating formation is based on plastic deformation. Plastic deformation is mostly concentrated on the particle boundaries and therefore, material jets (of coating and substrate materials) are formed in order to increase coating quality and adhesion [8]. Typically, plastic deformation is detected from an etched microstructure of cold-sprayed coatings by a flattening degree of the particles. On the other hand, generally, material properties depend on its microstructure which in turn depends on grain structure and treatments. Plastic deformation is originated from dislocation movements caused by critical shear stress. In principle, plastic deformation occurs in each grain in the individual powder particle which means that particle boundaries can restrict the deformation of some grains. This indicates different levels of plastic deformations in the inter-particle and hence, through the coating structure. In addition, hardening mechanisms of the coating structures, work hardening or strain hardening, takes place under high deformation [12].

For dense coating and tight bonds between particles, good metal–metal bonding is required. This needs clean contact surfaces under high-pressure conditions [8,13,14]. Material jets formation is also one of the requirements for the successful and tight bonding [14]. For that

---

* Corresponding author. Tel.: +358 408490188; fax: +358 331152330.
E-mail address: heli.koivuluoto@tut.fi (H. Koivuluoto).

0257-8972/$ – see front matter © 2010 Elsevier B.V. All rights reserved.
doi:10.1016/j.surfcoat.2010.01.001

oxide layers of powder particles should be broken down and removed from the metal surface during the impacts [6]. This occurs by high plastic deformation and material jets [6,8,13,14]. Destruction of oxide layer can be illustrated with an egg-cell-model. During impact, particles behaved similarly like an egg, hard cell (oxide) broke down and soft inside (metal) deformed. After oxide layer is broken down and gas flow removes oxides away [6].

Plastic deformation under high strain rate conditions creates several microscopic features into the microstructure. There may be high amount of dislocations, dislocation wall formations, formation of elongated sub-grains, break-ups of sub-grains and recrystallization. At a solid state under a high strain rate, localized heating (material is still under melting point) generates adiabatic shearing instabilities at the interfaces and localized shear bands form [15]. The structure with fine-sized grains without voids or oxide inclusions caused by dynamic recrystallization leads tight metal–metal bonding between particles [16].

The aim of this study was to investigate microstructural details of Cu and Ta coatings prepared with high-pressure cold spraying. Detailed analysis was carried out by using FESEM and TEM. In our previous studies, the cold-sprayed Cu [1] and Ta [2,3] coatings were revealed to have overall dense structure according to SEM characterization and in addition, according to corrosion tests. Thus, more specific evaluation was needed to identify the structural details needed for the impermeable coating microstructure. Material properties of Cu and Ta are summarized in Table 1 [17,18]. Cu and Ta as powder materials are both very suitable materials for cold spraying [4,19]. Nevertheless, properties are dissimilar. Ta is a heavy metal with high melting temperature whereas Cu is lighter with lower melting point. In addition, common for both materials, FCC and BCC metals have high amount of slip systems, indicating good capability to deform due to the dislocation movements [20].

2. Experiments

Cold-sprayed coatings were prepared at Linde AG Gas (Unterschliessheim, Germany) with the CGT's Kinetiks 4000 high-pressure cold spraying equipment. Cu powder was gas-atomized whereas Ta powder was fused and crushed. Powder characteristics are presented in Table 2. Both powders were from H.C. Starck (Cu: Amperit 190.068 and Ta: Amperit 151.065) and optimized by manufacturer (particle size and high purity level) for cold spraying [21]. Table 3 shows spraying parameters used in this study. Spraying parameters were chosen according to previous experiments [2] and experimental knowledge. Carbon steel (Fe52) sheets (50 × 100 × 2 mm) as substrate materials were grit-blasted (Mesh 18) prior to spraying.

Powder morphologies were characterized using a Philips XL30 scanning electron microscope (SEM). Cold-sprayed coating microstructures and fracture surfaces were analyzed using a Zeiss ULTRAplus field-emission scanning electron microscope (FESEM). Microstructures were studied from unetched metallographic cross-sectional coating samples. Coatings were manually bent up to the rupture for fracture surface analysis. In addition, inter-particle structures were characterized using a Jeol JEM 2010 analytical transmission electron microscope (TEM+EDS). In TEM characterization, samples were analyzed from top-view and cross-section directions. Top-view sample of the cold-sprayed Cu coating was electrolytically prepared with twin jet electrolytical polisher (Struers Tenu-Pol-5) using a solution of nitric acid in methanol (1:2) whereas cross-section of the cold-sprayed Cu coating and top-view sample of cold-sprayed Ta coatings were prethinned by hand, then thinned with dimple grinder (Gatan Dimpler 656) and final thinned with precision ion polishing system (Gatan PIPS 691). Coating denseness was evaluated using open-cell electrochemical potential measurements with long-time exposure. The electrochemical cell used consisted of a tube, of diameter 20 mm and volume 12 ml, glued on the surface of the coating specimen. A 3.5-wt.% NaCl solution was placed in the tube for 60-day measurements. Open-cell potential measurements were taken with a Fluke 79 III true RMS multimeter. A silver/silver chloride (Ag/AgCl) electrode was used as a reference electrode.

Table 1
Material properties of copper [17] and tantalum [18]. FCC means face-centered cubic and BCC means body-centered cubic crystal structure.

Material	Crystal structure	Atomic weight	Density (g/cm^3)	Melting point (°C)
Copper	FCC	63.5	8.9	1085
Tantalum	BCC	180.8	16.6	2996

Table 2
Powder characteristics.

	Cu powder	Ta powder
Particle size (μm)	−35 + 15	−30 + 10
Production method	Gas-atomized	Fused and crushed
Particle shape	Spherical	Blocky

3. Results and discussion

The aim of this study was to characterize the microstructures of cold-sprayed Cu and Ta coatings and evaluate the coating properties. The characterization was focused on the structure, fracture behavior and grain structure with other microstructural details using several microscopic techniques (SEM, FESEM, and TEM). In addition, denseness was demonstrated with open-cell potential measurements.

3.1. Powder characteristics

Cu powder was gas-atomized having a spherical shape (Fig. 1A) whereas Ta powder was fused and crushed with a blocky shape (Fig. 1B). Particle size distributions of the Cu and Ta powders were −35 + 15 μm and −30 + 10 μm, respectively, given by supplier. Coating quality depends reportedly strongly on powders as well as spraying parameters [22,23]. Optimal powder properties and further spraying parameters are material-dependent.

Moreover, particle impact velocity is one of the critical property and is influenced by powder characteristics and spraying parameters [24]. Schmidt et al. [22] have reported that particle size affects impact velocities of particles; finer particles have higher impact velocities which provide good bonds and adherence between particle–particle and particle–substrate. Moreover, process temperature is one of the most important spraying parameters due to its effect on particle velocity [22]. In addition, purity of the powder is crucial for the metal–metal bonding and oxide layer removal. High purity powder particles have thinner oxide layers on the particle surfaces, promoting more tendency to get metal–metal bonding on the impact. If the oxide layer is thick, removal of this layer is more difficult on the impacts and thus, possibility that oxides stay at particle boundaries in the structure and decrease the metal–metal bonding [6]. Secondly, increased oxide content in the powder increased the critical velocity needed for adhesion [25], reflecting the one reason for use of high purity powders in cold spraying.

Table 3
Spraying parameters. Process gas N_2, spraying distance 40 mm, distance between two adjacent spray beads 1.5 mm and traverse speed 20 m/min, amount of layers 2 for Cu and 3 for Ta coating.

Coating	Pressure (bar)	Gas temperature (°C)	N_2 flow rate (m^3/h)
CS Cu	32	490	85
CS Ta	38	800	82

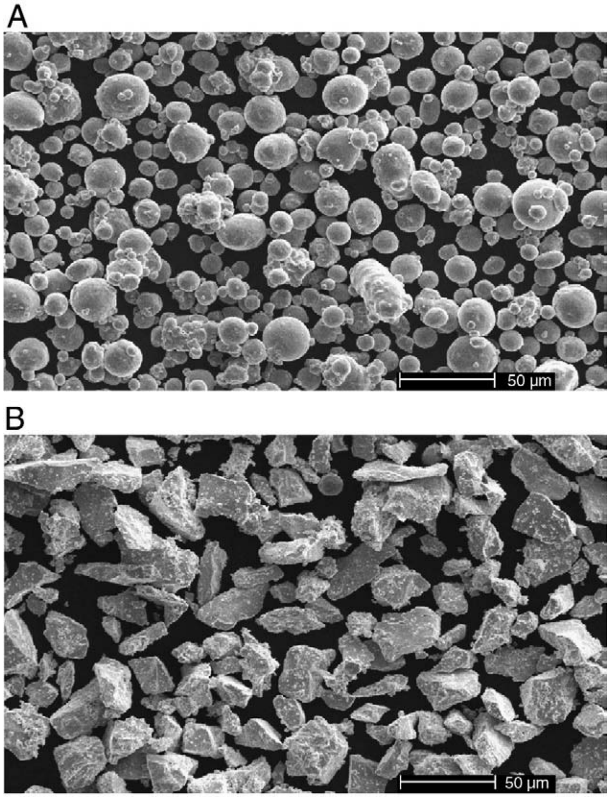

Fig. 1. Morphology of (A) Cu and (B) Ta powders. SEM images.

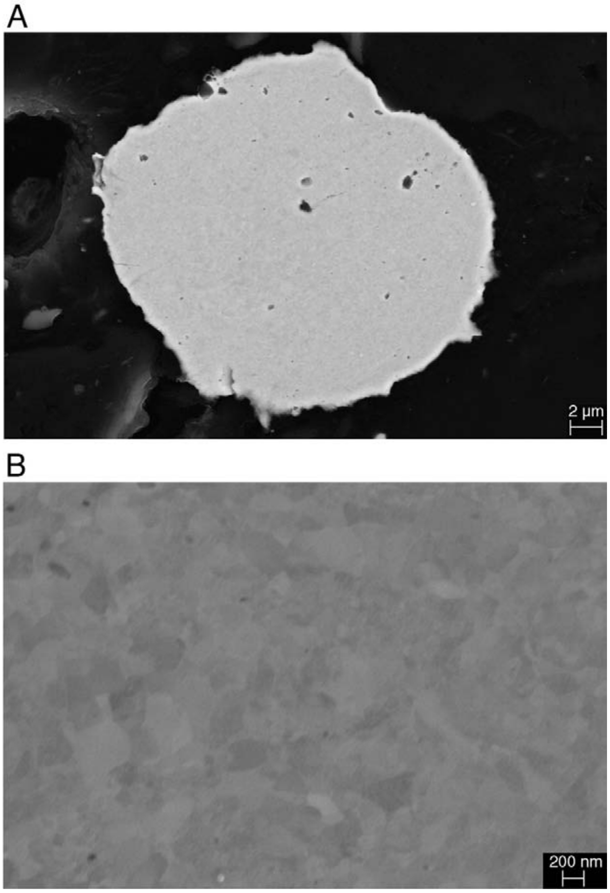

Fig. 2. Cross-section of Cu powder particle (A) individual particle and (B) internal structure. FESEM images.

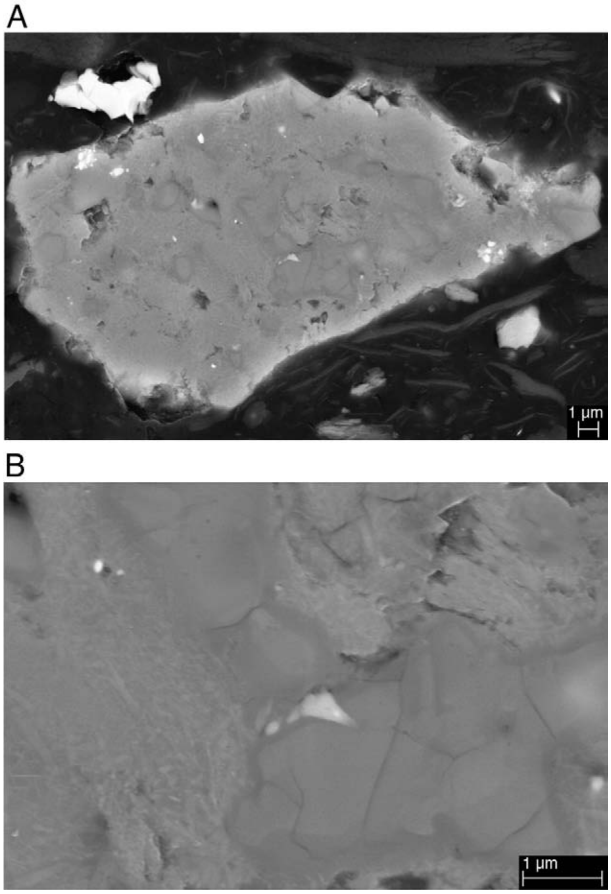

Fig. 3. Cross-section of Ta powder particle (A) individual particle and (B) internal structure. FESEM images.

Fig. 2 presents cross-section of an individual Cu powder particle. The particle has a relatively dense structure at the initial state (Fig. 2A), which is typical for the gas-atomized powder [26]. Internal structure of the Cu particle is shown in Fig. 2B. Different-sized grains are observed in the structure. The grain size is in the nano-scale (from ten to few hundred nanometers) and grains are randomly placed inside the powder particle. Typically, crushed powder particles have irregular shape. Cross-section of individual blocky-shaped Ta particle is shown in Fig. 3A and internal structure in Fig. 3B. Grain size distribution is somewhat wide from nano-scale to micro-scale grains.

The properties of the Cu and Ta powders differed relatively from each other. However, they both are optimized by manufacturer for cold spraying and capable to produce fully dense coating structures. Common properties were narrow particle size distribution and dense particle structure whereas main differences were in the particle morphology, spherical vs. blocky, and in the grain size; Cu powder had finer grain size and Ta powder had wider grain size distribution observed from cross-sections.

3.2. Coating denseness

Open-cell potential measurements were performed in order to show long-time impermeable behavior of these coatings. These measurements are a relevant method to characterize coating denseness, and in the other words, existing through-porosity, open-porosity or interconnected porosity in the coating structures. Open-cell potentials of the coatings were compared to the values of the corresponding bulk material and the carbon steel substrate material. If the value of the coating approaches the value of the bulk material, coating have a dense and impermeable structure and thus, similar corrosion protection with bulk material. However, if the value of the coatings approaches the value of the substrate material, it reflects existing through-porosity and thus, open path for the salt solution to penetrate from the coating surface to the interface between coating and substrate. Fig. 4 shows the open-cell potentials of the cold-sprayed Cu and Ta coatings, Cu and Ta bulk materials, and Fe52 substrate material. As the result, the coatings behaved similar with corresponding bulk materials, indicating the high impermeability and the real corrosion protection.

The cold-sprayed Cu and Ta coatings had overall dense structures according to the open-cell potential measurements. The coating structures were through-porosity-free without interconnected porosity due to the improved powder properties sprayed with advanced spraying equipment and optimized spraying parameters. On contrast, Van Steenkiste and Gorkiewicz [27] have reported the porosity level of kinetic-sprayed Ta coatings at about 3–16% (measured using a He pycnometer), depending on spraying conditions. Furthermore, the similar corrosion resistance of cold-sprayed Ta coating with Ta bulk material was evaluated in our previous studies [2,3]. The studies showed the open-cell potential behavior in the short-time exposure. In addition to that, the similar corrosion properties of the cold-sprayed Ta coatings and Ta bulk material in 3.5 wt.% NaCl, 40 wt.% H_2SO_4, and 20 wt.% HCl solutions at room temperature and elevated temperature were demonstrated with anodic polarization measurements.

3.3. Microstructures

General views of the cross-sections of the cold-sprayed Cu and Ta coatings on grit-blasted steel substrates are presented in Fig. 5. The coatings have visually dense structures. Powder particles underwent high level of plastic deformation during particle impacts which were presented in our previous study [1]. In addition, flattening of the cold-sprayed particles is observed from the etched structure due to the high plastic deformation [6,24]. Bonding between particles and substrate is tight due to the strong deformation of coating and substrate materials. Interface between the cold-sprayed Cu coating and the grit-blasted steel substrate is presented in Fig. 6A. Faultless interface is revealed. Fig. 6B shows microstructure of the cold-sprayed Cu coating. Similar randomly aligned grains can be seen in the Cu powder particle (Fig. 2B) and in the cold-sprayed Cu coating (Fig. 6B) as well.

Faultless interface between cold-sprayed Ta coating and grit-blasted steel substrate was presented in our previous studies [2,3]. Fig. 7A shows more specific details of the interface between Ta particles and between Ta particle and grit-blasted steel substrate. Arrows show the particle boundary between two Ta particles. Very fine grain structure is detected near to the particle–particle interface. Fig. 7B shows elongated grains due to the high deformation. Moreover, material jet between two Ta particles is observed in Fig. 7C presented with an arrow.

The microstructures of the cold-sprayed Cu (Fig. 6) and Ta (Fig. 7) coatings demonstrated localized deformed inter-particle structure.

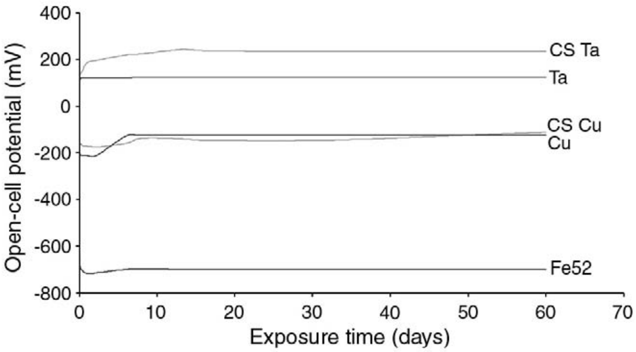

Fig. 4. Open-cell potentials of cold-sprayed (CS) Ta coating, Ta bulk material, cold-sprayed (CS) Cu coating, Cu bulk material, and Fe52 substrate material as a function of exposure time (in 3.5 wt.% NaCl). Ag/AgCl was used as a reference electrode.

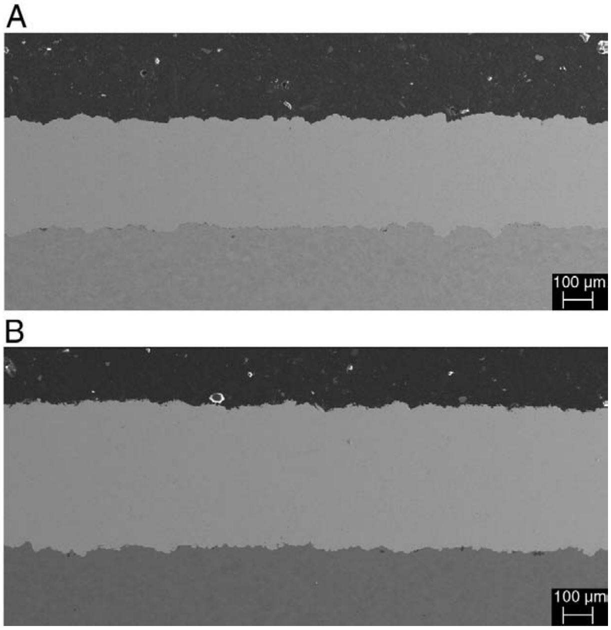

Fig. 5. Cross-sections of cold-sprayed (A) Cu and (B) Ta coatings on grit-blasted steel substrate. FESEM images.

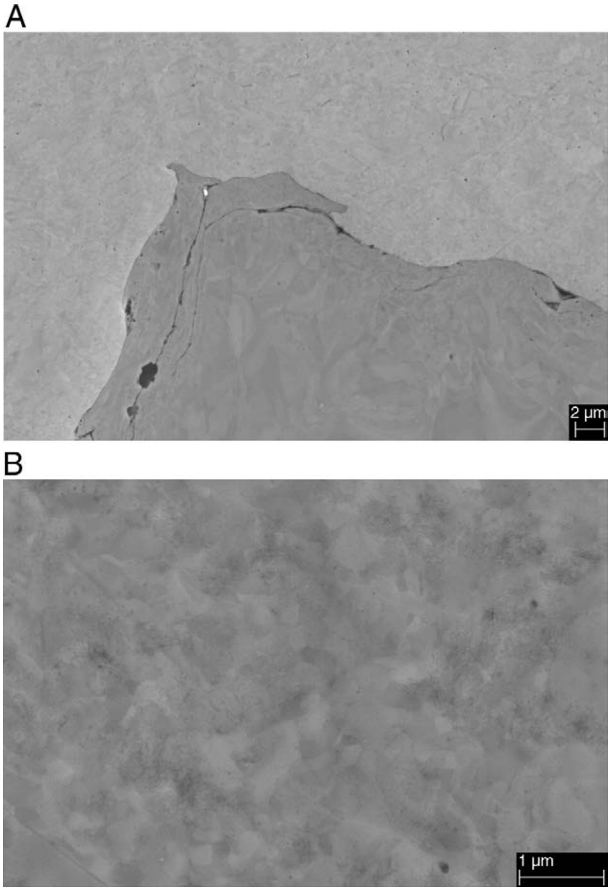

Fig. 6. Microstructure of cold-sprayed Cu coating (A) interface between coating (lighter gray) and grit-blasted steel substrate (darker gray) and (B) internal particle structure. FESEM images.

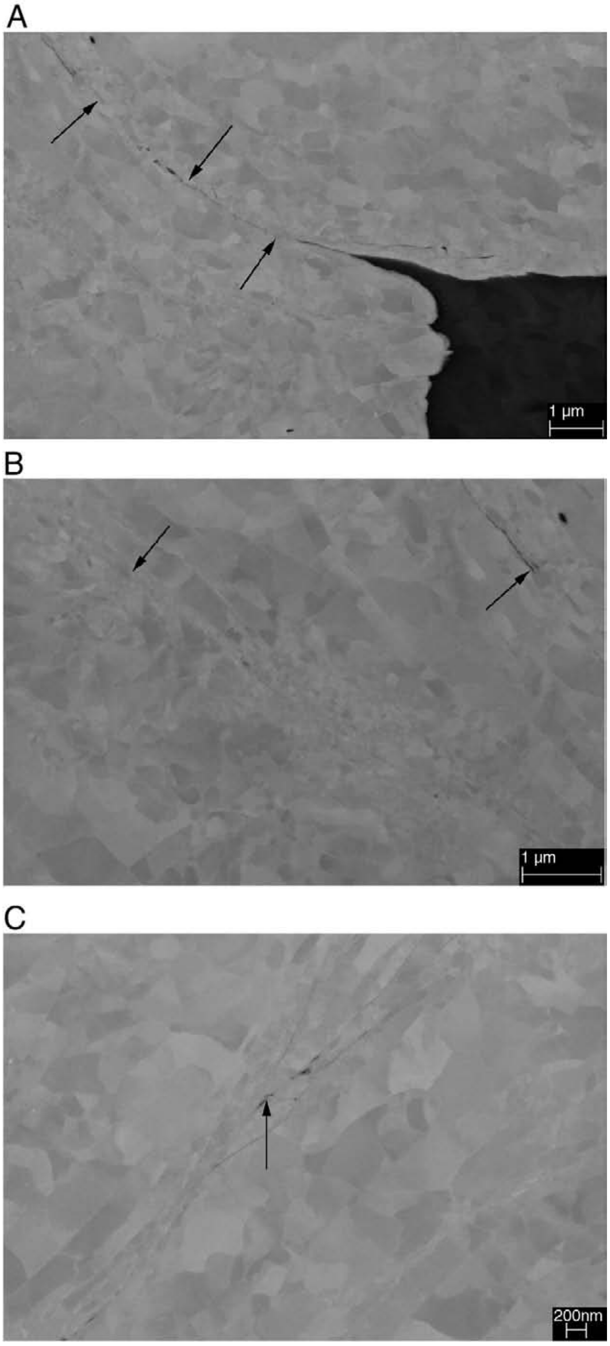

Fig. 7. Microstructure of cold-sprayed Ta coating A) interface between coating (gray area) and substrate (black area), B) grain structure, and C) elongated grains and material jet (arrow). Arrows show interfaces between particles. FESEM images.

This is due to the adiabatic shear instability and thermal softening [4,8,9]. The high plastic deformation is needed to remove oxide layers of the particles and thus, making it possible to form metal–metal bonding between particles. Therefore, the metal–metal bonds are required to receive dense structure and tight bonds between particles. Furthermore, the desired coating properties can be contributed by spraying parameters. Thermal softening causes adiabatic shear instability due to the localized heat distribution in the particle interface [8,9]. For the thermal softening, Ta (material with higher melting point) was sprayed with higher preheating temperature of process gas (800 °C vs. 490 °C). Additionally, the effect of gas temperature on the particle velocity should be detected. Higher particle velocity is achieved with higher gas temperature [6,22]. Moreover, higher gas pressure (together with high gas temperature) was used in order to get higher particle velocity and thus, high deformation.

3.4. Fracture behavior

Fracture surface analysis revealed structural details, e.g., particle deformation and particle bonding. The first criterion for denseness of the coating was high plastic deformation and thus, tight bonds between particles. Fracture surfaces (Figs. 8 and 9) showed the high level of plastic deformation occurred on the particle impacts. Fig. 8 presents the fracture surfaces of the cold-sprayed Cu coating. Partly brittle and partly ductile type fractures are observed. In addition to these, deformed material jets are seen from fracture surfaces. The

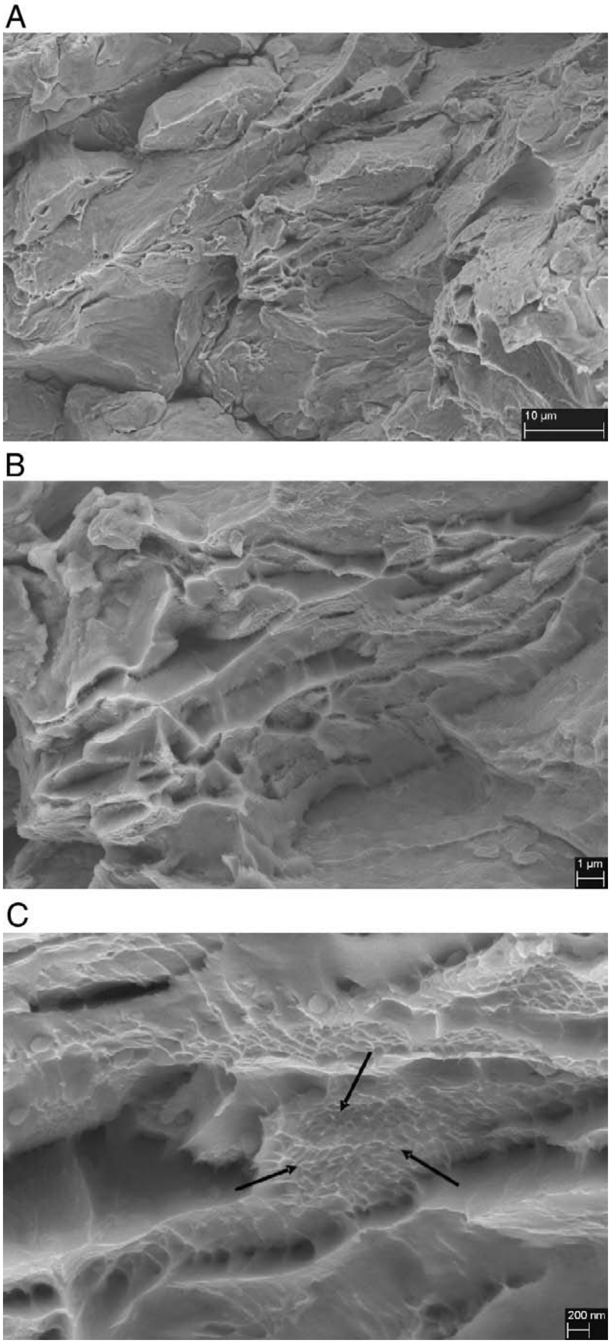

Fig. 8. Fracture surfaces of cold-sprayed Cu coating A) overview with deformed particles, B) ductile fracture, and C) recrystallized inter-particle structure indicated by arrows. FESEM images.

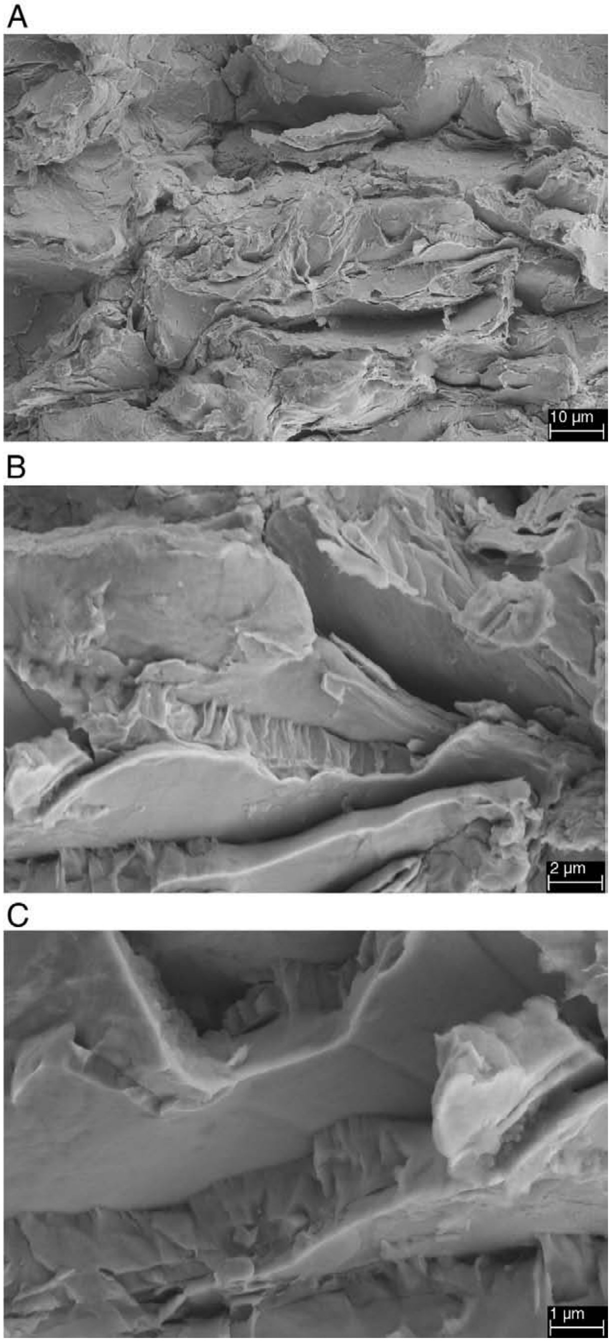

Fig. 9. Fracture surfaces of cold-sprayed Ta coating A) overview with flattened particles, B) highly deformed particle, and C) columnar inter-particle structure. FESEM images.

formation of material jets due to the thermal softening and adiabatic shear instability is very crucial for tight metal–metal bonding [8,14]. Dynamic recrystallization was also occurred on the Cu powder particle impacts due to the temperature and strain rate arising and is perceived as a fine-sized, recrystallized grain structure marked with arrows in Fig. 8C [28].

Partly brittle and partly ductile fractures were also observed from fracture surfaces of the cold-sprayed Ta coating, Fig. 9. The fracture surfaces of the cold-sprayed Ta coatings showed the high deformation level, flattened particle shape after deformation and in addition, tight bonds between particles. The fracture surfaces of the cold-sprayed Cu and Ta coatings differed from each other due to the different powder type and powder structure. The blocky Ta particles had columnar internal structure (Fig. 9B and C) whereas the spherical Cu particles had a flattened shape after impact and a fine-sized, recrystallized inter-particle structure (Fig. 8C).

3.5. Grain structures

Plastic deformation is known to be related to dislocations (i.e., microstructural defects). Under high strain, dislocation movement cause plastic flow and, hence permanent deformation and even more, cause work hardening. In the microstructure, plastic flow can be seen in the presence of slip planes due to the sliding [12] and shear bands due to the adiabatic shear localization [15]. The high dislocation density indicates high plastic strain and hence, high level of deformation. In addition to the high dislocation densities, twinning, i.e., formation of twins causes permanent deformation in the material [12].

Microscopic details by TEM analysis are performed in other studies [24,28–30]. Borchers et al. [24,28] found out high dislocation density areas, elongated grains, and ultra-fine grains as well as recrystallized structure areas in the cold-sprayed Cu coatings. In addition, Richter et al. [29] have reported grain refinement of cold-sprayed CoNiCrAlY coatings together with non-uniform inter-particle structures by TEM analysis. These observations correspond with our studies. Furthermore, the present study shows microstructural details both from cross-sectional and top-view direction. Fig. 10 presents microstructural details of the cold-sprayed Cu coating from cross-sectional direction. Particle boundary is seen in Fig. 10A and grain structure in Fig. 10B.

In Fig. 10A, holes in the structure arisen from ion milling are indicated as weak particle boundaries whereas other regions of the boundaries were tight. In addition, EDS analysis showed oxygen contents in these points in the structure: 1) 1.9 wt.% O, 2) 2.6 wt.% O, 3) 0.9 wt.% O, and 4) 0.5 wt.% O (Fig. 10A). These analyses show the oxygen contents at the present points and are not reflecting to the total amount of oxygen in the structure. Values are given here in order to get a comparison between different regions inside the coatings. The EDS analysis revealed lower amount of oxygen contents inside the particle (points 3 and 4 in Fig. 10A) than at the particle boundary. Furthermore, oxygen content was lower in point 1 than in point 2 (Fig. 10A), indicating tighter bonding region (point 1). On the other hand, it is possible that higher oxygen content in the open boundary (point 2) compared to the tight boundary (point 1) reflects the possibility that the oxide layers were not totally removed. There were still some weak points in the structures of this overall dense cold-sprayed Cu coating, however, tight bonds are dominant and thus, coating has the impermeable structure. High plastic deformation together with adiabatic localization is detected in microscopic characterization as the structure with a lot of nano-scale features. In addition, the cold-sprayed Cu coatings had not uniform structures [28]. Fig. 10B revealed slip bands (Fig. 10B, slip bands marked with number 1) and twinning (Fig. 10B, twins marked with number 2) due to the heavy plastic deformation and different grain sizes, indicating localized grain deformation on the impacts.

The etched microstructures of cold-sprayed coatings differed in the cross-sectional and top-view directions [1]. Particle deformation (and flattening) is detected in the cross-sectional direction whereas images from the top-view direction revealed additional information about microscopic details from the inter-particle structures. Fig. 11 presents inter-particle structure of the cold-sprayed Cu coating. A lot of shear bands due to the high deformation level is clearly seen in Fig. 11A (e.g., line-like structure inside the circle) and in addition to these, high dislocation density areas were observed in the structure, e.g., black lines marked with arrow. Fig. 11B shows fine-sized grains with the high amount of dislocations and on the other hand, dislocation-free grains due to the dynamic recrystallization. Finer inter-particle grain size is resulted from high plastic deformation whereas coarser grains

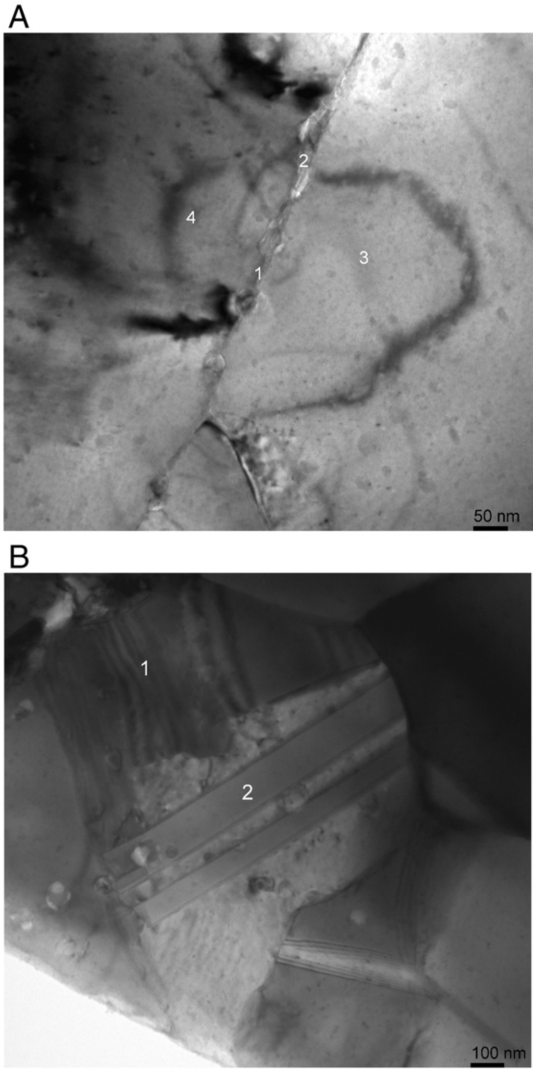

Fig. 10. Microstructural details from cross-sectional direction of cold-sprayed Cu coating A) particle boundary, EDS analysis taken from places 1–4, 1 and 2 are at the boundary, and 3 and 4 inside the particle, and B) grain boundaries and grain structure with slip bands (marked with 1) and twins (marked with 2). TEM images.

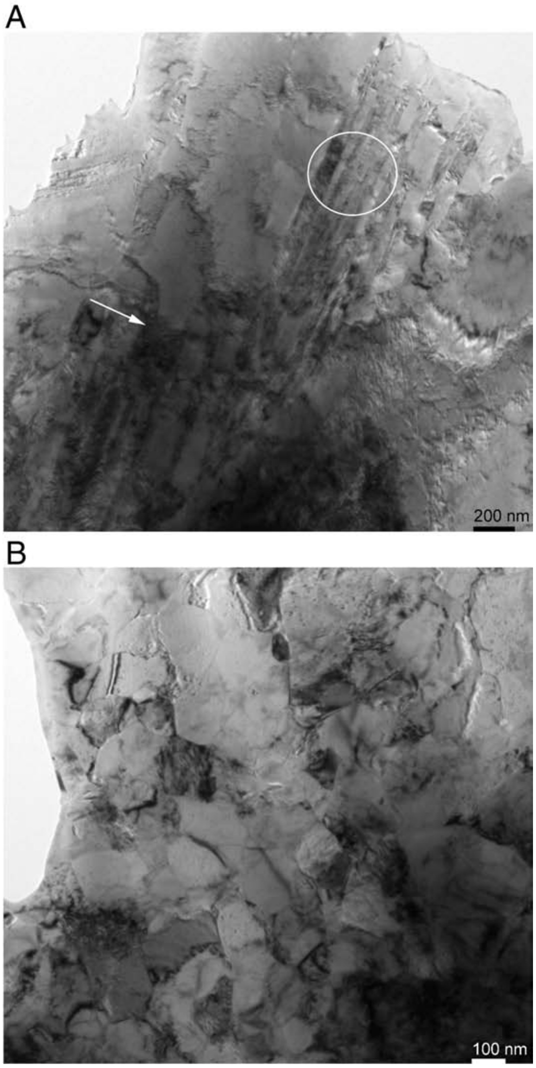

Fig. 11. Microstructural details from top-view direction of cold-sprayed Cu coating A) shear bands (line-like structure, e.g., inside the circle) and high dislocation density (black areas, example showed by arrow) and B) grain structure with fine-sized grains. TEM images.

are in the less deformed places [29]. Furthermore, randomly orientated fine-sized grains were observed in TEM investigations [30].

Deformation and inter-particle structure from top-view direction of Ta particles are shown in Fig. 12. High dislocation density areas are observed in the TEM images. Fig. 12A shows elongated grains with high dislocation density whereas dislocation walls are observed in Fig. 12B as black areas. Moreover, Fig. 12C shows tight particle bonds with shear bands (particle boundary is indicated with white arrows whereas black arrow shows shear bands) and Fig. 12D grain deformation with high dislocation density.

EDS analysis (Fig. 12C) revealed the low oxygen contents both in the particle boundary and in the inter-particle structure: 1) 0.7 wt.% O, 2) 0.7 wt.% O, 3) 0.5 wt.% O, and 4) 0.6 wt.% O. This indicated pure metal–metal bonding between particles. However, it should be observed that oxygen content reflects not the total amount of oxygen inside the coating structure. The cold-sprayed Ta coating had very dense and highly deformed structure with tight particle bonds. This coating contained high amount of dislocations and especially dislocation walls. Moreover, elongated grains indicated high plastic deformation and localized deformation levels due to the localized adiabatic shearing and thermal softening.

Highly deformed and tightly bonded structures of the cold-sprayed Cu and Ta coatings were observed with FESEM and TEM characterizations. In addition to that, high level of plastic deformation causes work hardening in the coating structure. On the contrary, high hardness indicates work hardening. Hardness of the cold-sprayed Ta coating was 230 $HV_{0.3}$ and of Ta bulk material 100 $HV_{0.3}$ [31]. The same trend was observed also with the cold-sprayed Cu compared to the Cu bulk material, 150 $HV_{0.3}$ vs. 80 $HV_{0.3}$ [31]. In both coatings, increment of the coatings' hardness was significant, indicating strain hardening and work hardening resulted from plastic deformation. On the other hand, dislocation density is increased in hardened material which makes a connection between work hardening (increased hardness) and highly deformed microstructure (high dislocation density). [20]

4. Conclusions

As a conclusion, the cold spraying is shown to be an optimal spraying method to prepare overall dense coatings with impermeable coating structures. Dependence between microstructure and coating quality, e.g., denseness, was clarified. In general, Cu is one of the most

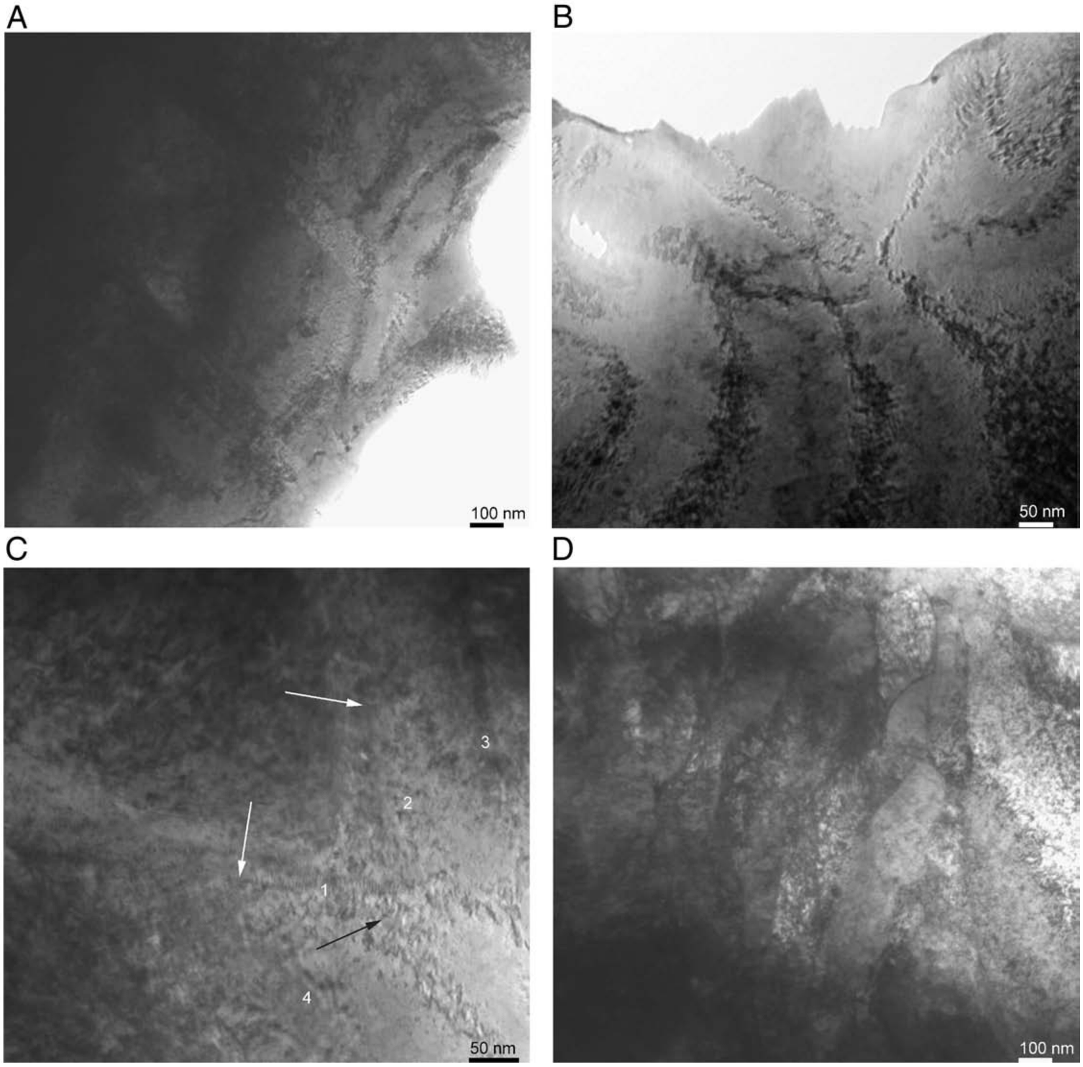

Fig. 12. Microstructural details from top-view direction of cold-sprayed Ta coating A) grain boundaries, elongated grains, B) dislocation walls (black areas), and C) particle boundaries (indicated with white arrows), EDS analysis taken from places 1–4 (1 is at the boundary, 2–4 are inside the particle), and shear bands (example showed by black arrow), and D) deformed grains with high dislocation density. TEM images.

used and researched material in the field of cold spraying. The cold-sprayed Cu coatings are typically used in the applications where electrical or thermal conductivity is needed. For this kind of applications, high purity and denseness of the coatings are advantageous properties. On contrast, Ta is used when extreme corrosion resistance is needed. For that reason, the denseness of the coating is the first criterion for corrosion protection due to the fact that Ta coating gives anodic protection to the steel substrate.

Firstly, denseness of the cold-sprayed Cu and Ta coatings was identified with a corrosion test. Secondly, FESEM evaluations showed faultless interfaces between coating and substrate which is also important for the particle adhesion. In addition, metal–metal bonding was found to be dominant in the particle bonding. Moreover, localized deformation of particles was observed from FESEM images. In the cold-sprayed Ta coating, fine-sized grains were concentrated at the particle boundaries. On the other hand, in the cold-sprayed Cu coating different-sized grains were mostly randomly orientated.

Thirdly, fracture surface analysis revealed particle deformation, bonding, structure, and fracture behavior, specifying coating quality. The fracture planes of the cold-sprayed Cu coatings appeared heavy plastic deformation of powder particles, having a partly brittle and partly ductile fracture behavior. In addition, material jets and elongated particle structures were perceived, indicating clearly localized deformation. Moreover, the cold-sprayed Cu coating had recrystallized grain structure. Additionally, Ta powder particles also underwent high deformation and flattening of the particles was observed from fracture surfaces. In addition, Ta particles had elongated and columnar grain structure.

And finally, TEM characterization provided valuable additional information about specific microstructural details (also in the nanoscale) of the cold-sprayed Cu and Ta coatings. High dislocation density areas and dislocation walls were observed mostly from top-view characterization. In addition, twins due to the deformation were noticed. In the cold-sprayed Cu coating, slip and shear bands were dominant whereas the cold-sprayed Ta coating contained more shear bands and dislocation walls. Common for both structures were different-sized grains with large and fine grain sizes and more elongated and less deformed grains. These details are caused by localized deformation due to the adiabatic shear instability. FESEM and TEM characterizations also showed metal–metal bonding. Tight bonds were dominant and thus, structures were dense. We can say that coatings still contained individual defects but so low amounts that they do not affect the completeness. After all, it can be said that microstructure defines the quality of the coatings.

Acknowledgements

Authors like to thank Mr. Werner Krömmer from Linde AG Gas (Unterschleissheim, Germany) for spraying the coatings and valuable discussion. The project was supported by the Academy of Finland and Finnish Graduate School of New Materials and Process.

References

[1] H. Koivuluoto, J. Lagerbom, P. Vuoristo, Microstructural studies of cold sprayed copper, nickel, and nickel–30%copper coatings, J. Therm. Spray Tech. 16 (4) (2007) 488.
[2] H. Koivuluoto, J. Näkki, P. Vuoristo, Corrosion properties of cold-sprayed tantalum coatings, J. Therm. Spray Tech. 18 (1) (2009) 75.
[3] H. Koivuluoto, J. Näkki, P. Vuoristo, Structure and corrosion behavior of cold-sprayed tantalum coatings, in: B.R. Marple, M.M. Hyland, T.-C. Lau, C.-J. Li, R.S. Lima, G. Montavon (Eds.), Thermal Spray 2009: Expanding Thermal Spray Performance and New Markets and Applications, ASM International, Las Vegas, Nevada, USA, May 4–7, 2009, p. 314.
[4] T. Schmidt, F. Gärtner, H. Assadi, H. Kreye, Development of a generalized parameter window for cold spray deposition, Acta Mater. 54 (2006) 729.
[5] A. Papyrin, V. Kosarev, S. Klinkov, A. Alkimov, V. Fomin, Cold Spray Technology, 1st ed, Elsevier, Netherlands, 2007, p. 328.
[6] V.K. Champagne (Ed.), The Cold Spray Materials Deposition Process, Fundamentals and applications, Woodhead publishing Limited, Cambridge, England, 2007, p. 362.
[7] J. Pattison, S. Celotto, A. Khan, W. O'Neill, Standoff distance and bow shock phenomena in the cold spray process, Surf. Coat. Technol. 202 (2008) 1443.
[8] M. Grujicic, C.L. Zhao, W.S. DeRosset, D. Helfritch, Adiabatic shear instability based mechanism for particles/substrate bonding in the cold-gas dynamic-spray process, Mater. Des. 25 (2004) 681.
[9] H. Assadi, F. Gärtner, T. Stoltenhoff, H. Kreye, Bonding mechanism in cold gas spraying, Acta Mater. 51 (2003) 4379.
[10] T. Van Steenkiste, D.W. Gorkiewicz, Analysis of tantalum coatings produced by the kinetic spray process, J. Therm. Spray Tech. 13 (2) (2004) 265.
[11] T.S. Price, P.H. Shipway, D.G. McCartney, E. Calla, D. Zhang, A method for characterizing the degree of inter-particle bond formation in cold sprayed coatings, J. Therm. Spray Tech. 16 (4) (2007) 566.
[12] T.H. Courtney, Mechanical Behavior of Materials, 2nd ed, McGraw-Hill Publishing Company, Singapore, 2000, p. 733.
[13] R. Gr, V. Leshchynsky Maev, Introduction to low pressure gas dynamic spray, physics & technology, Wiley-VCH Verlag GmbH & Co, KGaA, Weinheim, Germany, 2008. 328 pp.
[14] M. Grujicic, J.R. Saylor, D.E. Beasley, W.S. DeRosset, D. Helfritch, Computational analysis of the interfacial bonding between feed-powder particles and the substrate in the cold-gas dynamic-spray process, Appl. Surf. Sci. 219 (2003) 211.
[15] M.A. Meyers, Plasticity: Adiabatic Shear Localization, Encyclopedia of Materials: Science and Technology, p. 7093–7103
[16] T. Stoltenhoff, C. Borchers, F. Gärtner, H. Kreye, Microstructures and key properties of cold-sprayed and thermally sprayed copper coatings, Surf. Coat. Technol. 200 (2006) 4947.
[17] Metals Handbook, Volume 2, Properties and Selection: Nonferrous Alloys and Special-Purpose Materials, Properties of Pure Metals, Copper (Cu), ASM Online
[18] Metals Handbook, Volume 2, Properties and Selection: Nonferrous Alloys and Special-Purpose Materials, Properties of Pure Metals, Copper (Cu), ASM Online
[19] F. Gärtner, T. Stoltenhoff, T. Schmidt, H. Kreye, The cold spray process and its potential for industrial applications, J. Therm. Spray Tech. 15 (2) (2006) 223.
[20] W.D. Callister Jr., Materials Science and Engineering, An Introduction, 5th ed, John Wiley & Sons Inc, United State of America, 2000, p. 871.
[21] H.C. Starck, Amperit, Powders for Surface Technology and more..., Cold-Spray-Powderline, Powder procedure, available in http://www.hcstarck.de/index.php?page_id=2044.
[22] T. Schmidt, F. Gärtner, H. Kreye, New developments in cold spray based on higher gas- and particle temperatures, J. Therm. Spray Tech. 15 (4) (2006) 488.
[23] H. Kreye, T. Schmidt, F. Gärtner, and T. Stoltenhoff, The Cold Spray Process and Its Optimization, Thermal Spray 2006: Building on 100 Years of Success, B.R. Marple, M.M. Hyland, Y.-C. Lau, R.S. Lima, and J. Voyer (Eds.), May 15–18 (Seattle, Washington, USA), ASM International, p 5
[24] C. Borchers, F. Gärtner, T. Stoltenhoff, H. Assadi, H. Kreye, Microstructural and macroscopic properties of cold sprayed copper coatings, J. Appl. Phys. 12 (93) (2003) 10064.
[25] C.-J. Li, G.-J. Yang, C.-X. Li, H.S. Bang, W.-Y. Li, Examination of the estimating approaches for the critical velocity in cold spraying, in: B.R. Marple, M.M. Hyland, Y.-C. Lau, C.-J. Li, R.S. Lima, G. Montavon (Eds.), Thermal Spray 2007: Global Coating Solutions, ASM International, Beijing, China, May 14–16, 2007, p. 128.
[26] Metals Handbook, Volume 7, Powder Metal Technologies and Applications, Atomization, General Characteristics of Atomized Metal Powders, Atomization, ASM Online.
[27] T. Van Steenkiste, D.W. Gorkiewicz, Analysis of tantalum coatings produced by the kinetic spray process, J. Therm. Spray Tech. 13 (2) (2004) 265.
[28] C. Borchers, F. Gärtner, T. Stoltenhoff, H. Kreye, Microstructural bonding features of cold sprayed face centered cubic metals, J. Appl. Phys. 8 (96) (2004) 4288.
[29] P. Richter, A. Zúñiga, M. Yandouzi, B. Jodoin, CoNiCrAlY microstructural changes induced during Cold Gas Dynamic Spraying, Surf. Coat. Technol. 203 (3–4) (2008) 364.
[30] L. Ajdelsztajn, B. Jodoin, J. Schoenung, Synthesis and mechanical properties of nanocrystallize Ni coatings produced by cold gas dynamic spraying, Surf. Coat. Technol. 201 (3–4) (2006) 1166.
[31] H. Koivuluoto, M. Kotilainen, P. Vuoristo, Overview of structure and properties of high-pressure and low-pressure cold-sprayed coatings, Weld. Cutt. (2) (2009) 98.

Publication VI

Heli Koivuluoto and Petri Vuoristo

Structural Analysis of Cold-Sprayed Nickel-Based Metallic and Metallic-Ceramic Coatings

Journal of Thermal Spray Technology, DOI: 10.1007/s11666-010-9481-4, in press.

Reprinted from Journal of Thermal Spray Technology with permission of ASM International.
Copyright (2010) ASM International.

JTTEE5
DOI: 10.1007/s11666-010-9481-4
1059-9630/$19.00 © ASM International

Peer Reviewed

Structural Analysis of Cold-Sprayed Nickel-Based Metallic and Metallic-Ceramic Coatings

Heli Koivuluoto and Petri Vuoristo

(Submitted October 31, 2009; in revised form December 29, 2009)

In cold spraying, many factors, e.g., powder characteristics and compositions, spraying parameters, and post-treatments affect coating formation. Cold spraying is the optimal technique to produce highly dense coatings. Furthermore, denseness and impermeability are the criterions for the corrosion resistance of anodically protective coatings. Therefore, this study focuses on denseness improvement of cold-sprayed (CS) metallic coatings. The aim of this study was to characterize structural details of CS Ni, Ni-20Cu, Ni-20Cr, Ni-20Cr + Al_2O_3, and Ni-20Cr + WC-10Co-4Cr coatings in order to produce dense coatings by optimizing the affecting factors. Denseness of Ni coating was improved with optimized spraying parameters whereas denseness of Ni-20Cr coatings was increased with added hard particles in the powder mixture. In addition, denseness of Ni-20Cu coatings was improved by heat treatments. Denseness of the coatings is evaluated by corrosion tests. In addition, fracture behavior, microstructures, and hardness studies of the coatings are performed.

Keywords coating structure, cold spraying, denseness, heat treatment of coatings, Ni alloy coatings

1. Introduction

Cold spraying is a solid-state process wherein the coating is formed by powder particle impacts with a high kinetic energy and thus, with a high particle velocity (Ref 1, 2). In addition, ceramic particles with a metallic matrix can be sprayed using the cold spray system. At least one component of the sprayed powder needs to be ductile (Ref 3). During impacts, powder particles deform plastically and adhere to the substrate surface or to other particles and form the coating (Ref 4, 5). Formation of bonds between particles requires critical impact velocities of particles in order to obtain adequate bonding and adhesion (Ref 1). Furthermore, successful particle-substrate and particle-particle bonding requires a high level of plastic deformation and adiabatic shear instability. In addition, strong adhesion between particles requires the formation of material jets due to the thermal softening. Higher particle velocity leads stronger bonding and thus, affects the denseness of coatings (Ref 2). Cold spraying is a potential method of spraying dense (very low porosity) coatings for applications where corrosion protection is needed. Denseness and impermeability depend strongly on spraying process conditions, powder characteristics, and coating material, and moreover, the combination of these affecting factors (Ref 6). Additionally, coating quality relies on spraying conditions, higher velocity leads to stronger plastic deformation and furthermore, coating structure become denser and mechanical properties are improved (Ref 7, 8). The preheating temperature of process gas reportedly has influence on the coating quality. Higher temperature together with higher pressure leads to denser coating structure due to the thermal softening and local shear instability (Ref 1, 2).

Metal-ceramic composite coatings are reportedly produced by using cold spray processes (Ref 9-11). Furthermore, hardmetal coatings, e.g., WC-Co coatings have been prepared with the cold spraying (Ref 12, 13). Adhesion of metallic particles depends on particle velocity and temperature on impact. These parameters affect also the behavior of hard particles (e.g., erosion, activation, and sticking) (Ref 9). Ceramic particles activate the sprayed surface by removal of oxide layers of metallic particles. This improves the deposition efficiency. On the other hand, hard particles hammer the sprayed particles, providing a denser coating structure (Ref 14). However, the amount of ceramic particles in the sprayed coating is low compared to the initial powder composition. Usually, coatings contain ceramic particles below 5% from total amount of ceramic powder (Ref 11, 15). Hard particles can have higher or lower velocity than the metallic particles in the powder mixture. Velocity depends on powder characteristics (e.g., particle size) of the hard particles (Ref 9). Klinkov et al. (Ref 9) have shown that fine SiC particles (5 and 15 μm) have higher velocity than Al or Cu particles. However, a shock layer near to the surface decreases the velocity of 5 μm particles and thus, less

Heli Koivuluoto and **Petri Vuoristo**, Department of Materials Science, Tampere University of Technology, Tampere, Finland. Contact e-mail: heli.koivuluoto@tut.fi.

Published online: 11 February 2010

activation occurs with these particles in comparison with 15 μm particles (Ref 9). For a dense coating and tight bonds between particles, metal-metal bonding and material jet formation are required. This needs clean contact surfaces under high pressure conditions (Ref 3, 16, 17). For that, oxide layers of powder particles should be destroyed and removed from the metal surface on the impacts (Ref 18). This occurs with high plastic deformation and materials jets (Ref 3, 16-18). Removal of oxide layer can be illustrated with an egg-cell-model (during impact, particles behave similar like egg, hard cell (oxide) breaks down and soft inside (metal) deforms). After the oxide layer is broken down, a gas flow removes the oxides away (Ref 18).

Typically, the level of plastic deformation is detected from an etched microstructure of cold-sprayed (CS) coatings by the flattening degree of the particles. On the other hand, generally, material properties depend on their microstructure which in turns depends on grain structure and treatments. Therefore, plastic deformation is due to dislocation movements caused by critical shear stress. In principle, plastic deformation occurs in each grain in the individual powder particle which means that particle boundaries can restrict the deformation of some grains. This indicates different levels of plastic deformation in the particle and hence, through the coating structure (Ref 19).

The aim of this study was to investigate the structural properties of nickel-based metallic and metallic-ceramic coatings in order to improve the denseness and impermeability of these coatings. Ni, Ni-20Cu (NiCu), and Ni-20Cr (NiCr) were chosen because of their possibility to act as corrosion barrier coatings. In addition, hard Al_2O_3 and WC-10Co-4Cr (WC-Co-Cr) particles were mixed with the NiCr powder in order to decrease porosity and increase denseness of the coatings. The corrosion resistance of these coatings depends on denseness (existing through-porosity, impermeability) and chemical homogeneity. It can be said that microstructure of these coatings defines their corrosion protection capability. This study sought structural properties such as microstructures, fracture surfaces, corrosion properties, and mechanical properties of the CS Ni, NiCu, NiCr, NiCr + 50(vol.%)Al_2O_3, and NiCr + 30(vol.%)WC-Co-Cr coatings. In addition, the effects of spraying parameters and heat treatment as a post-treatment were studied.

2. Experimental Techniques

Ni, Ni20Cu, Ni20Cr, Ni20Cr + 50Al_2O_3, and Ni20Cr + 30WC-Co-Cr powders were CS with different spraying parameters. Metallic powders were gas-atomized having a spherical shape whereas added hard particles (Al_2O_3 and WC-Co-Cr) had an irregular blocky shape. Al_2O_3 powder was fused and crushed and WC-Co-Cr powder sintered and crushed. Table 1 shows powder characteristics and Fig. 1 morphologies of the powders used. Particle sizes are nominal given by supplier. Metallic-ceramic powder mixtures were manually mixed by hand.

Coatings were prepared at Linde AG Linde Gas Division (Unterschleissheim, Germany) with a CGT Kinetiks 4000 high-pressure cold spray system. Table 2 summarizes the spraying parameters used in this study. Two different beam distance-traverse speed combinations were tested with each powder (except NiCr). In addition to these, three different preheating temperatures of gas (500, 600, and 700 °C) were tested with the NiCr + 30WC-Co-Cr powder. In all experiments, nitrogen was used as a process gas. Substrates, carbon steel sheets ($50 \times 100 \times 1.5$ mm^3), were grit-blasted (1 mm Al_2O_3 grits) prior to spraying.

Cold-sprayed coatings were characterized both in the as-sprayed and heat-treated state. Heat treatments were done using a furnace in a protective (Ar-3%H_2) atmosphere. Figure 2 shows the heat treatment procedure with three different regions. The region I is the temperature rising up to the temperature of 600 °C, II the temperature holding with the holding time of 2 h at 600 °C, and III the temperature cooling. Samples were in the protective atmosphere during total heat treatment cycle. Heat treatment temperature of 600 °C was chosen according to our previous studies of CS Ni coatings (Ref 20) and Ni20Cr coatings (Ref 21).

Powder morphologies were characterized using a Philips XL30 scanning electron microscope (SEM). Coating structures and fracture surfaces were analyzed with a Zeiss ULTRAplus field-emission scanning electron microscope (FESEM). Microstructures were studied from unetched metallographic cross-sectional samples. Coating samples were bent for fracture surface analysis. Hard particle fractions were calculated from the coating cross sections using image analysis (ImageJ). Coating denseness and especially existing through-porosity were studied using open-cell electrochemical potential measurements and salt spray tests. The electrochemical cell used in the open-cell potential measurements consisted of a plastic tube, of diameter 20 mm and volume 12 mL, glued on the surface of the coating specimen. A 3.5 wt.% NaCl solution was placed in the tube for 9-day measurements. Open-cell potential measurements were taken with a Fluke 79 III true RMS multimeter. A silver/silver chloride (Ag/AgCl) electrode was used as a reference electrode. The salt spray test was done according to the ASTM B117 standard. Substrates were masked with epoxy paint before testing in order to allow the coating surfaces to be in contact only with the corroding salt spray. A 5 wt.% NaCl solution was used with an exposure time of 96 h, a temperature of 35-40 °C, a solution

Table 1 Powder characteristics

Powder	Particle size, μm	Production method	Supplier
Ni	−30 + 10	Gas-atomized	H.C. Starck
Ni-20Cu	−30 + 10	Gas-atomized	Sandvik Osprey
Ni-20Cr	−30 + 10	Gas-atomized	Sandvik Osprey
Al_2O_3	−90 + 45	Fused and crushed	H.C. Starck
WC-10Co-4Cr	−45 + 11	Sintered and crushed	Sulzer Metco

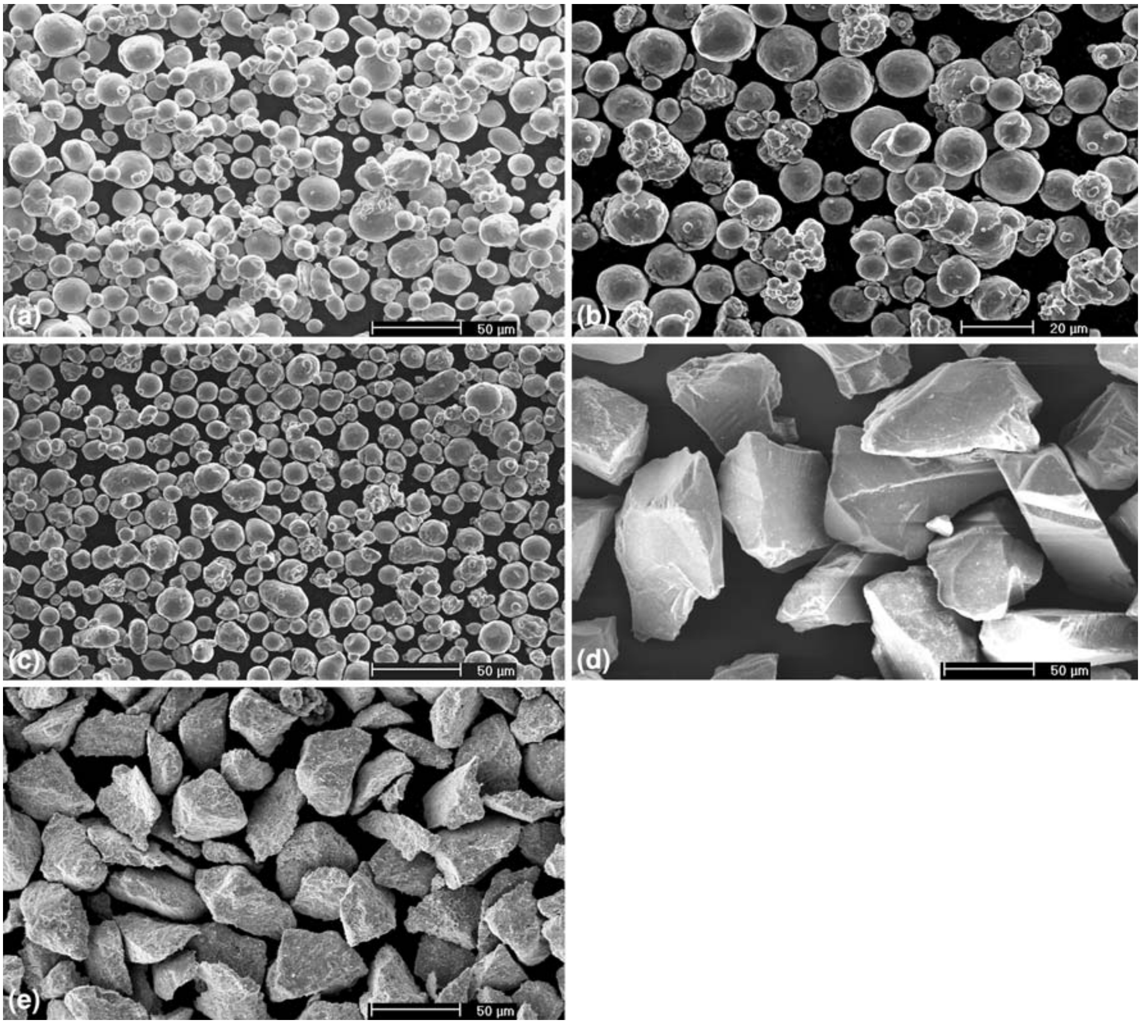

Fig. 1 Morphologies of (a) Ni (−30 + 10 µm), (b) Ni20Cu (−30 + 10 µm), (c) Ni20Cr (−30 + 10 µm) metallic powders and added hard particles, (d) Al_2O_3 (−90 + 45 µm), and (e) WC-10Co-4Cr (−45 + 11 µm). SEM images

Table 2 Spraying parameters

Coating	Gas pressure, bar	Gas temperature, °C	Gas flow, m^3/h	Beam distance, mm	Traverse speed, m/min
Ni-1	36	700	82	0.75	40
Ni-2	36	700	82	1.5	20
NiCu-1	39	650	89	0.75	40
NiCu-2	39	650	89	1.5	20
NiCr-1	38	600	89	0.75	40
NiCr + 50Al_2O_3-1	39	700	88	0.75	40
NiCr + 50Al_2O_3-2	39	700	88	1.5	20
NiCr + 30WC-Co-Cr-1	37	700	80	0.75	40
NiCr + 30WC-Co-Cr-2	37	700	80	1.5	20
NiCr + 30WC-Co-Cr-3	37	500	88	0.75	40
NiCr + 30WC-Co-Cr-4	37	600	84	0.75	40

Beam distance means distance between two adjacent spray beads

pH of 6.3, and a solution accumulation of 0.04 mL/cm^2 h. Surfaces of the coatings were analyzed visually and amounts (%) of corrosion spots were characterized using image analysis (ImageJ). Vickers hardness ($HV_{0.3}$) was measured as an average of ten measurements with a Matsuzawa hardness tester.

3. Results

The corrosion tests show clearly denseness and impermeability or existing through-porosity and therefore, weak bonding or structural defects in the coating structures (Ref 22). The densification effect of added hard Al_2O_3 particles on the denseness of the $NiCr + Al_2O_3$ coatings was clearly showed in the previous study (Ref 14). Denseness improvement was noticeable due to the hammering effect of hard particles together with possibility to use higher process temperature without clogging the nozzle (Ref 14). The main focus point of this study was to improve denseness in order to decrease through-porosity (open-porosity or interconnected porosity). Denseness, fracture behavior, microstructure, and hardness of these CS Ni, NiCu, NiCr, $NiCr + Al_2O_3$, and NiCr + WC-Co-Cr coatings were characterized.

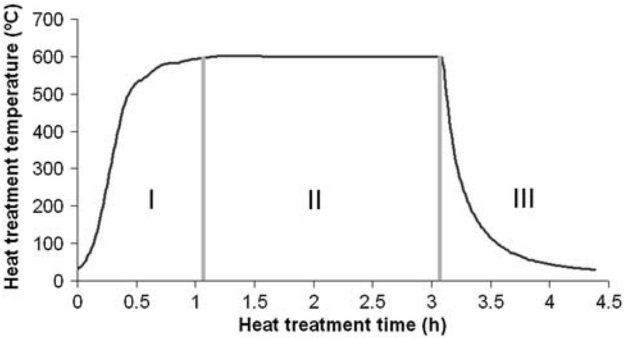

Fig. 2 Heat treatment procedure: (I) temperature rising, (II) temperature holding, and (III) temperature cooling

3.1 Denseness

Open-cell potential measurements and salt spray tests were done in order to investigate the impermeability of the coatings, i.e., is the coating impermeable or is there existing through-porosity (in the other words open-porosity or interconnected porosity) in the coating structures. The corrosion resistance of these coatings is based on anodic protection and hence, fully dense coating structure is the requirement. The results of the open-cell potential measurements are shown in Fig. 3 to 6. If the open-cell potential of the coating is close to the bulk material, it reflects the dense structure of the coating and hence, similar protection with bulk material. On the other hand, if the open-cell potential of the coating approaches the value of the substrate material, it reflects existing through-porosity in the coating structure, indicating open way for the salt solution to penetrate from coating surface to the interface between coating and substrate. The open-cell potential of as-sprayed and heat-treated Ni-1 and Ni-2 coatings, Ni bulk, and Fe52 substrate material are presented in Fig. 3.

Figure 4 shows the open-cell potential values of as-sprayed and heat-treated NiCu-1 and NiCu-2 coatings, Ni-30Cu bulk material, and Fe52 substrate material. Heat treatment improved the denseness of these coatings. The open-cell potential behavior of heat-treated coatings was closer to the bulk material compared with the substrate material, indicating denser coating structure. In addition, it should be noticed that spraying parameters had not as strong effect on the open-cell potential behavior of NiCu as with Ni coatings, reflecting that spraying parameters together with powder characteristics are strongly material-dependent in the cold spraying (Ref 6).

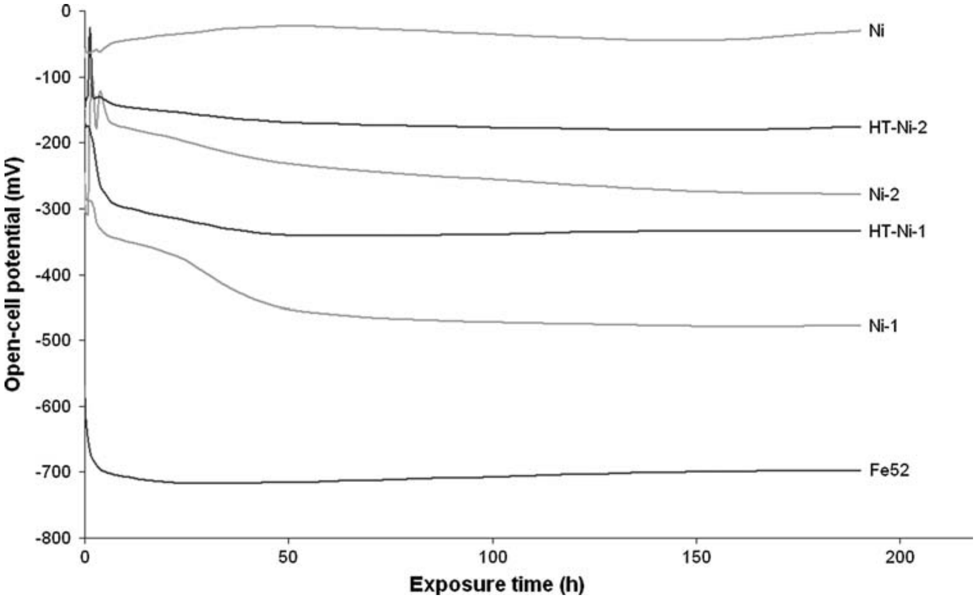

Fig. 3 Open-cell potentials of as-sprayed Ni-1 and Ni-2 coatings, heat-treated HT-Ni-1 and HT-Ni-2 coatings, Ni bulk material, and Fe52 substrate material as a function of exposure time in 3.5% NaCl solution. Ag/AgCl reference electrode

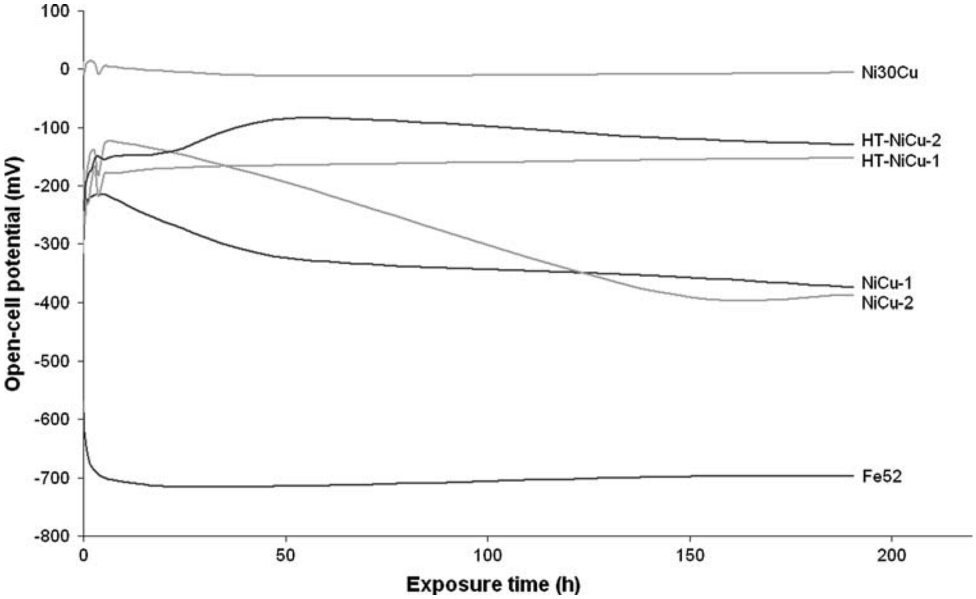

Fig. 4 Open-cell potentials of as-sprayed NiCu-1 and NiCu-2 coatings, heat-treated HT-NiCu-1 and HT-NiCu-2 coatings, Ni-30Cu bulk material and Fe52 substrate material as a function of exposure time in 3.5% NaCl solution. Ag/AgCl reference electrode

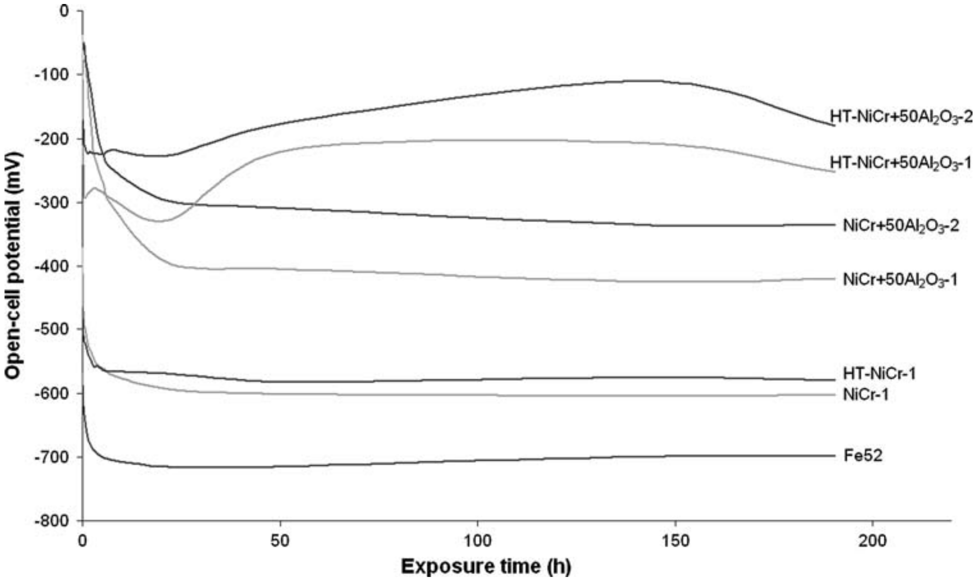

Fig. 5 Open-cell potentials of as-sprayed NiCr-1, NiCr + 50Al_2O_3-1 and NiCr + 50Al_2O_3-2 coatings, heat-treated HT-NiCr-1, HT-NiCr + 50Al_2O_3-1 and HT-NiCr + 50Al_2O_3-2 coatings and Fe52 substrate material as a function of exposure time in 3.5% NaCl solution. Ag/AgCl reference electrode

An addition of Al_2O_3 particles into the NiCr powder improved the denseness of the coating. The open-cell potential values of as-sprayed and heat-treated NiCr + Al_2O_3 and NiCr coatings and Fe52 substrate material are presented in Fig. 5. Pure NiCr coating contained through-porosity, and the denseness was increased with the ceramic particle addition. In addition, the improving effect of the heat treatments on denseness was noticeable also with NiCr + 50Al_2O_3 coatings. Our previous study (Ref 14) showed similar results of influence of the hard particle addition on coating structure. However, it should be notice that in this present study different NiCr powder was used, −30 + 10 μm instead of −22.5 + 10 μm. This provides crucial effect of powder-type together with spraying parameters (and optimal combinations of these factors) on the production of dense coatings.

Figure 6 presents the open-cell potential values of NiCr + 30WC-Co-Cr coatings in the as-sprayed and heat-treated state. The same effect of the hardmetal particles as the Al_2O_3 particles on the denseness improvement was

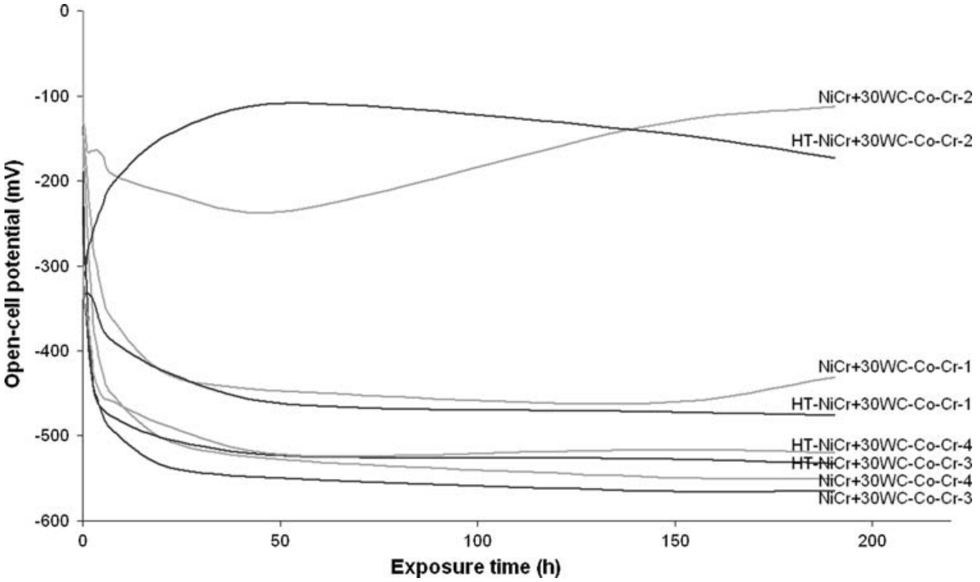

Fig. 6 Open-cell potentials of as-sprayed NiCr + 30WC-Co-Cr-1, NiCr + 30WC-Co-Cr-2, NiCr + 30WC-Co-Cr-3 and NiCr + 30WC-Co-Cr-4 coatings and heat-treated HT-NiCr + 30WC-Co-Cr-1, HT-NiCr + 30WC-Co-Cr-2, HT-NiCr + 30WC-Co-Cr-3, and HT-NiCr + 30WC-Co-Cr-4 coatings as a function of exposure time in 3.5% NaCl solution. Ag/AgCl reference electrode

Table 3 Amount of corrosion spots on the coating surface after salt spray test

	Amount of corrosion spots, %	
Coating	**As-sprayed**	**Heat-treated**
Ni-1	67.9	23.8
Ni-2	0.8	0.1
NiCu-1	54.2	11.9
NiCu-2	34.7	11.3
NiCr-1	98.5	98.9
NiCr + 50Al_2O_3-1	14.1	7.5
NiCr + 50Al_2O_3-2	12.7	8.5
NiCr + 30WC-Co-Cr-1	30.7	49.2
NiCr + 30WC-Co-Cr-2	24.7	30.0
NiCr + 30WC-Co-Cr-3	93.9	91.3
NiCr + 30WC-Co-Cr-4	67.1	97.7

observed. However, the influence of spraying parameters came clearly up with these NiCr + 30WC-Co-Cr coatings. Coatings sprayed with lower preheating temperatures (500 and 600 °C) and higher traverse speed (40 m/min versus 20 m/min) together with lower beam distance (0.75 mm versus 1.5 mm) contained more through-porosity inside the structure.

Salt spray tests showed corresponding results with the open-cell potential measurements. Table 3 shows the amount of corrosion spots analyzed by image analysis from the coating surfaces after the salt spray test. Two trends were seen in the results; (1) the heat treatment decreased the amount of corrosion spots with all coatings except NiCr + 30WC-Co-Cr coatings, and (2) the amount

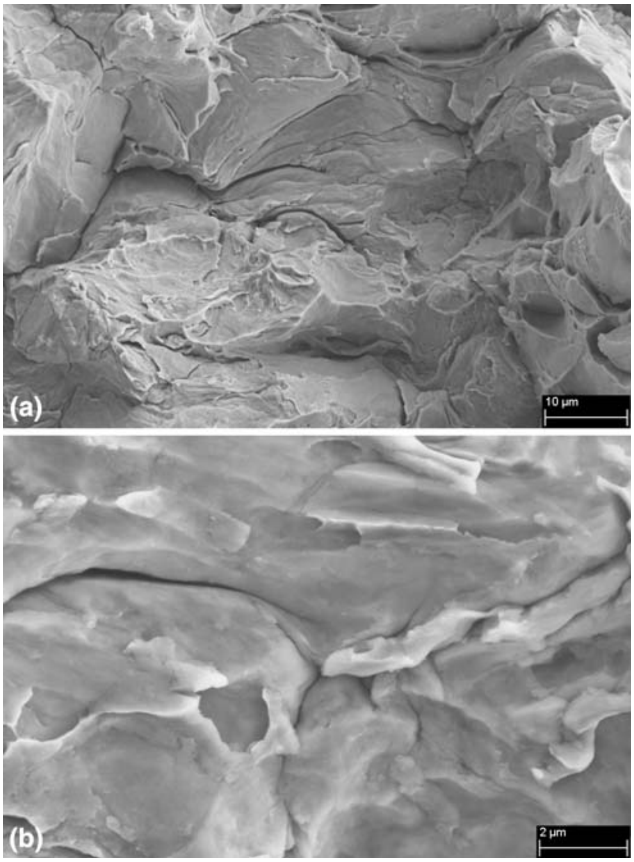

Fig. 7 Fracture surfaces of as-sprayed Ni-2 coating (a) general view and (b) crossing point of three Ni particles. FESEM images

of corrosion spots decreased with lower traverse speed and higher beam distance.

3.2 Fracture Surfaces

Fracture surface analysis was found to be a relevant method of evaluating microstructural details of the coatings. First, fracture surfaces were showed brittle and ductile fracturing behavior. Second, microscopic features, e.g., particle deformation, voids in the structure, material jets, particle bonds, and even interparticle structures were observed. As is shown in our previous studies (Ref 14, 22), existing through-porosity in the CS coatings is caused by the weak bonds between particles due to the undeformed or less deformed particles. This was seen also with the fracture surface of Ni-1 coating from which less deformed particles (spherical particles) were observed. The denseness of the CS Ni coating was improved by changing spraying parameters. With lower traverse speed and higher beam distance, coating structure became denser; see Ni-2 coating (Fig. 3 and Table 3). In addition, the higher level of plastic deformation was observed in the fracture surface (Fig. 7). Furthermore, Fig. 7(b) shows tight bonding between three Ni particles.

The fracture surface of heat-treated Ni-2 coating is presented in Fig. 8. The coating became stiffer after the heat treatment, indicating recrystallization occurred during annealing. The fracture surface of heat-treated coating was mostly ductile type whereas as-sprayed coating was partly brittle and partly ductile ruptured. The grain structure is perceived from Fig. 8(b). Figure 9 shows the fracture surfaces of NiCu-2 coatings both in the as-sprayed and heat-treated state. The strong deformation is observed in the NiCu-2 coating in Fig. 9(a). Additionally, more ductile fracture behavior (due to recrystallization) in the heat-treated state is seen in both NiCu coatings (NiCu-2 in Fig. 9b).

NiCr coatings contained porosity in their structure according to the corrosion tests. In addition to these, the fracture surfaces (Fig. 10) revealed that the deformation level was not as high as it should be (particles were not flattened enough), indicating weak bonds between particles and even pores in the particle boundaries. Heat-treated NiCr coating had similar fracture behavior with as-sprayed coating. Therefore, it can be said that heat treatment did not densify the structure due to the high amount of porosity in the boundaries. Heat-treated structure was slightly ductile, however, not as much as other coatings in this study.

The fracture surfaces of NiCr + 50Al_2O_3-2 coating in the as-sprayed state are presented in Fig. 11. Bonding between metallic and ceramic particles is received from

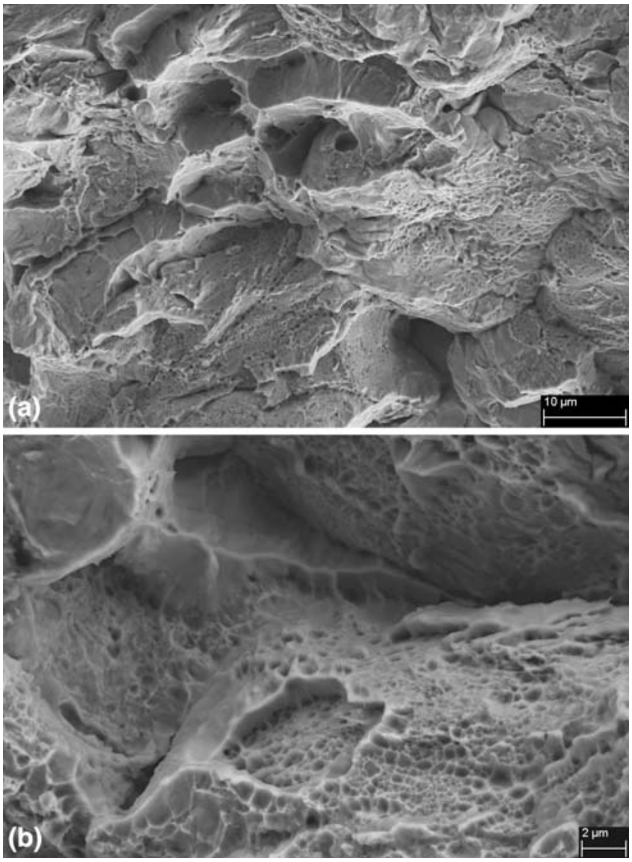

Fig. 8 Fracture surfaces of heat-treated Ni-2 coating (a) general view and (b) ductile fracture. FESEM images

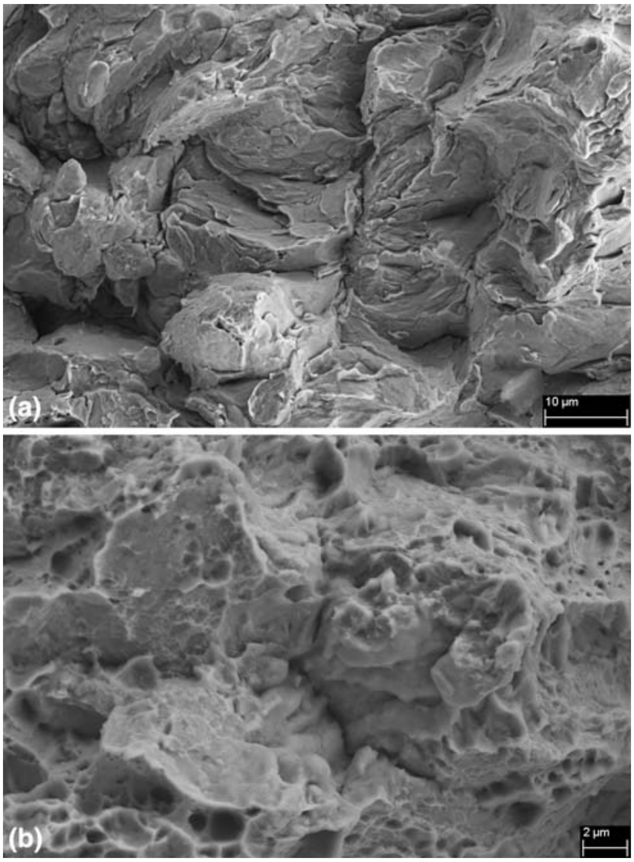

Fig. 9 Fracture surfaces of (a) as-sprayed NiCu-2 and (b) heat-treated NiCu-2 coatings. FESEM images

fracture surfaces and seemed to be tight. Arrows shows the interfaces between NiCr and Al_2O_3 particles. In addition, from Fig. 11(b), the hammering effect of the hard particles can be seen by the high level of deformation and the material jets formation of NiCr particle (NiCr particle below Al_2O_3 particle). Hard particles hammer or tamp the previous particles, densifying the entire coating structure.

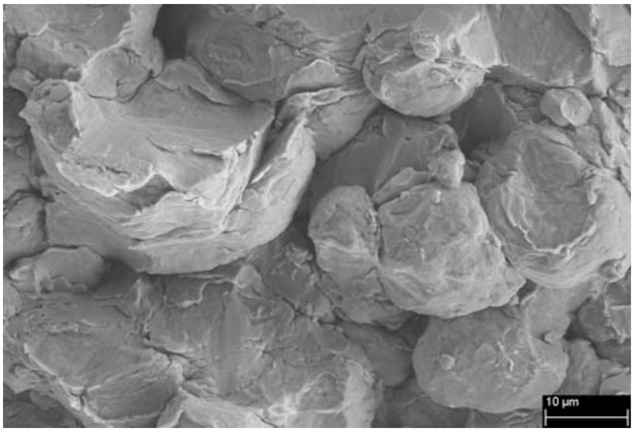

Fig. 10 Fracture surfaces of as-sprayed NiCr-1 coating. FESEM image

Another solution to improve the denseness of NiCr coatings was to add hardmetal, WC-Co-Cr, particles into the NiCr powder. The fracture surfaces showed that the hardmetal particles broke down on the impacts. Therefore, WC-Co-Cr particles were scattered inside the structure. Figure 12 shows the fracture surfaces of NiCr + 30WC-Co-Cr-2 coatings (as-sprayed). Also here, the hammering (tamping) effect of hard particles can be seen in the closed view (Fig. 12b). After heat treatment, the fracture plane became more ductile also in this case.

3.3 Microstructures

Cold-sprayed coatings are typically dense and porosity-free according to the microscopic observations. However, the corrosion tests appeared existing through-porosity in the CS Ni and Ni-30Cu coatings (Ref 22). In this study, the denseness improvement was done by optimizing powders and spraying parameters and in addition to these, with the heat treatments. The as-sprayed microstructure of Ni-2

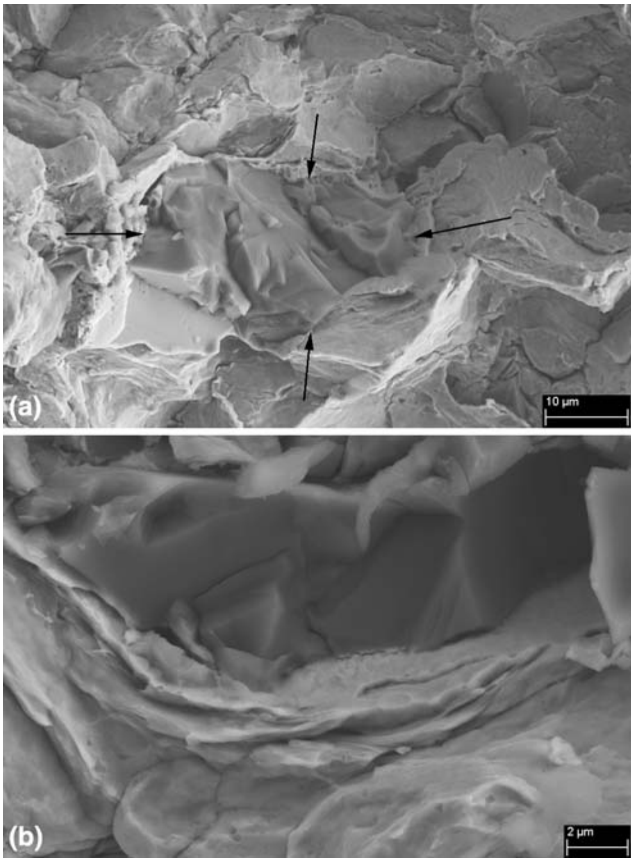

Fig. 11 Fracture surfaces of as-sprayed NiCr + $50Al_2O_3$-2 coatings (a) general view; arrows indicate interfaces between NiCr and Al_2O_3 particles (Al_2O_3 particle is inside the area) and (b) bonding between Al_2O_3 and NiCr particles. FESEM images

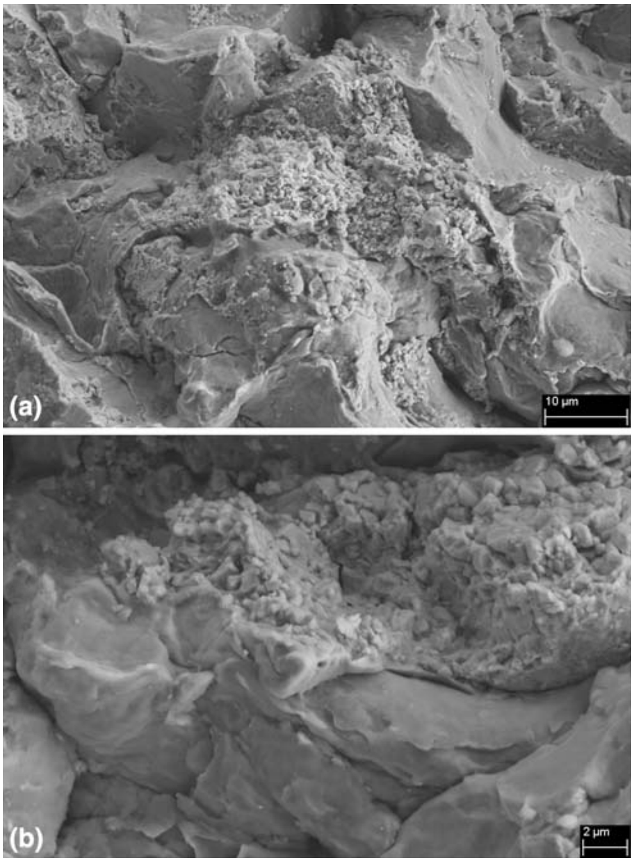

Fig. 12 Fracture surfaces of as-sprayed NiCr + 30WC-Co-Cr-2 coatings (a) general view, (b) bonding between WC-Co-Cr and NiCr particles. FESEM images

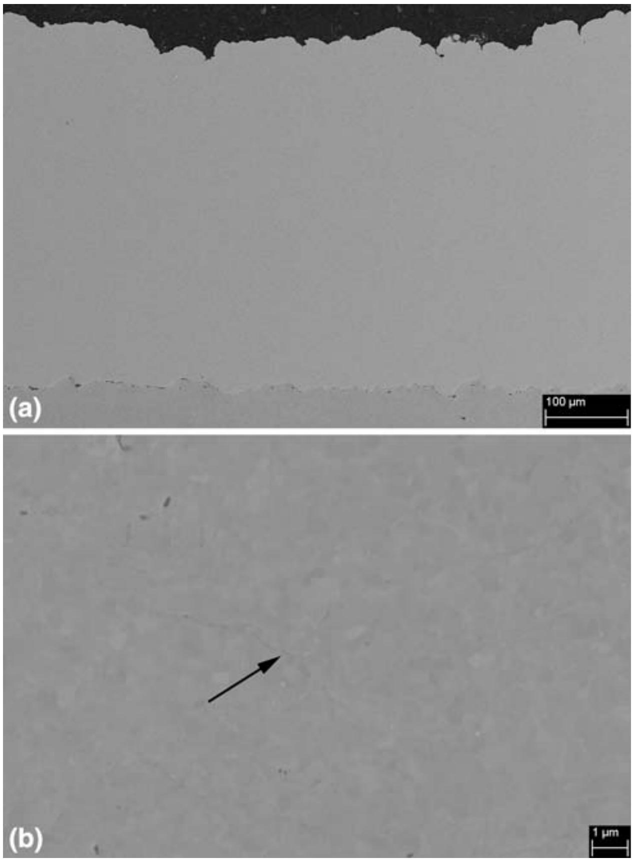

Fig. 13 Cold-sprayed Ni-2 coating in as-sprayed state (a) cross section and (b) microstructure, arrow shows crossing point of three Ni particles. FESEM images

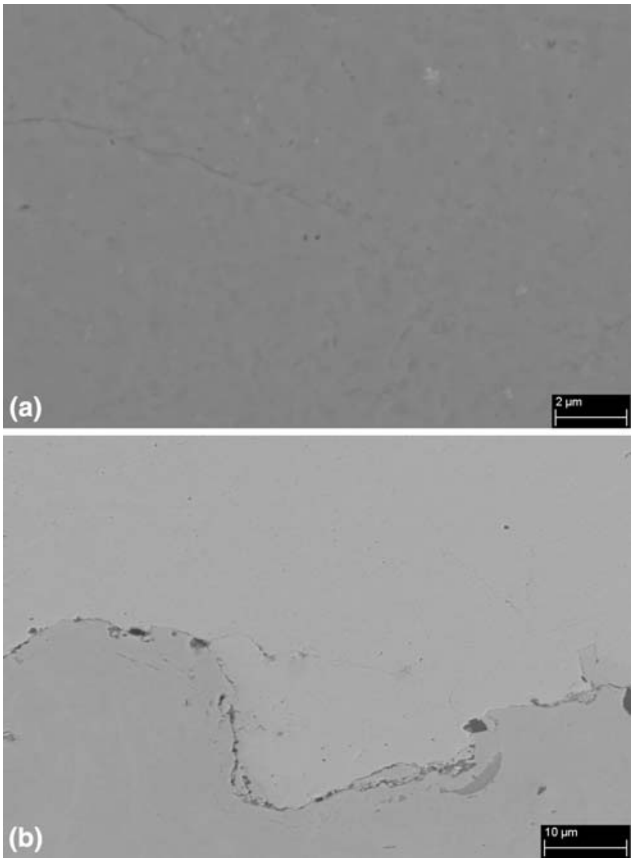

Fig. 14 Cold-sprayed NiCu-2 coating (a) as-sprayed microstructure, oxidized boundaries and (b) heat-treated structure and interface between coating and substrate. FESEM images

coating is presented in Fig. 13. The Ni-2 coating had better structural properties, i.e., denser structure than the Ni-1 coating had. The tight bond between Ni particles in the highly dense coating (Ni-2) is shown by an arrow in Fig. 13(b). The effect of heat treatment was clearly seen in the fracture surfaces, but microstructure did not reveal any more information. The cross section of heat-treated Ni-2 coating was appeared similar with the cross section of as-sprayed coating with very dense structure and without voids or pores.

The cross section of the NiCu-2 coating is presented in Fig. 14. The NiCu-2 coating seemed to be highly dense, defect-free, and faultless. However, slightly oxidized boundaries are still detected in the cross-sectional structures both in the as-sprayed and heat-treated state (Fig. 14a and b, respectively). According to the corrosion tests, NiCu coatings became denser, but still structures contained some weak points which can be explained with these oxidized particle boundaries.

The fracture surfaces of the as-sprayed and heat-treated NiCr-1 coatings already revealed undeformed particles with weak bonding. Additionally, microstructures of these coatings showed that coatings included porosity (Fig. 15a) and open or weak particle boundaries (Fig. 15b) in their structures in the as-sprayed state.

Figure 16 shows microstructure of NiCr + 50Al_2O_3-2 coating in the as-sprayed (Fig. 16a and b) and heat-treated state (Fig. 16c). Porosity inside the coating structure was significantly lower in the NiCr + Al_2O_3 coatings compared with NiCr coating. The amount of Al_2O_3 particles was 5% according to image analysis (ImageJ). The tight bonding between NiCr and Al_2O_3 particle is perceived in Fig. 16(b). Moreover, some oxidized boundaries are observed in the heat-treated structure (Fig. 16c). However, the amount of oxidized areas was much lower in the metallic-ceramic mixture coating compared with pure metallic coating due to the higher level of plastic deformation occurred on the impacts.

Figure 17 presents the microstructure of NiCr-30WC-Co-Cr-2 coating in the as-sprayed and heat-treated state. The amount of WC-Co-Cr particles was 18% according to image analysis (ImageJ). The structure of NiCr mixture coating included more WC-Co-Cr particles compared with Al_2O_3 particles. Hardmetal particles were not as dense as Al_2O_3 particles in the as-received state, and they deformed and broke down during impacts and thus, more embedded in the metallic structure. The addition of the ceramic particles to the powder-gas flow (Ref 9) or to metallic powder (Ref 14) has reportedly increased the deposition efficiency of the metallic coating due to the

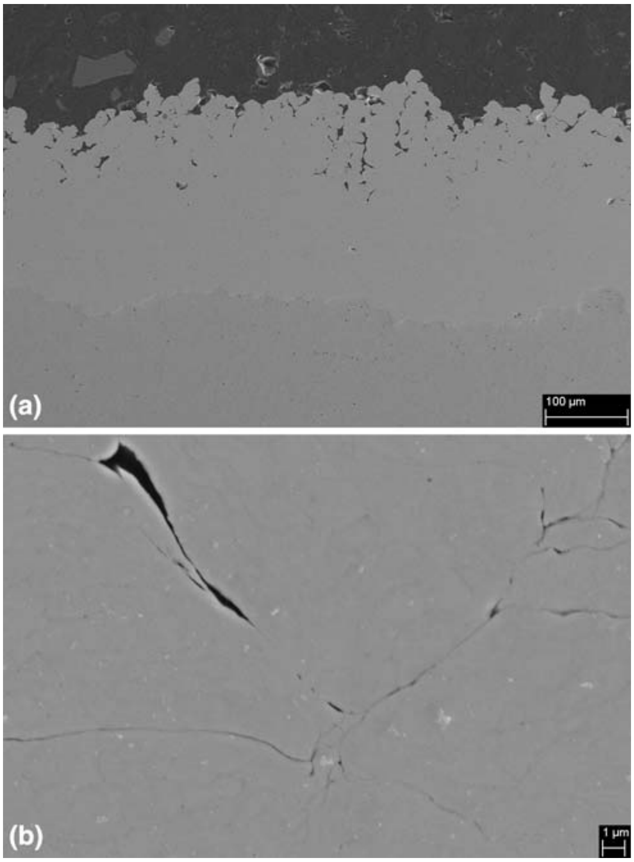

Fig. 15 Cold-sprayed NiCr-1 coating in as-sprayed state (a) cross section and (b) open particle boundaries. FESEM images

activation mechanism of hard particles. The increment of coating thickness compared NiCr coating with NiCr + $50Al_2O_3$ and NiCr + 30WC-Co-Cr coatings were noticeable also in this study, compare coating thicknesses of NiCr (Fig. 15a), NiCr + Al_2O_3 (Fig. 16a), and NiCr + WC-Co-Cr (Fig. 17a) coatings: 250 µm, 331 µm, and 386 µm, respectively.

3.4 Hardness

Vickers hardness was measured in order to characterize the mechanical behavior and hardening of the coatings. In addition, the effect of heat treatments on the properties was performed. Table 4 summarizes the Vickers hardness of the coatings in the as-sprayed and heat-treated state. The hardness measurements of the NiCr + $50Al_2O_3$ and NiCr + 30WC-Co-Cr coatings were done in the metallic areas of the coatings in order to analyze the behavior of metallic particles and hence, the effect of hard particles addition on the metallic area of the coating. Hardness of the Ni and NiCu coatings was significantly decreased after heat treatment due to the fact that coatings were softer state by recovery and recrystallization. However, the hardness of NiCr, NiCr + $50Al_2O_3$, and NiCr + 30WC-Co-Cr coatings were at the same level compared with the as-sprayed and heat-treated each others. This is possibly caused by the oxygen content of the coatings as weak points in the particle boundaries. The effect of oxidized areas was probably higher than recovery and thus, hardness was not decreased after heat treatments. Moreover, the hardness of NiCr with added hard particles was higher than pure NiCr (measurements were done from the metallic part of the coating), reflecting the hardening by hammering effect of hard particles.

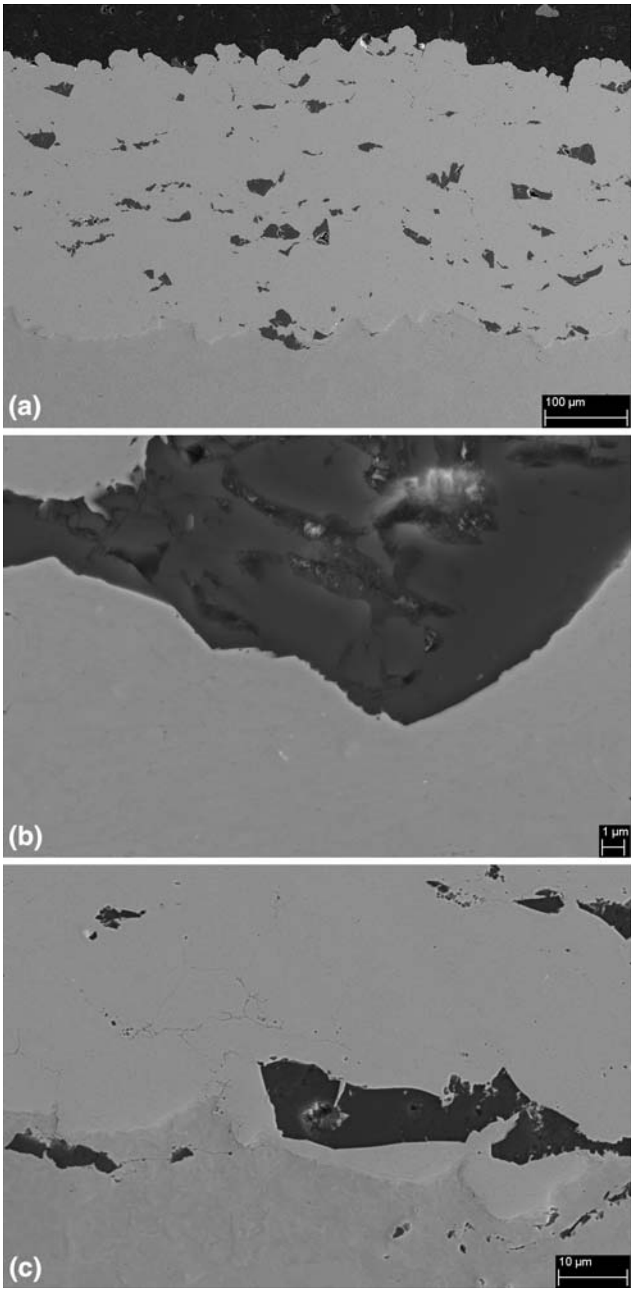

Fig. 16 Cold-sprayed NiCr + $50Al_2O_3$-2 coating (a) as-sprayed cross-sectional structure, (b) bonding between NiCr and Al_2O_3 particles (as-sprayed), and (c) heat-treated structure. FESEM images

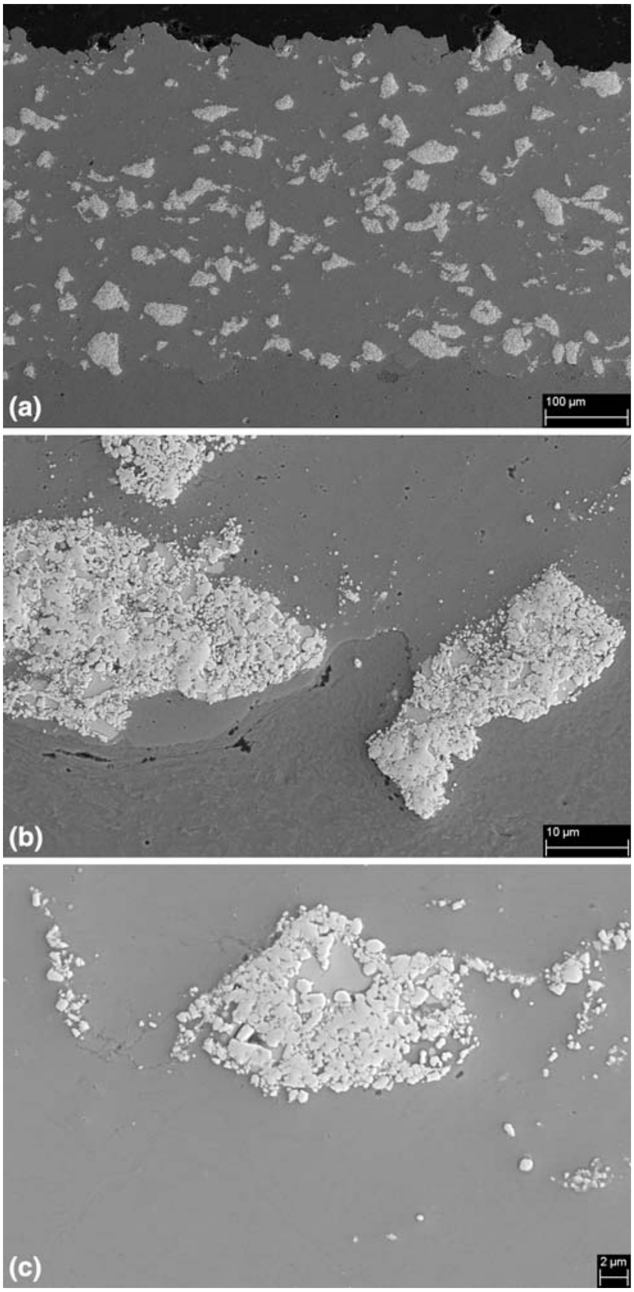

Fig. 17 Cold-sprayed NiCr + 30WC-Cr-Co-2 coating (a) as-sprayed cross-sectional structure, (b) interface between as-sprayed coating and grit-blasted steel substrate, and (c) heat-treated structure. FESEM images

As a summary of the hardness measurements, the hardness of the CS coatings was high due to the work hardening. The hardness was slightly higher in the coatings which were sprayed using lower traverse speed and higher beam distance, indicating high hardening and deformation occurrence. The hard particle addition increased the hardness of the metallic areas of the NiCr + Al_2O_3 and NiCr + WC-Co-Cr coatings. The effect was stronger with Al_2O_3 particles.

Table 4 Vickers hardness ($HV_{0.3}$) of cold-sprayed Ni, NiCu, NiCr, NiCr + 50Al_2O_3, and NiCr + 30WC-Co-Cr coatings in as-sprayed and heat-treated state

	Hardness, $HV_{0.3}$ (SD)	
Coating	As-sprayed	Heat-treated
Ni-1	233 (7.7)	105 (2.8)
Ni-2	238 (5.7)	124 (2.1)
NiCu-1	251 (19.5)	164 (7.5)
NiCu-2	266 (11.3)	185 (14.0)
NiCr-1	247 (31.5)	308 (38.3)
NiCr + 50Al_2O_3-1	375 (42.1)	371 (24.5)
NiCr + 50Al_2O_3-2	398 (46.8)	372 (41.4)
NiCr + 30WC-Co-Cr-1	340 (24.9)	357 (30.6)
NiCr + 30WC-Co-Cr-2	388 (39.7)	387 (40.1)
NiCr + 30WC-Co-Cr-3	337 (29.8)	325 (35.6)
NiCr + 30WC-Co-Cr-4	349 (33.3)	328 (28.9)

4. Discussion

This study shows affecting factors for the denseness of several CS coatings. Coating materials were chosen for their corrosion resistance behavior. Nickel and nickel alloys are known as corrosion resistant materials (Ref 23). However, the corrosion protection of these coatings is based on impermeability and thus, denseness plays very the important role in the corrosion resistance.

4.1 CS Ni Coatings

The denseness of Ni coating was improved significantly due to the optimized powder characteristics together with optimal spraying parameters. Furthermore, the structural details and denseness was affected by heat treatments. Ajdelsztajn et al. (Ref 24) have reported CS nanostructured Ni coating with dense structure according to microscopic analysis. Moreover, in the present study, the highly dense structure of CS Ni coatings was observed with microscopic characterization and in addition, with the corrosion tests. Ni-2 coating had impermeable microstructure without through-porosity in its structure.

The open-cell potential measurements and salt spray tests revealed the impermeability of Ni (Ni-2) coating sprayed with the high-pressure cold spray system. Additionally, the Ni powder was optimized by manufacturer for cold spraying. Furthermore, heat treatments improved the denseness of Ni coatings. The open-cell potential behavior of Ni-2 and HT-Ni-2 coatings was similar with Ni bulk material (Fig. 3), indicating fairly dense coating structure. Moreover, the salt spray test revealed differences in the corrosion behavior of Ni coatings (Table 3). The Ni-2 and HT-Ni-2 coatings contained the rather low amount of corrosion spots on the surface after the salt spray test, 0.8 and 0.1%, respectively. Furthermore, heat treatment decreased the amount of corrosion spots (67.9% Ni-1 and 23.8% HT-Ni-1) in the Ni-1 coatings also, reflecting the densifying effect of heat treatment. The most important affecting factor in the case of CS Ni coatings was optimized spraying parameters. It was observed that the lower traverse speed of the spraying nozzle together with higher beam distance produced the higher denseness of the coatings. Dense structure requires the high level of plastic deformation and hence, tight bonds between particles. Typically, existing weak points in the CS coatings were concentrated on the weak particle boundaries due to the undeformed particles. In addition, oxide layers were not removed and thus, caused weak bonds between particles.

Particularly, Ni particles were more deformed in the denser coating structure (Fig. 7). The high plastic deformation was observed in the flattened shape of particles. Moreover, tight bonding between three Ni particles (the crossing point of these three particles) was seen in Fig. 7(b) and dense microstructure in Fig. 13(b). The cross section of Ni-2 coating showed defect-free structures and faultless interfaces between coating and substrate. The dense structure of CS coatings depended strongly on the deformation of the particles and hence, the metallic bonds of metallic powder particles (Ref 17, 25). In addition to the spraying parameter optimization, the denseness improvement effect of heat treatments was observed with both Ni coatings (Ni-1 and Ni-2). Heat treatment increased the denseness of Ni-1 coating but did not eliminate all porosity. In addition to the results of corrosion tests and microscopic evaluation, the influence of heat treatment was detected in the hardness measurements. Hardness decreased after heat treatment due to the fact that structure became softer and more ductile (noticed also on the fracture surfaces). Ductile fracturing was dominant in the heat-treated Ni-2 coating (compare Fig. 7 and 8, as-sprayed and heat-treated fracture surfaces). During heat treatment, recrystallization occurred which was seen as decreased hardness values due to the softening.

4.2 CS NiCu Coatings

The denseness improvement was noticeable also in the case of NiCu coatings. Reportedly, particle velocity has strong influence on the coating formation and level of plastic deformation (Ref 4). This was also noticed in this study. Finer particle size (−30 + 10 versus −38 + 16 μm) together with higher process temperature (and advanced spraying system) was found to be better with NiCu powder according to comparison of the results between this present study and our previous study (Ref 22). The highest effect of heat treatment on the denseness improvement was observed with NiCu coatings according to the salt spray test. The amount of corrosion spots was reduced from 54.2% (NiCu-1) to 11.9% (HT-NiCu-1) and 34.7% (NiCu-2) to 11.3% (HT-NiCu-2) after heat treatment. Heat-treated structure was recrystallized and more ductile. The high level of plastic deformation occurred during spraying in the case of NiCu particles. The dense structure formation needs plastic deformation due to the localized shearing (Ref 26). This was seen mostly in NiCu-2 coating (Fig. 9a). Localized shearing is due the hardening by plastic deformation and/or due to the thermal softening caused by heating (Ref 26). However, the structure should be even more ductile in order to be fully dense. For NiCu coating, heat treatment made structure significantly stiffer which was observed on the fracture surfaces (Fig. 9b). In addition, recrystallization was noticed from hardness values by decreased values in comparison with hardness of the as-sprayed and heat-treated coating. This was due to the recrystallization and softening. Additionally, the structures became denser according to the corrosion tests. During recrystallization, the work-hardened structure (with the high amount of dislocations) starts to change positions and new grain structure forms (Ref 26). The same effect as with Ni coatings was observed with these NiCu coatings also.

As well as Ni particles, NiCu particles underwent the high level of deformation due to the thermal softening and adiabatic shear instability (Ref 25). Metal-metal contact under high pressure is the requirement for localized adiabatic shearing and thus, tight bond formation between metallic powder particles (Ref 26). However, in the case of NiCu coating slightly oxidized boundaries were still detected in the cross-sectional structures both in the as-sprayed and heat-treated states. This is due to the fact that oxide layers of powder particles were not totally removed on the particle impacts. According to the corrosion tests, NiCu coatings became denser but still structures contained some weak points which can be explained with these oxidized particle boundaries. As a summary, first, specialized powder characteristics together with optimized spraying parameters led denser coating structure. Second, the densification of NiCu coatings by heat treatment was significant.

4.3 CS NiCr Coatings

It was possible to manufacture NiCr coatings by using cold spraying. However, coatings contained porosity due to the less deformed particles and thus, weak bonds between particles. The highest process temperature (700 °C) was not possible to use due to the fact that NiCr particles clogged the nozzle. For that reason, particles were not underwent as high deformation level as is needed for generating tight bonds between particles and revealing metal-metal bonding between particles. The open particle boundaries together with oxidized boundaries were perceived in the cross sections of NiCr coating as structural defects (Fig. 15). The corrosion tests showed existing through-porosity in the NiCr coating structure (Fig. 5 and Table 3). After the salt spray test, the surface of NiCr coating was strongly corroded with 98.5% amount of corrosion spots. Heat treatment did not have much influence on microstructural details and not improved the denseness of the coating. The NiCr coating contained over-amount defects in its structure and thus, heat treatment was not capable of densify structure enough. However, partly ductile fractures were found in the fracture surface of heat-treated NiCr coating. Weak bonds between particles due to the too low amount of deformation can cause porosity between particle boundaries (Ref 24). In addition to this, the porous layer on the top of the coating is influenced by the fact that the densifying (or tamping) effect of next particles is missing (Ref 20, 24). One solution to densify the CS NiCr coatings is to add hard particles into the metallic NiCr powder. As it is found out the functions of the hard particles are (1) keep the nozzle clean, (2) activate the sprayed surface, and (3) densify the structure. In this study, we showed the denseness improvement effect of hard, Al_2O_3 and WC-Co-Cr, particles.

4.4 CS NiCr + 50Al_2O_3 Coatings

Typically, a ceramic addition mixed with metallic powder is used in low-pressure cold spraying. Powder mixtures, e.g., Cu + Al_2O_3, Ni + Al_2O_3, Zn + Al_2O_3, and Al + Zn + Al_2O_3 are commercially available (Ref 27). In addition, metal-ceramic composite (e.g., Al-Al_2O_3) coatings have sprayed successfully (Ref 28). Furthermore, we have demonstrated the capability to improve the denseness of high-pressure CS NiCr coating by adding the hard ceramic particles into the metallic NiCr powder. Furthermore, coating thicknesses increased with the hard particle addition, indicating higher deposition efficiency. Powder characteristics are one of the important factors in the cold spraying. Optimal powder properties (e.g., particle size, particle size distribution, and morphology) depend on coating material. According to previous study (Ref 14) added Al_2O_3 particles affected significantly on the microstructural properties of CS NiCr + Al_2O_3 coatings. The best characteristics of Al_2O_3 particles were achieved to be the coarsest particle size ($-90+45$ versus $-45+22$ and $-22+5$ μm) and the highest composition (50 vol.% versus 30 vol.%). Therefore, the particle size of $-90+45$ μm and amount of 50 vol.% were chosen. Moreover, coarser NiCr ($-30+10$ versus $-22.5+10$ μm) particles were used in this study compared with previous study (Ref 14). Moreover, NiCr + Al_2O_3 coatings were heat-treated in order to analyze the effect of annealing.

The corrosion tests demonstrated the densification of NiCr coatings with added Al_2O_3 particles, comparing the results of NiCr and NiCr + Al_2O_3 coatings in both corrosion tests (Fig. 5 and Table 3). The denseness improvement was significant (the amount of corrosion spots on the surfaces of NiCr and NiCr + Al_2O_3 98.5% and 14.1%, respectively). The effect of spraying parameters on the coating formation is material-dependent. In this study, the traverse speed and beam distance combination had the minor effect on the coating formation in the case of NiCr + Al_2O_3 coating. On the other hand, the hard particle addition had the major effect on the coating formation and denseness improvement due to the cleaning, activating, and densifying effects of hard particles. The hammering effect had appeared from the fracture surface (Fig. 11b); indicating the high plastic deformation of NiCr particle due to the localized shear instability and material jets formation. Ceramic particles are more brittle than metallic particles and thus, fracture instead of deform. Fracturing of ceramic particles might be necessary for the coating formation (Ref 10). Fracturing of hard particles was reported (Ref 11). On the other hand, some ceramic particles were embedded in the structure. Furthermore, the oxide layers of metallic particles should also be fractured and removed, revealing metallic surfaces of the particles for metal-metal bonding. Added hard particles help to destroy the oxide layers from metal surfaces by activating, hammering, and tamping the sprayed surfaces. Bonding between metallic and ceramic particles was observed in Fig. 11(b) and 16(b). Sticking between these different material-type particles had occurred by mechanical interlocking due to the embedding of the hard ceramic particles into the softer metallic matrix.

Additionally, heat treatment had influence on the denseness by improving it. Denser coating structures were achieved after heat treatment (see Fig. 5 and Table 3). The amount of corrosion spots was decreased from 14.1% and 12.7% to 7.5% and 8.5% after the salt spray test. However, the effect of heat treatment on microstructure was not significant (Fig. 16) whereas the fracture surface analysis showed slightly more ductile fractures in the heat-treated coating than in the as-sprayed state (Fig. 11a). In addition, the hardness of the metallic part of the coatings were at the same level in both as-sprayed and heat-treated states. With these coatings, recovery occurred during heat treatment which was seen in the slight denseness improvement. However, recrystallization would need higher annealing temperature or longer annealing time. The most important result was denseness improvement of NiCr coating by using hard particles in order to reinforce the structure due to the high level of localized deformation, material jets and adiabatic shear instability.

4.5 CS NiCr + 30WC-Co-Cr Coatings

Hardmetal particles were added into the NiCr powder in order to improve the denseness and corrosion properties compared with the pure NiCr coating. WC-Co-Cr was chosen because of its better corrosion resistance than WC-Co (Ref 29). WC-Co-Cr particles acted like Al_2O_3 particle with three ways: (1) activate the sprayed surface, (2) reinforce the coating structure, and (3) keep the nozzle clean (Ref 14). Coating forms on the solid-state impacts (Ref 2) and no melting of WC-Co particles during impacts were observed (Ref 12). Hard particle addition makes possible to use higher gas temperature, which affects particle velocity by increasing it (Ref 10). On the other hand, higher particle velocity leads stronger deformation and thus, denser coating structure. The effect of preheating temperature of gas on the denseness of NiCr + WC-Co-Cr coatings was significant according to the corrosion tests (Fig. 6 and Table 3). The highest temperature (700 °C) led the lowest porosity into the coatings. The reason for that was the higher velocity causes higher deformation and thus, denser structure. In addition, void reduction occurs with high deformation (Ref 10). In addition to the process temperature, open-cell potential measurements showed that lower traverse speed together with higher beam distance had remarkable effect on the denseness of the coating.

The fracture surface analysis revealed the high level of deformation of NiCr particles whereas hardmetal particles were broken down and fragmented. Therefore, hardmetal particles were placed all over the coating structure (Fig. 12). Lee et al. (Ref 28) were found out the same kind of occurrence were hard particles fragmented during impact. They have used agglomerated Al_2O_3 whereas we used sintered and crushed WC-Co-Cr particles. Heat treatment had only minor effect in the case of NiCr + WC-Co-Cr coating. After heat treatment, the fracture surface of the coating was slightly more ductile. In addition, the hardness of the as-sprayed and heat-treated NiCr + WC-Co-Cr coatings were similar, reflecting only the minor effect of heat treatment. Only the lower traverse speed and higher beam distance combination caused higher hardness, indicating the higher level of work hardening and plastic deformation.

Microstructures of NiCr + 30WC-Co-Cr coatings were dense without noticeable pores or other defects (Fig. 17). Moreover, the structure of NiCr + 30WC-Co-Cr coating contained more added hard particles than NiCr + Al_2O_3 coating in proportion to initial powder compositions. WC-Co-Cr particles were more deformed, fell to parts, and stuck to the previous particles and thus, more entered into the structure. Summing up, the metallic structure of NiCr coating can be densified with hardmetal particles. However, spraying parameters had strong influence on the coating formation. High process temperature with lower traverse speed together with higher beam distance was needed in order to produce highly dense coating structure.

5. Conclusions

Cold spraying is proven to be an optimal thermal spray method in order to prepare fully dense or low-porosity coatings from metallic or metallic-ceramic composite mixture powder feedstock. This study showed that structural details, i.e., microstructure, fracture behavior, and denseness, and hardness depend strongly on powder characteristics, spraying parameters, and post-treatments. In optimal situation, fully dense coating structures are able to manufacture with the optimal combination of powder and spraying parameters. In this study, the Ni (Ni-2) coating had overall dense structure. In the contrast to this, sometimes when the optimal combination was not achieved, then structural details can be improved with post-treatments. In this study, the denseness improvement of NiCu coatings was done with heat treatments. Heat-treated NiCu coatings were the softer state due to the recrystallization and structures became denser according to the corrosion tests. In addition to these, one solution to decrease through-porosity is powder mixing. Hard particle addition into the metallic powder has shown significant denseness improvement. This was clarified with NiCr coatings added hard particles (NiCr + $50Al_2O_3$ and NiCr + 30WC-Co-Cr). Al_2O_3 particles embedded in the structure of NiCr coatings whereas WC-Co-Cr particles broke down and stuck into the structure. Both particle additions made the structure of NiCr coating denser due to the fact that higher gas temperature was able to use and due to the hammering and tamping of the coating structure.

Acknowledgments

The authors thank Mr. Werner Krömmer of Linde AG Gas for spraying the coatings and for his valuable advice. They also thank Mr. Jonne Näkki of KETEK for the salt spray tests. The project was funded by Academy of Finland and Finnish Graduated School of New Materials and Processes.

References

1. T. Schmidt, F. Gärtner, H. Assadi, and H. Kreye, Development of a Generalized Parameter Window for Cold Spray Deposition, *Acta Mater.*, 2006, **54**, p 729-742
2. H. Assadi, F. Gärtner, T. Stoltenhoff, and H. Kreye, Bonding Mechanism in Cold Gas Spraying, *Acta Mater.*, 2003, **51**, p 4379-4394
3. M. Grujicic, C.L. Zhao, W.S. DeRosset, and D. Helfritch, Adiabatic Shear Instability Based Mechanism for Particles/Substrate Bonding in the Cold-Gas Dynamic-Spray Process, *Mater. Des.*, 2004, **25**, p 681-688
4. A. Papyrin, V. Kosarev, S. Klinkov, A. Alkimov, and V. Fomin, *Cold Spray Technology*, 1st ed., Elsevier, the Netherlands, 2007, p 328
5. R. Maev and V. Leshchynsky, Air Gas Dynamic Spraying of Powder Mixtures: Theory and Application, *J. Therm. Spray Tech.*, 2006, **15**(2), p 198-205
6. H. Koivuluoto, J. Näkki, and P. Vuoristo, Corrosion Properties of Cold-Sprayed Tantalum Coatings, *J. Therm. Spray Tech.*, 2009, **18**(1), p 75-82
7. T. Van Steenkiste and D.W. Gorkiewicz, Analysis of Tantalum Coatings Produced by the Kinetic Spray Process, *J. Therm. Spray Tech.*, 2004, **13**(2), p 265-273
8. T.S. Price, P.H. Shipway, D.G. McCartney, E. Calla, and D. Zhang, A Method for Characterizing the Degree of Inter-particle Bond Formation in Cold Sprayed Coatings, *J. Therm. Spray Tech.*, 2007, **16**(4), p 566-570
9. S.V. Klinkov, V.F. Kosarev, A.A. Sova, and I. Smurov, Calculation of Particle Parameters for Cold Spraying of Metal-Ceramic Mixtures, *J. Therm. Spray Tech.*, 2009, **18**(5-6), p 944-956
10. T.H. Van Steenkiste, J.R. Smith, and R.E. Teets, Aluminum Coatings Via Kinetic Spray with Relatively Large Powder Particles, *Surf. Coat. Technol.*, 2002, **154**, p 237-252
11. H.Y. Lee, Y.H. Yu, Y.C. Lee, Y.P. Hong, and K.H. Ko, Cold Spray of SiC and Al_2O_3 with Soft Metal Incorporation: A Technical Contribution, *J. Therm. Spray Tech.*, 2004, **13**(2), p 184-189
12. R.S. Lima, J. Karthikeyan, C.M. Kay, J. Lindemann, and C.C. Berndt, Microstructural Characteristics of Cold-Sprayed Nanostructured WC-Co Coatings, *Thin Solid Films*, 2002, **416**, p 129-135
13. H.-J. Kim, C.-H. Lee, and S.-Y. Hwang, Fabrication of WC-Co Coatings by Cold Spray Deposition, *Surf. Coat. Technol.*, 2005, **191**, p 335-340
14. H. Koivuluoto and P. Vuoristo, Effect of Ceramic Particles on Properties of Cold-Sprayed Ni-20Cr + Al_2O_3 Coatings, *J. Therm. Spray Tech.*, 2009, **18**(4), p 555-562
15. A. Shkodkin, A. Kashirin, O. Klyuev, and T. Buzdygar, The Basic Principles of DYMET Technology, *Thermal Spray 2006: Pushing the Envelope of Materials Performance*, B.R. Marple, M.M. Hyland, Y.C. Lau, R.S. Lima, and J. Voyer, Ed., May 15-18, 2006 (Seattle, Washington, USA), ASM International
16. R. Maev and V. Leshchynsky, *Introduction to Low Pressure Gas Dynamic Spray, Physics & Technology*, Wiley-VCH Verlag GmbH & Co, KGaA, Weinheim, Germany, 2008, p 328
17. M. Grujicic, J.R. Saylor, D.E. Beasley, W.S. DeRosset, and D. Helfritch, Computational Analysis of the Interfacial Bonding Between Feed-Powder Particles and the Substrate in the

Cold-Gas Dynamic-Spray Process, *Appl. Surf. Sci.*, 2003, **219**, p 211-227

18. V.K. Champagne, Ed., *The Cold Spray Materials Deposition Process, Fundamentals and Applications*, Woodhead publishing Limited, Cambridge, England, 2007, p 362
19. T.H. Courtney, *Mechanical Behavior of Materials*, McGrae-Hill Publishing Company, Singapore, 1990, p 710
20. H. Mäkinen (Koivuluoto), J. Lagerbom, and P. Vuoristo, Mechanical Properties and Corrosion Resistance of Cold Sprayed Coatings, *Thermal Spray 2006: Pushing the Envelope of Materials Performance*, B.R. Marple, M.M. Hyland, Y.C. Lau, R.S. Lima, and J. Voyer, Ed., May 15-18, 2006 (Seattle, Washington, USA), ASM International, 6 p
21. H. Mäkinen (Koivuluoto), J. Lagerbom, P. Vuoristo, Adhesion of Cold Sprayed Coatings: Effect of Powder, Substrate, and Heat Treatment, *Thermal Spray 2007: Global Coating Solutions*, B. Marple, M. Hyland, Y.-C. Lau, C.-J. Li, R. Lima, and G. Montavon, Ed., ASM International, May 14-16, 2007 (Beijing, China), p 31-36
22. H. Koivuluoto, J. Lagerbom, and P. Vuoristo, Microstructural Studies of Cold Sprayed Copper, Nickel, and Nickel-30%Copper Coatings, *J. Therm. Spray Tech.*, 2007, **16**(4), p 488-497
23. P. Crook, Corrosion of Nickel and Nickel-Base Alloys, *Corrosion: Materials*, Vol. 13B, *ASM Handbook*, ASM International, 2005, p 228-251
24. L. Ajdelsztajn, B. Jodoin, and J.M. Schoenung, Synthesis and Mechanical Properties of Nanocrystalline Ni Coatings Produced by Cold Gas Dynamic Spraying, *Surf. Coat. Technol.*, 2006, **201**, p 1166-1172
25. T. Stoltenhoff, C. Borchers, F. Gärtner, and H. Kreye, Microstructures and Key Properties of Cold-Sprayed and Thermally Sprayed Copper Coatings, *Surf. Coat. Technol.*, 2006, **200**, p 4947-4960
26. M. Meyers, Plasticity: Adiabatic Shear Localization, *Encyclopedia of Materials: Science and Technology*, p 7093-7103
27. Obninsk Center for Powder Spraying, Website: http://www.amazonit.ru/ocpn/eindex.html
28. H.Y. Lee, S.H. Jung, S.Y. Lee, Y.H. You, and K.H. Ko, Correlation Between Al_2O_3 Particles and Interface of Al-Al_2O_3 Coatings by Cold Spray, *Appl. Surf. Sci.*, 2005, **252**, p 1891-1898
29. L.-M. Berger, P. Ettmayer, P. Vuoristo, T. Mäntylä, and W. Kunert, Microstructure and Properties of WC-10%Co-4%Cr Spray Powders and Coatings: Part 1. Powder Characterization, *J. Therm. Spray Tech.*, 2001, **10**(2), p 311-325

Publication VII

Heli Koivuluoto and Petri Vuoristo

Effect of Powder Type and Composition on Structure and Mechanical Properties of $Cu+Al_2O_3$ Coatings Prepared by Using Low-Pressure Cold Spray Process

Journal of Thermal Spray Technology, DOI: 10.1007/s11666-010-9491-2, in press

Reprinted from Journal of Thermal Spray Technology with permission of ASM International.
Copyright (2010) ASM International.

JTTEE5
DOI: 10.1007/s11666-010-9491-2
1059-9630/$19.00 © ASM International

Effect of Powder Type and Composition on Structure and Mechanical Properties of Cu + Al_2O_3 Coatings Prepared by using Low-Pressure Cold Spray Process

Heli Koivuluoto and Petri Vuoristo

(Submitted December 28, 2009; in revised form February 4, 2010)

Powder type and composition have a very important role in the production of metallic and metallic-ceramic coatings by using the low-pressure cold spray process. Furthermore, structure and mechanical properties of Cu and Cu + Al_2O_3 coatings are strongly influenced by powder characteristics of Cu particles. The aim of this study was to evaluate the effect of different particle types of Cu powder and different compositions of added Al_2O_3 particles on the microstructure, fracture behavior, denseness, and mechanical properties, i.e., hardness and bond strength. Spherical and dendritic Cu particles were tested together with 0, 10, 30, and 50 vol.% Al_2O_3 additions. Coating denseness and particle deformation level increased with the hard particle addition. Furthermore, hardness and bond strength increased with increasing Al_2O_3 fractions. In the comparison between different powder types, spherical Cu particles led to the denser and less oxide-contenting coating structure due to the highly deformed particles.

Keywords Cu, Cu + Al_2O_3, low-pressure cold spraying, mechanical properties, structure

1. Introduction

Cold spraying is based on the utilization of significantly low process temperatures with high particle velocities. A coating is formed when powder particles impact at high velocities (above the material-dependent critical velocity) with high kinetic energy on the sprayed surface, deform and adhere to the substrate or to other particles (Ref 1, 2). Successful bonding between particles requires a high level of plastic deformation, adiabatic shear instabilities, and even more, material jets formation on the impacts (Ref 2-6). Typically, in the cold spray process, a gas is accelerated to supersonic velocity by a converging-diverging type nozzle (Ref 7). Cold spraying can be divided into two different processes: high-pressure (HPCS) and low-pressure cold spraying (LPCS). In LPCS, firstly, gas and powder are mixed in the diverging part of the nozzle from where particles are accelerated to the high-velocity particle-gas flow. Then after the exit of the nozzle, this particle-gas jet flows and impacts on the sprayed surface. The main differences between these two cold spray processes are the pressure level, 10 versus 40 bar, and type of powder injection, radial versus axial (Ref 8).

In LPCS, the preheating temperatures of the process gas are between room temperature and 650 °C, and pressures between 5 and 10 bar. Typically, in the low-pressure cold spray process, compressed air is used as the process gas to spray powder mixtures (Ref 9). Furthermore, particle velocities are reported to be in the range of 350-700 m/s in this spray process (Ref 10). Irissou et al. (Ref 11) have reported particle velocities for Al_2O_3 particles (mean size 25.5 μm) 580 m/s. In addition, Ning et al. (Ref 12) have presented mean particle velocities for Cu particles (30 μm) 450 m/s (sprayed with helium). Furthermore, irregular particles have reportedly higher in-flight velocities compared with spherical particles with the same particle sizes (Ref 12) due to the higher drag forces (Ref 13).

The LPCS is a relevant method to manufacture metallic coatings (e.g., Cu, Al, Ni, Zn, and Sn) with an addition of ceramic particles in the blended spray powder. There are three purposes for the use of hard ceramic particles in the powder mixtures. First, hard particles keep the nozzle clean and further, eliminate the nozzle clogging. Second, hard particles activate the sprayed surface by removing impurities, contamination, and oxide layers from the surface and additionally, roughening the surface. Third, hard particles reinforce the coating structure (Ref 14). Ceramic particles affect by the mechanical hammering of the substrate/sprayed layers or by the so-called shot peening via particle impacts (Ref 15). Furthermore, Shkodkin et al. (Ref 14) have reported increased bond strength and coating density with the increasing ceramic addition. Reportedly, the amount of ceramic particles in the sprayed coating structure is low in comparison with the initial powder composition. A hard

---

Heli Koivuluoto and **Petri Vuoristo**, Department of Materials Science, Tampere University of Technology, Tampere, Finland. Contact e-mail: heli.koivuluoto@tut.fi.

Published online: 18 March 2010

phase can be used to the purpose of reinforcement to strengthen the metallic matrix in LPCS process (Ref 16).

LPCS coatings similar with the HPCS coatings have highly deformed structure due to the high-velocity particle impacts. Plastic deformation level by the flattening of the sprayed metallic particles upon impacts is the relevant indicator to the quality of the coatings. Furthermore, the denseness and impermeability of the cold-sprayed coatings depend on the amount of deformation. High deformation levels lead to high denseness (Ref 5). Our previous study (Ref 17) showed microstructural details and existing through-porosity in the structure of LPCS $Cu + Al_2O_3$ coating. Additionally, powder characteristics are found to have the very crucial influence on coating formation and hence, coating properties in cold spraying (Ref 18, 19). Furthermore, suitable powders for cold spraying have specific particle size with narrow particle size distribution, depending on powder materials (Ref 18).

The aim of this study was to characterize Cu and $Cu + Al_2O_3$ coatings produced by using LPCS. Powder characteristics have a very important role in the coating and structure formation and thus, this study focuses on the characterization of LPCS Cu coatings sprayed from various feedstock material compositions. Furthermore, the effect of powder type (Cu) and composition ($Cu + Al_2O_3$) on structural details, e.g., microstructure and denseness, and mechanical properties were analyzed. Two different types of Cu powders are tested with four different compositions of added hard particles. Structural properties were evaluated using electron microscopy. In addition to these investigations, hardness and bond strength were measured in order to evaluate the mechanical behavior of the coatings.

2. Experimental Techniques

Two different Cu powders, a spherical and dendritic, were used as pure metallic powders with three different manually mixed compositions of Al_2O_3 particles. The production method of spherical particles was gas atomization whereas the dendritic particles got their morphologies by the electrolytic production method. In addition to these, a commercial powder mixture was tested as a reference. Table 1 summarizes powders and sample codes used. Morphologies of powders are presented in Fig. 1. Figure 1(a) shows the morphology of D_Cu powder, (b) added Al_2O_3 particles, (c) E_Cu dendritic Cu powder, and (d) O_Cu spherical Cu particles. All powders are commercially available. K-01-01 powder was supplied by Twin Trading Company (Moscow, Russia), and Ecka M15 by Ecka Granules (Furth, Germany), and Osprey Cu by Sandvik Osprey (Neath, UK). Oxygen content of E_Cu was $<0.15\%$ and of O_Cu it was 0.071% given by suppliers.

The LPCS Cu and $Cu + Al_2O_3$ coatings were prepared at Tampere University of Technology with the DYMET 304 K equipment (Obninsk Center for Powder Spraying, Obninsk, Russia). Compressed air was used as a process gas. Spraying parameters used are summarized in Table 2. The DYMET equipment was installed into an industrial robot. A round (∅ 5 mm) tubular nozzle was used. Substrates were grit-blasted (mesh 24, Al_2O_3 grits) Fe52 steel plates with the dimensions of 100 mm × 50 mm × 5 mm. In the bond strength tests, coatings sprayed with traverse speed of 7.4 m/min whereas in the other examinations, coatings sprayed with a traverse speed of 5 m/min were used. With O + 30 and O + 50 powders, feed rate was continuously regulated in order to gain smooth particle flow.

Powder morphologies were characterized using a Philips XL30 scanning electron microscope (SEM, Philips, Eindhoven, the Netherlands) whereas coating structures and fracture surfaces were characterized using a Zeiss ULTRAplus field-emission scanning electron microscope (FESEM, Carl Zeiss NTS GmbH, Oberkochen, Germany). The microstructures of LPCS coatings were studied from unetched metallographic cross-sectional samples. Denseness and particularly existing through-porosity (open-porosity/interconnected porosity) of the LPCS coatings were tested with corrosion tests; open-cell electrochemical potential measurements and salt spray tests. The electrochemical cell used in the open-cell potential measurements consisted of a tube, of diameter 20 mm and volume 12 mL, glued on the surface of the coating specimen. A 3.5 wt.% NaCl solution was put into the tubes for nine-day measurements. Open-cell potential measurements were done with a Fluke 79 III true RMS multimeter (Everett, WA). A silver/silver chloride (Ag/AgCl) electrode was used as a reference electrode. The salt spray test was done

Table 1 Powder characteristics of Cu and $Cu + Al_2O_3$ powders

Sample	Powder composition	Cu powder	Particle size of Cu powder, µm	Morphology of Cu powder	Amount of Al_2O_3, vol.%
D_Cu	$D\_Cu + Al_2O_3$	K-01-01	ca 15 (a)	Dendritic	~50 (a)
E_Cu	E_Cu	Ecka M15	<63	Dendritic	0
E + 10	$E\_Cu + 10Al_2O_3$	Ecka M15	<63	Dendritic	10
E + 30	$E\_Cu + 30Al_2O_3$	Ecka M15	<63	Dendritic	30
E + 50	$E\_Cu + 50Al_2O_3$	Ecka M15	<63	Dendritic	50
O_Cu	O_Cu	Osprey Cu	−25 + 5	Spherical	0
O + 10	$O\_Cu + 10Al_2O_3$	Osprey Cu	−25 + 5	Spherical	10
O + 30	$O\_Cu + 30Al_2O_3$	Osprey Cu	−25 + 5	Spherical	30
O + 50	$O\_Cu + 50Al_2O_3$	Osprey Cu	−25 + 5	Spherical	50

Particle sizes are given by producers

(a) With Dymet Cu powder particle size and amount of Al_2O_3 are visually analyzed from morphology images

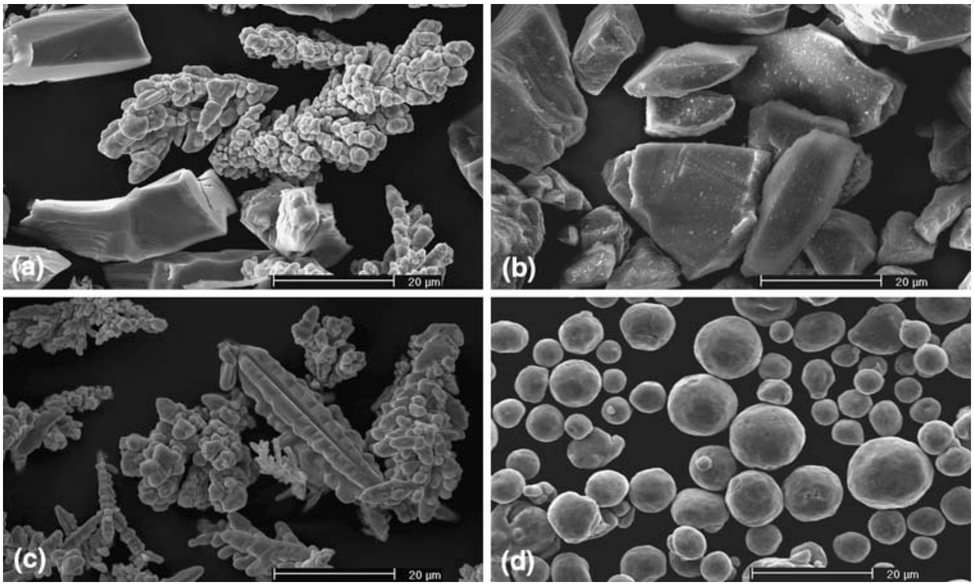

Fig. 1 Morphologies of (a) D_Cu, (b) Al_2O_3, (c) E_Cu, and (d) O_Cu powders. SEM images

Table 2 Spraying parameters of LPCS coatings

Spraying parameter	D_Cu	E_Cu, E + 10, E + 30, E + 50	O_Cu, O + 10	O + 30, O + 50
Pressure, bar	6	6	6	5
Preheating *T*, °C	540	540	540	540
Powder feed (equipment setting scale 1-8)	4.5	4.5	5.5	5-7 (a)
Traverse speed, m/min	5, 7.4	5, 7.4	5, 7.4	5, 7.4
Beam distance, mm	1	1	1	1
Spraying distance, mm	10	10	10	10
Number of layers	4	4	2	3

Beam distance stands for distance between two adjacent spray beads
(a) Powder feeding was continuously regulated

according to the ASTM B117 standard. A 5 wt.% NaCl solution was used with an exposure of 96 h, a temperature of 35-40 °C, a solution pH of 6.3, and a solution accumulation of 0.04 mL/cm^2 h. Coating surfaces after the salt spray test were visually analyzed. An amount of corrosion spots on the surfaces were evaluated by using image analysis program, ImageJ, which was also used in the analysis of Al_2O_3 fractions inside the coatings. Furthermore, mechanical properties were studied. Vickers hardness ($HV_{0.3}$) was measured as an average of 10 measurements with a Matsuzawa MMT-X7 hardness tester (Akita, Japan). Bond strength values were determined according to the standard EN582 in a tensile pull test (Instron 1185 mechanical testing machine, Norwood, MA). Three measurements were carried out to calculate the average values of bond strengths.

3. Results and Discussion

This study shows microstructural details using electron microscopic techniques, fracture surface analysis and denseness evaluations with corrosion tests. In addition to these, hardness and bond strength were investigated in order to find the relationship between the microstructure and the macroscopic properties of different LPCS Cu + Al_2O_3 mixture coatings.

3.1 Microstructures

The microstructural features of LPCS Cu + Al_2O_3 coating prepared from K-01-01 powder are presented in our previous study (Ref 17). This same powder was used also in the present study as a reference. Figure 2 shows cross-sectional structure (Fig. 2a) of D_Cu coating and interface between coating and grit-blasted steel substrate (Fig. 2b). Coating thickness was 276 µm (thickness of 1 layer 69 µm). Black particles are Al_2O_3 particles, arising from an initial powder mixture. The amount of Al_2O_3 particles inside the coating was 5.2% according to image analysis. Dendritic Cu particles were deformed on the impacts. However, some oxidized boundaries are observed in the microstructure as slightly darker gray areas between primary particles. Oxidized areas were caused by initial oxidized layers on the particle surfaces in the as-received

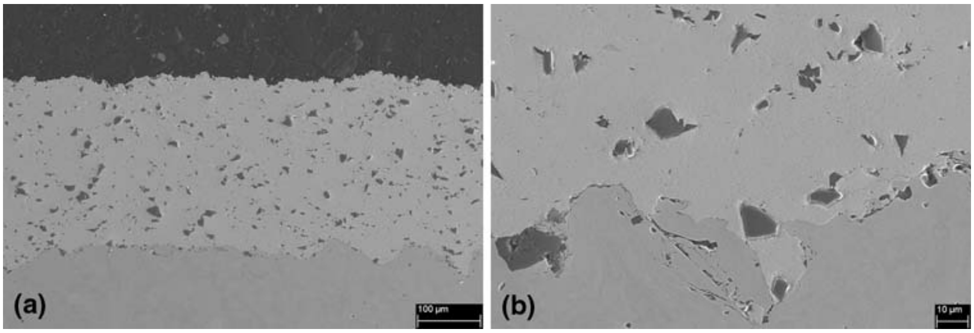

Fig. 2 Structure of D_Cu coating on grit-blasted steel substrate (a) general view and (b) interface between coating and substrate. FESEM images

state. Furthermore, dendritic particles had large surface areas due to the dendritic morphology of particles (Fig. 1c, powder particle consists of primary particles) and thus, high number of oxidized primary particle boundaries compared with spherical particles. An interface between coating and substrate was faultless and tightly adhered. Moreover, the interface seemed to be highly deformed (Fig. 2b).

Usually, hard particles are mixed with metallic particles in the LPCS process. There are three functions of use of ceramic particles: (i) cleaning the nozzle, (ii) activating the sprayed surface, and (iii) densifying the structure (Ref 17). In this study, pure Cu powders were also tested. The structure of E_Cu (dendritic) coating is presented in Fig. 3. The E_Cu coating contained some porosity and open boundaries in its structure concentrated mostly near to the coating surface. One reason for that could be that densifying effect of next incoming particles was missing and thus, coating had a porous layer on the top of the coating (Ref 20). Coating thickness was 258 μm (thickness of 1 layer 65 μm). In order to eliminate the porosity, Al_2O_3 particles were mixed with Cu powder.

The coating thicknesses increased with increasing amount of Al_2O_3 particles. The coating thicknesses of E + 10, E + 30, and E + 50 coatings were 328 μm (thickness of 1 layer 82 μm), 379 μm (thickness of 1 layer 95 μm), and 391 μm (thickness of 1 layer 98 μm), respectively. This indicates deposition efficiency improvement by using metallic-ceramic mixture powders. Figure 4 presents the structures of E + 10 (Fig. 4a) and E + 30 (Fig. 4b) coatings. These coatings contained also the porous layer near to the coating surface. However, the amount of porosity and open boundaries was decreased with the Al_2O_3 addition. This was due to the hammering effect of hard particles and thus, densification of the structure.

The strongest influence of hard particles on microstructure was detected with the highest amount of Al_2O_3 particles in the case of powder mixtures with dendritic Cu powder particles. The porous top layer was eliminated in the E + 50 coating which is seen in Fig. 5(a). Additionally, the detailed microstructure of E + 50 coating is presented in Fig. 5(b). Particle boundaries are partly seen in the structure, indicating that all oxide layers were not removed during particle impacts. In addition, very small-sized pores can be observed in the primary particle boundaries. The dendritic particles were plastically deformed, but even higher deformation would be needed for eliminating all initial oxide layers of the powder particles. After removal of the oxide layers, it is possible to reveal the pure metallic surface and together with high contact pressure achieve the metallic bonding between primary Cu particles (Ref 6). However, the cross-sectional structure showed localized deformed grain structure inside the individual primary particles (Fig. 5b).

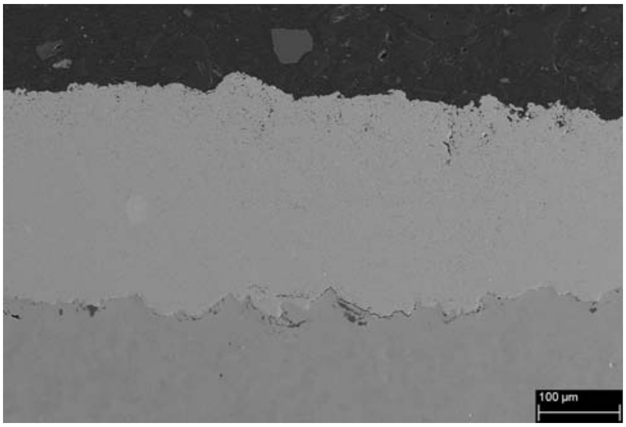

Fig. 3 Structure of E_Cu coating on grit-blasted steel substrate. FESEM image

In addition to the dendritic Cu feedstock, the LPCS coatings were prepared from spherical Cu powders mixed with different amounts of Al_2O_3 particles. The structure of pure O_Cu (spherical) coating is presented in Fig. 6. The coating was mainly dense, containing only a few pores near to the coating surface. The porous layer was not received as well as in the coatings sprayed from dendritic Cu particles. It should be noticed that there is a lower amount of primary particle surfaces in the spherical, atomized particles arose from the higher primary particle size (ca 12.5 μm versus few microns) and thus, the higher volume of the individual primary particle (spherical powder particle versus dendritic primary particle in the powder particle), indicating possibility to have lower amount of oxidized particle boundaries. Additionally, oxide layers from initial Cu powder (direct reduction,

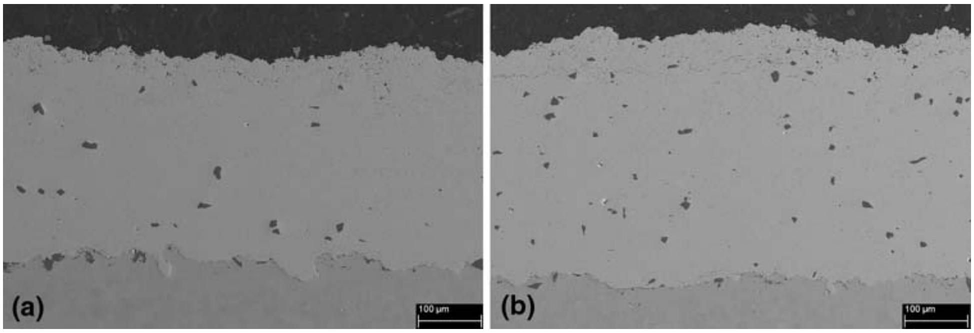

Fig. 4 Structures of (a) E + 10 and (b) E + 30 coatings on grit-blasted steel substrates. FESEM images

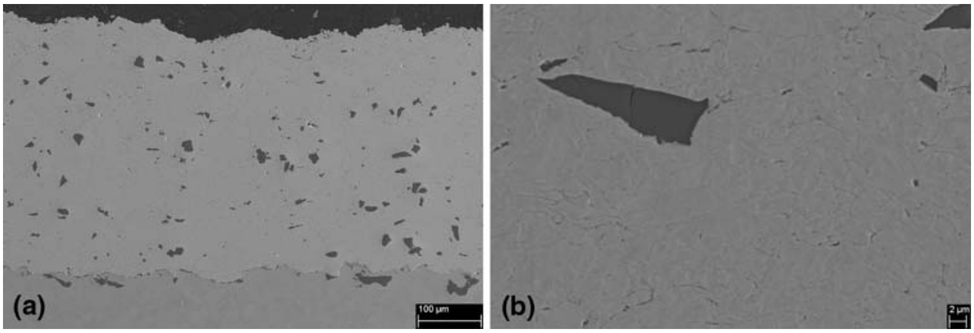

Fig. 5 Structure of E + 50 coating on grit-blasted steel substrate (a) general view and (b) detailed microstructure. FESEM images

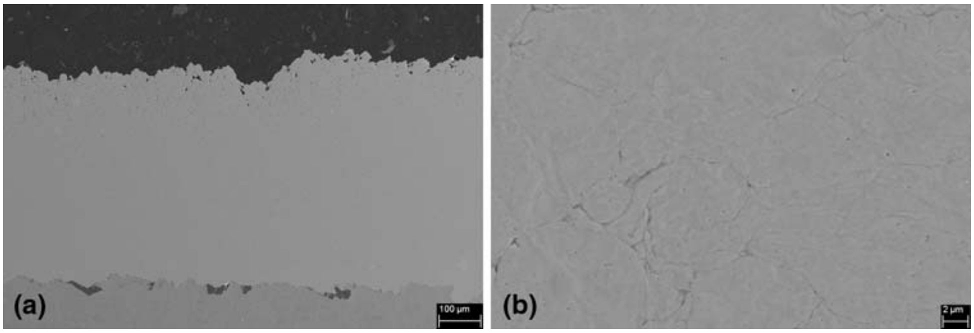

Fig. 6 Structure of O_Cu coating on grit-blasted steel substrate (a) general view and (b) detailed microstructure. FESEM images

convoluted particles) have reportedly incorporated as well in the HPCS Cu coating whereas the HPCS Cu coating sprayed from spherical powder was oxide-free (Ref 21). The coating thickness of O_Cu coating was 504 µm (thickness of 1 layer 252 µm). However, it should be noticed that coating thicknesses between coatings prepared from dendritic powder (Ecka M15) and spherical powder (Osprey) are not comparable because of different powder feed rates. The powder feed rate was continuously controlled in order to gain smooth powder flow in the case of O_Cu coatings. Figure 6(b) reveals the detailed microstructure of O_Cu coating. Oxidized particle boundaries, which were not removed during impacts, are detected inside the structure arose from initial oxide layers on the surfaces of the as-received powder particles as slightly darker gray boundaries in Fig. 6(b).

The structure of O + 10 coating is shown in Fig. 7. The coating had a relatively dense structure. Black particles inside the structure are Al_2O_3 particles arose from the powder mixture. The coating thickness was 441 µm (thickness of 1 layer 221 µm). More detailed structure is presented in Fig. 7(b). The addition of the hard particles was reinforced and hammered the structure and particles were undergone high plastic deformation. Therefore, more oxide layers were removed and metal-metal particle bonds were revealed. However, some oxidized boundaries

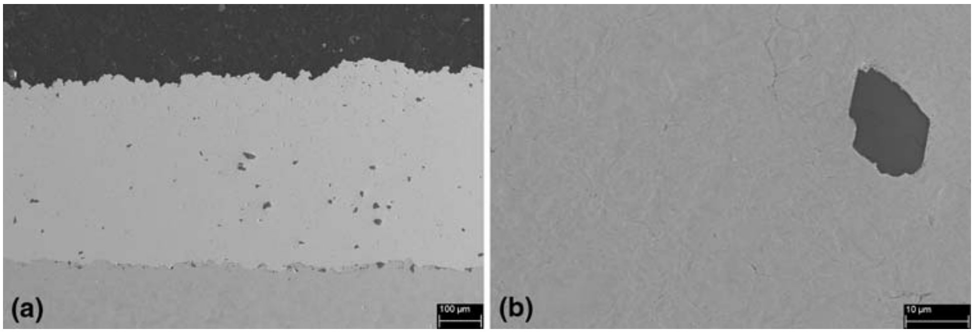

Fig. 7 Structure of O + 10 coating on grit-blasted steel substrate (a) general view and (b) detailed microstructure. FESEM images

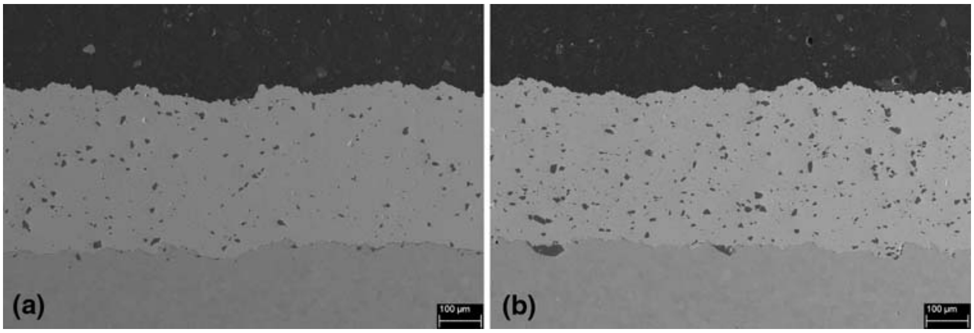

Fig. 8 Structure of (a) O + 30 and (b) O + 50 coatings on grit-blasted steel substrates. FESEM images

are still observed in the structure. In addition to the particle boundaries, localized grain deformation is detected in the interparticle structures.

Bonding between particles depends on powder materials, e.g., metallic and ceramic particles. In the optimal situation, metal-metal bonds are formed between metallic particles. Meanwhile, ceramic particles cannot be plastically deformed and hence, bonding mechanism between metallic and ceramic particles will be interlocking. The ceramic particles just stick to the metallic matrix. The amount of the hard particles has an effect on the coating formation of these composite coatings. In the case of spherical particles, the amount of 30% and 50% leads higher amount of Al_2O_3 particles to the coating structure. In turn, the higher amount of Al_2O_3 particles inside the coating possesses the higher amount of weaker ceramic-metallic bonds between particles. Bonding between metallic particles is stronger than between metallic and ceramic particles due to the bonding mechanisms (metal-metal bonds lead to the tighter adhesion between particles than sticking between metallic-ceramic particles). Figure 8 presents the structures of O + 30 (Fig. 8a) and O + 50 (Fig. 8b) coatings. The coating thicknesses were 370 μm (thickness of 1 layer 123 μm) and 364 μm (thickness of 1 layer 121 μm), respectively.

Al_2O_3 fractions were analyzed using image analysis and the amounts of Al_2O_3 particles inside the coating structures are presented in Table 3. Usually, coatings contain ceramic particles below 5% from total amount of ceramic powder, indicating erosion and on the other hand, activation occurred by ceramic particles (Ref 14, 22, 23). The similar behavior was also detected in this study.

Table 3 Amount of Al_2O_3 particles in the powder and inside the coating

Sample	Amount of Al_2O_3 particles in the powder, vol.%	Amount of Al_2O_3 particles inside the coating, %
D_Cu	~50	5.2
E_Cu	···	···
E + 10	10	0.9
E + 30	30	1.5
E + 50	50	3.6
O_Cu	···	···
O + 10	10	0.7
O + 30	30	2.0
O + 50	50	3.3

Amount inside the coating was done using image analysis (ImageJ)

Structures of LPCS Cu + Al_2O_3 coatings differed from each other, depending on sprayed feedstock. Obviously, coating sprayed with spherical Cu particles had larger primary particle size in the coating structure compared with the particle size of primary particles in the coating sprayed from dendritic Cu particles. The visually densest coating sprayed with dendritic powder (E_Cu) was achieved with the composition 50% Al_2O_3, whereas in the case of spherical Cu powder, the densest structure was gained with composition of 10% Al_2O_3 particles.

However, grain sizes are equal in these both coatings. The structure of LPCS Cu + Al_2O_3 coating prepared from spherical powder (O + 10) was denser and purer than the coating structure of E + 50 coating (compare Fig. 5b and Fig. 7b).

Spraying parameters have also influence on coating formation and deposition efficiency in LPCS process. Maev and Leshchynsky (Ref 4) have shown that deposition efficiency increased with the increasing preheating temperature of gas. Therefore, high preheating temperature (540 °C) of compressed air was used in this study. Additionally, this study is perceived the noticeable deposition efficiency increment with increasing amount of added Al_2O_3 particles with the dendritic Cu particles by comparison between coating thicknesses: 258 µm for E_Cu and 328-391 µm for E + Al_2O_3 coatings. Furthermore, the amount of Al_2O_3 particles in the coatings structures was obviously increased with increasing amount of hard particles in the powder mixture. Further, this trend was similar with spherical and dendritic Cu particles (Table 3).

3.2 Fracture Surfaces

Fracture surface analysis reveals particle deformation. Figure 9 presents the fracture surface of D_Cu coating. Localized deformation is detected in the structure (Fig. 9b). Powder particle boundaries are not clearly seen in the structure whereas primary particle boundaries are observed from the fracture surface. The blocky particles in Fig. 9 are Al_2O_3 particles which are embedded into the metallic structure. The coating structure prepared from dendritic feedstock contains high amount of primary particle boundaries and thus, probability to have oxidized boundaries is higher (Ref 17). In the other words, particles need to be deformed even higher level in order to get metal-metal bonding between Cu particles compared with the spherical Cu particles which have initially higher primary particle size and thus, lower amount of particle boundaries, and additionally, denser and purer particle structure in as-received state.

Figure 10 shows the fracture surface of Cu coating prepared from dendritic particles. The pure E_Cu coating is presented in Fig. 10(a) and E + 50 in Fig. 10(b). The densifying effect due to the more deformed particle structure with added hard particles (E + 50) is perceived from the structures. The primary particle boundaries are more clearly seen in the structure of E_Cu coating. The open particle boundaries were also detected in the microstructure of this coating (Fig. 3), indicating less deformed particles and hence, weak bonding between Cu particles. The primary Cu particles are strongly deformed in the coating structure with Al_2O_3 particles (Fig. 10b), reflecting the high effect of hard particles on the coating formation by increasing the deformation level of metallic particles.

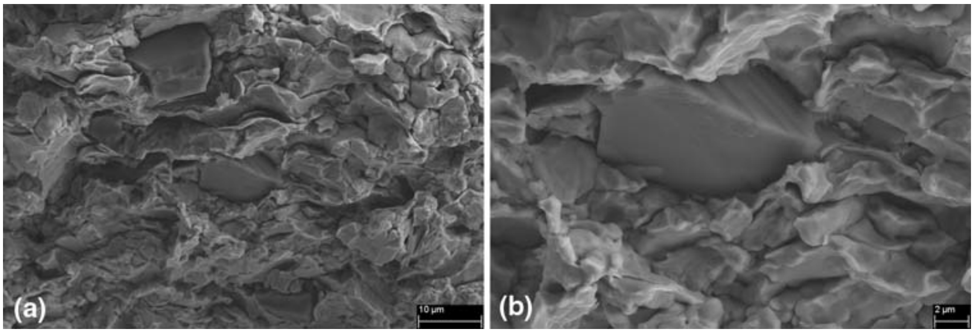

Fig. 9 Fracture surfaces of D_Cu coating (a) general and (b) detailed view. FESEM images

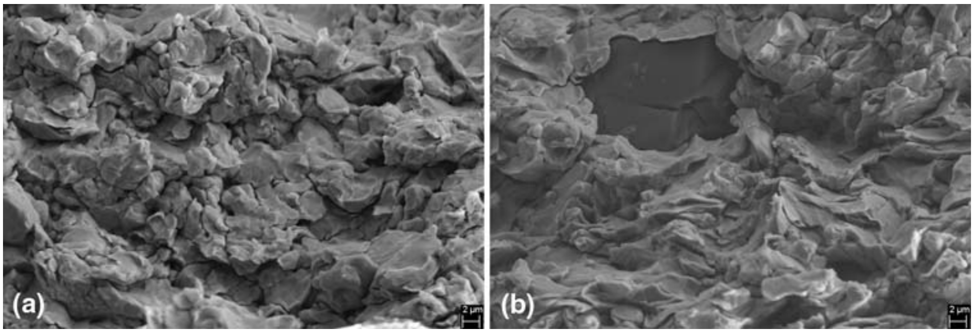

Fig. 10 Fracture surfaces of (a) E_Cu and (b) E + 50 coatings. FESEM images

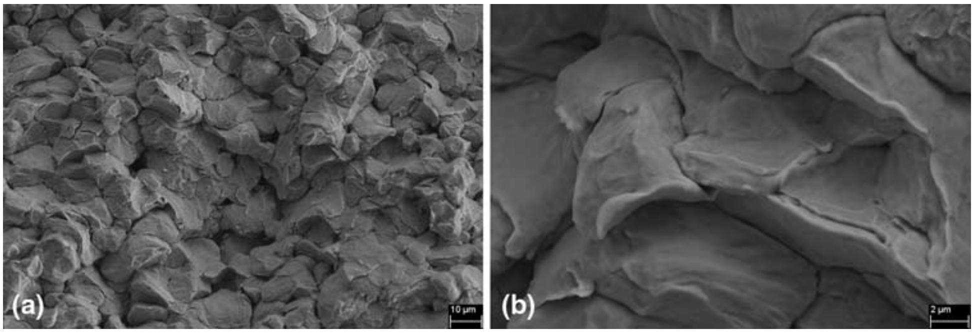

Fig. 11 Fracture surfaces of O_Cu coating (a) general and (b) detailed view. FESEM images

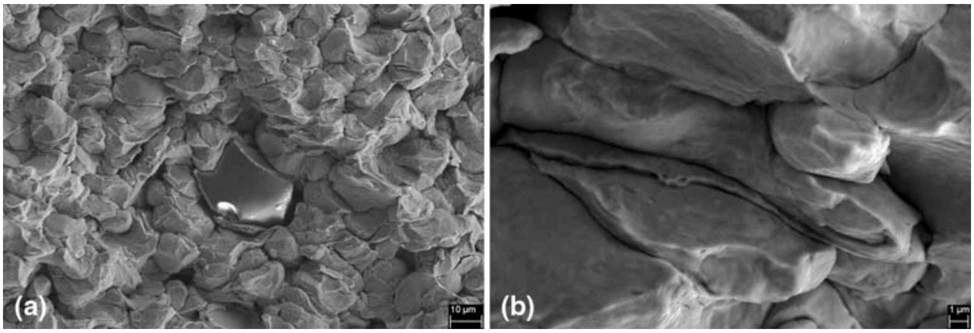

Fig. 12 Fracture surfaces of O + 10 coating (a) general and (b) detailed view. FESEM images

According to the salt spray test (in following "Denseness" section) and evaluation of microstructures, the densest coating prepared from spherical Cu particles was gained with 10% Al_2O_3 addition. In addition, the fracture surface of O + 10 showed tighter structure with higher deformation level compared with O_Cu coating without the ceramic addition. However, Cu particles in the O_Cu coating were also relatively highly deformed. Common for these both coatings and actually, also for D_Cu and E_Cu coatings, the fracture planes were mostly brittle type. The fracture surfaces of O_Cu and O + 10 coating are shown in Figs. 11 and 12, respectively. Figures 11(b) and 12(b) reveal high particle deformation as the flattened particle shapes. Additionally, material jets are observed inside the structure. Especially, in Fig. 12(b) narrow material jet is detected in the middle of the fracture surface. Formation of material jets is due to the thermal softening and adiabatic shear instability (Ref 6).

As a summary of the fracture surface analysis, particles were strongly deformed on the particle impacts. Moreover, Al_2O_3 addition hammered the structure, causing the higher level of plastic deformation occurrence and thus, highly deformed metallic structure. This was particularly seen with E + Al_2O_3 coatings. Particle bonds were tighter in the coatings prepared from spherical particles (O_Cu and O + Al_2O_3 coatings) compared with dendritic particles (D_Cu, E_Cu, and E + Al_2O_3 coatings). This was strongly influenced by the amount of particle boundaries. Larger primary particle size indicates denser coating structure arising from lower amount of particle boundaries as the weak points in the structure. On the other hand, material jets also clean the surfaces and promote metallic surfaces for the tight metal-metal bonding (Ref 6).

3.3 Denseness

Open-cell potential measurements showed existing through-porosity in all LPCS Cu coatings. The open-cell potentials of the LPCS Cu and Cu + Al_2O_3 coatings were between −519 and −610 mV, whereas open-cell potential of Fe52 substrate material was −700 mV. The open-cell potentials were close to the value of Fe52 substrate material, reflecting open way for test solution (3.5% NaCl) to penetrate from coating surface to the interface between coating and substrate. In addition, salt spray tests were gained as a supplementary evaluation. Existing through-porosity in the structure of coatings was also performed in the salt spray test. The amount of corrosion spots on the coating surfaces after the salt spray test was visually analyzed by using image analysis (ImageJ). Results are presented in Fig. 13. The amount of corrosion spots decreased with Al_2O_3 addition. The LPCS Cu coatings prepared from spherical feedstock had denser structure compared with the coatings prepared from dendritic feedstock. These results indicate that bonds between particles were tighter in these O_Cu coatings. Moreover, denseness was improved mostly with 10% Al_2O_3 addition to the O_Cu powder and 30% Al_2O_3 addition to the E_Cu

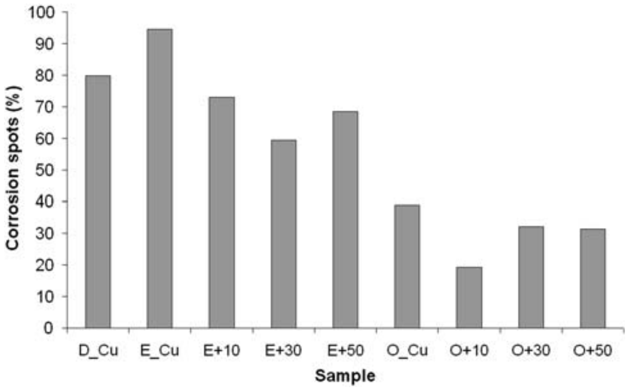

Fig. 13 Amount of corrosion spots (%) on coating surfaces after salt spray test analyzed by image analysis (ImageJ)

powder. The structure consisted mostly of metallic bonding have denser structure. However, low amount of added hard particles hammer the metallic structure, reinforcing the entire coating and thus, O + 10 coating had the highest denseness. Meanwhile, powder composed of dendritic Cu particles needed higher amount of hard particles to hammer the structure enough. On the other hand, amount of weaker bonds between metallic and ceramic particles than between metal-metal particles increases with higher amount of Al_2O_3 particles, reflecting to the denseness by again decreasing it. These different behaviors of dendritic and spherical mixture powders indicate clearly the importance of specific powder properties which should be chosen case by case.

Microstructural characterization together with corrosion tests clearly showed the effect of powder type of Cu particles and composition of added hard particles on coating formation and structure and therefore, also on the denseness (impermeability) of the coatings. The densest structures were achieved with coatings prepared from spherical powder particles (O_Cu and O + Al_2O_3 coatings). This was affected by the density of the powder particle and the number of primary particle boundaries (oxidized boundaries). Therefore, lower number of particle boundaries with lower number of oxidized particle surfaces generates tighter structure and thus, the higher denseness of the coating. With the spherical particle mixtures, the effect of hard particles was not as high as in the case of dendritic particles. The highest denseness of O_Cu coatings was detected with 10% Al_2O_3 particle addition into the initial powder mixture. In the case of dendritic particles, the highest denseness was gained with 30% and 50% Al_2O_3 addition. In conclusion, salt spray tests showed that all coatings tested in this study contained through-porosity in their structure. However, denseness improvement was clearly observed with Al_2O_3 additions, reflecting their significant effect on coating formation.

3.4 Hardness

Vickers hardness was measured in order to evaluate differences in the mechanical properties of coatings prepared from different-type powder characteristics. Hardness indicates level of work hardening. Table 4 summarizes Vickers hardness $HV_{0.3}$ of LPCS coatings. LPCS Cu coating sprayed with dendritic feedstock powder particles (E_Cu) have lower hardness than coating sprayed with spherical particles (O_Cu). McCune et al. (Ref 21) have reported similar behavior where the HPCS Cu coating sprayed from spherical (gas-atomization) Cu particles possessed higher hardness compared with coating sprayed from convoluted (direct reduction) Cu particles. Furthermore, hardness increases with increasing Al_2O_3 addition, indicating the high deformation and thus, the higher hardening effect. It should be noticed that indentation was taken from metallic area of the coating in order to analyze the behavior of metallic Cu particles. In addition, if we compare Cu + 50Al_2O_3 coatings, it can be noticed that O + 50 coating had the highest hardness, then D_Cu coating and after that E + 50 coating had the lowest hardness in this comparison. The trend in the hardness values was comparable to the microscopic evaluations, reflecting the strong effect of powder type and composition on the deformation, denseness, particle bonding, and work hardening.

Table 4 Vickers hardness $HV_{0.3}$ of LPCS Cu and Cu + Al_2O_3 coatings

Sample	Vickers hardness $HV_{0.3}$	SD
D_Cu	117	3.4
E_Cu	83	3.9
E + 10	95	7.6
E + 30	96	4.3
E + 50	103	4.6
O_Cu	106	6.0
O + 10	113	4.1
O + 30	127	3.3
O + 50	127	8.9

3.5 Bond Strength

The bond strength of LPCS Cu coating prepared from dendritic powder (K-01-01) was cohesive type in our previous study (Ref 17). In this study, the bond strength of D_Cu coating which was prepared from the same powder as feedstock showed also cohesive type bond strength. On the contrary, in the cases of E_Cu and E + Al_2O_3 coatings samples fractured partly from the coating-substrate interface and partly close to the interface in the coating side. However, it can be said that bond strength was mostly adhesive type because the rupture was still occurred mostly at the interface. In the case of O_Cu and O + Al_2O_3 coatings, bond strength was clearly adhesive type due to the fact that the weakest point in the tensile test was the interface between coating substrate. The adhesive rupture and thus, the adhesive-type bond strength in both cases, O_Cu and E_Cu coatings mixed with Al_2O_3 particles was possibly due to the hammering effect of Al_2O_3 particles. The Al_2O_3 particles tamped the coating structure, leading higher cohesion between particles compared with adhesion between coating and

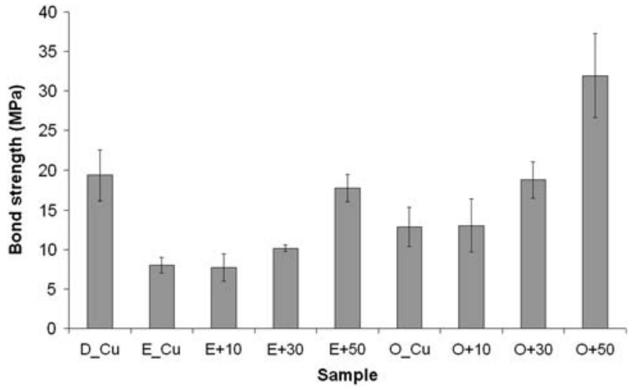

Fig. 14 Bond strengths (and standard deviations) of LPCS Cu and Cu + Al_2O_3 coatings. D_Cu coating had cohesive type, E_Cu and E + Al_2O_3 coatings mostly adhesive type, and O_Cu and O + Al_2O_3 coatings adhesive-type bond strengths

substrate. Bonds between Al_2O_3 and Cu particles were weaker than bonds between the metallic particles (sticking versus metallic bonding). Thus, it is more probable that fracture occurs inside the D_Cu coating where the amount of Al_2O_3 particles was higher and bonds between particles weaker. Besides, the lower amount of hard particles inside the coating (compare D_Cu coating with E + 50 and O + 50 coatings) indicates more bonding areas between the metallic particles. Figure 14 summarizes the bond strengths of the coatings. It can be clearly seen that the bond strengths increase with the increasing amount of Al_2O_3 particles in the initial manually mixed powder mixtures. This effect was also detected in Ref 14, 24, and 25. In addition, coatings prepared from spherical particles (O_Cu and O + Al_2O_3) had the higher bond strengths caused by higher plastic deformation together with more oxidized-free particle boundaries (purer coatings). Maev and Leshchynsky (Ref 8) have reported the adhesion strength of Cu-based coating on steel substrate ~27 MPa which is comparable with results in this study.

Generally speaking, the bond strengths of the LPCS coatings are reasonable. However, bonding and as well as bond strengths are strongly influenced by powder characteristics and compositions. Regardless of the powder characteristics of Cu particles, the bond strength of the LPCS Cu coatings depends on the amount of Al_2O_3 particles in the powder mixtures. This study showed that bond strength was the highest with 50% Al_2O_3 addition. This was due to the activation effect of hard particles (also hammering and tamping effects) together with increased contact areas (Ref 24) on the substrate surfaces. Bonding between grit-blasted steel substrate and powder particles was stronger, reflecting higher plastic deformation occurred on the impacts. Moreover, higher deformation level was also detected in the microscopic evaluations. Spherical particles underwent higher plastic deformation (lower content of oxidized primary particle boundaries) and hence, also the bond strengths of the coatings prepared from spherical particles (Osprey) are relatively higher than in the case of the coating prepared from dendritic particles (K-01-01 and Ecka). This was clearly observed in both O_Cu and E_Cu mixture coatings with all powder composition (0%, 10%, 30%, and 50% Al_2O_3 addition).

4. Conclusions

The LPCS process is the relevant method to prepare Cu and Cu + Al_2O_3 coatings. These coatings were relatively dense according to visual examination. However, corrosion tests revealed through-porosity inside the coating structures. Moreover, powder characteristics and compositions affected the denseness and mechanical properties of the coatings. In this study, the effect of powder type, i.e., dendritic versus spherical Cu particles, and the amount of Al_2O_3 particles in the powder mixtures were characterized. The study was focused on the microstructural details and mechanical behavior of the LPCS Cu coatings manufactured by using different feedstock.

The LPCS Cu and Cu + Al_2O_3 coatings prepared from the spherical Cu particles contained less through-porosity in their structures compared with coatings prepared from the dendritic particles, indicating denser coating structures. It was possible to produce pure Cu coatings from both spherical and dendritic feedstock by using LPCS process; however, the quality of the coatings can be improved with the hard particle additions. This study has clearly shown that more deformed and denser coating structure together with higher hardness and bond strength were gained with Al_2O_3 particle addition into the Cu powder. Densification was noticeable with the E + Al_2O_3 coatings (dendritic Cu particles) and according to corrosion tests; the densest structure was achieved with the amount of 30% Al_2O_3 particles. Porosity was significantly diminished with increasing amount of Al_2O_3 particles in the initial powder mixture. In addition to that, fracture surface analysis showed much higher level of deformation of Cu particles when Al_2O_3 particles were mixed with Cu particles, reflecting the densifying and hammering effect of hard particles.

On the other hand, O_Cu and O + Al_2O_3 coatings had denser structures than E_Cu and E + Al_2O_3 coatings. This can be explained by the powder characteristics; particle morphologies, primary particle sizes and purity of the initial powder particles. Usually, if the coating has weak points in its structure, they are detected on the particle boundaries and because of that affect particle bonding. The dendritic particles have more boundaries in the structure due to the finer particle size of primary particles and thus, more possibilities to have weak bonds between the particles due to the higher amount of oxidized particle boundaries. The O + 10 coating had the densest structure according to the microscopic evaluation and in addition to that, the corrosion tests. Meanwhile, the O + 50 coatings had the highest hardness and bond strength. Firstly, the higher amount of Al_2O_3 particles causes the higher level of work hardening which is reflected on the hardness values. On the other hand, bond strengths (adhesive strength, fracture surface was between coating and substrate) were higher due to the stronger activation effect of Al_2O_3 particles on substrate surface by increasing and cleaning the contact areas. Second, metallic bonding makes the structure denser and thus, 10% Al_2O_3 addition forms denser structure than 50% addition and thus, 10% was enough to hammer the structure.

The hardnesses and bond strengths of the coatings were strongly depended on the powders used. The hardness and bond strength were increased with the increasing amount of hard particles in both cases of LPCS Cu mixture coatings prepared from either spherical or dendritic feedstock. However, it should be noticed that the hardness and bond strengths were higher when using the spherical Cu particles compared with the dendritic particles. Denser powder particles with higher primary particle size can be explained this effect due to the fact that spherical particles underwent the higher level of plastic deformation. Thus, they have probability to have the lower number of weak particle boundaries.

This study presented the effect of powder characteristics on the coating properties. Densification was significantly detected, but still LPCS Cu and $Cu + Al_2O_3$ coatings contained through-porosity. However, this study has clearly shown the importance of the powders in the cold spraying and shown the possibility to improve coating quality by using the metallic-ceramic mixture powders with optimized characteristics together with optimized compositions, depending on the coating properties desired.

Acknowledgments

The authors thank Mr. Mikko Kylmälahti, of Tampere University of Technology, Department of Materials Science, for the spraying the LPCS coatings and Mr. Sakari Tolvanen of Tampere University of Technology, Department of Materials Science for the carrying out the bond strength tests. In addition, the authors express thanks to Mr. Jonne Näkki of KETEK for the salt spray tests. This study was supported by Academy of Finland and Finnish National Graduate School on New Materials and Processes.

References

1. A. Papyrin, V. Kosarev, S. Klinkov, A. Alkimov, and V. Fomin, 2007, *Cold Spray Technology*, 1st ed., Elsevier, the Netherlands, 328 p
2. T. Schmidt, F. Gärtner, H. Assadi, and H. Kreye, Development of a Generalized Parameter Window for Cold Spray Deposition, *Acta Mater.*, 2006, **54**(3), p 729-742
3. C. Borchers, F. Gärtner, T. Stoltenhoff, H. Assadi, and H. Kreye, Microstructural and Macroscopic Properties of Cold Sprayed Copper Coatings, *J. Appl. Phys.*, 2003, **93**(12), p 10064-10070
4. R. Maev and V. Leshchynsky, Air Gas Dynamic Spraying of Powder Mixtures: Theory and Application, *J. Therm. Spray Technol.*, 2006, **15**(2), p 198-205
5. H. Assadi, F. Gärtner, T. Stoltenhoff, and H. Kreye, Bonding Mechanism in Cold Gas Spraying, *Acta Mater.*, 2003, **51**, p 4379-4394
6. M. Grujicic, C.L. Zhao, W. DeRosset, and D. Helfritch, Adiabatic Shear Instability Based Mechanism for Particles/Substrate Bonding in the Cold-Gas Dynamic-Spray Process, *Mater. Design*, 2004, **25**, p 681-688
7. T. Stoltenhoff, H. Kreye, and H. Richter, An Analysis of the Cold Spray Process and Its Coatings, *J. Therm. Spray Technol.*, 2001, **11**(4), p 542-550
8. R. Maev and V. Leshchynsky, *Introduction to Low Pressure Gas Dynamic Spray, Physics & Technology*, Wiley-VCH Verlag GmbH&Co, KGaA, Weinheim, Germany, 2008, p 328
9. A. Kashirin, O. Klyuev, T. Buzdygar, and A. Shkodkin, DYMET Technology Evolution and Application, *Thermal Spray 2007: Global Coating Solutions*, B. Marple, M. Hyland, Y. Lau, C.-J. Li, R. Lima, and G. Montavon, Ed., May 14-16, 2007 (Beijing, China), ASM International, 2007, p 141-145
10. X.-J. Ning, J.-H. Jang, H.-J. Kim, C.-J. Li, and C. Lee, Cold Spraying of Al-Sn Binary Alloy: Coating Characteristics and Particle Bonding Features, *Surf. Coat. Technol.*, 2008, **202**(9), p 1681-1687
11. E. Irissou, J.-G. Legoux, B. Arsenault, and C. Moreau, Investigation of Al-Al_2O_3 Cold Spray Coating Formation and Properties, *J. Therm. Spray Technol.*, 2007, **16**(5-6), p 661-668
12. X.-J. Ning, J.-H. Jang, and H.-J. Kim, The Effects of Powder Properties on In-Flight Particle Velocity and Deposition Process During Low Pressure Cold Spray Process, *Appl. Surf. Sci.*, 2007, **253**(18), p 7449-7455
13. B. Jodoin, L. Ajdelsztajn, E. Sansoucy, A. Zúñiga, P. Richter, and E. Lavernia, Effect of Particle Size, Morphology, and Hardness on Cold Gas Dynamic Sprayed Aluminum Alloy Coatings, *Surf. Coat. Technol.*, 2006, **201**, p 3422-3429
14. A. Shkodkin, A. Kashirin, O. Klyuev, and T. Buzdygar, The Basic Principles of DYMET Technology, *Thermal Spray 2006: Building on 100 Years of Success*, B. Marple, M. Hyland, Y. Lau, R. Lima, J. Voyer, Ed., May 15-18, 2006 (Seattle, Washington), ASM International, 2006
15. B. Djordjevic, and R. Maev, SIMAT™ Application for Aerospace Corrosion Protection and Structural Repair, *Thermal Spray 2006: Building on 100 Years of Success*, B. Marple, M. Hyland, Y. Lau, R. Lima, J. Voyer, Ed., May 15-18, 2006 (Seattle, Washington), ASM International, 2006
16. H. Weinert, E. Maeva, and E. Leshchynsky, Low Pressure Gas Dynamic Spray Forming Near-net Shape Parts, *Thermal Spray 2006: Building on 100 Years of Success*, B. Marple, M. Hyland, Y. Lau, R. Lima, and J. Voyer, Ed., May 15-18, 2006 (Seattle, Washington), ASM International, 2006
17. H. Koivuluoto, J. Lagerbom, M. Kylmälahti, and P. Vuoristo, Microstructure and Mechanical Properties of Low-Pressure Cold Sprayed (LPCS) Coatings, *J. Therm. Spray Technol.*, 2008, **17**(5-6), p 721-727
18. V. Champagne, Ed., *The Cold Spray Materials Deposition Process: Fundamentals and Applications*, Woodhead Publishing Limited, Cambridge, England, 2007, p 362
19. H. Mäkinen (Koivuluoto), J. Lagerbom, and P. Vuoristo, Adhesion of Cold Sprayed Coatings: Effect of Powder, Substrate, and Heat Treatment, *Thermal Spray 2007: Global Coating Solutions*, B. Marple, M. Hyland, Y.-C. Lau, C.-J. Li, R. Lima, and G. Montavon, Ed., May 14-16, 2007 (Beijing, China), ASM International, 2007, p 31-36
20. H. Mäkinen (Koivuluoto), J. Lagerbom, and P. Vuoristo, Mechanical Properties and Corrosion Resistance of Cold Sprayed Coatings, *Thermal Spray 2006: Building on 100 Years of Success*, B. Marple, M. Hyland, Y. Lau, R. Lima, and J. Voyer, Ed., May 15-18, 2006 (Seattle, Washington), ASM International, 2006
21. R.C. McCune, W.T. Donlon, O.O. Popoola, and E.L. Cartwright, Characterization of Copper Layers Produced by Cold Gas-Dynamic Spraying, *J. Therm. Spray Technol.*, 2000, **9**(1), p 73-82
22. A. Shkodkin, A. Kashirin, O. Klyuev, and T. Buzdygar, Metal Particle Deposition Stimulation by Surface Abrasive Treatment in Gas Dynamic Spraying, *J. Therm. Spray Technol.*, 2006, **15**(3), p 382-386

23. S.V. Klinkov, V.F. Kosarev, A.A. Sova, and I. Smurov, Calculation of Particle Parameters for Cold Spraying of Metal-Ceramic Mixtures, *J. Therm. Spray Technol.*, 2009, **18**(5-6), p 944-956
24. H.Y. Lee, S.H. Jung, S.Y. Lee, Y.H. You, and K.H. Ko, Correlation Between Al_2O_3 Particles and Interface of Al-Al_2O_3 Coatings by Cold Spray, *Appl. Surf. Sci.*, 2005, **252**, p 1891-1898
25. K. Spencer, D.M. Fabijanic, and M.-X. Zhang, The Use of Al-Al_2O_3 Cold Spray Coatings to Improve the Surface Properties of Magnesium Alloys, *Surf. Coat. Technol.*, 2009, **204**, p 336-344